

TABLE OF CONTENTS

DECLARATION	v
SUMMARY OF RESEARCH	vi
ACKNOWLEDGEMENTS	viii
LIST OF FIGURES	xvi
LIST OF TABLES	xix
LIST OF EQUATIONS	xx
LIST OF ACRONYMS	xxi
CHAPTER 1 – INTRODUCTION AND PROBLEM STATEMENT	1
1.1 INTRODUCTION	1
1.2 PROBLEM STATEMENT AND MOTIVATION	4
1.2.1 Motivation for the research study	4
1.2.2 Research hypotheses and questions	9
1.3 RESEARCH AIM AND OBJECTIVES	10
1.4 RESEARCH METHODOLOGY	11
1.4.1 Literature study	11
1.4.2 Empirical research.....	12
1.4.2.1 Data collection	13
1.4.2.2 Data analysis	14
1.4.2.3 Research overview	15
1.5 ETHICAL ASPECTS	16
1.6 CONTRIBUTION OF THE STUDY	16
1.7 CHAPTER SUMMARY	17
CHAPTER 2 – LITERATURE STUDY: THE ART AND SCIENCE OF CONDUCTING ORTHORECTIFICATION WITH AN OVERVIEW ON REMOTE SENSING (RS)	19
2.1 INTRODUCTION	19
2.2 REMOTE SENSING PLATFORMS	20
2.2.1 Evolution of satellite platforms.....	20
2.2.2 Properties of satellite systems.....	25
2.2.2.1 Regions of the electromagnetic spectrum.....	26

2.2.2.2	Converting recorded digital data into images.....	27
2.2.3	Characteristics of satellite systems	29
2.2.4	Modernisation of optical satellite systems	30
2.2.5	Definition of resolution capabilities	33
2.2.6	Satellite image distortions	34
2.2.6.1	Radiometric distortions	35
2.2.6.2	Geometric distortions.....	36
2.3	WAYS AND MEANS TO IMPROVE THE GEOMETRICAL ACCURACY OF SATELLITE IMAGERY	38
2.3.1	The application of image processing systems.....	39
2.3.2	Geometric correction methods	40
2.3.2.1	Parametric approach	41
2.3.2.2	Non-parametric approach	44
2.4	THE REQUIREMENTS AND ACQUISITION OF GCPS AND DEMS TO CREATE ACCURATE ORTHO-IMAGES.....	46
2.4.1	The application of GCPs	47
2.4.2	The application of DEMs	49
2.5	ASSESSMENT OF AN ORTHO-IMAGE	51
2.5.1	Calculating RMSE	53
2.5.2	Utilising the ERDAS IMAGINE® 2015 MAA tool	55
2.5.3	Performing visual inspections.....	56
2.6	CHAPTER SUMMARY	57
CHAPTER 3 - RESEARCH METHODOLOGY		59
3.1	INTRODUCTION	59
3.2	PROBLEM STATEMENT AND MOTIVATION.....	59
3.2.1	Motivation for the research study	59
3.2.2	Research hypotheses and questions	61
3.3	RESEARCH AIM AND OBJECTIVES	61
3.4	RESEARCH METHODOLOGY	62
3.5	RESEARCH DESIGN.....	64
3.6	DATA ACQUISITION AND COLLECTION	65
3.6.1	Study area.....	65

3.6.2	Data types (components) used during this study	66
3.6.2.1	Image data.....	66
3.6.2.2	Elevation data.....	67
3.6.2.3	Ground control points	70
3.6.2.3.1	GPS device based GCPs.....	70
3.6.2.3.2	TerraSAR-X GCPs.....	75
3.6.2.4	Vector layer	77
3.7	DESIGN OF EXPERIMENTS	78
3.7.1	Description of the stage 1 experiments	79
3.7.2	Description of the stage 2 experiments	80
3.7.3	Description of the stage 3 experiments	80
3.7.4	Validity and reliability of the data collected.....	81
3.8	DATA ANALYSIS	82
3.9	CHAPTER SUMMARY.....	83
CHAPTER 4 – EMPIRICAL RESEARCH: ORTHORECTIFICATION EXPERIMENTS		
AND METHODOLOGICAL CONTRIBUTION		
		85
4.1	INTRODUCTION	85
4.2	PROCESS FOLLOWED TO PERFORM ORTHORECTIFICATION	85
4.2.1	Limitations of manually selecting and placing input GCPs	88
4.3	ORTHORECTIFICATION TESTS: STAGE 1 EXPERIMENTS	89
4.3.1	Experiment 1(a): Utilising 5 GCPs and 30 m SRTM DEM.....	91
4.3.2	Experiment 1(b): Utilising 5 GCPs and 12 m DTM	93
4.3.3	Experiment 1(c): Utilising 5 GCPs and 2 m DTM	94
4.3.4	Experiment 2(a): Utilising 13 GCPs and 30 m SRTM DEM.....	95
4.3.5	Experiment 2(b): Utilising 13 GCPs and 12 m DTM	96
4.3.6	Experiment 2(c): Utilising 13 GCPs and 2 m DTM	97
4.3.7	Experiment 3(a): Utilising 25 GCPs and 30 m SRTM DEM.....	98
4.3.8	Experiment 3(b): Utilising 25 GCPs and 12 m DTM	99
4.3.9	Experiment 3(c): Utilising 25 GCPs and 2 m DTM	100
4.4	ANALYSIS OF STAGE 1 EXPERIMENTS.....	101
4.5	ORTHORECTIFICATION TESTS: STAGE 2 EXPERIMENTS	105
4.5.1	Independent experiment 01: Using TerraSAR-X GCPs and 2 m DTM.....	105

4.5.2	Independent experiment 02: Using sensor model and 2 m DTM	106
4.6	ANALYSIS OF STAGE 2 EXPERIMENTS.....	107
4.7	ORTHORECTIFICATION TESTS: STAGE 3 EXPERIMENTS	110
4.7.1	Experiment 01: GCPs concentrated on the west side of the image	111
4.7.2	Experiment 02: GCPs concentrated on the east side of the image	112
4.7.3	Experiment 03: GCPs concentrated on the north side of the image.....	113
4.7.4	Experiment 04: GCPs concentrated on the south side of the image	114
4.7.5	Experiment 05: Random distribution of GCPs covering the entire image....	115
4.8	ANALYSIS OF STAGE 3 EXPERIMENTS.....	116
4.9	STUDY CONTRIBUTIONS.....	118
4.9.1	Requirements necessary to create accurate ortho-images	119
4.9.2	Contributions derived from the stage 2 experiments	121
4.9.3	The influence of inadequate and irregular GCPs on orthorectification	121
4.9.4	Concluding notes	123
4.10	FINAL OUTCOME.....	124
4.11	REALISING THE NEED FOR DEVELOPING AN AUTOMATIC GCP EXTRACTION SCRIPT (A-GCP-ES)	125
4.12	CHAPTER SUMMARY.....	126
CHAPTER 5 – DEVELOPMENT OF AN AUTOMATIC GCP EXTRACTION SCRIPT		127
5.1	INTRODUCTION.....	127
5.2	MEASURES FOLLOWED TO VERIFY PLACEMENT OF GCPS.....	128
5.3	BACKGROUND CONCEPT OF THE A-GCP-ES	129
5.4	DEVELOPMENT OF THE A-GCP-ES.....	130
5.4.1	Creating the required chip database utilising PCI Geomatica®.....	132
5.4.2	Executing the A-GCP-ES on Microsoft (MS) Windows operating system ...	136
5.5	TESTING AND EVALUATING THE A-GCP-ES	138
5.5.1	Comparing the accuracy of manually placed GCPs by an operator to the GCPs extracted by the A-GCP-ES	142
5.6	CHAPTER SUMMARY.....	144
CHAPTER 6 – CONCLUSIONS AND RECOMMENDATIONS		145
6.1	INTRODUCTION	145

6.2	STUDY REVIEW	145
6.2.1	Background.....	145
6.2.2	Literature study	146
6.2.3	Empirical research.....	146
6.3	ACHIEVEMENT OF STUDY OBJECTIVES AND AIM	147
6.4	CONCLUSIONS	148
6.5	RECOMMENDATIONS	149
6.6	FUTURE RESEARCH.....	151
6.7	CHAPTER SUMMARY.....	152
	REFERENCES.....	153
	APPENDICES.....	162
	APPENDIX A: SRTM DEM METADATA AND IDENTIFICATION INFORMATION	162
	APPENDIX B: LETTER OF REQUEST TO UTILISE DTM TO PERFORM ORTHORECTIFICATION EXPERIMENTS.....	166
	APPENDIX C: LETTER OF REQUEST TO UTILISE GPS DEVICES FOR CAPTURING GCPS	167
	APPENDIX D: GPS POST-PROCESSING LOG FILES.....	168
	APPENDIX E: GCP COLLECTION CHECKLISTS.....	175
	APPENDIX F: TERRASAR-X GCP LOCATION SHEETS	188
	APPENDIX G: MAA REPORT FOR STAGE 1 – EXPERIMENT 1(a) (ORTHO-IMAGE USING 5 GCPS AND THE 30 M SRTM DEM)	198
	APPENDIX H: MAA REPORT FOR STAGE 1 – EXPERIMENT 1(b) (ORTHO-IMAGE USING 5 GCPS AND THE 12 M DTM)	205
	APPENDIX I: MAA REPORT FOR STAGE 1 – EXPERIMENT 1(c) (ORTHO-IMAGE USING 5 GCPS AND THE 2 M DTM)	212
	APPENDIX J: MAA REPORT FOR STAGE 1 – EXPERIMENT 2(a) (ORTHO-IMAGE USING 13 GCPS AND THE 30 M SRTM DEM)	219
	APPENDIX K: MAA REPORT FOR STAGE 1 – EXPERIMENT 2(b) (ORTHO-IMAGE USING 13 GCPS AND THE 12 M DTM)	226
	APPENDIX L: MAA REPORT FOR STAGE 1 – EXPERIMENT 2(c) (ORTHO-IMAGE USING 13 GCPS AND THE 2 M DTM)	233

APPENDIX M: MAA REPORT FOR STAGE 1 – EXPERIMENT 3(a) (ORTHO-IMAGE USING 25 GCPS AND THE 30 M SRTM DEM)	240
APPENDIX N: MAA REPORT FOR STAGE 1 – EXPERIMENT 3(b) (ORTHO-IMAGE USING 25 GCPS AND THE 12 M DTM)	247
APPENDIX O: MAA REPORT FOR STAGE 1 – EXPERIMENT 3(c) (ORTHO-IMAGE USING 25 GCPS AND THE 2 M DTM)	254
APPENDIX P: MAA REPORT FOR STAGE 2 – EXPERIMENT 01 (ORTHO-IMAGE USING 10 TERRASAR-X ACQUIRED GCPS AND THE 2 M DTM).....	261
APPENDIX Q: MAA REPORT FOR STAGE 2 – EXPERIMENT 02 (ORTHO-IMAGE USING ONLY SENSOR MODEL AND THE 2 M DTM)	265
APPENDIX R: MAA REPORT FOR STAGE 3 – EXPERIMENT 01 (CLUSTER OF GCPS ON THE WEST SIDE OF THE IMAGE)	269
APPENDIX S: MAA REPORT FOR STAGE 3 – EXPERIMENT 02 (CLUSTER OF GCPS ON THE EAST SIDE OF THE IMAGE)	273
APPENDIX T: MAA REPORT FOR STAGE 3 – EXPERIMENT 03 (CLUSTER OF GCPS ON THE NORTH SIDE OF THE IMAGE)	277
APPENDIX U: MAA REPORT FOR STAGE 3 – EXPERIMENT 04 (CLUSTER OF GCPS ON THE SOUTH SIDE OF THE IMAGE)	281
APPENDIX V: MAA REPORT FOR STAGE 3 – EXPERIMENT 05 (GCPS DISTRIBUTED RANDOMLY ACROSS THE ENTIRE IMAGE)	285
APPENDIX W: A-GCP-ES DEVELOPMENT REQUEST LETTER	289
APPENDIX X: AUTOMATIC GCP EXTRACTION SCRIPT (A-GCP-ES)	290
APPENDIX Y: OPERATOR MAA REPORTS FOR INPUT GCPS ACCURACY COMPARISON	296

LIST OF FIGURES

<i>Figure 1.1: Varying numbers of uniformly distributed GCPs per experiment and DTM resolution</i>	<i>7</i>
<i>Figure 1.2: Various scenarios to simulate the lack and irregular distribution of GCPs</i>	<i>8</i>
<i>Figure 1.3: Research overview.....</i>	<i>15</i>
<i>Figure 2.1: First television picture from space: TIROS-1 satellite, 01 April 1960</i>	<i>21</i>
<i>Figure 2.2: Data flow and components of satellite systems</i>	<i>25</i>
<i>Figure 2.3: Regions of the electromagnetic spectrum.....</i>	<i>26</i>
<i>Figure 2.4: Raster representation displaying shades of grey and corresponding DN ...</i>	<i>28</i>
<i>Figure 2.5: Colour composite image</i>	<i>29</i>
<i>Figure 2.6: Effect of solar illumination in atmosphere.....</i>	<i>35</i>
<i>Figure 2.7: Distortions created by platform altitude changes</i>	<i>37</i>
<i>Figure 2.8: Proposed theoretical placement of 13 GCPs to achieve a uniform distribution.....</i>	<i>48</i>
<i>Figure 2.9: Good features for capturing GCPs.....</i>	<i>49</i>
<i>Figure 2.10: The illustrated difference between a DTM and a DSM.....</i>	<i>50</i>
<i>Figure 2.11: Utilising a DTM to create an ortho-image.....</i>	<i>50</i>
<i>Figure 2.12: ERDAS IMAGINE® 2015 RMSE report when utilising the Multipoint Geometric Correction tool</i>	<i>54</i>
<i>Figure 2.13: Relationship between RMSE and residuals of individual GCPs.....</i>	<i>54</i>
<i>Figure 2.14: Layout of MAA tool report</i>	<i>56</i>
<i>Figure 3.1: Geographical study area in the City of Tshwane Metropolitan Area</i>	<i>66</i>
<i>Figure 3.2: Pléiades DIMAP v2 structure</i>	<i>67</i>
<i>Figure 3.3: Illustrating the differences in the spatial resolution between the three DEMs</i>	<i>70</i>
<i>Figure 3.4: Trimble’s GeoExplorer 6000 series handheld (model: GeoXH 3.5G) GPS device.....</i>	<i>71</i>
<i>Figure 3.5: South African TrigNet Stations.....</i>	<i>72</i>
<i>Figure 3.6: Trimble Pathfinder Office 5.6 software post-processing settings</i>	<i>73</i>
<i>Figure 3.7: TerraSAR-X GCP-3 point distributions.....</i>	<i>76</i>
<i>Figure 4.1: Evaluate rough irregular edges of ortho-image.....</i>	<i>88</i>
<i>Figure 4.2: Placement of input point to correspond to reference points</i>	<i>89</i>
<i>Figure 4.3: Stage 1 – Experiment 1(a): Measured deviations and errors against CPs... ..</i>	<i>92</i>

Figure 4.4: Stage 1 – Experiment 1(b): Measured deviations and errors against CPs... 93

Figure 4.5: Stage 1 – Experiment 1(c): Measured deviations and errors against CPs... 94

Figure 4.6: Stage 1 – Experiment 2(a): Measured deviations and errors against CPs... 95

Figure 4.7: Stage 1 – Experiment 2(b): Measured deviations and errors against CPs... 96

Figure 4.8: Stage 1 – Experiment 2(c): Measured deviations and errors against CPs... 97

Figure 4.9: Stage 1 – Experiment 3(a): Measured deviations and errors against CPs... 98

Figure 4.10: Stage 1 – Experiment 3(b): Measured deviations and errors against CPs 99

Figure 4.11: Stage 1 – Experiment 3(c): Measured deviations and errors against CPs 100

Figure 4.12: Stage 1 – Experiments: Accuracy assessments 102

Figure 4.13: Effect of quality of elevation source on the overall accuracy of an ortho-image 104

Figure 4.14: Stage 2 – Experiment 01: Measured deviations and errors against CPs . 106

Figure 4.15: Stage 2 – Experiment 02: Measured deviations and errors against CPs . 107

Figure 4.16: Stage 3 – Experiments GCP distribution settings 110

Figure 4.17: Stage 3 – Exp 01: GCPs distributed on the west side of the image 111

Figure 4.18: Stage 3 – Exp 02: GCPs distributed on the east side of the image..... 112

Figure 4.19: Stage 3 – Exp 03: GCPs distributed on the north side of the image 113

Figure 4.20: Stage 3 – Exp 04: GCPs distributed on the south side of the image..... 114

Figure 4.21: Stage 3 – Exp 05: Random distribution of GCPs 115

Figure 4.22: Stage 3 – Experiments: Accuracy assessments 117

Figure 4.23: Stage 3 – Experiments: Measured distance errors 118

Figure 4.24: Requirements necessary to achieve high accurate ortho-images..... 120

Figure 5.1: Screen capture of reference document used to verify the accurate placement of GCPs 129

Figure 5.2: The PPFs utilised by the A-GCP-ES..... 130

Figure 5.3: The A-GCP-ES output ASCII text document..... 131

Figure 5.4: Inputs required by the A-GCP-ES 132

Figure 5.5: Creating Chip Database – Open the PCI Geomatica® software and load the reference sources 133

Figure 5.6: Creating Chip Database – Open the Algorithm Library window 133

Figure 5.7: Creating Chip Database – Complete the PNT2CHIP parameters for the Input Ports..... 134

Figure 5.8: Creating Chip Database – Complete the PNT2CHIP parameters under the Input Params 1 tab..... 135

Figure 5.9: Evaluating chips by utilising the PCI Geomatica® Chip Manager 136

Figure 5.10: Execute the A-GCP-ES with the required inputs provided 137

Figure 5.11: Executed script summary..... 137

Figure 5.12: Import the ASCII GCP file into the ERDAS IMAGINE® Coordinate Calculator dialogue 139

Figure 5.13: Settable fields to format the ERDAS IMAGINE® Import Data dialogue so as to correctly import the ASCII GCP file 139

Figure 5.14: ASCII GCP file imported into the Coordinate Calculator 140

*Figure 5.15: Verifying the saved *.gcc (GCP coordinate) file* 140

Figure 5.16: ASCII GCP file loaded into the ERDAS IMAGINE® Multipoint Geometric Correction workspace..... 141

Figure 5.17: Operator input GCP accuracy comparison..... 142

Figure 5.18: Input GCP accuracy comparison between A-GCP-ES and operator 143



LIST OF TABLES

<i>Table 2.1: Summary of the most common HR and VHR satellite systems.....</i>	<i>24</i>
<i>Table 2.2: Pléiades satellite image processing levels</i>	<i>42</i>
<i>Table 3.1: Sample of the GCP Checklist used during the fieldwork</i>	<i>75</i>
<i>Table 3.2: TerraSAR-X GCP-3 coordinate specification and accuracy assessments</i>	<i>77</i>
<i>Table 4.1: Overall accuracies achieved from the stage 1 experiments</i>	<i>101</i>
<i>Table 4.2: Overall accuracies achieved from the stage 2 experiments</i>	<i>108</i>
<i>Table 4.3: Pléiades image quality performances.....</i>	<i>109</i>
<i>Table 4.4: Overall accuracies achieved from the stage 3 experiments</i>	<i>116</i>

LIST OF EQUATIONS

(1) <i>Collinearity Equation</i>	43
(2) <i>Rational Polynomial coefficients (RPC) equation</i>	45
(3) <i>Equation to determine minimum GCPs required</i>	47
(4) <i>Calculating RMSE</i>	53
(5) <i>Calculating RMSE of individual GCPs</i>	54
(6) <i>Calculating the total RMSE for all GCPs</i>	55
(7) <i>Error contribution of each GCP in relation to the total RMSE</i>	55
(8) <i>Alternative method for calculating $RMSE_x$</i>	90
(9) <i>Alternative method for calculating $RMSE_y$</i>	90
(10) <i>Measure the radial distance from control to data point</i>	90

LIST OF ACRONYMS

2D	two-dimensional
3D	three-dimensional
A-GCP-ES	Automatic Ground Control Point Extraction Script
ASCII	American Standard Code for Information Interchange
ASTER	Advanced Spaceborne Thermal Emission and Reflection Radiometer
CBD	Central Business District
CCD	charge-coupled device
CI	Confidence Interval
CMD	MS Windows' Command Prompt interface
CNES	Centre National d'Etudes Spatiales
CP(s)	Check Point(s)
CSIR	Council for Scientific and Industrial Research
DEM(s)	digital elevation model(s)
DGPS	Differential Global Positioning System
DHM(s)	digital height model(s)
DIMAP	Digital Image Map
DLR	German Aerospace Centre
DN	Digital number
DSM(s)	digital surface model(s)
DTED	Digital Terrain Elevation Data
DTM(s)	digital terrain model(s)
EADS	European Aeronautical Defence and Space Company
EML	ERDAS Macro Language
ENVI®	Environment for Visualizing Images owned by Exelis, Inc. The company was acquired by Harris Corporation in 2015. ENVI® is a software solution for processing and analysing geospatial imagery.

ERDAS	Previously an acronym for <i>Earth Resource Data Analysis Software</i> , but is now the trademark name for <i>Earth to Business Company</i> .
ES	electromagnetic spectrum
ESA	European Space Agency
ESSA	Environmental Science Services Administration
GCP(s)	ground control point(s)
GDEM	Global Digital Elevation Map
GIS(s)	Geographic Information System(s)
GLONASS	Global Orbiting Navigation Satellite System
GNSS	Global Navigation Satellite Systems
GPS	Global Positioning System
GSD	Ground sampling distance
HAE	Height Above Ellipsoid
HartRAO	Hartebeesthoek Radio Astronomy Observatory
HOV	hold-out validation
HR	high-resolution
IKONOS	A commercial Earth observation satellite owned by Digital Globe.
IPS	Image processing system
LOOCV	leave-one-out cross validation
LiDAR	Light Detection and Ranging
L-MR	low- to medium resolution
MAA	Metric Accuracy Assessment
MHz	megahertz
MS	Microsoft
MSL	mean sea level
NASA	National Aeronautics and Space Administration
NGI	National Geospatial Information
NSSDA	National Standard for Spatial Data Accuracy
PCI Geomatics	A privately held Canadian corporation and developer of PCI

	Geomatica®. A complete and integrated desktop software that features tools for remote sensing, digital photogrammetry, etc.
PPF	PCI Pluggable Function
RINEX	Receiver Independent Exchange
RMSE	root mean square error
RPC(s)	Rational Polynomial Coefficient(s)
RS	Remote Sensing
RTK	Network Real Time Kinematic
SA	South Africa
SITA	State Information Technology Agency
SPOT	Système Pour l'Observation de la Terre (French Remote Sensing Satellite)
SRTM	shuttle radar topography mission
T&E points	Test and Evaluation points
TDI	time delay integration
Tracks4Africa	Tracks4Africa is a SA based company that creates paper and raster maps from tracks and waypoints collected by private persons that travel across Africa.
TIROS	Television Infrared Observation Satellite
TOS	TIROS Operational System
UAV	Unmanned Aerial Vehicle
US(A)	United States (of America)
USGS	United States Geological Survey
USSR	Union of Soviet Socialist Republic
UTM	Universal Transverse Mercator
VHR	Very high-resolution



CHAPTER 1 – INTRODUCTION AND PROBLEM STATEMENT

1.1 INTRODUCTION

The use of satellite images have become an integral part of many modern technologies and disciplines (Stallmann et al., 30 July 2015). Satellite images are used in many applications and are widely used by civil engineers, environmental planners, cartographers, geologists, hydrographers, agricultural technicians, military and other state departments. Satellite images are mainly used to provide a base map layer for digital analysis purposes and/or as a visual source to perform observations, detect changes and for other statistical analysis such as disaster predictions and management (Saha, 2004; Gao, 2009). During such applications, the visual and accuracy properties of the satellite images must be improved by means of performing radiometric (spectral) and geometric (spatial) corrections (Gao, 2009). However, when satellite images are used for specific applications, such as navigation and military operations, the location accuracy of the images becomes an important factor to consider.

Orthorectification¹ is a method that provides accurate remotely sensed images and provides real-ground coordinates (including x, y and z values) for all image pixels. This is achieved by eliminating positional displacement of image pixels caused by topographic relief, lens distortions and camera tilt (Yang and Williams, 1997). Orthorectification is based on collinearity equations derived from three-dimensional (3D) ground control points (GCPs). Orthorectification comprises four basic components, namely an image, a geometric sensor model, elevation data (for example a digital elevation model (DEM)) and GCPs that are selected as input and reference control points from the input satellite image and reference data source (Yang and Williams, 1997). The product of the orthorectification process is an ortho-image.

The geometric correction of satellite imagery, by means of georectification and orthorectification in specific, is common practice in the modern remote sensing (RS)

¹ Two types of orthorectification processes exist, namely:

- a) **Automatic:** Block triangulation is the process to tie numerous images together through automatically generating tie points using automatic point match algorithms.
- b) **Manual:** Single frame orthorectification is the process to orthorectify one image at a time by means of manual point collection. This process entails orthorectifying a raw image by using an accurate reference data set from which input parameters are collected.



domain. Essentially this is to ensure that the positional accuracy of the resulting ortho-image is improved considerably by accounting for any positional errors or distortions present in raw satellite imagery as caused by sensor-Earth geometry variations. Ground control points and the underlying reference elevation surface play a pivotal role during this rectification process in the sense that it provides the link between image and ground-coordinates. The challenge remains to capture the appropriate number of high quality GCPs and using the correct quality digital elevation model available.

It is important to realise that an ortho-image is only as accurate as the input and reference sources used. Therefore, it is imperative to use accurate elevation data and ground control as input and reference data sources. In general, when deciding on the elevation data to use, a lower resolution DEM will be sufficient such as the Shuttle Radar Topography Mission (SRTM) 30 m DEM. This is especially true when orthorectifying low- to medium resolution (L-MR)² satellite imagery. However, a much more accurate DEM is needed when higher accuracy is required and when performing orthorectification on high-resolution (HR)³ and very high-resolution (VHR)⁴ satellite imagery. This accounts for a DEM to have a ground sample distance (GSD) accuracy of 15 m or better (e.g. WorldDEM™). It is also important to utilise accurate and a sufficient number of GCPs, which are collected/acquired by means of:

- a) Global positioning system (GPS): During this study, the Trimble's GeoExplorer 6000 series handheld (model: GeoXH 3.5G) receiver device was used to manually collect specific GCPs. The accuracy of the manually collected GCPs are described in Chapter 3, refer to Paragraph 3.6.2.3.1.
- b) Sensor automated GCPs: Satellites can collect GCPs anywhere on the Earth's surface by means of an automated process, e.g. automatic GCPs created by TerraSAR-X. TerraSAR-X ground control points are delivered in two standard accuracies, namely TerraSAR-X GCP-1 with an accuracy of 1 m and TerraSAR-X GCP-3 with an accuracy of 3 m (Airbus Defence and Space, August 2014).

² L-MR satellite imagery: imagery with a ground sampling distance (GSD) of > 15 m, for example Landsat-8 and Aster images.

³ HR satellite imagery: imagery with a GSD of 1 m - 15 m, for example Système Pour l'Observation de la Terre (SPOT-5 and SPOT-6) and IKONOS.

⁴ VHR satellite imagery: imagery with a GSD of < 1 m, for example Pléiades, QuickBird, GeoEye and WorldView.



Some organisations and departments (for example, the United States Geological Survey (USGS)) generate their own DEMs by means of semi-automatic DEM extraction software from various satellite image stereo scenes. Other remote sensing techniques are also used to perform orthorectification such as radar interferometry or Light Detection and Ranging (LiDAR). However, for most organisations and departments these different techniques of acquiring suitable DEMs and GCPs are unrealistic, as the financial implications are too great and resources unavailable. Considering the different accuracies and applications that satellite imagery are being used for, the question that arises is "*what is the required accuracy of an ortho-image?*" The required accuracy is purely dependent on the application for which the ortho-image will be used. For instance, military target acquisition and navigational purposes will require higher accuracy ortho-images than applications such as mapping and agricultural assessments. In this study, one goal was to create an optimal accurate ortho-image that could be used for benchmarking purposes and could then serve as the reference measurement source for quantifying ortho-images created. The accurate ortho-image was determined to be the image with the smallest root mean square error (RMSE) and positional accuracy displacement from the orthorectification experiments performed. The following data sources were used to perform orthorectification procedures:

- a) Image data: it is important to use 'raw' satellite images when simulating any orthorectification process by utilising manually collected GCPs or any other independently acquired GCPs. A Pléiades-1B primary panchromatic image with a spatial resolution of 0.5 m was selected as the image type to use during this study.
- b) Elevation data: three elevation sources of different quality, namely SRTM 30 m DEM, 12 m DTM and a 2 m DTM derived from a LiDAR point dataset were used.
- c) GCPs: ground control points were collected by using a GPS receiver through fieldwork as well as acquired TerraSAR-X GCPs from Airbus Defence and Space.
- d) Vector layer: a road vector layer was created by driving a motor vehicle and capturing GPS tracks, covering the required sample area. The GPS tracks were converted to a vector layer (polyline), which was divided into smaller segments to simulate the scenarios that occur when using a vector road layer as a source for collecting GCPs. It was assumed that segmentation would affect the accuracy of the resulting ortho-image, because extracting GCPs from road vector layers makes it very difficult to achieve a uniform distribution of GCPs.



1.2 PROBLEM STATEMENT AND MOTIVATION

1.2.1 Motivation for the research study

The geometric correction of satellite imagery has been a pivotal topic since the launch of the first Earth observation satellite system in the 1960's. Various methods exist to perform geometric correction, such as georectification and georeferencing methods, which focus on the horizontal position of image pixels. In contrast, orthorectification consider the pixel positional shift caused by the Earth's curvature and provides real ground coordinates (x, y and z values) for all pixels. The conditions and data sources to use when performing orthorectification to achieve a certain level of geometric accuracy are well known, but in practice, it is more difficult to meet all conditional requirements (Henrico et al., 2016).

Ground control points and the underlying reference elevation surface play a pivotal role during this rectification process in the sense that it provides the link between image and ground-coordinates. In general, when deciding on the elevation data to use, a lower resolution digital elevation model will be sufficient. However, a much more accurate DEM is a prerequisite when higher accuracy is required. Typically, DEMs are either available as public products or more precise and fine scale DEMs which can be obtained from commercial suppliers. Easily available public products are described as (Rexes and Hirt, 2014; Henrico et al., 2016):

- a) Shuttle Radar Topography Mission (SRTM): available as 1 arc-second resolution (30 m) and 3 arc-second resolution (90 m);
- b) Digital Terrain Elevation data (DTED): resolution is available in levels 0 (900 m), 1 (90 m) and 2 (30 m); and
- c) Advanced Spaceborne Thermal Emission and Reflection Radiometer (ASTER) Global Digital Elevation Map (GDEM): available in 30 m resolution.

More precise and fine scale DEMs, for example the WorldDEM™ product (12 m resolution) can be acquired from Airbus Defence and Space. However, the collection of suitable GCPs presents a significant problem, since existing sources of GCPs may not be available and one of the major challenges remains, i.e. to accurately capture the appropriate number of GCPs. Collecting new GCPs for a specific area is an expensive





exercise and in some cases, areas are inaccessible, which makes it impossible to collect new GCPs due to environmental conditions, security and mobility restrictions.

Ideally, when performing orthorectification, sufficient input data sets (i.e. a digital elevation model and ground control points) are required. In most cases, the acquisition of a suitable DEM is not problematic, as various formats and good quality DEMs are easily available for acquisition from various organisations and institutions. However, the collection of suitable GCPs presents a significant problem, as mentioned above. It is easy to manually collect GCPs within the South African (SA) borders (as a South African citizen) by using a GPS receiver and driving to remote areas. It is also relatively easy to acquire other spatial data from various organisations and institutions necessary to perform orthorectification, for example DEMs and image data. However, when moving outside the South African borders, the collection of GCPs becomes problematic. Only limited data sets are available in these areas to use as possible sources for collecting GCPs, for example Tracks4Africa (<https://tracks4africa.co.za/>) and OpenStreetMap (<https://www.openstreetmap.org/#map=5/51.500/-0.100>). Other methods to consider for collecting GCPs in areas in Africa are to:

- a) Approach private organisations, for example TomTom SA (https://www.tomtom.com/en_za/) that captures vector data sets of Africa from satellite images and aerial photographs, for operational and reselling purposes.
- b) Manually collect the required GCPs of a specific area by using a GPS receiver device. This method has extreme limitations that will restrict the collection of GCPs:
 - i. time consuming: a method like this will take a considerable amount of time to complete. The area needs to be physically visited, which will entail covering a vast area that will sometimes be inaccessible and difficult to reach due to environmental conditions and access restrictions;
 - ii. financial implication: to embark on such a project will have an enormous financial implication, especially when considering accommodation and travelling expenses, for example petrol and vehicle maintenance; and
 - iii. travelling authorisation: authorisation will need to be acquired from every country being entered. Every country has its own immigration laws for foreigners travelling to or through their country. It will therefore be imperative



to acquire the necessary travelling documentation (for example passports and visa) from the required departments and embassies.

As a rule of thumb (Tao and Hu, 2001), a uniform distribution of GCPs covering an entire image scene is needed when performing orthorectification of remotely sensed images (Liu et al., 2007). The minimum and optimum GCP required to perform single frame orthorectification is dependent on various factors, such as the accuracy of usable GCPs, scattering of GCPs and topographical characteristics of the land (e.g. mountainous, flat plateau, etc.). Good practice is to use as many GCPs as possible that are spread over the entire image, covering the centre and four corners of the image when the terrain variation and geometric distortion are great. However, it should also be realized that more GCPs would not necessarily render better results. The quality and distribution of accurate GCPs both have a major influence on the orthorectification process (Ke, 2006).

During this study, various orthorectification experiments were conducted. Firstly, nine orthorectification experiments were performed where the number of GCPs in the image scene and the DEM quality were altered in each case. This design is illustrated below in Figure 1.1, where the Pléiades image acts as backdrop for the desired number of uniformly distributed GCPs used in each experiment, as well as indicating the three DEMs mentioned earlier.

All experiments were conducted in the same manner with only the number of GCPs utilised and quality of the DEM that differed. Experiments 1(a), (b) and (c) were performed using 5 GCPs and altering the elevation sources for each experiment. Experiment 1(a) used the 30 m DEM, experiment 1(b) the 12 m DTM and 1(c) the 2 m DTM. Experiments 2(a), (b) and (c) as well as experiments 3(a), (b) and (c) were performed in exactly the same manner as experiment 1, the only differences being that experiment 2 utilised 13 GCPs and experiment 3 used 25 GCPs. This allowed for testing the effect that the number of GCPs and the quality of an elevation source has on the location accuracy of an ortho-image.

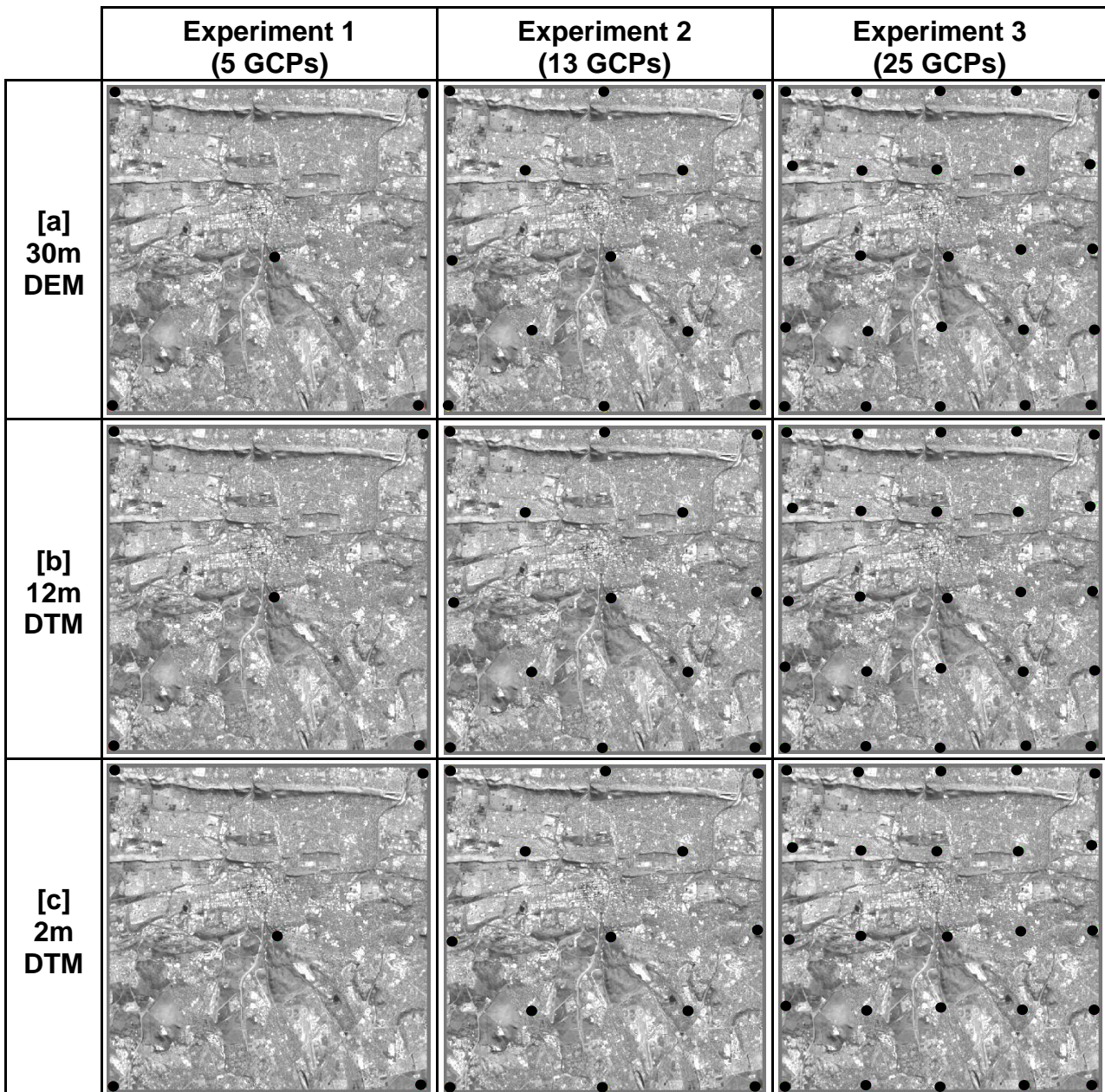


Figure 1.1: Varying numbers of uniformly distributed GCPs per experiment and DTM resolution

After these experiments were conducted, one ortho-image was identified and used as the benchmarked image for comparing and evaluating all other ortho-images produced from simulated orthorectification experiments to follow. To identify and choose the best ortho-image for the benchmarking, all ortho-images produced by these experiments were independently and objectively assessed. This was achieved by qualitatively and quantitatively measuring the RMSE of each individual image (the smaller this error is, the better the positional accuracy of the ortho-image) as well as measuring the positional accuracy of individual features identified on the image compared to the collected and

acquired GCPs locations. During this study, the image identified and selected for use as the benchmark image are referred to as the 'master image'.

Secondly, one orthorectification experiment was conducted with TerraSAR-X GCPs acquired from Airbus Defence and Space, which included utilising the 2 m DTM. Another experiment was performed utilising only the specific sensor geometric model and an elevation source. The resulting images were compared to the master image to determine the accuracy of ortho-images when using the TerraSAR-X GCPs as well as performing orthorectification without the use of any GCPs. Thirdly, orthorectification experiments were conducted to simulate various scenarios when GCPs are irregularly distributed and selected from vector road layers to cover only specific areas within an image scene (Figure 1.2).

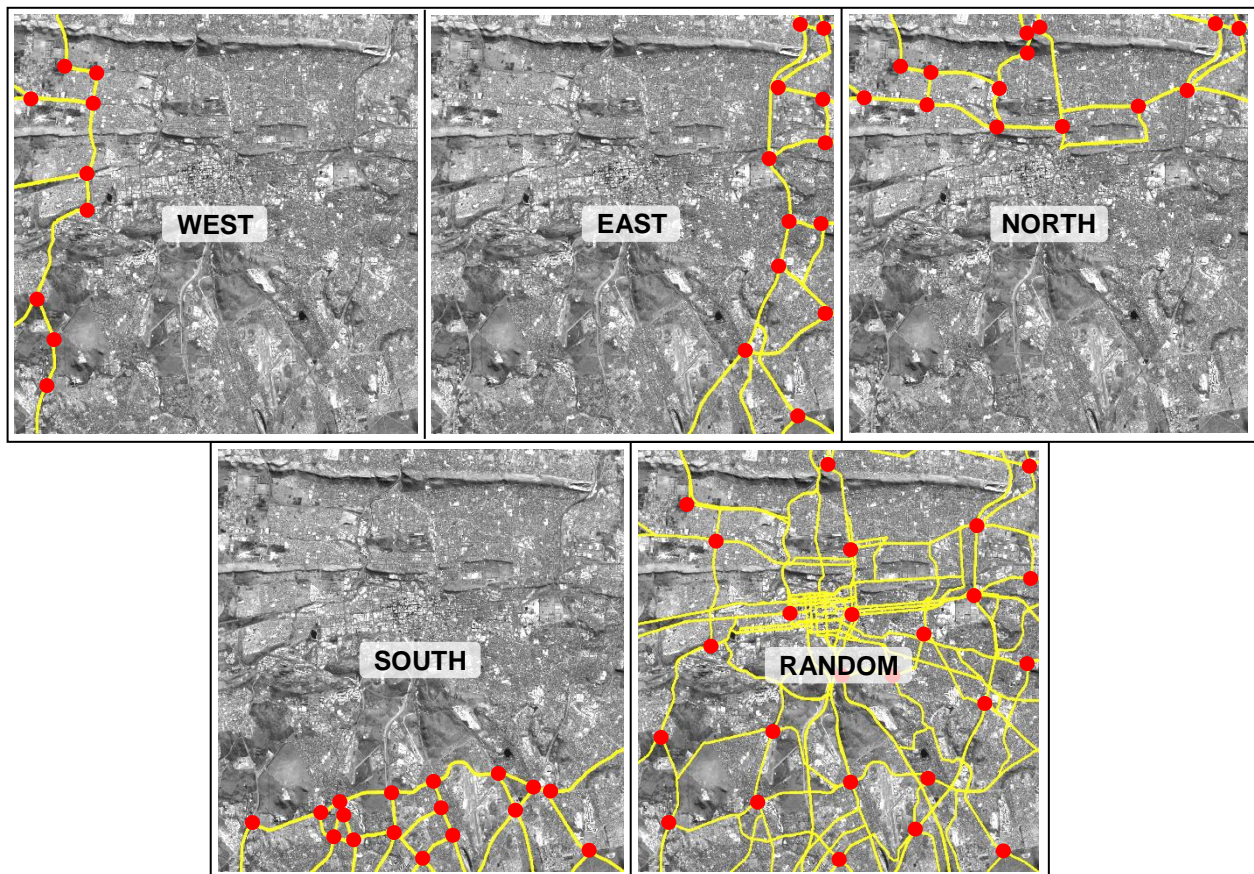


Figure 1.2: Various scenarios to simulate the lack and irregular distribution of GCPs

All ortho-images produced from these experiments were compared, measured and analysed against the master image.

1.2.2 Research hypotheses and questions

Performing orthorectification with available and adequate data sets does not pose any problems. However, the accuracy of an ortho-image is significantly influenced when poor quality DEMs are used or when limited GCPs are irregularly distributed. Vector road layers are in some instances the only data source available for collecting GCPs. It is evident from Figure 1.2 that using a vector road layer as a source for collecting GCPs will affect the accuracy of the resulting ortho-image. Roads, in some instances, only cover certain areas in an image scene, which will make it very difficult to achieve a uniform distribution of GCPs, as is illustrated in Figure 1.1. This is even more problematic in Africa where roads are widely dispersed. Some image scenes will only have one road running across a very small area or it might even be that some satellite image scenes will not have any roads covering an image scene. In such cases, methods such as block triangulation, utilising automated acquired GCPs, performing RPC orthorectification⁵ (Grodecki and Dial, 2002) or orthorectification without the use of GCPs are the only processes that can be applied to ensure orthorectification. However, these various alternative methods of performing orthorectification was not considered, as this study was to investigate the effect that GCPs and elevation sources have on the execution of orthorectification following the parametric approach. The focus of this study was to analyse the use of irregularly distributed GCPs that are varying in number as well as the influence of elevation data when performing single frame orthorectification.

As mentioned in Paragraph 1.1, orthorectification necessitates four basic components, namely an image, a geometric sensor model, a DEM and GCPs. Image distributors provide the image data and image processing software engineers and architectures design the software to include a library of all well-known and required geometric sensor models. Elevation data sources (e.g. DEMs) are also no problem to acquire and are easily available online as well as from commercial companies, such as National Geospatial Information (NGI) and United States Geological Survey (USGS). However, acquiring GCPs can be a discouraging and very difficult task and in most cases limit the accuracy of ortho-images. A study by Jakubowicz and Jaszczak (09 February 2005)

⁵ During Rational Polynomial Coefficient, orthorectification geolocation information (x, y and z) is provided to individual image pixels. RPC files are normally pre-computed by image vendors and provided with the image data during acquisition.



revealed that the GCP collection method has a direct influence on the accuracy of the GCPs, which has an even greater influence on the results of the orthorectification process. Considering the foregoing, this thesis study was conducted while considering the following hypotheses:

- a) Hypothesis 1 (H₁): There is an increase in the accuracy of ortho-images when accurate DEMs are used.
- b) Hypothesis 2 (H₂): There is a decrease in the accuracy of ortho-images when an inadequate number of GCPs are randomly distributed in an image scene.
- c) Hypothesis 3 (H₃): Using TerraSAR-X GCPs in conjunction with a high-resolution elevation model renders a high quality and accurate ortho-image, the equivalent to utilising manually collected GCPs.
- d) Hypothesis 4 (H₄): Creating an ortho-image by utilising only the geometric sensor model and an elevation source can be used as a substitute for the process of acquiring GCPs.

From the preceding section, the following research questions were formulated:

- a) Question 1: Does the accuracy of a DEM and the uniform distribution of GCPs influence the accuracy of an ortho-image?
- b) Question 2: Does the number of GCPs that are uniformly distributed across a single satellite image scene influence the accuracy of an ortho-image?
- c) Question 3: To what extent does the lack of GCPs that only cover a specific area in an image scene influence the accuracy of an ortho-image?
- d) Question 4: Instead of manually collecting GCPs through fieldwork by utilising a GPS receiver device, is it possible to utilise TerraSAR-X GCPs to create accurate ortho-images?
- e) Question 5: Does a stand-alone geometrical sensor model combined with a DEM result in a comprehensive accurate ortho-image when compared to other GCP experiments?

1.3 RESEARCH AIM AND OBJECTIVES

The aim of this study was to investigate and compare the positional accuracies of ortho-images under various orthorectification scenarios and provide improved geometric accuracies of VHR satellite imagery when diverse ground control and elevation data



sources are available. To achieve the aim of this study, the following objectives were identified:

- a) Objective 1: Create an accurate ortho-image (master image) to be used as the benchmarked image for comparing and evaluating all ortho-images produced from the simulated orthorectification experiments.
- b) Objective 2: Identify an ortho-image's grade of accuracy when using various accuracy DEMs.
- c) Objective 3: Analyse the accuracy of an ortho-image by manipulating the number of uniformly distributed GCPs covering an image scene.
- d) Objective 4: Investigate and examine the influence of an inadequate number of GCPs that are only distributed in a specific area of an image scene.
- e) Objective 5: Analyse the accuracy of an ortho-image created from using TerraSAR-X GCPs compared to an ortho-image created from using highly accurate manually collected GCPs.
- f) Objective 6: Investigate the feasibility of creating an ortho-image utilising only the image specific geometric sensor model and a high-resolution DEM without the use of GCPs.

1.4 RESEARCH METHODOLOGY

Primary and secondary data were collected, investigated and analysed to address the problem of this study that was discussed in Paragraph 1.2.2. This study therefore consisted of two phases, namely to conduct a literature study and to conduct empirical research. A methodology was developed for improving the geometric accuracy of VHR satellite imagery applying orthorectification procedures when there are inadequate GCPs available that are irregularly distributed across an image scene. The two research phases mentioned above comprised the elements discussed in the Paragraphs that follow.

1.4.1 Literature study

An in-depth literature study was conducted by investigating secondary sources such as books, journals, articles and the internet. The focus was on the various methods

available for use when performing orthorectification on satellite imagery, the input data necessary and parameters required in order to create an accurate ortho-image.

The importance of selecting accurate DEMs and the significance of accurate GCPs that are uniformly distributed across an entire image scene were investigated. Google was the main search engine used to search for information on the process of performing orthorectification.

1.4.2 Empirical research

Empirical research was used to determine the influence of the number and distribution of GCPs and elevation data required during the orthorectification process to create an accurate ortho-image. The empirical component of this study was pragmatically executed to collect and analyse primary data. The empirical research of this study was conducted in three stages. These stages are outlined below and are discussed in more detail in Chapter 3:

- a) Stage 1: nine orthorectification experiments (Figure 1.1) were performed utilising the various quality DEMs and accurate GCPs to identify one ortho-image that are referred to as the 'master image'. The master image was used as the benchmarked image for comparing and evaluating all other ortho-images produced from the orthorectification experiments performed.
- b) Stage 2: two independent orthorectification experiments were conducted. The first experiment utilised the TerraSAR-X GCPs acquired from Airbus Defence and Space and the 2 m DTM was used as the selected input elevation data. The second experiment followed the parametric georectification approach without utilising GCPs as a means to create an ortho-image.
- c) Stage 3: numerous orthorectification experiments (Figure 1.2) were performed by means of simulating various scenarios where GCPs are selected from vector road layers that are irregularly distributed to cover only specific areas within an image scene. All ortho-images produced from these experiments were compared, measured and analysed against the master image to determine the accuracy of the orthorectification.



1.4.2.1 Data collection

As mentioned in Paragraph 1.1, orthorectification comprises four basic components, namely:

- a) a 'raw' image;
- b) a dataset (e.g. an accurate ortho-image or vector layer) to use as a reference source for determining tie-points between the 'raw' image and the reference image. Individual GCPs that are manually collected or automatically created can also be used as a reference source;
- c) elevation data (e.g. DEM) to use as an input reference data source, which accounts for variations in terrain height; and
- d) a geometric sensor model that is image type specific and are embedded in most image processing systems. These models are used for correcting satellite data recording errors that are caused by sensor orientation, sensor altitude and position, systematic errors associated with the sensor, topographic variations and the Earth's shape and rotation.

During this study, a Pléiades primary image covering the Pretoria Central Business District (CBD), the capital of South Africa, was used to conduct all necessary orthorectification experiments. The GCPs were manually collected by using GPS receiver devices. Numerous suitable locations were identified on the Pléiades image scene covering the Pretoria CBD for capturing accurate GCPs. Other GCPs which were used for control point purposes consisted of TerraSAR-X GCPs from Airbus Defence and Space. The following different quality DEMs covering the area mentioned above were acquired from various vendors:

- a) SRTM 30 m DEM: the SRTM DEM was acquired from the USGS website⁶.
- b) 12 m DTM: this digital terrain model was extracted from the 2 m DTM (discussed below) by way of resampling, using a bilinear interpolation method.
- c) 2 m DTM: this elevation data source was derived from LiDAR data collected during August 2013 that included the sample area of this study. Captured at ± 8 observations per square meter using a Leica ALS50 sensor and thirty percent overlap, the point cloud returns were subsequently classified into ground and non-ground layers. These classified x, y and z measurements formed the primary

⁶ USGS Website: <http://earthexplorer.usgs.gov/>



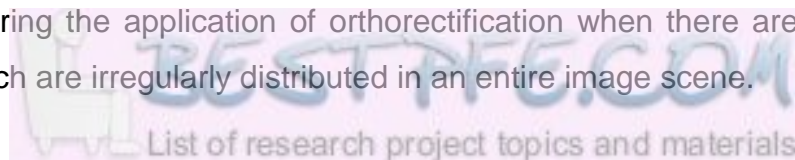
input to generate the seamless DTM at two meter GSD. The procedure followed to create this DTM is discussed in Chapter 3 (Paragraph 3.6.2.2).

1.4.2.2 Data analysis

Data analysis was performed by following two steps:

- a) Step 1: determining the accuracy of an ortho-image by means of altering the number of GCPs and the quality of the DEMs. Nine experiments were performed where the number of uniformly distributed GCPs (Figure 1.1) in an image scene and the quality of the elevation sources were altered. These experiments were performed on a Pléiades-1B primary panchromatic image covering the Pretoria CBD. The first experiment used five GCPs that were evenly distributed to cover the entire image scene (Figure 1.1(a)). The second experiment used 13 GCPs (Figure 1.1(b)) and the third experiment 25 GCPs (Figure 1.1(c)). During each experiment, the various quality DEMs mentioned in Paragraphs 1.1 and 1.2 were used to determine the effect that different quality DEMs have on the orthorectification process. From these nine experiments, the most accurate ortho-image was selected as the master image to be used as the benchmarked image for comparing and evaluating the resulting ortho-images produced during step 2.
- b) Step 2: create various scenarios to simulate the lack of GCPs that are irregularly distributed across an image scene. By using a vector road layer, five experiments were performed to create scenarios to simulate the lack of as well as the irregular distribution of GCPs (Figure 1.2) which were used to perform orthorectification. These experiments were also performed on the same Pléiades primary image covering the Pretoria CBD that was used during step 1.

The results acquired from the numerous experiments were analysed by using qualitative and quantitative research methods to assess and present the data results in a descriptive and statistical manner. Data results were triangulated for the purpose to determine accuracy, reliability and validity. From the experiments performed during step 2 and by comparing the orthorectification results to the accurate master image, a methodological approach was developed for improving the geometric accuracy of satellite imagery during the application of orthorectification when there are inadequate GCPs available which are irregularly distributed in an entire image scene.



1.4.2.3 Research overview

This study was conducted by following the research overview illustrated in Figure 1.3.

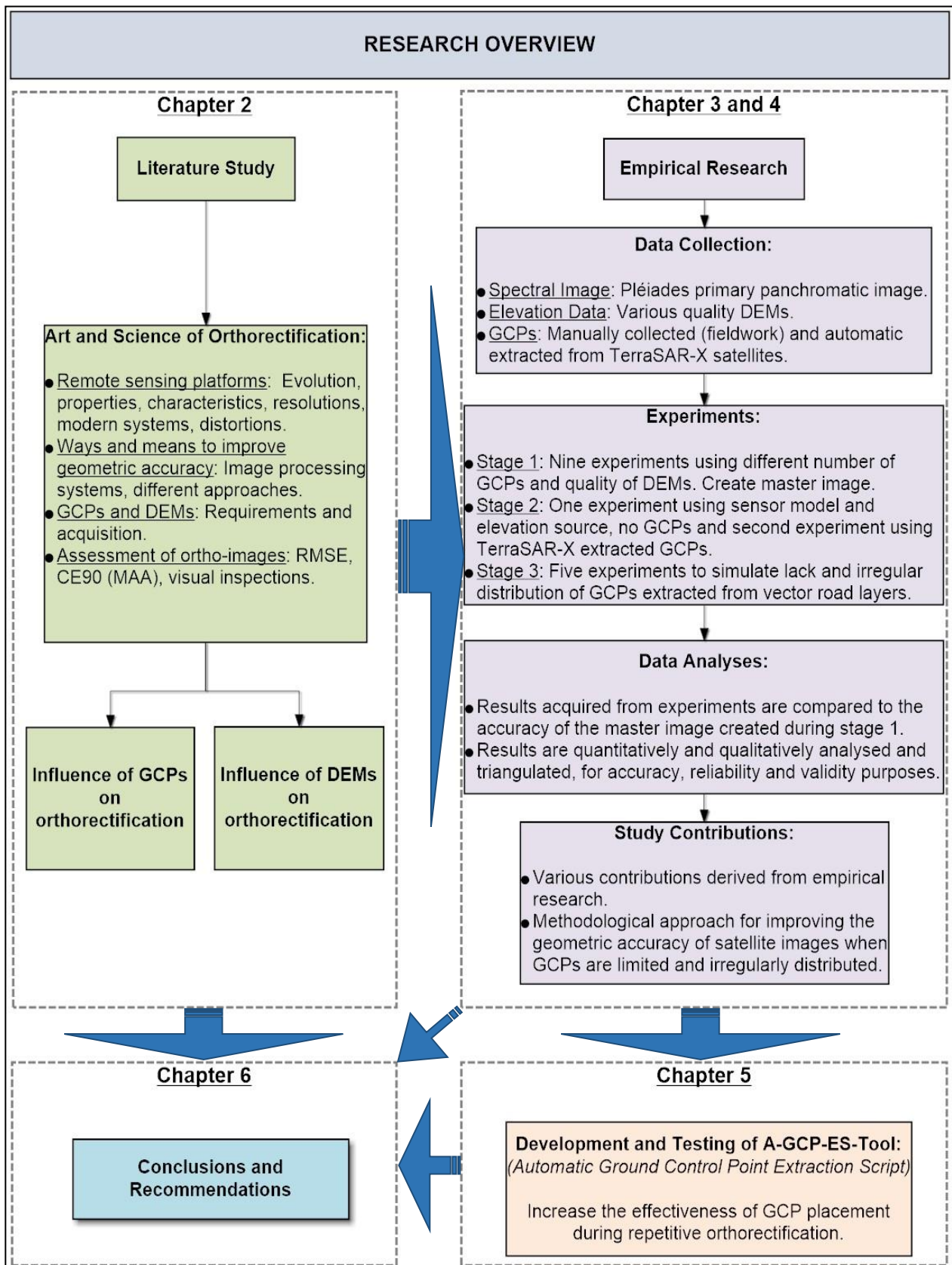


Figure 1.3: Research overview



1.5 ETHICAL ASPECTS

The necessary references to copyright were included in the text when applicable to the Pléiades primary images used during this study. Permission for the use of the elevation data source (2 m DTM) and the TerraSAR-X GCP-3 product was received from the relevant providers. Consent was also acquired for the use of the two Trimble® GeoExplorer® 6000 series handheld (GeoXH 3.5G) devices. All necessary request letters are included as addendums.

1.6 CONTRIBUTION OF THE STUDY

Geographers view the world from a spatial perspective. A spatial perspective requires knowledge of the locations of phenomena (spatial location), their distribution over the Earth's surface (spatial distribution), as well as their variation across the surface of the Earth (spatial variation). The observed spatial patterns of distribution and variation also have to be explained by asking “*when?*”, “*why?*” and “*how?*” questions about a phenomenon under investigation. These questions cannot be answered by considering a phenomenon in isolation. In order to explain the spatial patterns displayed by a phenomenon, it is also essential to investigate spatial associations – in other words, how two or more phenomena vary and conform in space. Considering the complex interrelationships in the human-environment system, this is often easier said than done.

Throughout history, maps were a prominent visualization tool used by geographers to depict spatial location, distribution and variation of phenomena and to explain patterns of spatial association. Maps are flat-surfaced, scaled-down, generalised and simplified representations of reality. It serves as a model that can be used to visualise, analyse and explain spatial patterns in an area of interest. Maps are still the most prominent tool used by geographers, but the methods employed to source and map the base information for maps changed radically in recent times. The first maps were based on explorers visiting unknown territories and making crude measurements to plot physical features relative to one another. Today we are fortunate to have access to space-age technology, such as satellite remote sensing. As the word *remote* implies, it is no longer necessary to visit an area of interest for mapping purposes. Satellite images provide a



synoptic bird's eye view of the location and distribution of phenomena on the Earth's surface.

Since 1999, with the launch of IKONOS - the first high-resolution commercial satellite - HR satellite imagery has become commercially available and attracted interests from various organisations and institutions (Brovelli et al., 2006). High-resolution satellite imagery has advanced since 2007 with the launch of sub-one metre spatial resolution satellites, such as WorldView and GeoEye, which have become the primary sources for performing spatial analysis in the scientific and commercial field. However, the challenge that users face currently is the uncertainty in the spatial accuracy of these images, which has a significant effect on further reduction of data derived from the images. Spatial accuracy is vital when these images are used for specific applications when the spatial location of features is of critical importance, such as for target acquisition (military operations), change-detection analysis (environmental management), navigational purposes, rapid and digital mapping and crisis and disaster monitoring. The contribution of this study is three-fold. Firstly, it provides an overview of the input requirements necessary to produce a high quality ortho-image. The background to these requirements is discussed in detail in Chapter 2. Secondly, investigating the influence that the number of GCPs and the quality of DEMs has on the positional accuracy of an ortho-image. Tests were conducted by increasing the number of uniformly distributed GCPs as well as various accurate DEMs. The results showed that when more GCPs were applied, the smaller the difference in accuracy was between the different DEMs utilised. Thirdly, this study addressed the problems associated with an irregularly distributed, inadequate number of GCPs and their influence on the accuracy of the derived ortho-images.

1.7 CHAPTER SUMMARY

In this chapter, an introduction to the topic was discussed. The specific problem, research framework and methodology, were briefly presented and defined. This chapter concluded with an overview to the contribution of this study. In the next chapter, a literature review on the science and art of conducting orthorectification with an overview on remote sensing will be presented.



CHAPTER 2 – LITERATURE STUDY: THE ART AND SCIENCE OF CONDUCTING ORTHORECTIFICATION WITH AN OVERVIEW ON REMOTE SENSING (RS)

2.1 INTRODUCTION

The use of satellites for remote sensing dates back to the 1950's with the launch of Sputnik-1. At first, satellite remote sensors were basic television cameras that captured crude panchromatic images in low resolution. Over time, sensors developed to take images using the electromagnetic spectrum (ES) beyond the visible and into the near and thermal infrared regions. On 23 July 1972 the satellite, named Earth Resources Technology Satellite (ERTS-1), was launched. The ERTS-1 was specifically designed to collect information about Earth resources. This sensor operated in multispectral mode as opposed to the panchromatic mode of the Television Infrared Observation Satellite (TIROS-1), which was launched on 01 April 1960 (Paragraph 2.2.1). The ERTS program was later renamed Landsat, which is to this day still operational (Short, 2000). Currently, many different types of aircraft and Earth-orbiting spacecraft use modern photographic cameras to detect and record information about objects on the Earth's surface (Avery and Berlin, 1992). Satellite images can contain as many as 200 (or more) continuous spectral bands (known as hyperspectral imagery) and the best commercially available spatial resolution of an image is 50 cm. In fact, the GeoEye-1 satellite has a ground sample distance of 41 cm, but due to US Government restrictions on civilian imaging, these images are resampled to a spatial resolution of 50 cm before they are made commercially available. Satellite imagery, especially VHR satellite imagery, has become increasingly important in recent times. Since the launch of the first two VHR satellites, IKONOS in September 1999 and QuickBird in October 2001, satellite imagery has been applied in numerous diverse fields and is widely used by professionals including civil engineers, environmental planners, cartographers, geologists, hydrographers, agricultural technicians and military image analysts.

Every application of satellite imagery needs a certain geometric accuracy. In the case where L-MR satellite imagery is used for land cover classification over large areas, the geometric accuracy is not a great concern. However, when HR satellite imagery and VHR satellite imagery are used during applications for the purpose to perform object identification or navigation then higher geometric accuracy is required. Therefore, the

geometric accuracy assessment of HR and VHR satellite imagery proves to be fundamental.

It is unavoidable that recorded remote sensed data typically contains distortions and errors in the image data such as geometry errors. These errors can arise in many ways, e.g. the errors resulting from relative motions of the sensor platform and its scanners, as well as those due to curvature and rotation of the Earth, which can exhibit as a skewed image product (Richards and Xiuping, 2006). Most of these errors are corrected at the ground station when the data are initially received from the satellite sensor. However, there are geometric distortions that are difficult to account for mathematically, for instance altitude and speed. To correct these distortions, an image analyst can perform a procedure called image rectification (georectification), also known as image transformation. It is essential to realise that all images need to be rectified to a map projection, using either georeferencing or ortho-correction approaches according to the local terrain characteristics. Some images may only require georeferencing without considering the Earth's curvature (elevation of ground pixels), while other images may require to be orthorectified. Orthorectification considers the elevation shift in image pixels by removing the positional displacement of image pixels caused by topographic relief, lens distortions and camera tilt.

2.2 REMOTE SENSING PLATFORMS

One way to classify remote sensing systems is according to the type of platform carrying the imaging system. Three main types of remote sensing platforms exist, namely manned aircraft, unmanned aircraft vehicles (UAV) and satellite systems (i.e. optical and radar). In this thesis, optical satellite platforms are the focal point. This study touches on low and medium resolution satellite platforms as well as SAR systems, but the primary focus is on HR and VHR optical satellite platforms and imagery.

2.2.1 Evolution of satellite platforms

One of the direct results of the Cold War that started in 1947 between the US and the Soviet Union (officially the Union of Soviet Socialist Republic (USSR)) was the 'Space Race' for supremacy in space exploration. The honour went to the USSR when they

launched Sputnik-1 on 04 October 1957, which provided the first space views of our planet's surface and atmosphere – and consequently the era of satellites was born. This had the effect that the US accelerated its space programme and launched its first orbiting satellite, Explorer-1 on 31 January 1958. The Television Infrared Observation Satellite (TIROS-1) was the first meteorological satellite and this satellite platform was equipped with Vidicon wide-scanning camera sensors that captured crude panchromatic images and was mainly devoted to looking at clouds (Figure 2.1). TIROS-1 had a lifespan of 78 days and a spatial resolution of 2.5 to 3.0 km (Kramer, 2002).

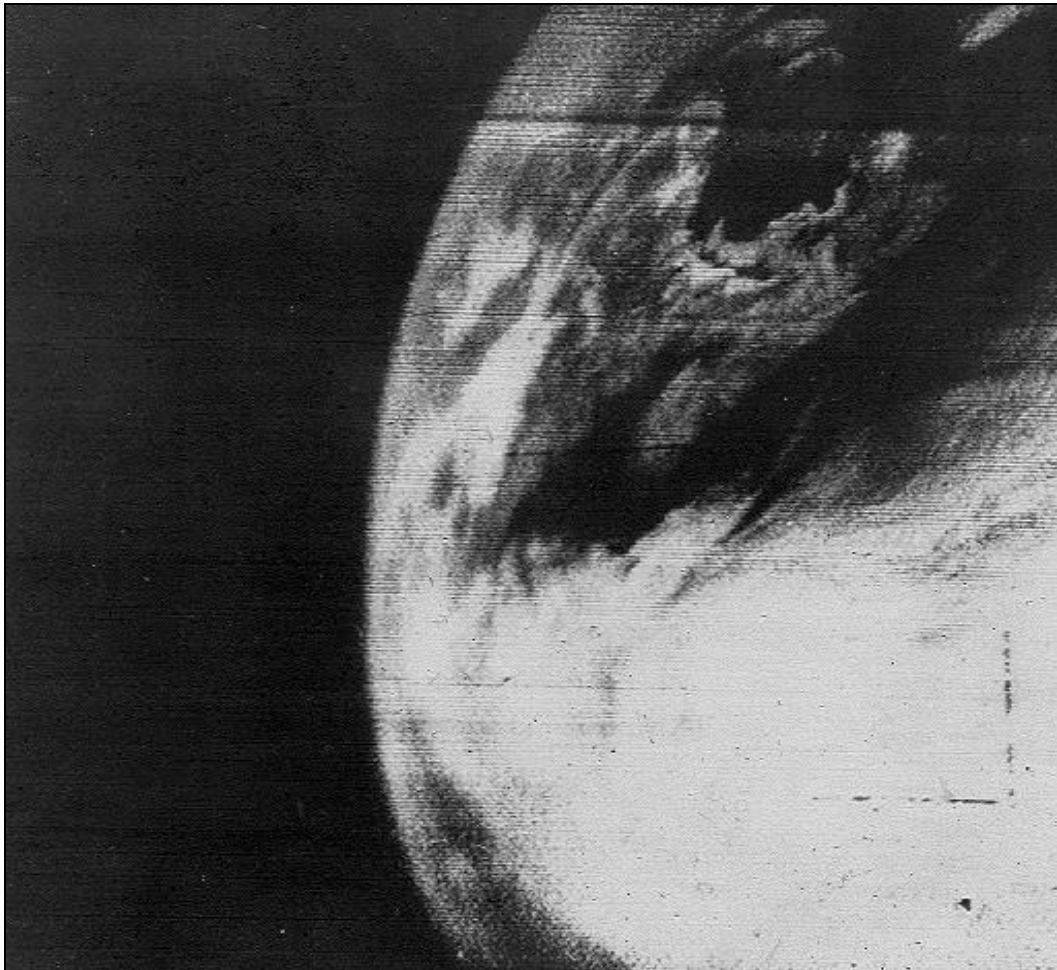


Figure 2.1: First television picture from space: TIROS-1 satellite, 01 April 1960
(Copyright © NASA)

The satellite programme evolved rapidly after the success of the TIROS-1 satellite. A series of nine TIROS satellites was launched in quick succession after TIROS-1 with TIROS-10 launched on 02 July 1965, being the last of the experimental TIROS series. The TIROS Operational System (TOS) paved the way for nine satellites named Environmental Science Services Administration (ESSA-1 through 9), launched between 1966 and 1969. The same time the ESSA satellites were developed and launched, the



National Aeronautics and Space Administration (NASA) developed and sustained seven NIMBUS satellites with NIMBUS-1 launched on 28 August 1964. The NIMBUS series were significant in the fact that it served as the proving ground for future polar orbiting satellite platforms, having a 3-axis stabilizer and carrying a number of instruments such as microwave and infrared radiometers, advanced Vidicon camera systems, atmospheric sounders, ozone mappers and a coastal zone colour scanner (Allison et al., 1978). Haas and Shapiro (1982) mentions that the NIMBUS series led to the Landsat programme, which dates back to its initiation in 1966 when it was initially named the Earth Resources Technology Satellite (ERTS) programme. The ERTS-1 satellite was launched on 23 July 1972 and was eventually renamed to Landsat-1 in 1975. The Landsat project is the longest active satellite imagery acquisition programme, with Landsat-8 (the latest satellite) that was launched on 11 February 2013. Its sensors have spatial resolutions of 15 m (panchromatic), 30 m (multispectral) and 100 m (thermal).

After the launch of the first satellite in 1957, numerous different types of satellites were launched, with sensor resolution ranging from low to medium resolution merely for meteorology, agricultural, communications and navigational purposes. However, none of these satellites were appropriate for mapping purposes due to their insufficient ground sampling distance. This changed with the launch of the first French SPOT satellite (SPOT-1) in 1986, which had stereoscopic capacity and GSD of 10 m. The next big leap in the evolution of satellite platforms and imaging sensors came with the launch of the very high spatial resolution satellite, named IKONOS that was launched on 24 September 1999. IKONOS is still operational and carries two sensors which are capable of capturing 0.82 m panchromatic resolution and 3.2 m multispectral resolution, respectively.

Today there are large varieties of HR and VHR satellite systems available for commercial use. The most common Earth observation satellites are (indicating the satellite name and launch date) IKONOS (24 September 1999), QuickBird (18 October 2001), SPOT-5 (04 May 2002), WorldView-1 (18 September 2007), GeoEye-1 (06 September 2008), Worldview-2 (08 October 2009), Pléiades-1A (17 December 2011), SPOT-6 (09 September 2012), Pléiades-1B (02 December 2012), SPOT-7 (30 June 2014) and the most recent WorldView-4, formerly known as GeoEye-2 which was launched on 11 November 2016.

The satellite systems mentioned above are passive systems, meaning that these systems record radiation from the naturally illuminated Earth's surface. A summary of the HR and VHR satellite systems as mentioned above is included in Table 2.1. Another major leap in the development of remote sensing platforms came in 1978 with the launch of the first commercial satellite carrying space-borne synthetic aperture radar (SAR)⁷, named SEASAT. The SEASAT satellite was designed to primarily observe the Earth's oceans and sea ice. Even though the importance and feasibility of space-borne SAR satellites were soon realized by the wealth of information received, the applications of optical satellites were still preferred above SAR satellites. The main reasons for this were due to the low spatial resolution and the salt and pepper (black-and-white) affect that SAR imagery delivers. It provides an unfamiliar visual representation of the Earth's surface as opposed to optical images, which can make the identification and analyses of SAR images a daunting task.

Synthetic Aperture Radar imagery is mainly used as a complementary source to optical images and has many advantages such as the effect of radar shadow, detect motion of objects, determine elevation and measurement of slight changes to surface conditions, but the most common one is that it is weather and daytime independent. In recent years, the application of SAR imagery has come into its own with the increased availability of HR and VHR commercial SAR imagery. Examples of such imagery are the VHR TerraSAR-X images, which can deliver 0.25 m spatial resolution (in Staring SpotLight mode) and up to 1 m spatial resolution in the high-resolution SpotLight mode. Synthetic Aperture Radar satellite imagery is still a complementary source to optical images, but nowadays bring about a new genre to applications such as object identification, natural disasters, change detection, ocean surveillance, elevation modelling, land cover and soil monitoring.

⁷ Synthetic aperture radars are active systems that emit their own artificial radiation and measure the radar pulses reflected back from the ground surface.

Table 2.1: Summary of the most common HR and VHR satellite systems

Satellites	Launch Date	Orbit	Altitude	Spectral Bands and Resolution	Image Swath	Revisit Time
<i>Current operational HR and VHR satellite systems</i>						
IKONOS	24 September 1999	Sun-synchronous	681 km	PAN (0.82 m), MS (3.2 m)	11.3 km X 11.3 km	3 days
QuickBird	18 October 2001	Sun-synchronous	450 km	PAN (0.6 m), MS (2.44 m)	16.5 km X 16.5 km	3 to 7 days
SPOT-5	04 May 2002	Sun-synchronous	822 km	2 PAN (5 m) – combined to create 2.5 m product, MS (10 m) and short-wave infrared (20 m)	60 km X 60 km to 80 km	2 to 3 days
WorldView-1	18 September 2007	Sun-synchronous	496 km	PAN (0.5 m)	17.6 km X 17.6 km	5 days
RapidEye	29 August 2008	Sun-synchronous	630 km	Constellation of 5 satellites with blue, green, red, red-edge and NIR bands. 6.5 m spatial resolution resampled to 5 m pixel size.	77 km X 77 km	5.5 days
GeoEye-1	06 September 2008	Sun-synchronous	681 km	PAN (0.41 m), MS (1.65 m). PAN sold at 0.5 m and MS at 2.0 m due to US government regulations	15.2 km X 15.2 km	3 days
WorldView-2	08 October 2009	Sun-synchronous	770 km	PAN (0.46 m), MS (1.84 m). PAN sold at 0.5 m and MS at 2.0 m due to US government regulations	16.4 km X 16.4 km	3.7 days
Pléiades-1A	17 December 2011	Sun-synchronous	694 km	PAN (0.5 m), MS (2.0 m)	20 km, 100 km X 100 km mosaic	2 days
SPOT-6	09 September 2012	Sun-synchronous	694 km	PAN (1.5 m), MS (6 m)	60 km swath strips and up to 600 km length	1 to 3 days
Pléiades-1B	02 December 2012	Sun-synchronous	694 km	PAN (0.5 m), MS (2.0 m)	20 km, 100 km X 100 km mosaic	2 days
SPOT-7	30 June 2014	Sun-synchronous	694 km	PAN (1.5 m), MS (6 m)	60 km swath strips and up to 600 km length	1 to 3 days
WorldView-3	13 August 2014	Sun-synchronous	617 km	PAN (0.31 m), MS (1.24 m) and short-wave infrared (3.7 m)	13.1 km X 13.1 km	< 1 day
WorldView-4	11 November 2016	Sun-synchronous	617 km	PAN (0.31 m), MS (1.24 m)	13.1 km X 13.1 km	< 1 day

Adapted from Satellite Image Corporation (2016)

2.2.2 Properties of satellite systems

Passive satellite remote sensing is the means of measuring radiation (energy) emitted from the Earth's surface using a remote sensor mounted on a satellite platform (Richards and Xiuping, 2006). The image data delivered from this radiation are primarily based on the properties of the electromagnetic spectrum (ES) and the geometry of the satellite platform. Satellite systems are unique in their engineering to detect variations of this emitted and reflected radiation and can collect radiation from the visible or other parts of the spectrum to construct an image of the Earth's surface. Satellite platforms are intricate systems and processing the image data recorded by these systems require the use of complex mathematical calculations to account for distortions inherent in the image data. These distortions are created by systematic sensor and platform-induced geometry errors (Paragraph 2.2.6). Other considerations include the effect of the atmosphere on the emitted and reflected radiation and the transmission of the recorded data back to the ground receiving station for processing (Richards and Xiuping, 2006). More detail concerning these errors are discussed in Paragraph 2.2.6.

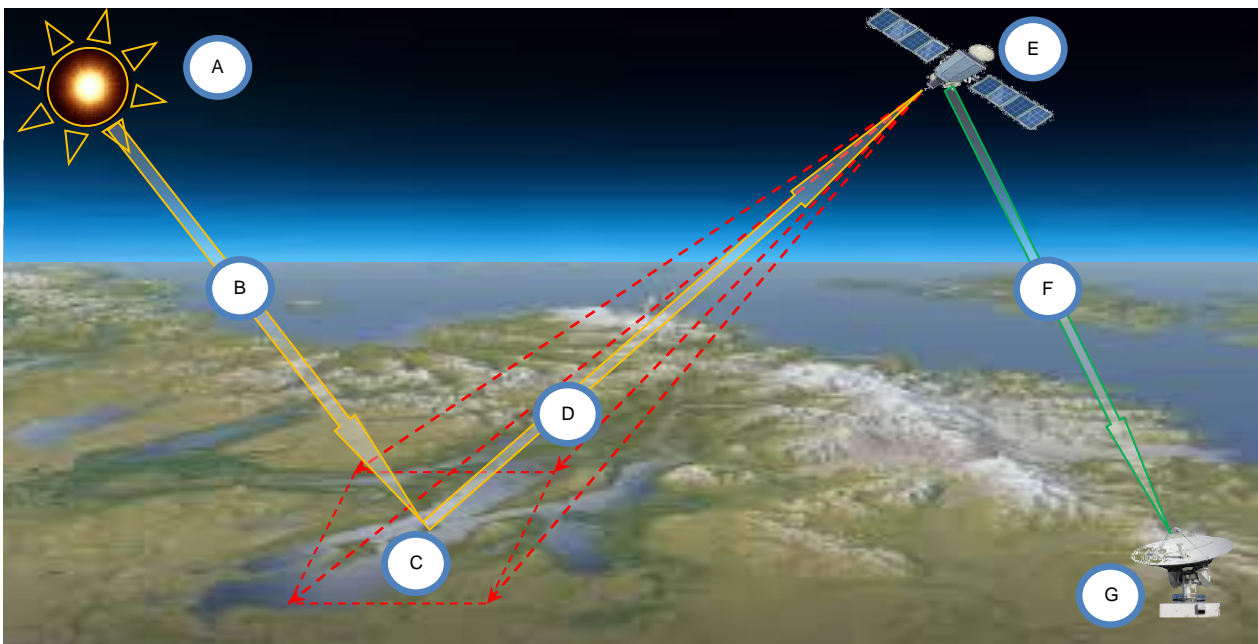


Figure 2.2: Data flow and components of satellite systems

Adapted from Natural Resources Canada: Canada Centre for Remote Sensing (2015)

The data flow and components of satellite systems are illustrated in Figure 2.2:

- (A) - Energy or illumination source, e.g. the Sun.
- (B) - Electromagnetic radiation emitted from illumination source.
- (C) - Target area.

- (D) - Electromagnetic radiation reflected by the Earth's surface and recorded by the satellite system.
- (E) - Satellite platform.
- (F) - Transmission of the recorded data back to the ground receiving station.
- (G) - Ground receiving station and processing for delivering data as an image.

2.2.2.1 Regions of the electromagnetic spectrum

Wavelength, or range of wavelengths, is probably the most significant characteristic of satellite image data. Different wavelengths and frequency correlate to different regions of the ES, which can provide unique information about an object. Most satellite systems operate in the visible and infrared ranges of the ES. These are known as optical satellite systems, whereas SAR satellites emit microwave radiation, which is the longest wavelength used for remote sensing. Understanding the regions of the ES and its correlation to its wavelength and frequency, which is inversely related to each other, is important to understanding the information extracted from satellite-recorded data. The ES ranges from short wavelengths or high frequency to long wavelengths or low frequency, as is illustrated in Figure 2.3.

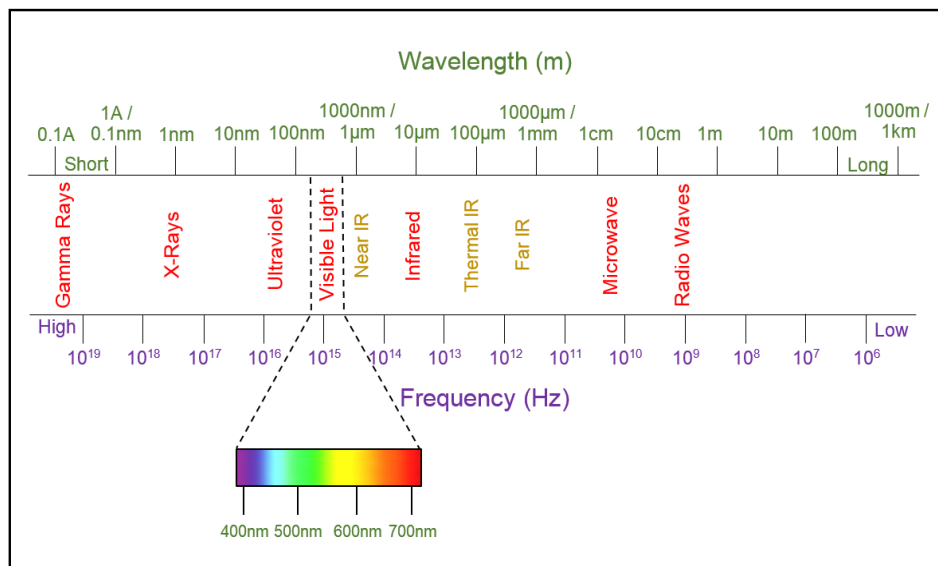


Figure 2.3: Regions of the electromagnetic spectrum

Source: Natural Resources Canada: Canada Centre for Remote Sensing (2015)

Objects absorb and reflect electromagnetic radiation that travels through space at the speed of light. Remote sensors are specifically designed to detect and record only specific radiation that is reflected from objects. However, certain factors influence the

reflected radiation from objects, which might create a misrepresentation of the spectral value of objects and thus make the identification of such objects very difficult. These influential factors affect the brightness and contrast of measured image pixels, which are known as radiometric distortions. Richards and Xiuping (2006) states that radiometric errors are a result of, but not limited to the following influential factors:

- a) wavelength dependence of solar radiation and
- b) the effect of the atmosphere on the wavelengths.

Radiometric errors as well as geometric errors that occur during the acquisition of radiation data will be discussed in more detail later in this chapter (Paragraph 2.2.6).

2.2.2.2 Converting recorded digital data into images

The electromagnetic radiation recorded by satellite systems are coded and stored in the satellite system and when in range of a satellite ground receiving station the coded data are attached to a high frequency electromagnetic wave signal and transferred to the receiving station. The received satellite signal is then filtered from the coded data, which is decoded to create the image (US Army Corps of Engineers, October 2003).

Image data are displayed by an array of pixels or cells, which is usually square and represents geographical space, referred to as a raster image. Each pixel contains a digital number (DN) that represents the object radiation recorded by the sensor, which is based on the brightness value of the radiation. The location of objects or conditions is defined by the row and column positions of the pixels they occupy, it is therefore not necessary to generate geographical coordinates for each pixel. Each pixel can only contain one DN that represents the average of the recorded radiation of an object or surface area. The pixels in an image that are not associated with a specific object or surface area are in most cases populated with the value '0', which represents 'no data' (US Army Corps of Engineers, October 2003) and is represented by the colour black. An 8-bit cell value scale, where values can range from 0 – 255, is used to represent most recorded radiation, because its small in data size and provides a good representation of the recorded scene. The more cells there are, the sharper the image and the better the quality. Recently, with the increase computing capability of computers, 16-bit (values

range from 0 – 65 535) and even 32-bit (values range from 0 – 4 294 967 295) images are used for processing purposes.

Panchromatic images consist of only one spectral band and all brightness values recorded will appear as shades of grey, which is stored in this one band. Therefore, different objects and features will reflect different shades of grey, such as with water and trees that have a very low reflectance will represent very dark areas, whereas man-made features such as roads and buildings that have high reflectance will represent bright areas. This effect is illustrated by Figure 2.4, with the use of an 8-bit panchromatic image.

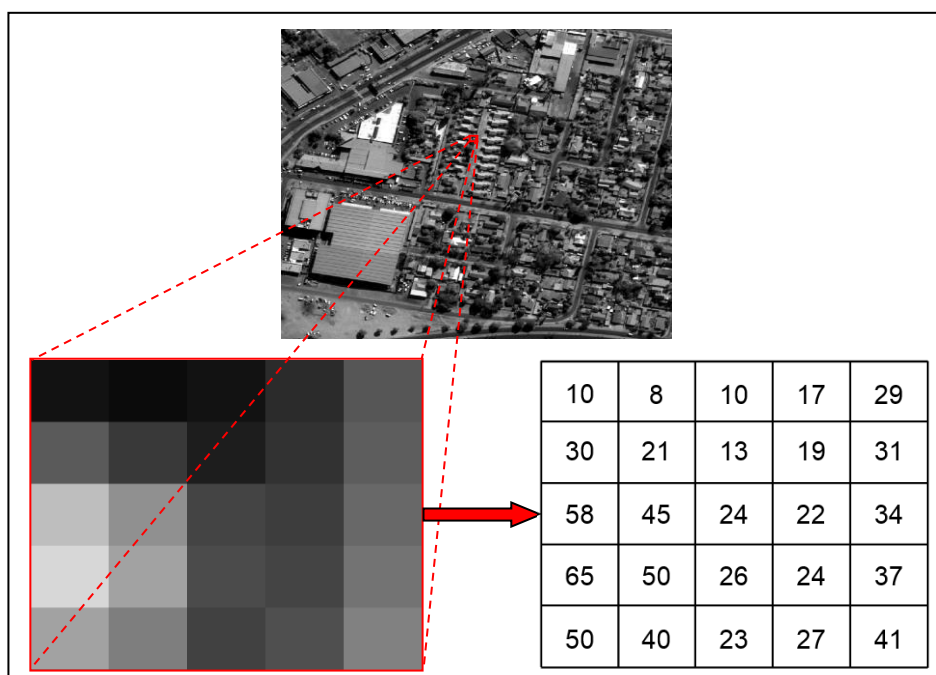


Figure 2.4: Raster representation displaying shades of grey and corresponding DN
 Modified from Natural Resources Canada: Canada Centre for Remote Sensing (2015)

In comparison to panchromatic images, multispectral images usually have between three and 10 different bands, while hyper-spectral imagery measures reflectance energy in narrower and more bands than multispectral imagery and can contain as many as 200 (or more) continuous spectral bands. Multispectral images display the information stored in each band by using the three primary colours (red, green and blue). As is the case with panchromatic images, each multispectral band consists of pixels represented by various digital numbers signifying the brightness reflected by an object or feature. The primary colours are combined in different magnitudes to display a multispectral image (Figure 2. 5).

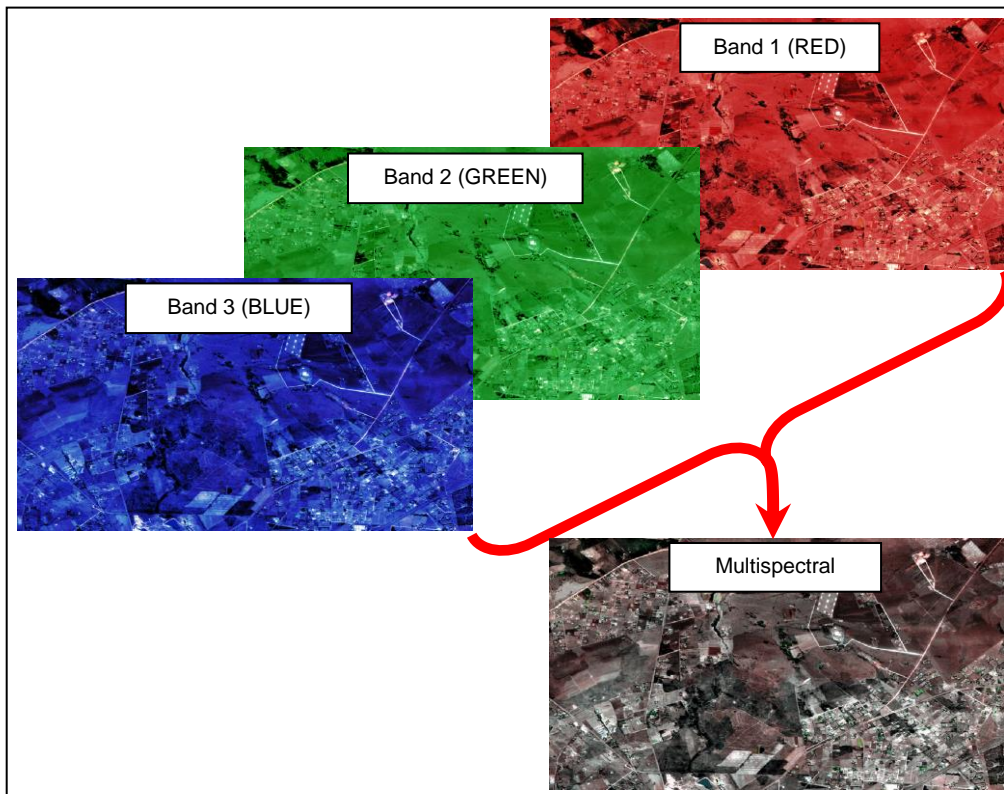


Figure 2.5: Colour composite image

(Copyright © CNES 2013, Distribution Airbus Defence and Space / SPOT Image, all rights reserved)

2.2.3 Characteristics of satellite systems

As referred in Paragraph 2.2.1, satellite remote sensing systems can be placed on a variety of platforms. Satellites provide numerous advantages such as to present a continuous coverage of the Earth's surface at very high quality and have a number of unique and useful characteristics (Natural Resources Canada: Canada Centre for Remote Sensing, 2015), namely:

- a) Orbit: an orbit is the path a satellite follows, which is unique for every satellite system specifically in terms of its altitude, orientation and rotation in relation to the Earth (Natural Resources Canada: Canada Centre for Remote Sensing, 2015). Two common remote sensing orbits used are:
 - i. Geostationary orbits: satellites that view the same portion of the Earth's surface follow a geostationary orbit. These satellites have a high altitude and orbit in unification with the Earth's rotation at speeds that match the Earth's rotation.
 - ii. Polar orbits: satellites following a north-south orbit, relative to an imaginary line stretching between the North and South poles, follow a polar orbit. One

characteristic of these orbits is that they are normally Sun-synchronous – meaning that a satellite system covers a specific areas of the Earth’s surface at a constant local time. One major advantage of Sun-synchronous satellite systems is that they produce consistent illumination images.

- b) Swath: swath is the portion of the Earth’s surface that a satellite system can view or image. The swath of satellites can vary between a few kilometres wide to hundreds of kilometres wide.
- c) Instantaneous field of view (IFOV): the IFOV of a satellite sensor refers to the area on the Earth’s surface that is sampled at a specific moment in time. This is also described as the pixel size of the sensor relative to the ground sampling distance.
- d) Resolution: the detail that can be extracted from an image is dependent on the spatial resolution of a satellite sensor, which can vary from coarse or low resolution to fine or high-resolution. Data collected by satellite systems are characterized in terms of spatial, spectral, temporal and radiometric resolution. This is described in more detail in Paragraph 2.2.5.

2.2.4 Modernisation of optical satellite systems

It is evident from the previous discussions that satellite technologies have developed tremendously since the 1950’s. The difficulty is to predict future advances of satellite systems, since so many improvements have been achieved over the last three to five years. Current trends and improvements achieved can be described as follows:

- a) Improved agility platforms and avionics: satellites are becoming more agile with the development of Control Management Gyros that improves the sensor stability and therefore deliver increased pointing accuracies and instantaneous stereo images consequently enlarging the field of view. The Control Management Gyros allow for super-resolution imaging due to the yaw and pitch capabilities achievable. These systems have incredible reaction times and manoeuvrability to acquire images in any direction. The advantages of improved agility and sensor avionics are evident in the architecture of the Pléiades satellites. These satellites have a very compact design characterised by rigid solar panels, a high-resolution instrument and sophisticated control moment gyros. High attitude accuracies are achieved through the installation of 4 fibre-optic gyroscopes and 3 star trackers

(Gleyzes et al., 2012). Satellites are also becoming smaller and more agile. Small satellites can operate at different altitude and therefore provide better revisit times. Sensors are enhanced to collect more light from a specific scene and hence deliver higher quality images at different times of the day.

- b) Integrated use of satellite constellations: the integrated use of satellite constellations was revolutionised with the launch of the RapidEye satellite system on 29 August 2008 that consists of 5 identical satellites operating in the same orbital plane (Maxwell et al., 2014). Individual satellite systems consist of unique capabilities and provide specific application elements. However, recently these individual systems are being challenged by satellite constellations, such as RapidEye, SPOT, Pléiades and TerraSAR-X. Satellite constellations have the advantage of minimising revisit times and acquiring information over larger areas. In recent times, there has also been a trend to interconnect different satellite systems. Petrat and Eloff (2014) states that through interconnecting radar and optical sensors, it is possible to acquire information that is cloud and weather independent and to perform change detection by analysing the spectral signatures of features recorded by both radar and optical sensors.
- c) Improved communication technologies: there are currently great leaps been made in communication science and integrating these technologies in satellite systems. Fibre optic technologies will play an important role in future space missions by enhancing communications between satellite systems and ground stations. Optical fibre amplifiers will be able to boost signal optical power to increase communication reach in space (Stampoulidis, 2014). Laser technologies are responsible for high-speed data links between satellites and until recently, satellite systems have transmitted data via radio frequencies. The increase in image quality created the problem of increased data storage and transmission capabilities. These problems are neutralised with the use of laser technologies to transmit data speedily and efficiently between different satellites and ground stations, which is already evident with TerraSAR-X (German Aerospace Centre (DLR) and European Aeronautical Defence and Space Company (EADS)) and Alphasat (European Space Agency (ESA)). In 2008, teams responsible for TerraSAR-X successfully set up a laser-optical data link between two satellites located 5 000 km apart that transferred data at a transmission rate of 5.5 GB/s. Alphasat was launched on 25 July 2013 and is designed to expand

telecommunications. It is positioned in a geostationary orbit and is capable of extending the range of laser communications to tens of thousands of kilometres. Alphasat will enable future satellites equipped with laser terminals to transmit data at a rate of 1.8 GB/s to Alphasat, which will in turn relay the data to the ground stations (Powell, 2013).

- d) Enhance space situational awareness and satellite protection: space situational awareness can be described as the means to identify, track, monitor and predict future locations of space objects or debris. Improvements to space situational awareness are achieved through collaborative activities, such as ground-based radar systems, optical telescopes and space-based sensors to locate and track space objects. Satellite systems are vulnerable to objects as small as several millimetres in diameter and the protection of satellite systems is achieved by maintaining accurate orbits and tracking of satellite systems, which are enhanced by the development of new and improved satellite tracking technologies (Becker et al., 2012).
- e) Detection enhancements: the charge-coupled devices (CCDs) have been the backbone of space optical instruments since the 1970's. They are high-performance imaging sensors, but CCD noises are its biggest drawback such as the lack of integrated functions and degraded image data caused by limited response time in the space radiation environment (Mobasherya and Dastfard, 2013). Currently, standard CCDs are being replaced by time delay integration (TDI), one of the most sophisticated and revolutionary imaging detection devices to date. The TDI image sensor is based on CCD technology, hence the name TDI-CCD image sensor. This imaging technique utilises 2D arrays to capture multiple image samples of an image scene and average these samples in order to improve the signal (Fox, 2015). These TDI-CCD sensors are quantum efficient and captures high-resolution satellite images during high-speed imaging and are advantageous during low-light levels applications (Gleyzes et al., 2012).

Considering the satellite technology innovations achieved in recent times, it is still tricky to predict future developments. It is evident that developments have enhanced satellite performances by improving all aspects of satellite systems, to include sensors, data storage and data-link systems. Future advances will increase as technologies improve and it is almost unthinkable to comprehend the fact that these systems can still become

better. However, to predict future trends one has to look into the past. It was less than 50 years ago, that ERTS-1 was launched – the first satellite to monitor the Earth's surface. Since then, advances to satellite systems have increased steadily. The biggest technological leaps have happened over the past ten years with the introduction of sub 50 cm spatial resolutions. Considering the abovementioned, the question then arises: *What will the future hold?*

There are already aims to develop satellite systems that will have the capability to perform on-board image processing for improving data and product delivery. It is certain that improvements will still encompass all aspects of satellite systems. Ultimately, improvements will have the aim to reduce costs, increase data quality (better resolution capabilities), interoperability and manoeuvrability. Satellite systems will also be developed to be a reconfigurable spacecraft, which will be capable to be used for different application. Such satellite systems will have reconfigurable sub-apertures to simultaneously be used for conducting astronomy, Earth observation and planetary exploration (Costlow, 21 March 2014).

2.2.5 Definition of resolution capabilities

Tempfli et al. (2009), states that the characteristics of a satellite sensor determine the quality of an image. Resolution is established by the influence of distance (spatial), wavelength band of ES radiation (spectral), time (temporal) and the quantity of radiation (radiometric):

- a) Spatial resolution: indicates the smallest size of objects that can be detected by a remote sensor and is often referred to as the ground resolution or ground sampling distance, which is described as the ground surface area that forms one pixel. However, spatial resolution and pixel size is not interchangeable. An image with a spatial resolution of 50 cm will have a pixel size of 50 cm X 50 cm, but the image can be resampled to display and represent a pixel size that is different to the spatial resolution.
- b) Spectral resolution: refers to the different wavelength intervals in the electromagnetic spectrum that a sensor can record. Coarse spectral resolution refers to the wide intervals in the ES (e.g. SPOT-5 panchromatic band records ES

- radiation between 480 – 710 nm) and fine spectral resolution refers to narrow intervals (e.g. SPOT-5 red band records ES radiation between 610 – 680 nm).
- c) Temporal resolution: refers to the length of time for a satellite system to obtain imagery of a particular area. It is directly associated to the revisit period and orbit cycle of a satellite system. A system that takes 2 days (e.g. Pléiades-1A) to revisit a specific area on the Earth's surface has a higher temporal resolution than a system that take 5 days (e.g. WorldView-1).
 - d) Radiometric resolution: refers to a satellite system's sensitivity to variations in the spectral reflection of objects or features. Radiometric resolution is directly related to the number of bits into which the recorded radiation is divided. For instance, an image with a data type of 8-bits (data file values range from 0 – 255 for each pixel) has a higher radiometric resolution than a 4-bit image, where data file values only range from 0 – 15. Therefore, the finer the radiometric resolution of a sensor the more sensitive it is to detect small differences in reflected or emitted energy. The dynamic depth of modern sensors has moved from 8-bit to 12-, 16- and even 32-bit.

These four resolution domains contain valuable information that can be extracted from raw satellite data, which will assist in the analysis of specific applications such as agriculture where the health and viability of crops are examined.

2.2.6 Satellite image distortions

In recent years, improvements of the spatial, spectral, radiometric and temporal resolution of satellite sensors had the effect of delivering high- and very high-resolution satellite imagery to the commercial sector. The use of this imagery is very effective for various applications, as were mentioned in Paragraph 1.1 (Zhang and Cheng, 2009). However, Harrison and Jupp (1989) and Olsen (2007) note that it is imperative to remove image noise and distortions, caused due to the characteristics of the satellite system and the imaging conditions, before any analyses can be performed. Two general distortions related to satellite image acquisition can be distinguished, namely radiometric and geometric distortions.



2.2.6.1 Radiometric distortions

Radiometric errors result from the instrumentation used to record the data, e.g. from the wavelength dependence of solar radiation and from the effect of the atmosphere on the wavelengths (Richards and Xiuping, 2006). Liew (2001) states that “*the atmospheric constituents cause wavelength dependent absorption and scattering*” of solar radiation. This is illustrated by Figure 2.6:

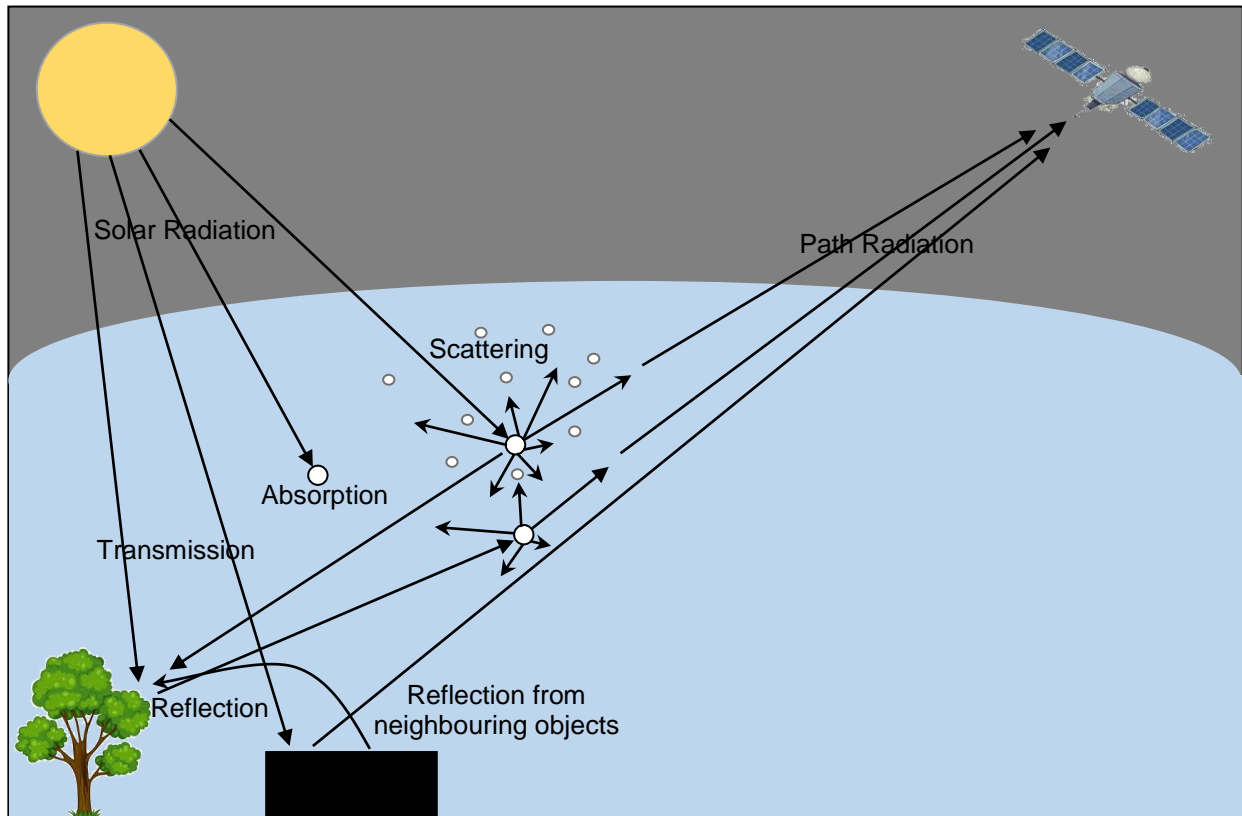


Figure 2.6: Effect of solar illumination in atmosphere

Adapted from USGA (2016)

Radiometric distortions refer to errors in the measured brightness values of image pixels. According to Richards and Xiuping (2006), distorted brightness values of image pixels can lead to two broad types of radiometric distortions. Firstly, the distribution of data brightness in an image band is altered and secondly the brightness of a single pixel from band to band is different. Radiometric correction methods can eliminate the distortions and noise caused by the atmosphere and sensor instrumentation. However, the applied radiometric correction methods must be specific to the nature of the distortion (Lillesand et al., 2008). The following common radiometric correction methods

are described by Lillesand et al. (2008), Horn and Woodham (1978) and in the ERDAS IMAGINE® Field Guide (Hexagon Geospatial, October 2013):

- a) rescaling: resizing image pixels can improve the smoothness and sharpness of an image. An image will become smoother by increasing the pixel size of the image. Conversely, an image will appear sharper when the pixel size is reduced;
- b) haze reduction: the effect of atmospheric scattering appears as a whitish haze on an image. This effect can be removed by means of applying a haze reduction function to the image. This is achieved by firstly determining how much each image band has shifted in brightness value away from the original value and then to subtract this value from each of the pixel brightness values in that image band;
- c) noise reduction: by applying one or more of a variety of possible noise-reducing filters, these image errors are minimised and removed;
- d) de-stripping: regular striping on images is caused by the sensor instrumentation using different small sets of sensors (detectors) to collect the image data (Horn and Woodham, 1978). This effect can be removed by applying a de-stripping algorithm;
- e) histogram matching: rearrange the pixel values of one image to be identical to the pixel distribution in another image. This is performed in order to eliminate or reduce the tonal inconsistency of an image, which is caused when creating a mosaic from multiple images;
- f) histogram equalisation: correct an image by evenly distributing tight clustering of pixels values in an image scene;
- g) brightness adjustment: an image with an even brightness can be created by way of adjusting the digital value of image pixels for each pixel distribution range; and
- h) solar illumination angle corrections: solar illumination angle errors are caused by factors such as the time of the day and the day of the year when the image is captured. These factors have an effect on the reflected radiation being transmitted, reflected and scattered. However, radiative transfer equations exist that can be used to rectify these distortions (Hexagon Geospatial, October 2013).

2.2.6.2 Geometric distortions

Geometric distortions consist of errors in the absolute location of features relative to other features in the image scene. It is important to correct geometric distortions,

because spatial data are jointly integrated to provide a total picture of the image scene. Data will be inadequate and worthless if the absolute location of these data sets is incorrect or left uncorrected. Webber (1973) states that there are two types of geometric distortions, namely:

- a) internal distortions (systematic distortions): caused by variations of the sensor beam width and sampling and
- b) external distortions (non-systematic distortions): caused by variations of the location (affect viewing angles, e.g. nadir and oblique), altitude (see Figure 2.7), attitude (affect image scale), speed of the sensor platform (dependent on the nature of the motion relative to the sampling rate which might create a blurry image), the curvature of the ground surface and the Earth's rotation (affect image scale). The effect of an imaging systems' pitch, roll and yaw on causing distortions are illustrated as follows:

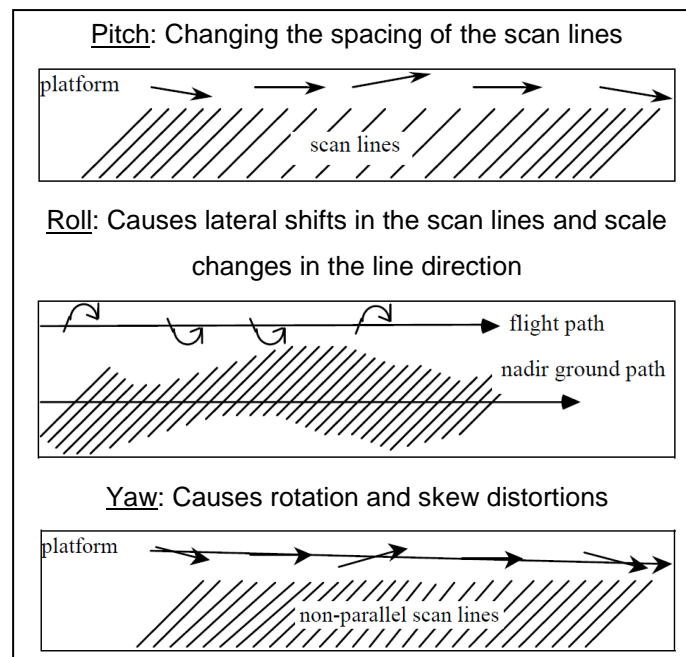


Figure 2.7: Distortions created by platform altitude changes

Source: Richards (2012)

Richards and Xiuping (2006) note that geometric distortions occur for many reasons and most of these errors are corrected at the ground station when the data are initially received from the satellite sensor. However, there are geometric distortions that are difficult to account for mathematically, for instance altitude and speed. To correct these distortions, an image analyst can perform a procedure called image rectification (georectification), also known as image transformation. This procedure entails the

transformation of the unknown image coordinates into known ground coordinates (Richards and Xiuping, 2006). Consequently, georectification is described as a process to geometrically correct an image so that it can be represented on a planar surface and is regarded as a necessity when accuracy, distance and direction are some of the significant factors that need to be derived from the data (Kumar, 2004). During this study, the focus was on investigating geometric distortions and the way and means to improve the geometric accuracy of satellite imagery.

2.3 WAYS AND MEANS TO IMPROVE THE GEOMETRICAL ACCURACY OF SATELLITE IMAGERY

Geometric distortions are an inherent phenomenon in all remote sensing platforms, which are caused when an attempt is made to represent the 3D surface of the Earth onto a 2D plane. As were mentioned in Paragraph 2.2.6.2, these distortions may be due to a variety of reasons. However, ways and means exist to remove or at least minimise these distortions, which is a necessity before analysing or extracting information from the imagery. Not all data sets need to be rectified. Some images may only require to be georeferenced, which entails that the images are planar (has a projection), but require the redefining of map coordinate information for an image. Yang (1997) cites that one of the most common image georeferencing methods to apply when redefining map coordinates is to perform conventional polynomial rectification. This method entails simple image-wide scaling and rotation without considering localised relief distortions (Yang, 1997; Kumar, 2004).

Georectification and georeferencing methods focus on the horizontal position of pixels in the produced image without considering the Earth's curvature (elevation of ground pixels). These methods are efficient when using medium and low spatial resolution remotely sensed images, where the elevation shift in pixel position is not a primary concern. However, when working with high- and very high-resolution satellite imagery, the pixel positional shift caused by the Earth's curvature also needs to be considered (Gao, 2008). A method known as orthorectification can be used to consider the elevation shift in image pixels. Yang and Williams (1997) state that orthorectification is achieved by means of removing the positional displacement of image pixels caused by topographic relief, lens distortions and camera tilt and providing real ground coordinates

(including x, y and z values) for all pixels. Orthorectification is based on collinearity equations derived from 3D GCPs. It is accomplished by applying image elevation data (e.g. Digital Elevation Model (DEM)) to a rectification sensor-specific or sensor-generic model and selecting input and reference GCPs from the input satellite image and reference data source (Yang and Williams, 1997). A procedure named resampling is then used to geometrically correct the original distorted image, which uses DN values to transfer distorted image pixel locations to new corrected image pixel locations. Four common resampling methods exist, namely:

- a) Nearest neighbour: this is the simplest method and uses the digital value of the pixel in the distorted image that is nearest to the location of the pixel in the corrected image.
- b) Bilinear interpolation: this process takes a weighted average of four pixels in the distorted image that is nearest to the location of the pixel in the corrected image and creates new digital values for every new pixel.
- c) Cubic convolution: this process is an extension to the bilinear interpolation method and takes a weighted average of sixteen pixels in the distorted image that is nearest to the location of the pixel in the corrected image and creates new digital values for every new pixel.
- d) Bicubic spline interpolation: this method is very similar to bilinear interpolation, but much slower and produces a smoother finish. It uses a block size of 5 x 5 or larger to fit the current block of points.

The sections to follow will describe the application of image processing systems and the various geometric correction methods that can be applied to improve the geometrical accuracy of satellite imagery.

2.3.1 The application of image processing systems

It is important to realise that no processing or analysis of satellite imagery can be performed without the use of an image processing system (IPS). These systems are Geographic Information Systems (GIS), which consist of a collection of tools that are primarily designed to input, store, retrieve, manipulate and process or analyse image data. There are various commercial image processing systems available for working with image data and consist of various ways and means to perform geometric

corrections. However, only a few (PCI Geomatica®, ERDAS IMAGINE®, ENVI®, *et cetera*) include all important geometric sensor models (Paragraphs 2.3.2.1 and 2.3.2.2) that can be manipulated to alter input parameters and input sources. For the purposes of this study, the ERDAS IMAGINE® 2015 IPS was used to perform all necessary processing, manipulation, analyses and illustrations. This software was selected due to the fact of the extensive knowledge and skills acquired over numerous years in operating this system. All experiments performed during this study emphasis the ERDAS IMAGINE® methods and procedures.

2.3.2 Geometric correction methods

As was mentioned in Paragraph 2.1, two approaches exist to geometrically correct satellite imagery (Chmiel et al., 2004), namely:

- a) 2D polynomial based approach: this approach include the use of georectification and georeferencing methods, which focus on the horizontal position of pixels in the produced image without considering the Earth's curvature (elevation of ground pixels). These methods are often sufficient when using medium and low spatial resolution remotely sensed images, where the elevation shift in pixel position is not a primary concern.
- b) 3D geometric correction approach: this approach is known as the orthorectification method and is achieved by means of removing the positional displacement of image pixels caused by topographic relief, lens distortions and camera tilt and providing real ground coordinates (x, y and z values) for all pixels.

This study focused on the 3D geometric correction approach (orthorectification method) by employing a single frame orthorectification technique, which consist of orthorectifying one image at a time (as opposed to block triangulation) using a technique known as space resection. According to Moffitt and Mikhail (1980), the term space resection *“is the name given to the process in which the spatial position and orientation of photograph is determined based on photogrammetric measurements of the images of ground control points appearing on the photograph.”* The theoretical basis to perform orthorectification methods of satellite imagery are well documented (Grodecki and Dial, 2002; Toutin et al., 2002; Jacobsen, 2002; Maxwell et al., 2014; Stampoulidis, 2014; Toutin, 2006). There are various requirements that need to be adhered to when performing

orthorectification, especially the application of auxiliary data, which in practice it is always difficult due to the availability of good quality auxiliary data. The orthorectification of satellite images is sensitive to subtle changes in sensor parameters, acquisition conditions and target accuracy and it is therefore essential to use accurate auxiliary data.

Orthorectification requires the use of good quality GCPs and digital elevation models, as well as the application of a geometric correction model. Aguilar et al. (2008) states that a geometric correction model, also known as a sensor model, consists of a mathematic equation that connects the ground coordinates (x, y and z values) of objects to their matching 2D image coordinates (x and y values; z will have a value of 0). Various sensor models exist to use for performing geometric correction on satellite imagery. Most of these models, especially the commonly used ones are supported by image processing systems and are associated with the two general orthorectification categories, namely parametric and non-parametric (Hemmler and Wiedemann, 1997).

The approach to use when performing orthorectification depends mainly on the accuracy required and the availability of auxiliary data and sensor parametric (Chmiel et al., 2004). The parametric approach utilises unique and physical sensor models corresponding to specific sensor platforms and types, which is very reliable and produces very high modelling accuracies. However, when the data are not available to use the parametric approach then the non-parametric approach can be applied. The non-parametric approach consists of generalised sensor models that are independent of sensor platforms and sensor types and are very attractive and a very good substitute for physical sensor models.

2.3.2.1 Parametric approach

The parametric approach requires internal and external orientation parameters and consists of sensor models (known as 3D physical, rigorous, physical and/or deterministic sensor models) with complicated mathematical modelling for considering physical geometry components. Each sensor model is specific to the sensor type, which means that an image processing system needs a library of models to perform orthorectification on various types of images and the sensor model library has to be updated each time a

new sensor is available (Chmiel et al., 2004). These types of sensor models can be described as 2D/3D physical and deterministic models (e.g. Frame, Pushbroom, Whiskbroom, Panoramic and SAR) that have physical meaning by reflecting the physical reality of the viewing geometry, such as the satellite platform, imaging sensor and the Earth. These required parameters are distributed by image vendors in the form of image acquisition metadata that are usually included in raw image delivery packages or as an occupying file with certain processing level products. Processing levels differs for all types of sensor platforms. In the case of the Pléiades systems of which the Pléiades-1B image data were used during this study, the processing levels available are (Airbus Defence and Space, 2017):

- a) Primary: processing level closest to the image acquired by the sensor and reinstates perfect collection conditions;
- b) Ortho: represents a georeferenced image which is corrected from off-nadir acquisition and terrain effect; and
- c) Radiometric adjustments: corrections include colour stretching, contrast enhancements and atmospheric offset adjustments.

According to Panem et al. (2012), the Pléiades-HR system also introduces the following processing levels (see Table 2.2):

Table 2.2: Pléiades satellite image processing levels

Mission Requirements	Corresponding Processing Levels	Main Characteristics
Level 0	Raw level	Raw data
Level 1A	Radiometric corrected level	Level 0 + radiometric corrections
Level 1B	“Perfect” sensor level	Image resembles an acquisition by a perfect pushbroom sensor
Level 1C	Ortho-corrected level	Image is enhanced by removing terrain variations, without the use of GCPs

Adapted from Panem et al. (2012)

The use of 2D/3D physical models to orthorectify satellite imagery differs with respect to the type of sensor and platform and its geometry (Toutin, 2004), such as rotating or oscillating scanning mirrors (e.g. Landsat satellite) and Pushbroom scanners (e.g.

SPOT, Pléiades, IKONOS, QuickBird, WorldView and GeoEye). These models are based on mathematical equations, named collinearity equations, which include parameters for camera timing, alignment, focal plane and satellites altitude and ephemeris⁸ (Aguilar et al., 2008). Collinearity equations refer to a set of two equations to transmit sensor coordinates (2D) to object coordinates (3D). Captured GCPs correspond to x, y and z image coordinates and therefore two well-known collinearity equations for visible infra-red images are formulated (Bonneval, 1972; Wong, 1980) which are indicated by Equation 1:

$$\begin{aligned}
 x &= (-f) \frac{m_{11}(X - X_0) + m_{12}(Y - Y_0) + m_{13}(Z - Z_0)}{m_{31}(X - X_0) + m_{32}(Y - Y_0) + m_{33}(Z - Z_0)} \\
 y &= (-f) \frac{m_{21}(X - X_0) + m_{22}(Y - Y_0) + m_{23}(Z - Z_0)}{m_{31}(X - X_0) + m_{32}(Y - Y_0) + m_{33}(Z - Z_0)}
 \end{aligned}
 \tag{1}$$

where: (x, y) are the image coordinates,
 (X, Y, Z) are the map/ground coordinates,
 (X₀, Y₀, Z₀) are the projection centre coordinates,
 (-f) is the sensor's focal length and
 (m_{ij}) are the nine elements of the orthogonal 3-rotation matrix.

The variable m, indicated above can be described as follows (Politecnico, 2017):

$$\underline{m = m_3(\kappa)m_2(\varphi)m_1(\omega)}:$$

$$m_1(\omega) = \begin{pmatrix} 1 & 0 & 0 \\ 0 & \cos \omega & \sin \omega \\ 0 & -\sin \omega & \cos \omega \end{pmatrix},$$

$$m_2(\varphi) = \begin{pmatrix} \cos \varphi & 0 & -\sin \varphi \\ 0 & 1 & 0 \\ \sin \varphi & 0 & \cos \varphi \end{pmatrix},$$

$$m_3(\kappa) = \begin{pmatrix} \cos \kappa & \sin \kappa & 0 \\ -\sin \kappa & \cos \kappa & 0 \\ 0 & 0 & 1 \end{pmatrix}$$

⁸ According to Wade & Sommer (2006), ephemeris is “A table of the predicted positions of a satellite within its orbit for each day of the year, or for other regular intervals.”

An orthogonal matrix preserves lengths of vectors and angles. A rotation matrix transforms the set of coordinates (representing a 3D object) to an orthogonal Cartesian frame, without altering the shape or size of the object. Therefore, lengths of vectors and angles between two or more vector pairs stay unchanged.

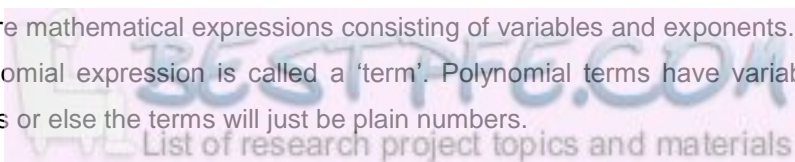
2.3.2.2 Non-parametric approach

The non-parametric approach uses sensor models that are much simpler than the parametric approach and can be used when the parametric of the satellite system or a rigorous 3D physical model is not available. The orthorectification result for using general sensor models is not as accurate as the results obtained by using physical sensor models.

However, the geometric accuracy achieved is still very high, for example in the case of orthorectifying a Pléiades image, the accuracy errors are less than 0.02 pixels (Aguilar et al., 2008). This approach only requires ground control points and does not reflect the source of distortions (Toutin, 2003), but rather signify the remote sensing system as a mathematical transformation between objects on the ground and image pixels (Aguilar et al., 2008).

The sensor models used during the non-parametric approach are known as 2D/3D general, implicit and/or empirical sensor models, which take the form of polynomials⁹ (Purplemath, 2014) or ratios of polynomials, named Rational Polynomial Coefficients (RPC). These models are based on various mathematical functions (Toutin, 2003), indicated by Equation 2:

⁹ Polynomial functions are mathematical expressions consisting of variables and exponents. Each piece or part added to the polynomial expression is called a 'term'. Polynomial terms have variables, raised to whole-number exponents or else the terms will just be plain numbers.



(a) 2D polynomial functions:

$$P_{2D}(XY) = \sum_{i=0}^m \sum_{j=0}^n a_{ij} X^i Y^j$$

(b) 3D polynomial functions:

$$P_{3D}(XYZ) = \sum_{i=0}^m \sum_{j=0}^n \sum_{k=0}^p a_{ijk} X^i Y^j Z^k$$

(c) 3D rational functions: (2)

$$R_{3D}(XYZ) = \frac{\sum_{i=0}^m \sum_{j=0}^n \sum_{k=0}^p a_{ijk} X^i Y^j Z^k}{\sum_{i=0}^m \sum_{j=0}^n \sum_{k=0}^p a_{ijk} X^i Y^j Z^k}$$

where: (X, Y, Z) are the terrain or cartographic coordinates,
 (i, j, k) are integer increments,
 (m, n, p) are integer intervals, usually between 0 and 3 and
 $(m+n+p)$ are the order of the polynomial functions, usually 3.

The order of polynomials (namely 1st order, 2nd order and 3rd order) can be described as follows (Toutin, 2003) by considering the above-mentioned polynomial mathematical functions:

- a) 2D polynomial functions: the simplest way to geometrically correct satellite images.
 - i. 1st order will only correct a translation and scaling in both axes, rotation and obliquity and has 3-term unknowns.
 - ii. 2nd order will in addition to the 1st order parameters also correct for torsion and convexity in both axes and has 6-term unknowns.
 - iii. 3rd order correct for the same distortions as mentioned in the 2nd order as well as other distortions and has 10-term unknowns, but do not necessarily portray any physical reality of the satellite system. However, 3rd order 2D polynomial functions have been known to introduce errors in the relative pixel position of ortho-images (Caloz and Collet, 2001).

- b) 3D polynomial functions: these functions are extensions to 2D polynomial functions by adding Z-values to compensate for terrain relief distortions. Each 1st, 2nd and 3rd order 3D polynomial function has 4-, 10- and 20-term unknowns.
- c) 3D rational functions: these models are the most commonly used alternative for the physical models of satellite images (National Imagery and Mapping Agency [NIMA], 16 November 2000) and are becoming the new standard in georectification of HR satellite imagery. The polynomial order used in these functions is usually less than or equal to three, because greater polynomial orders do not necessarily improve the results and a higher number of GCPs, at least 39 GCPs are then required (Kaichang et al., 2003). The 3D rational functions have the disadvantages of needing large numbers of GCPs and being highly sensitive to the GCPs distribution. They provide interior and exterior sensor orientation and the use of GCPs is not a mandatory requirement. Each 1st, 2nd and 3rd order 3D polynomial function has 8-, 20- and 40-term unknowns.

It is evident from the description of the numerous types of geometric correction methods and sensor models that various ways and means exist to improve the geometrical accuracy of satellite imagery. The method to use is dependent on the type of imagery and the availability of associated auxiliary data. During this study, the parametric approach is applied by utilising a specific physical sensor model to perform all required orthorectifications. As mentioned above, this approach ensures that geometrically accurate images are produced due to the availability of sensor auxiliary data and highly accurate GCPs and DEMs.

2.4 THE REQUIREMENTS AND ACQUISITION OF GCPs AND DEMs TO CREATE ACCURATE ORTHO-IMAGES

As were mentioned in Paragraph 1.1, orthorectification comprises four basic components. The image is a fixed variable and the type of image to use is dependent on the acquisition, the availability and task at hand. The geometric sensor model that relates to the image type is dependent on the accuracy required and the available of auxiliary data and sensor parameters. Therefore, the focus will now shift to the requirements and acquisition of GCPs and elevation data, which provide the link between image and ground-coordinates.

2.4.1 The application of GCPs

It is critical to collect precise and sufficient GCPs that have a uniform distribution across the entire image scene. Care should therefore be taken when selecting and identifying possible GCPs to be collected during a field study. It is imperative to realise that the number, distribution and accuracy of GCPs have a direct influence on the effect of geometric correction (Jakubowicz and Jaszczak, 09 February 2005; Zhang and Cheng, 2009). As a rule of thumb, GCPs should be uniformly distributed across an entire image scene. It is widely disputed among researchers as to the minimum and optimum number of GCP required to perform single frame orthorectification (Zhang and Cheng, 2009). The minimum required GCPs mainly depend on the type of sensor model used and the mathematical function. It is theorised that only six GCPs are required to compute 3D physical models (Paragraph 2.3.2.1). However, the minimum GCPs required with the order of transformation associated with empirical sensor models (Paragraph 2.3.2.2) are calculated by using Equation 3 (Hexagon Geospatial, October 2013):

$$\frac{(t+1)(t+2)}{2} = \text{minimum required GCPs} \tag{3}$$

where: (t) is the order of transformation (1^{st} , 2^{nd} or 3^{rd})

It is evident by applying this mathematical equation to the non-parametric approach that a minimum of three GCPs are required to calculate 1^{st} order transformations, six GCPs to calculate 2^{nd} order transformations, ten GCPs to calculate 3^{rd} order transformations and so on. The question still arises: *How many GCPs will constitute the optimum number of GCPs required to orthorectify satellite images?* The answer to this question has been broadly disputed and part of this study is to provide a proven answer to this question (Aguilar et al., 2008; Chmiel et al., 2004; Jakubowicz and Jaszczak, 09 February 2005; Toutin, 2004; Zhang and Cheng, 2009; Toutin and Chénier, July 2004; Tahar, 27-29 November 2013). Good practice is to use as many GCPs as possible that are spread over the entire image, covering the centre and four corners of the image when the terrain variation and geometric distortion are great. However, it should also be realise that more GCPs will not necessarily render better results (Toutin, 2004). Rather

spend more time on the quality and distribution of accurate GCPs than on the quantity of GCPs (Figure 2.8).

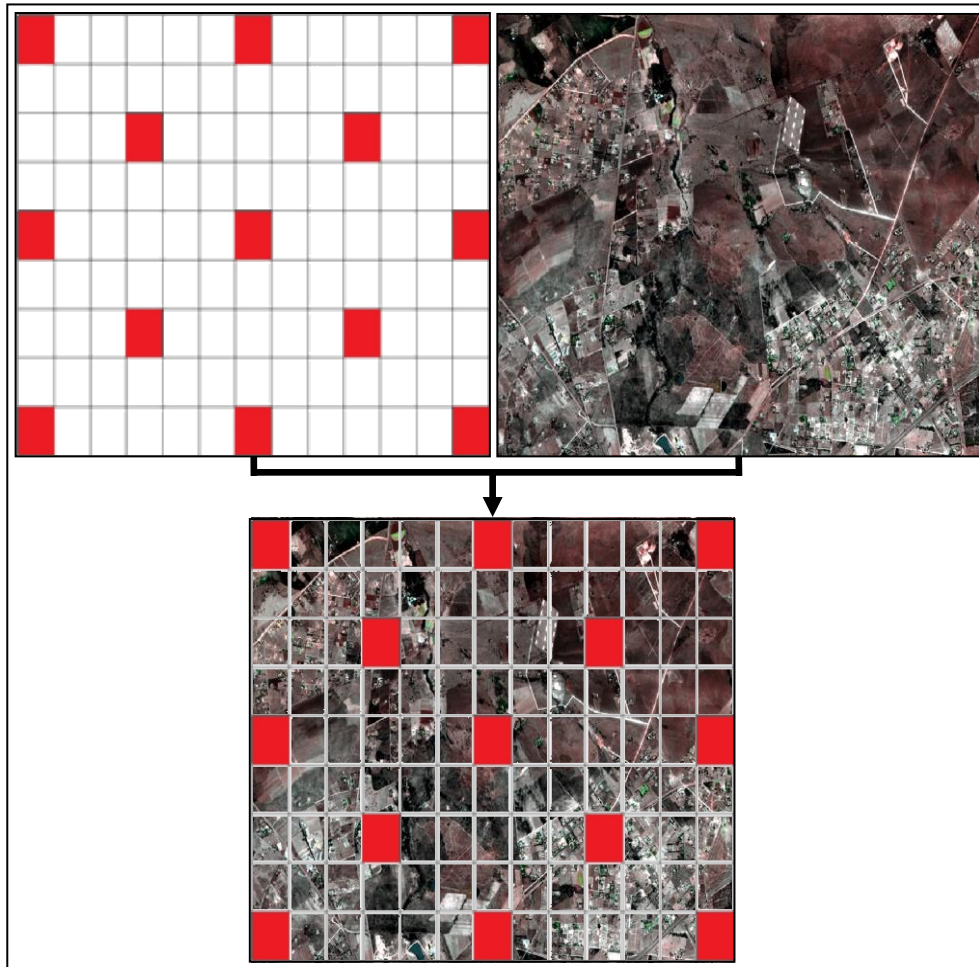


Figure 2.8: Proposed theoretical placement of 13 GCPs to achieve a uniform distribution
 (Copyright © CNES 2013, Distribution Airbus Defence and Space / SPOT Image, all rights reserved)

GCPs can be acquired by means of manual collection utilising a GPS or by means of an automated process where GCPs are automatically extracted, such as the TerraSAR-X GCP-1 and GCP-3 products (Paragraph 1.1). However, whether GCPs are manually or automatically acquired, the quality of GCPs will heavily depend on good planning. Areas to capture GCPs should be identified on the image and the GCPs should have the characteristic to easily distinguish features on the image and corresponding features on the ground, such as road intersections, building and/or swimming pool corners, centre point or markings on sport fields and centre point of traffic circles (Figure 2.9).

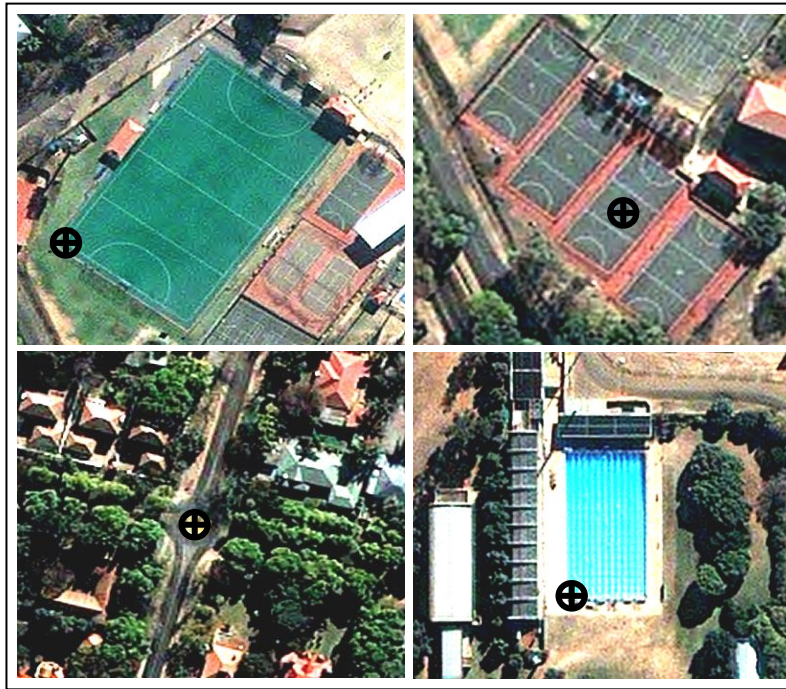


Figure 2.9: Good features for capturing GCPs

(Copyright © CNES 2013, Distribution Airbus Defence and Space / SPOT Image, all rights reserved)

2.4.2 The application of DEMs

As in the case of GCPs, the use of digital elevation models plays a vital role during the orthorectification process. Digital elevation models are applied during the 3D parametric and 3D non-parametric approaches through eliminating terrain distortions and transforming an image into an orthogonal projection. Digital elevation models are a regular array of x, y and z coordinates that describe the surface of the Earth above sea level, which are also known as digital height models (DHM), digital terrain models (DTMs) and digital surface models (DSMs). The term DEM is most of the time used as a generic term for a DTM and DSM (Jacobsen, 2003). However, in practice these terms are actually different products (Figure 2.10):

- a) DEM/DTM: both DEM and DTM are for all practical reasons the same product. DTMs are a broader term and include heights and elevations, but also refer to geographical elements and natural features on the surface of the Earth, such as rivers and ridges (Tighe et al., 2009).
- b) DSM: is a raster representation of the Earth's surface including all objects on it, such as the reflective surface of trees, buildings and powerlines (Tighe et al., 2009).

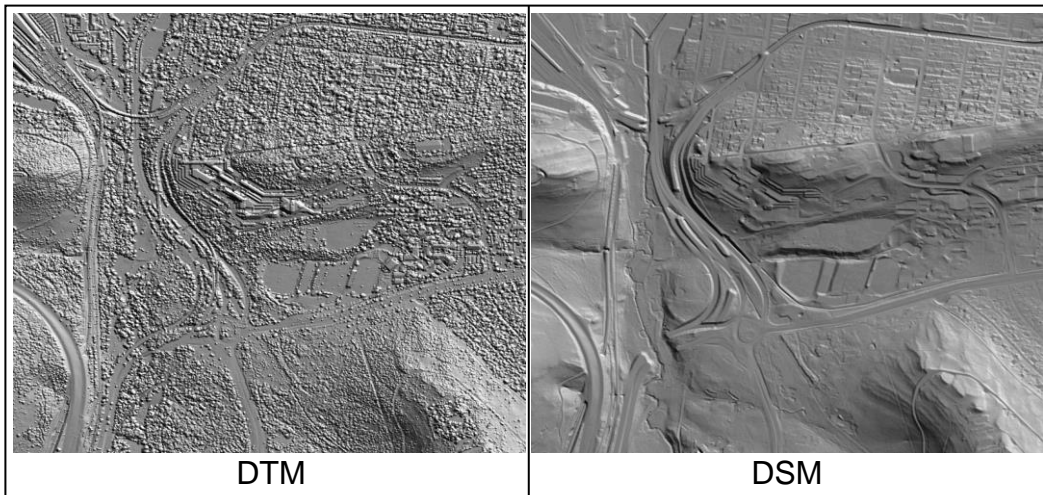


Figure 2.10: The illustrated difference between a DTM and a DSM

During the process of orthorectification, the regular array of a DEM is transformed to a matrix that corresponds to the input image. Orthorectification takes place by assigning grey-level values to each element in the matrix that is projected to the input image. Therefore, the DEM provides ground elevation and grey-level values to the input image, which are then used to create an ortho-image. This transformation is illustrated in Figure 2.11.

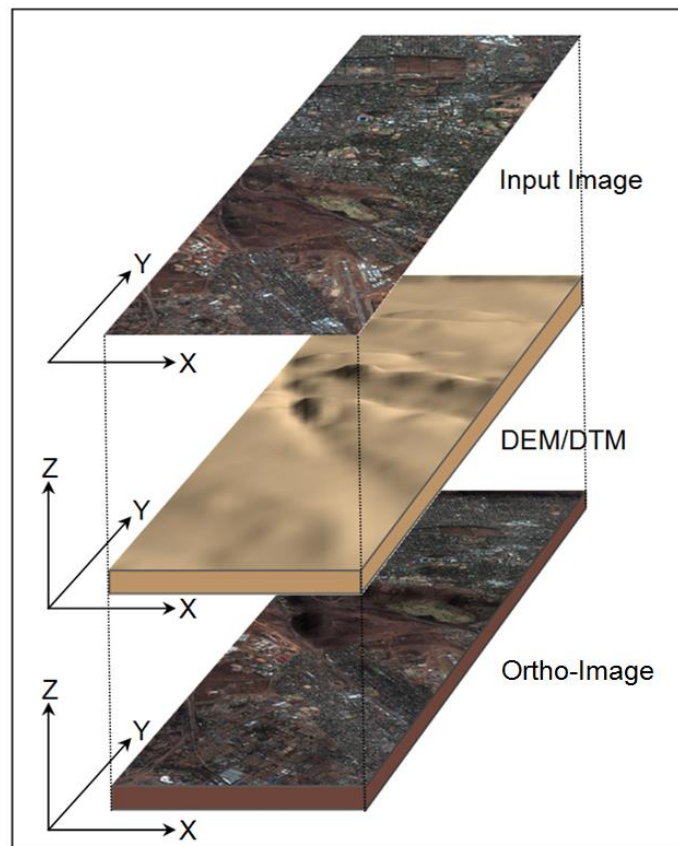


Figure 2.11: Utilising a DTM to create an ortho-image

2.5 ASSESSMENT OF AN ORTHO-IMAGE

One of the fundamental steps of performing orthorectification takes place after the ortho-image is created. Assessment of the ortho-image is a necessity that needs to be performed in order to determine the accuracy achieved from the final product. Performing orthorectification mainly depends on the type of sensor model utilised, which is based on measured ground control points. Therefore, any accuracy assessment of geometric correction is based on the accuracy assessment of independent checkpoints (CP), which are known ground control points that were not used during the orthorectification process. As were the case with GCPs, CPs should also be well distributed to cover the entire image scene (Brovelli et al., 2006). Two common validation methods are normally used to determine the accuracy of HR and VHR satellite images (Brovelli et al., 2006), namely:

- a) Hold-out validation (HOV): this is the most used and classic method to assess the spatial accuracy of ortho-images. Root mean square error (RMSE)¹⁰ of residuals is used to estimate the positional accuracy between the coordinates of GCPs and CPs. This method is simple and easy to compute, however some disadvantages are:
 - i. normally not reliable, because if poor quality CPs are used then the accuracy assessment is biased and
 - ii. not applicable when a low number of GCPs are available, because most of the GCPs would have been utilised during the orthorectification process and therefore very few CPs would remain to compute the accuracy.
- b) Leave-one-out cross validation (LOOCV): this method is an alternative to the HOV method and entails the process to divide the original dataset into smaller equal subsets. Each subset is alternatively used as a test set and training set and cross validates against each other. The accuracy is obtained by computing the average of accuracy values obtained from each subset by calculating the RMSE or a strong accuracy index such as the median Absolute Deviation. During this method, all GCPs are used except one (different in each subset iteration), which is used as the CP.

¹⁰ RMSE is the square root of the average in differences of the x and y location for identical points between GCPs and independent CPs.

The National Standard for Spatial Data Accuracy (NSSDA) by the Federal Geographic Data Committee (1998), states that accuracy of spatial data are normally reported in ground distances at the 95% confidence level. The meaning of a 95% confidence level can be explained by considering a 1.25 m RMSE of GCPs used to create an ortho-image. This means that 95% of the GCPs utilised will have a ground position error equal to or smaller than 1.25 m. The normal guideline for calculating RMSE is that the residual error should not be more than the pixel size of the particular image that is being orthorectified. This error in some instances can only be approximated (Smith, 2005). A large error for a specific GCP might be an indication that an error was made when the point was placed or that the point was incorrectly captured. The image used during the empirical phase of this study was a Pléiades-1B primary panchromatic image with a special resolution of 50 cm. Adhering to the normal guideline, mentioned above, the RMSE calculated for orthorectifying this image should then not be more than 0.5 m. It is important to realise that RMSE provides only a guideline as to which GCPs contribute to the overall accuracy of the image as well as the error value of GCPs. Four options to consider for achieving acceptable RMSE are:

- a) To eliminate the GCPs with high RMSE, which will provide a better fit result;
- b) To tolerate the level of RMSE;
- c) Use a higher order transformation, but this option might result to a distorted image; and
- d) Utilise only high-confidence points and exclude all other points.

The problem with the options to eliminate high error GCPs and to utilise only high-confidence points are that certain areas in the image might not be covered anymore by any reference points. This will result to an image being highly accurate in certain areas and distorted in other areas. A balance therefore needs to be achieved between including and excluding GCPs. It is derived from the study that the best choice will be to tolerate the level of RMSE. As was stated earlier, RMSE is only a guideline/indication to the contribution of GCPs to the accuracy of an image. Other factors also need to be considered when transforming an image to achieve a high level of accuracy, such as the elevation source.

Another method to consider for assessing or determining the accuracy of an ortho-image is to perform visual inspections. Visual inspections is as important, if not more important,

than any automated accuracy assessment tool. It is possible to assess GCPs and find that there is a high correspondence to CPs, which resulted in a high level of accuracy. It might even be that a poor correspondence exist, but still a high level of accuracy is achieved. In such cases, the visual assessment is more important than the RMSE, which can then be disregarded or removed if necessary (Federal Geographic Data Committee, 1998). Each experiment performed during this study (see Chapter 4, Paragraphs 4.3 – 4.5), is described in terms of the total RMSE achieved and accuracy is assessed using the ERDAS IMAGINE® 2015 Metric Accuracy Assessment (MAA) tool and through visual inspections that entails manually measuring the deviation between image pixels and matching control point locations, which indicates the ground position error of the GCPs. These three assessment methods used during this study are described below.

2.5.1 Calculating RMSE

To calculate RMSE, known GCP coordinates are compared to retransformed coordinates of the same points of the introduced reference GCPs by calculating a transformation matrix¹¹ from the GCPs. The reference GCPs are converted to the input coordinate system and the distance between these retransformed coordinates and the original input coordinates is the RMSE. The root means squared method is used to calculate RMSE. Various mathematical equations exist that can calculate RMSE, one of these equations is illustrated below by Equation 4, (Hexagon Geospatial, 2015):

$$RMSE = \sqrt{(x_r - x_i)^2 + (y_r - y_i)^2} \tag{4}$$

where: $(x_i$ and $y_i)$ are the source coordinates
 $(x_r$ and $y_r)$ are the retransformed coordinates

The ERDAS IMAGINE® 2015 software reports the RMSE for each respective GCP and indicates the total RMSE when utilising the GCP tool, illustrated in Figure 2.12 by the red squares.

¹¹ According to the ERDAS IMAGINE® 2015 Help Guide, a transformation matrix “is a set of numbers computed from the GCPs that can be plugged into polynomial equations.”

X Ref.	Y Ref.	Z Ref.	Type	X Residual	Y Residual	RMS Error	Contrib.
28.113	-25.835	1390.000	Control	-2.388	-1.514	2.828	0.602
28.280	-25.847	1536.000	Control	-2.345	-3.673	4.358	0.928
28.244	-25.829	1499.000	Control	3.899	3.110	4.988	1.062
28.163	-25.842	1425.274	Control	1.286	-4.326	4.514	0.961
28.198	-25.850	1449.000	Control	4.877	1.443	5.086	1.083
Resolution is current.				Control Point Error: (X) 3.8006 (Y) 2.7557 (Total) 4.6945			

Figure 2.12: ERDAS IMAGINE® 2015 RMSE report when utilising the Multipoint Geometric Correction tool

The RMSE is expressed as a distance in pixel width. For example, an RMSE of 4 means that the reference GCP is 4 pixels away from the input GCP. It also reports on the X and Y Residuals, which are the distances in one direction between the input and retransformed coordinates. The root mean square error of each individual GCP are indicated in the RMSE column and calculated by Equation 5:

$$R_i = \sqrt{XR_i^2 + YR_i^2}$$

- where:
- (R_i) is RMSE for GCP₁ (5)
 - (XR_i) is X Residual for GCP₁
 - (YR_i) is Y Residual for GCP₁

The relationship between RMSE and Residuals of individual GCPs are illustrated in Figure 2.13.

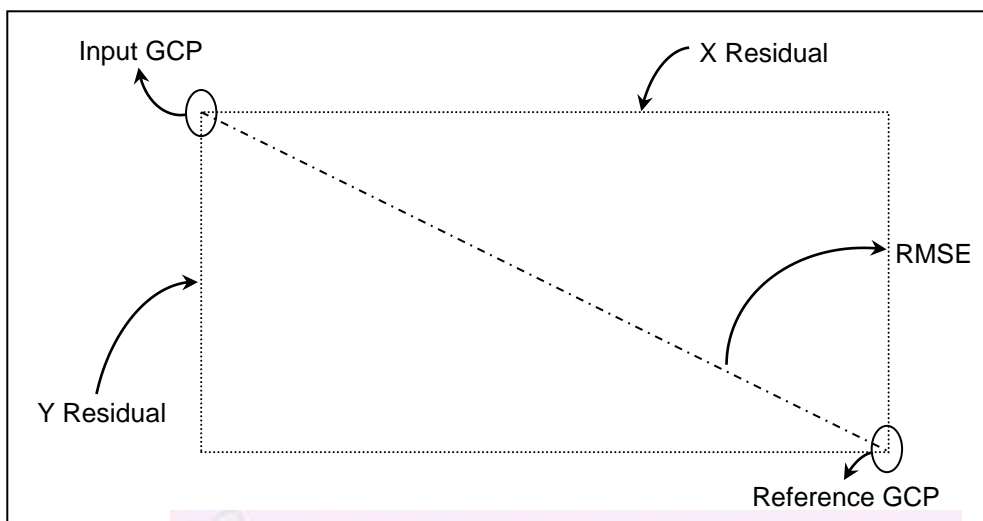


Figure 2.13: Relationship between RMSE and residuals of individual GCPs
 Adapted from Hexagon Geospatial (2015)
 List of research project topics and materials

The total X and Y RMSE can now be calculated to determine the total RMSE for all GCPs. These calculations are done utilizing the formulations of Equation 6:

$$R_x = \sqrt{\frac{1}{n} \sum_{i=1}^n XR_i^2}$$

$$R_y = \sqrt{\frac{1}{n} \sum_{i=1}^n YR_i^2}$$

$$T = \sqrt{R_x^2 + R_y^2} = \sqrt{\frac{1}{n} \sum_{i=1}^n XR_i^2 + YR_i^2} \quad (6)$$

where:

- (R_x) is X RMSE
- (R_y) is Y RMSE
- (T) is Total number of GCPs
- (i) is GCP number
- (XR_x) is X Residual for GCP_{*i*}
- (YR_y) is Y Residual for GCP_{*i*}

The values in the contribution table display the error contribution (RMSE) of each GCP in relation to the total RMSE. These values are calculated by applying Equation 7.

$$E_i = \frac{R_i}{T}$$

where:

- (E_i) is Error contribution of GCP_{*i*}
- (R_i) is RMSE for GCP_{*i*}
- (T) is Total RMSE

(7)

2.5.2 Utilising the ERDAS IMAGINE® 2015 MAA tool

The MAA tool used to assess all experiments performed creates a report indicating all calculated statistics based on the error between the image coordinates and control point coordinates. Figure 2.14 (below) shows the typical layout of the MAA report and indicates the description of one measured control point.

According to the ERDAS IMAGINE® 2015 Help Guide for utilising the MAA tool (Hexagon Geospatial, 2015), “Error computations are based on MIL-STD-600001¹², with bias taken into account. The CE90 (circular error 90%) is computed using horizontal error as input to the LE90 (linear error 90%) formula with bias.” The accuracy derived from these reports, which is indicated as the Test and Evaluation (T&E) points and mensuration error (CE90), is included in the descriptions of the accuracy achieved for all experiments performed. These reports, created during this study, are attached at the back of this document as addendums.

Distance values are in meters						
Mean latitude error: 1.171999						
Mean longitude error: 0.255882						
Mean horizontal error (average HE): 1.461420						
Standard deviation latitude error: 0.998900						
Standard deviation longitude error: 0.450726						
Standard deviation horizontal error: 0.710115						
90% Circular Error (against T&E): 2.371433						
90% Circular Error (T&E and mensuration error included): 2.371433						

ID	T&E Latitude	T&E Longitude	T&E Elevation	T&E CE90	T&E LE90	
1	-25 40 48.898	+28 05 58.648	1378.640	0.000	0.000	

						T&E Description
						CP #1

Measured Latitude		Measured Longitude		Measured Elevation		
-25 40 48.873		+28 05 58.666		1378.640		

Delta Latitude		Delta Longitude		Delta Elevation		Mensuration Error
0.788		0.479		0.000		0.000

Individual HE				Individual VE		
0.923				0.000		

Figure 2.14: Layout of MAA tool report

2.5.3 Performing visual inspections

Performing visual inspections is a subjective assessment. In this study, the ERDAS IMAGINE® 2015 measurement tool was used to measure the directional deviation (measured in degrees) and distance error (measured in metres) of specific image coordinates (relating to image pixels) against predetermined control point coordinates.

¹² MIL-STD-600001 is a United States Department of Defence approved military standard that defines Mapping, Charting and Geodesy product accuracy and provides a common basis for the appropriate application of these definitions. US DEPARTMENT OF DEFENSE. 26 February 1990. Department of Defense Standard Practice: Mapping, Charting and Geodesy Accuracy. Available: http://eart-info-nga.mil/publications/specs/printed/600001/600001_Accuracy.pdf [Accessed 26 March 2015].

The results are illustrated using a PolarPlot diagram and shows the directional deviation and distance error of each measured point (Chapter 4, Paragraphs 4.3).

2.6 CHAPTER SUMMARY

This chapter was emphasised by a literature review relating to the orthorectification of satellite imagery. A brief history to the evolution of satellite platforms was provided and the characteristics of the most common HR and VHR observation satellite systems were indicated in the form of a table. The focus then shifted to the properties and characteristics of satellite systems, with specific reference to the electromagnetic spectrum, converting recorded digital data into images, resolution capabilities and types of image distortions embedded in satellite imagery. The modernisation of optical satellite systems was also briefly described by indicating the current technological advancements and possible future improvements of these systems. Next, the ways and means to improve the geometrical accuracy of satellite imagery were discussed in detail. The emphasis was on geometric correction methods by referring to the parametric and non-parametric approaches. The requirements and role of GCPs and DEMs were investigated and the chapter concluded by emphasising the importance of performing accuracy assessment as a final step during orthorectification.

The literature study performed during this chapter indicated that the highest level of geometric accuracy is achieved by following the parametric approach and utilising a physical sensor model. Although the non-parametric approach (using empirical sensor models) is a good substitute for the use of physical sensor models, especially when there is a lack of available auxiliary data. Physical sensor models will provide the ways and means to create accurate ortho-images. This is especially true when accurate GCPs and elevation data are utilised. It is the intention of this study to perform numerous types of orthorectification experiments for the purpose to improve the geometric accuracy of HR satellite imagery. Therefore, it is imperative to create accurate ortho-images during each experiment, which will be provided by the use of physical sensor models, in order to compare and triangulate the orthorectification results. The methodological approach followed during this study is described in the next chapter.



CHAPTER 3 - RESEARCH METHODOLOGY

3.1 INTRODUCTION

This study made use of an extended literature study and empirical research to solve a specific problem. The torment to orthorectify satellite imagery when there are limited GCPs available that are irregularly distributed, encouraged the investigation of this problem and develop a methodological approach to follow for improving the geometric accuracy of VHR satellite imagery when there is a lack of quality GCPs available. In addition to the literature study (Chapter 2) that was conducted to provide insight into the evolution and modernisation of satellites, how they operate, their characteristics, inherent distortions and the role auxiliary data play during the process of rectification, the empirical research was conducted to answer the research questions identified for this study. According to Niaz (2008), the research problem that needs to be resolved will determine the research methodology to utilise. Research methods (quantitative and qualitative approaches) describe the research strategy and empirical techniques used to resolve specific research problems. Both research approaches are used to devise, investigate and resolve research problems. However, the nature of reality, knowledge and the principles that inspire scientific research, will lead to the preferred and specific research method to be used. This is normally based on the relevance of this method in the specific methodological orientation (Onwuegbuzie et al., 2009).

In this chapter, a brief statement of the research problem and motivation, the research questions and hypotheses and the aim and objectives are included, as it was already discussed in detail in Chapter 1. Thereafter, a detailed breakdown is provided of the methodology and methods that this research is based on.

3.2 PROBLEM STATEMENT AND MOTIVATION

3.2.1 Motivation for the research study

It is inevitable that remote sensed imagery will inherit geometric distortions during data capturing, due to many influential factors that affect the positional accuracy of satellite imagery. Factors such as acquisition geometry, topographic properties of the image

area, optical fidelity of the sensor and positional steadiness all play a vital role in the extent of geometric errors imbedded in remotely sensed imagery (Exelis VIS, 2013). Orthorectification is the process that eliminates the geometric distortions introduced during image acquisition. It produces a planimetric image that has a consistent image scale and is accurately registered to real-world map projections and ground coordinate systems.

Traditionally, orthorectification was a semi-automated process that required user inputs regarding the sensor platform, GCPs and terrain elevation to process the image data accurately using commercial image processing software. However, recently with the development of newly designed sensor systems this traditional approach has changed dramatically (Petrat and Eloff, 2014; Hoja et al., 2008). Automated orthorectification of imagery is now possible based on the comprehensive metadata embedded in remotely sensed data and utilising new and improved sensor models and algorithms to process the image data. As was mentioned in Chapter 2 (Paragraph 2.2.4), the modernisation of satellite systems brought about a new and improved dimension to the pointing accuracies of current and future generations of satellite systems (Petrat and Eloff, 2014).

These days, orthorectification are more and more performed by using RPCs, elevation data and optional GCPs to achieve highly accurate ortho-images, due to the fact that not all 3rd party image processing software have extended sensor model libraries to include all rigorous sensor models (Dial and Grodecki, 2005; Toutin, 2006). As were discussed in Chapter 2 (Paragraph 2.3.2), this method of using RPCs (non-parametric approach) are simpler empirical mathematical models compared to using rigorous sensor models (parametric approach) with complicated mathematical modelling (Dial and Grodecki, 2005). The non-parametric approach is usually followed due to the lack of suitable auxiliary data such as the non-availability of sensor specific parameters. However, when highly accurate ortho-images are required and auxiliary data are readily available, then the use of rigorous sensor models will be the most suitable option. Most ortho-image applications require very high registration accuracy. For instance, a registration error of less than 1/5 of a pixel will produce a change detection error of less than 10% and for measurement accuracies of less than 1 m (e.g. measurements of ice flow and cosmic ground deformation) even better registration accuracies are required (Leprince et al., 2007). In practice, the acquisition of raw image data with detailed sensor information and

sufficient elevation data to achieve high registration accuracies are not problematic. However, the collection of ground control points poses a significant problem when performing single frame orthorectification, as were discussed in Chapter 1 (Paragraph 1.2.1). In such cases, the only available source for extracting GCPs is vector layers. Therefore, the following question arises: *How accurate will an ortho-image be when GCPs are used that were extracted from a vector layer?* Various orthorectification experiments were conducted during this study to determine the effect of such GCPs that are irregularly distributed, covering an entire image scene.

3.2.2 Research hypotheses and questions

In Chapter 1 (Paragraph 1.2.2), a detailed description of the research hypotheses and questions were formulated. The specific experiments conducted during the empirical research (Chapter 4) enabled the testing of the research hypotheses and answer the research questions which were formulated. The experiments conducted during stages 1, 2 and 3 tested the research hypotheses and answered research questions 1, 2 and 3 (these are discussed in detail below in Paragraphs 3.7.1 – 3.7.3). To answer research questions 4 and 5, two separate independent orthorectification experiments were conducted during stage 2. Firstly, utilising the TerraSAR-X-based GCPs acquired from Airbus Defence and Space and the 2 m DTM to create an ortho-image and determine if it is possible to create accurate ortho-images without manually collecting GCPs. Secondly, create an ortho-image by utilising only the geometric sensor model and an elevation source (i.e. 2 m DTM) – without the use of GCPs – and determine if an accurate ortho-image can be produced.

3.3 RESEARCH AIM AND OBJECTIVES

The aim of this study was to investigate and compare the positional accuracies of ortho-images under various orthorectification scenarios and provide improved geometric accuracies of VHR satellite imagery when diverse ground control and elevation data sources are available. Considering the aim, a methodological approach was developed for improving the geometrical accuracy of VHR imagery when there are inadequate GCPs available that are irregularly distributed in an entire image scene. The parametric approach was followed to conduct all orthorectification experiments. Sufficient auxiliary

data were available to create a highly accurate ortho-image (e.g. master image), which were used to measure the accuracy of ortho-images created by utilising GCPs extracted from a vector layer. In order to achieve the aim of this study, specific objectives were formulated (Chapter 1, Paragraph 1.3). Achieving the objectives and ultimately the aim of this study contributed to the formulation of the methodological approach (see Paragraph 4.9, Chapter 4), which are described in terms of the procedure to follow, with specific reference to the:

- a) number of GCPs necessary;
- b) distribution and placement of GCPs; and
- c) effect of the elevation data and quality DEM necessary.

This approach highlighted the precise optimum data and reference sources necessary to use when performing orthorectification on VHR satellite imagery. It indicated expected location accuracy limitations when:

- a) utilising various quality elevation data sources and
- b) using a limited number of GCPs that are irregularly distributed.

3.4 RESEARCH METHODOLOGY

Methodology is defined as the rules, principles and formal conditions that govern scientific research for the purpose of organising and broadening ones knowledge of the phenomena that is being researched (Gelo et al., 2008). Gelo et al. (2008) specifically refers to methodologies as the relationship between the researcher's views, theory, research questions, hypotheses and research methods. Two types of research approaches exist, namely quantitative and qualitative approaches. Quantitative approaches dominated science research until the 1960's. Since the 1960's, researchers started to criticise the use of pure quantitative approaches and proposed a naturalistic, contextual and holistic method – this came to known as qualitative research (Gelo et al., 2008). Quantitative research (also known as traditional or experimental approaches) is a positivistic research paradigm that promotes the status of experimental research and the quantitative methods of analysis (Cohen et al., 2004; Creswell, 2012; Doll, 1970). Gelo et al. (2008, p 267) cites that quantitative research describes the “*how much of an entity there is*”, which means that quantitative research consists of calculating the frequency of events and the volume or the size of associations between variables (Maree, 2007).

Controversially, qualitative research is based in the post-positivism that promotes powerful descriptions of the phenomena being investigated (Gelo et al., 2008). Gelo et al. (2008, p 267) state that qualitative research implies “*describing the constituent properties of an entity*”, meaning that qualitative research focus rather on the clarification of phenomena. Addition to the foregoing differences between quantitative and qualitative research, both these approaches also differ regarding methodological assumptions and research methods:

- a) Quantitative research: according to Gelo et al. (2008), quantitative research requires a nomographical methodology. Nomography refers to the science of common law that manage generalisation. This means that facts are collected, confirmed and processed with the purpose to generalise. The methods to collect quantitative data are directly from the source of the data (primary data) or indirectly by using personal or official documents and archive material (secondary data). Qualitative data collection methods can be used to collect quantitative data, as long as the data are statistically analysed by awarding numerical values to the collected data. Therefore, quantitative data collection requires redirecting phenomena to numerical values for statistical analysis, while qualitative data collection constitutes non-numerical representations (texts, pictures, photos, videos, etc.). Quantitative research stresses meanings, concepts, characteristics, metaphors, symbols and descriptions of phenomena (Berg, 2004). The researcher’s role during quantitative data collection is one of objectivity and is limited to the collection of data for confirming research questions and hypotheses and focuses on the validity of what is being observed (Johnson and Christensen, 2008).
- b) Qualitative research: ideology (qualitative research), in contrast, refers to the complete representation of a particular event with the aim to record and develop an understanding of the event. Qualitative data collection also entails the collection of primary and secondary data, but uses different methods to collect data (Gelo et al., 2008). According to Howe (2003), the procedure for qualitative data collection is not as strictly defined as with quantitative data collection. The range is boundless and results are provided in descriptive or narrative form. Quantitative and qualitative research methods differ in several respects and Dreyer (1998) warns that “*Whether one conducts quantitative or qualitative*

research, one has to be both insider and outsider, engaged participant and detached observer.”

The difference between the two approaches is also evident in the dichotomy *descriptive* and *concept formation*. Quantitative approaches tend to be more descriptive, in that phenomena and their relationships are described, to confirm predictions made by theory. Qualitative approaches, in contrast, refer to concept formation, meaning personal perspectives, experiences and understandings of phenomena. Therefore, quantitative and qualitative research approaches do not need to be mutually exclusive. The one approach can complement the other. Some researchers even prefer to combine both research methods, which are known as mixed method research (Bergman, 2008; Strydom, 2009). According to Denzin as cited in (Keeves, 1988), reality is better understood when mixed research methods are used and it is therefore deemed as the ideal research approach to interpret reality. For this study, mixed research methods were utilised to collect and analyse data.

3.5 RESEARCH DESIGN

Both quantitative and qualitative research approaches make use of specific research designs. A research design is the blueprint/structure to conduct research (De Vos et al., 1998) and link the research methodology of a research approach to the research methods (Gelo et al., 2008). Therefore, research designs are used to obtain reliable and legitimate answers to research questions (Johnson and Onwuegbuzie, 2004). Quantitative research design can be experimental or non-experimental and qualitative research design is naturalistic. The research methods used during this study were specifically applied to collect data that coherently addressed the problem of this study. The use of both quantitative and qualitative research approaches, which refers to concept generation, meaningful personal perspectives, experiences and conducting experiments, as described by (Gelo et al., 2008), established the environment to analyse and interpret the collected data in order to achieve the aim of this study. This encouraged the execution of numerous experiments to provide statistical analyses and descriptions of the procedures and methods followed during the empirical research phase of this study.



The empirical component of this study was pragmatically executed, which means that the study was context-driven (Gelo et al., 2008; Onwuegbuzie et al., 2009). The data were collected in a specific manner (systematically and empirically) by conducting various experiments. The TerraSAR-X GCPs were acquired from Airbus Defence and Space covering the Pretoria CBD, South Africa. All other GCPs were manually collected from the pre-selected area by conducting a field experiment. The Pretoria CBD area was deliberately and consciously selected to be the sample area, due to the following reasons:

- a) This area is characterised by a diverse topographical layout ranging from mountainous areas to relative flat plateaus;
- b) Easy access was available to this area where GCPs could be manually collected; and
- c) The image data covering the sample area was easily acquired.

The research methodology followed during this study allowed the researcher to have complete control over the selection of GCPs to use for performing orthorectification experiments to create the master image. This ensured that an optimum ortho-image was created that would be used as the benchmark image. This image was used to test and evaluate the orthorectification results of all other ortho-images produced from simulated orthorectification experiments using vector layers as a means to acquire GCPs in remote areas.

3.6 DATA ACQUISITION AND COLLECTION

There are three components central to the orthorectification processes that were used in this study, namely the spectral imagery, topographic (elevation) data and GCPs. Each of these items is discussed in more detail in the sections to follow, including how the selected data elements were incorporated into the study design.

3.6.1 Study area

The region of interest or study area identified for conducting the study was Pretoria, which is located within the South African borders. As part of the greater City of Tshwane metropolitan area, the 395 km² region of interest was deliberately selected to perform

the orthorectification tests, mainly for two reasons: primarily because the landscapes surrounding the Pretoria central business district are characterised by diverse topographical layouts with up to 375 m between the lowest and highest locations. It ranges from mountainous areas with natural ecosystems to relative flat plateaus covered by a variety of settlement patterns, typical urban activities and land uses (Figure 3.1). Secondly, it also made logistical and economic sense to conduct the study close to where the investigative entity reside due to the required field data collection and verification activities (Henrico et al., 2016).

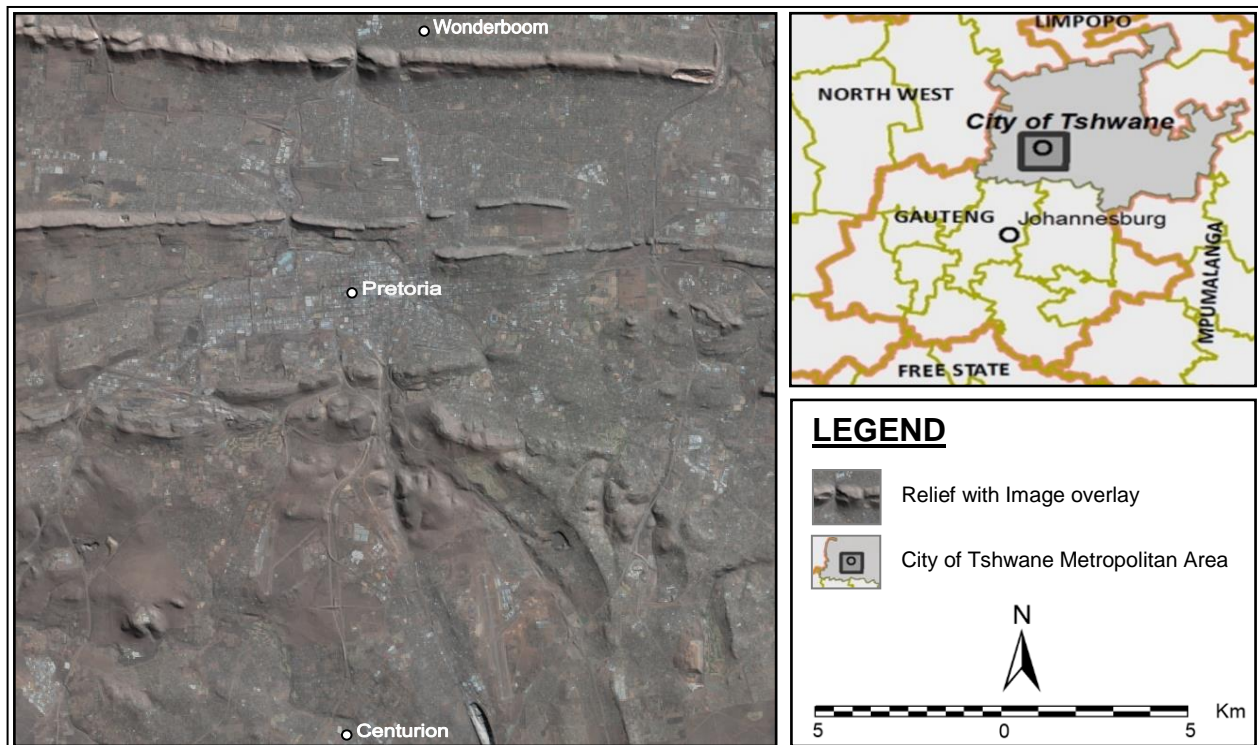


Figure 3.1: Geographical study area in the City of Tshwane Metropolitan Area

3.6.2 Data types (components) used during this study

3.6.2.1 Image data

It is imperative to use ‘raw’ satellite images when simulating any orthorectification process. For this reason, one Pléiades-1B primary panchromatic image was acquired from Airbus Defence and Space to perform all orthorectification experiments. Available at ~50 cm ground sampling distance (GSD), the primary product can be described as the processing level closest to the natural image acquired by the sensor. This image retains perfect collection conditions meaning that it is positioned in rectilinear geometry free from all radiometric distortions. The primary product is based on the Digital Image

Map (DIMAP)¹³ v2 structure (Figure 3.2) and consist of image files, DIMAP file (xml), KMZ file (kml), Icon.JPG, Preview.JPG, RPC file (xml), J2W file as well as Lineage, Masks, Library and an Index.htm (Airbus Defence and Space, October 2012; Panem et al., 2012).

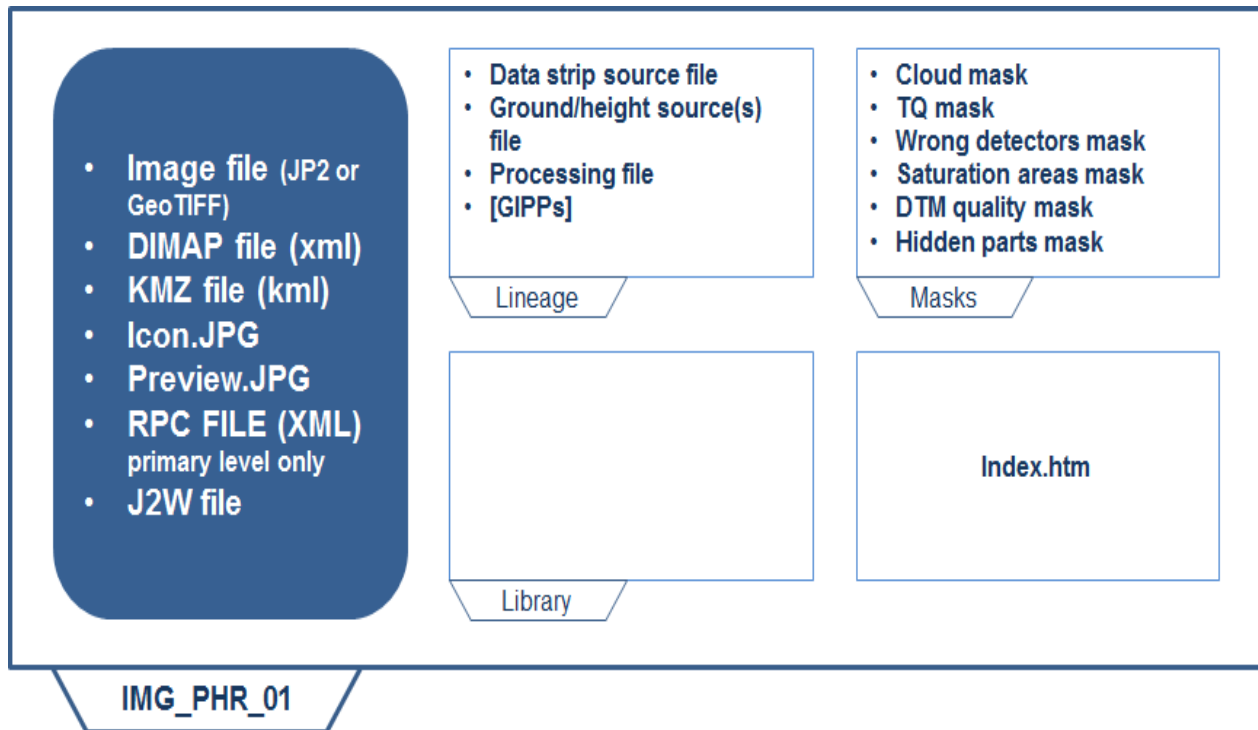


Figure 3.2: Pléiades DIMAP v2 structure

3.6.2.2 Elevation data

A digital elevation model signifies terrain relief by representing continuous elevation values through a regular collection of x, y and z values. These values are referenced to a shared datum to represent a topographic surface. DEMs, often known as digital height models (DHM) and digital terrain models (DTMs) are sometimes confused with the term digital surface models (DSMs). DTMs are digital representations of variables relating to a topographic surface and include heights and elevations, but also refer to geographical elements and natural features on the surface of the Earth, such as riverbeds and ridges. In contrast, a DSM reflects a land surface that includes the elevation of off-terrain objects, most commonly man-made features and vegetation. DEMs are either available as public products such as SRTM DTED1, ASTER GDEM v2, etc. or more precise and

¹³ The DIMAP format is a communal format that defines geographic data. It was developed by Centre National d'Etudes Spatiales (CNES), specifically for SPOT products.

fine scale DEMs can be obtained from commercial suppliers, for example the WorldDEM™ product from Airbus Defence and Space. Whichever is utilised during orthorectification, the DEM provides the necessary ground elevation and grey-level values to the input image, which are then used to create an ortho-image. The elevation data included in this study was acquired from two sources: one a subset from a well-known global DEM derived from synthetic aperture radar (SAR), the other from an airborne LiDAR campaign. The medium to high spatial resolutions of the DEMs included in the orthorectification test design were ultimately set at 30 m, 12 m and 2 m respectively, each covering the entire study region.

The Shuttle Radar Topography Mission (SRTM) was executed from 11 to 22 February 2000, using the Endeavour space shuttle. This mission was jointly executed by NASA and the NGA in an attempt to create elevation data of the entire Earth's surface. During the mission, eighty percent of the Earth's surface was covered in 1 arc-second data-points. The data were processed from raw C-band radar signals to create elevation data with a resolution accuracy of 30 m as measured at the equator. These data were resampled to 90 m (3 arc-second) for open distribution outside the United States (Farr et al., 2000). However, on 23 September 2014, the US Government announced the worldwide release of the base SRTM data. For this study, the 1 arc-second (~30 m) SRTM elevation data (v3) were downloaded in GeoTIFF format from the dedicated USGS site (<http://earthexplorer.usgs.gov/>). The SRTM DEM metadata and identification information that accompanied this data are attached at the back of this documents as Appendix A. Based on other local preliminary study results, the absolute horizontal accuracy expected from this popular global DEM product across the target area was ≤ 11.9 m (90% Confidence Interval (CI)) and the absolute vertical accuracy ≤ 5.6 m (90% CI). The current DEM version still contains significant localised non-ground values (e.g. dense vegetation or large and tall built-up structures), rendering it more of a DSM than a true DTM, which represents a 'bare Earth' model. Although not present in this study area, other known artefacts could include voids and systematic errors in the SRTM elevation surface. Using the appropriate software, these artefacts are commonly reduced or eliminated with standard DEM post-processing routines.

Conversely, the highest spatial resolution DEM used in this study were derived from LiDAR data collected over the entire City of Tshwane during August 2013. In an e-mail

on 15 February 2016, A. Breytenbach¹⁴ stated that the point cloud data were captured at ± 8 observations per square meter using a Leica ALS50 sensor and thirty percent overlap. The point cloud returns were subsequently classified into ground and non-ground layers. These classified x, y and z measurements (ground and non-ground) formed the primary input when generating both a seamless 32-bit DTM and DSM base product at two meter GSD. This was achieved mainly by executing the well-known ANUDEM algorithm¹⁵ (Hutchinson, 2011) and other DEM quality enhancements routines (e.g. terrain filtering, interpolation and removing noise) during a DEM processing chain customized specifically for this task. This DTM – with a recorded absolute horizontal (and vertical) accuracy of sub-meter proportions – then served as input in the orthorectification tests. Permission to utilise this data was granted by the City of Tshwane Metropolitan Municipality (refer to Appendix B for Letter of Request).

The remaining third DEM used in this study, a 12 m DTM, was created by resampling the 2 m DTM (using a bilinear interpolation method): first by creating a 5 m product, which in turn was resampled to create a 12 m DTM. This was done to create an acceptably smooth and spatially accurate digital elevation source that could represent the highly anticipated WorldDEM™ product, which became commercially available since the latter part of 2015, but was unobtainable for this study. Again, the recorded absolute accuracy of this 12 m elevation surface was comparable to that of the 2 m base DTM (≤ 1.0 m). The quality and detail of these DTMs are visually shown (hill-shaded) in Figure 3.3 compared to the 30 m SRTM DEM over a portion of the study area.

¹⁴ Breytenbach, A. (abreytenbach@csir.co.za), (15 February 2016). *2 m DTM creation and processing*. E-mail to: Henrico, I. (ivan.henrico@sita.co.za).

¹⁵ It is stated in the ANUDEM Version 5.3 User Guide (Hutchinson, 2011) that the ANUDEM a program is which was developed by Professor M. F. Hutchinson (Professor of Spatial and Temporal Analysis, Fenner School of Environment and Society, Australian National University, Canberra). It “*calculates values on a regular grid of a discretised smooth surface fitted to large numbers of irregularly spaced elevation data point, contour lines, streamlines, sink points, lake boundaries and cliff lines. The program imposes a global drainage condition that automatically removes spurious sinks where possible.*”

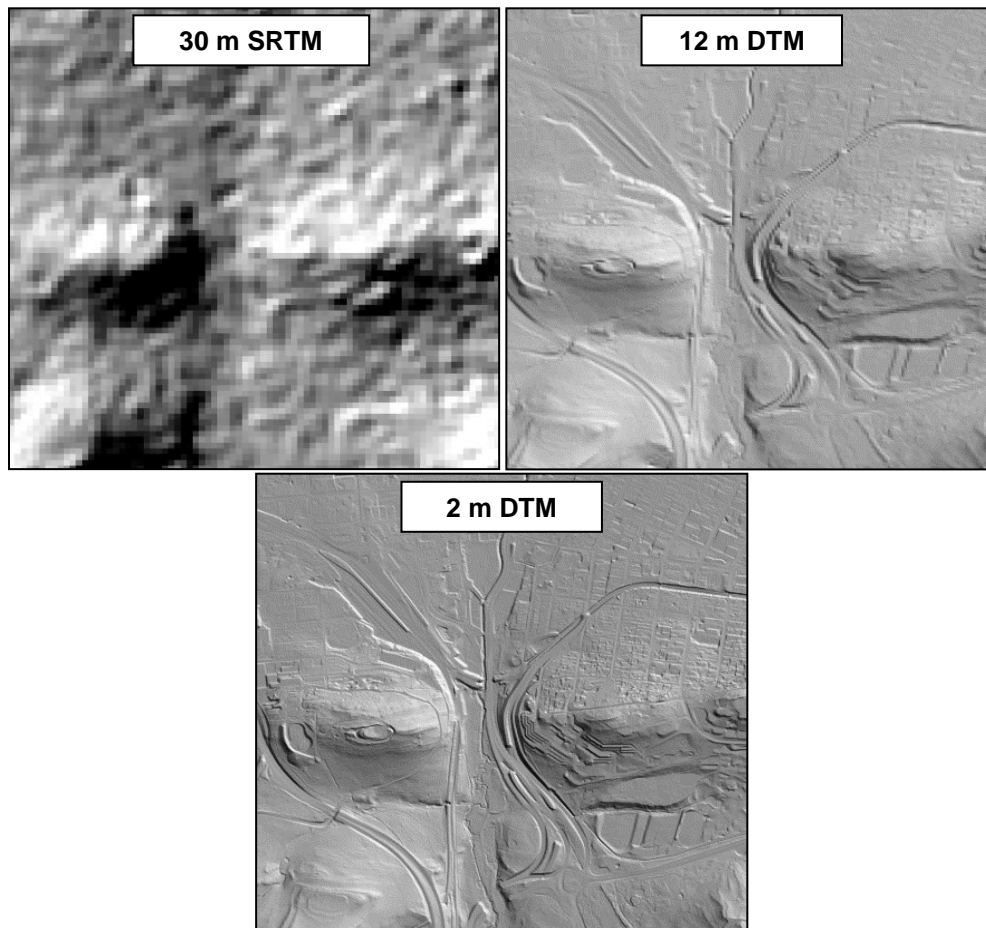


Figure 3.3: Illustrating the differences in the spatial resolution between the three DEMs

3.6.2.3 Ground control points

3.6.2.3.1 GPS device based GCPs

Twenty-five GCPs were captured using two Trimble® GeoExplorer® 6000 series handheld (model: GeoXH 3.5G) GPS devices (Figure 3.4), preloaded with the Trimble® TerraSync software. Permission to acquire and utilise these devices was requested from Optron (Pty) Ltd., see Appendix C for Letter of Request). The GeoXH 3.5G handheld uses both EVEREST and H-Star technology to obtain 10 cm accuracy during real-time operation or after post-processing (Trimble, February 2011). It is stated by Trimble (August 2014) that the Trimble® GeoExplorer® collects all Global Navigation Satellite Systems (GNSS) data in “*the World Geodetic Datum of 1984, the latitude/longitude coordinate system and the Height Above Ellipsoid*”¹⁶ (HAE) altitude reference.

¹⁶ Ellipsoid is a mathematical model of the Earth’s size and shape and HAE represents the distance from the ellipsoid to the geoid (MSL).

Configuring the TerraSync software to a different coordinate system only affects the display of the coordinates. It does not convert the data. Height values can be expressed as height above the ellipsoid (HAE) or as height above mean sea level (MSL), the latter was selected during this study. Post-processing of these points is discussed in more detail below. Mean sea level is an approximated distance between the geoid¹⁷ and the ellipsoid, known as geoid height. Conversions between these two height references are performed by the TerraSync software for display purposes on the device and by the Trimble Pathfinder Office software for importing and exporting the data (see Figure 3.6).



Figure 3.4: Trimble's GeoExplorer 6000 series handheld (model: GeoXH 3.5G) GPS device (Copyright © Trimble Navigation 2014)

South African TrigNet data were utilised to achieve accurate GCPs after post-processing. TrigNet consists of GNSS base stations that are permanently and continuously in operation to record 1-second epoch data on both L1 (1575.42 MHz – 10.23 MHz x 154) and L2 (1227.60 MHz – 10.23 MHz x 120) GPS frequencies (Geoconnect, 2016). Global Navigation Satellite Systems consists of a constellation of satellite-based systems which data are utilised for navigation and positioning on the

¹⁷ Geoid a reference system that considers the Earth's gravitational pull, which varies from place to place, to model the true size and shape of the Earth.

Earth's surface, in the air or in orbit (Combrinck, 2009). Combrinck (2009) states that the GNSS constitute four systems, namely:

- a) Global Positioning System (GPS) – developed by the USA;
- b) Global Orbiting Navigation Satellite System (GLONASS) – developed by the USSR;
- c) Galileo – created by the European Union (EU) in partnership with the European Space Agency (ESA); and
- d) Beidou (meaning 'Compass') – developed by the People's Republic of China.

In South Africa, the data received from GNSS are streamed in real-time to the TrigNet control centre situated in the offices of the Chief Directorate: National Geospatial Information located in the Western Cape. There are currently three TrigNet Network Real Time Kinematic (RTK)¹⁸ solutions (Figure 3.5) created within a Virtual Reference Station (VRS) network, which are situated in the Western Cape, Gauteng and Kwa-Zulu Natal provinces (<http://www.trignet.co.za>). The following real-time data are provided:

- a) Differential GPS (DGPS) at ~35 cm;
- b) RTK at ~5 cm; and
- c) Network RTK at ~3 cm.

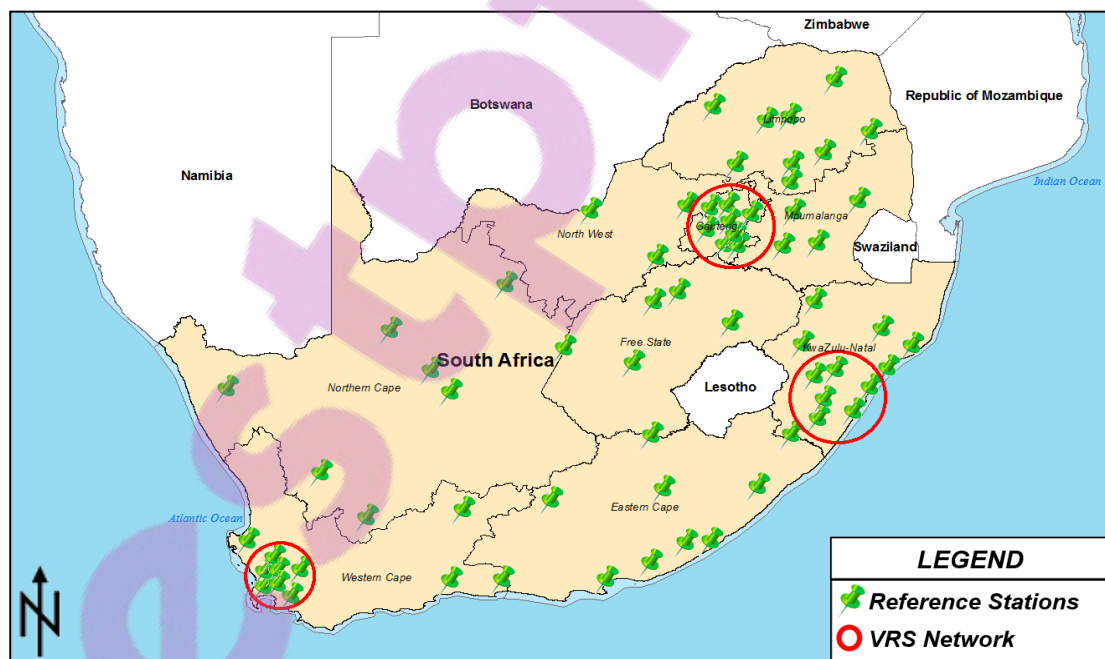


Figure 3.5: South African TrigNet Stations (Copyright 2014, Trimble Navigation Limited)

Adapted from National Geospatial Information (2014)

¹⁸ RTK is a satellite navigation technique used to enhance the positional accuracy derived from satellite-based positional systems.

The distribution of the manual collected GCPs were pre-determined by identifying the precise locations on the Earth’s surface where the GCPs need to be collected. This was done by evaluating the satellite based image data of the geographical area of interest in order to achieve a uniform distribution of GCPs covering the entire sample area. The centre and four corners of the image were used as the starting point for determining the position of the GCPs. Post-processing of the GCPs consisted of differential correction by utilising the TrigNet Pretoria GNSS data as the base and reference provider. One-second epoch data were downloaded in Receiver Independent Exchange (RINEX) format from the TrigNet Web Application for the specific period during the capturing of the GCPs. The post-processing was performed by importing the data which were captured in HAE, into the Trimble Pathfinder Office 5.6 software. The default settings were used on the software the import the captured points (*.ssf) and export the data to shapefile format (*.shp). If the data were captured in MSL, the settings had to be altered to select MSL as the altitude measured reference type and the EGM96 Geoid (Global), which is the default Geoid selected by the software. However, the data was captured in HAE (only displaying it in MSL on the device) and therefore the default HAE settings were used on the software. See Figure 3.6, for default settings used:

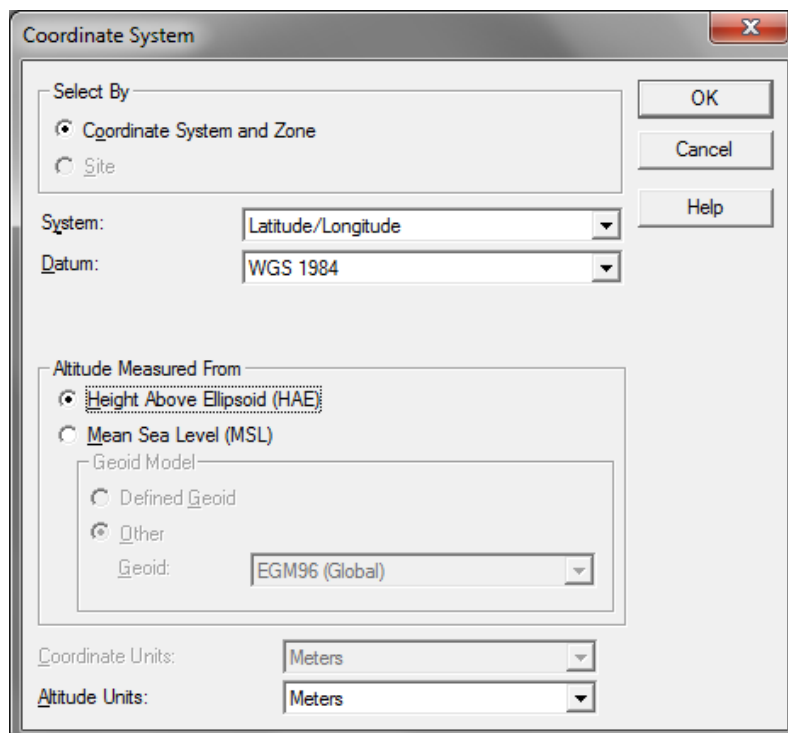


Figure 3.6: Trimble Pathfinder Office 5.6 software post-processing settings

The accuracy results of the GCPs achieved from performing the post-processing shows that 85.63% of all GCPs have a 3D (vertical and horizontal) positional accuracy between

0.05 – 0.5 m and 14.37% of the GCPs have a 3D positional accuracy between 0.5 – 1.0 m (see Appendix D) It can therefore be stated that all GCPs have a positional accuracy of less than 1.0 m. However, since 85% of all GCPs have an accuracy of less than 50 cm, the error measurements considered during this study are 50 cm with a Circular Error probability of 85% (CE85). It is also important to realise that when determining the accuracy of the ortho-images from the experiments performed and presented in Chapter 4, the GCP error is added to determine the total location accuracy of each ortho-image (Henrico et al., 2016).



In this study, qualitative research methods were used to capture GCPs by means of conducting fieldwork. Each pre-determined location was physically visited to capture the required GCPs using the Trimble GeoXH 3.5G handheld device. Harrison and List (2004) state that field experiments provide a meeting ground for empirical science and differ from laboratory experiments in that they are less controlled. However, field experiments are methodological complementary to laboratory experiments (Harrison and List, 2004) in the sense that sampling is conducted without the perception that controls exercised are unnatural without any deception. Fieldwork started on 19 June 2014 and carried over to 24 June 2014 with the help and assistance of members from the Directorate Geospatial Information (SANDF) and from Hartebeesthoek Radio Astronomy Observatory (HartRAO). Figure 1.1 (Chapter 1) illustrates the selected distribution of the 25 GCPs. A GCP Checklist was compiled for each captured GCP. Most of the checklist detail was retrieved from the GeoXH 3.5G handheld devices. The checklist comprised of the following components (Table 3.1):

- a) The GCP number;
- b) The GCP coordinates in latitudes and longitudes;
- c) GPS altitude, which was measured in above mean sea level (MSL);
- d) Position error estimation, which indicates the real-time predicted horizontal positional accuracy of the device;
- e) Number of satellites, represents the satellites that the receiver is using to compute its current GNSS position;
- f) Description of feature provides a brief description of the feature that was captured as well as a photograph of the feature and the location identified on the Pléiades satellite image;



- g) Terrain type provides a short description of the topographical layout of the area surrounding the feature; and
- h) Remarks to state whether this feature is clearly visible and identifiable on the Pléiades satellite image.

Table 3.1: Sample of the GCP Checklist used during the fieldwork

GCP #	GCP #1	
GCP Coordinates (Lat & Long)	25° 48' 43.697" S 28° 09' 05.420" E	
GPS Altitude (above sea level)	1444 m MSL	
Position Error Estimation	16 cm	
No. of Satellites	16	
Description of Feature	Southern T-Connection of the 3 rd Tennis Court from the Right	
	<u>Photo</u>	<u>Satellite Image</u>
		
Terrain Type	Flat open surroundings with plexipave tennis court surface	
Remarks	This feature is clearly visible and identifiable on the satellite image	

GCP Checklists were compiled for all 25 GCPs collected during the fieldwork. These Checklists are attached at the back of this study as Appendix E.

3.6.2.3.2 TerraSAR-X GCPs

TerraSAR-X satellites provide accurate and outstanding quality GCPs from space. The accuracy of these GCPs is reliant on the TerraSAR-X orbit accuracy, the precise radar X-band beam and the high-resolution and location accuracy of the imagery, which is up to 0.25 m in range and azimuth for both Staring Spotlight and Stripmap products.

In a study conducted by Hummel (2011), using HR Spotlight scenes acquired from a four-flight TerraSAR-X data acquisition flight-plan, it is stated that TerraSAR-X GCPs are delivered with an unrivalled accuracy where GCPs have a horizontal accuracy of 1.0 m and a vertical accuracy of 0.5 m. These accuracies were achieved by measuring the

data against GPS measurements and the precise coordinates of corner-reflectors in a very diverse topographical area. TerraSAR-X-based GCPs are delivered in two standard accuracy products, namely:

- a) TerraSAR-X GCP-1: multiple Spotlight scenes are used to extract 5 GCPs with an accuracy of approximately 1 m, covering an area of ~20 km² and
- b) TerraSAR-X GCP-3: multiple Stripmap acquisitions are used to deliver 10 GCPs with an accuracy of approximately 3 m, covering an area of ~1 000 km².

This study used the TerraSAR-X GCP-3 product from Airbus Defence and Space, who was requested to provide a random distribution of 10 GCPs that covers the entire 395 km² sample area (Figure 3.7) to create a near ideal distribution for creating an ortho-image (Henrico et al., 2016).

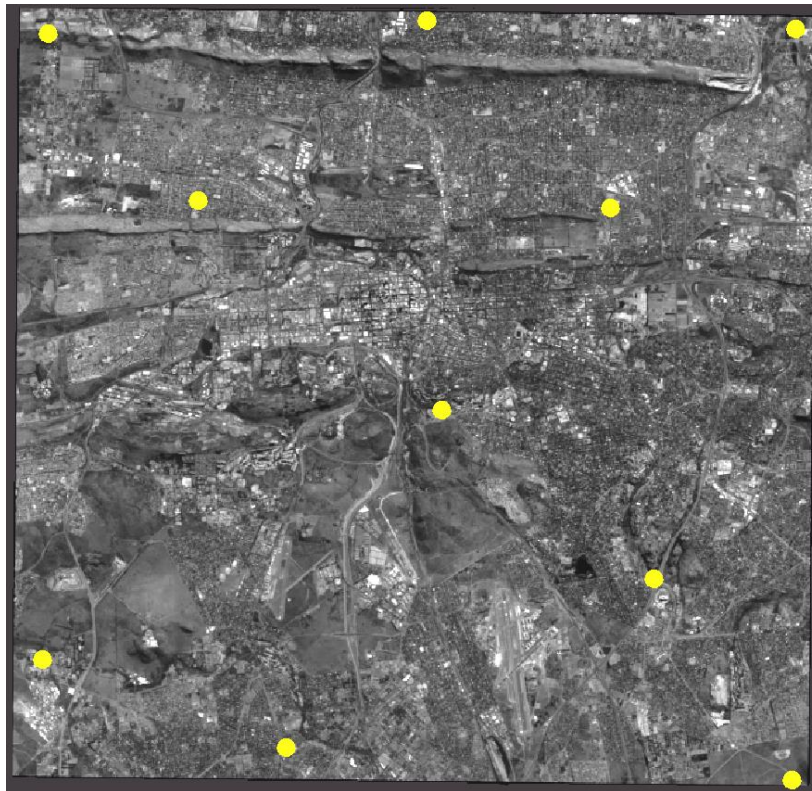


Figure 3.7: TerraSAR-X GCP-3 point distributions

It is stated in the TerraSAR-X GCP-3 Coordinate Specification and Accuracy Assessment file that the horizontal (H) and vertical (V) accuracy of each of the 10 GCPs acquired are 1 m for x, y and z locations (Table 3.2). These accuracies achieved from multiple Stripmap acquisitions are very good, which is equivalent to the stated TerraSAR-X GCP-1 product accuracy. The TerraSAR-X GCP location sheets, as received from Airbus Defence and Space, are attached as Appendix F.

Table 3.2: TerraSAR-X GCP-3 coordinate specification and accuracy assessments

ID	Coordinates (UTM)*		Ellipsoid Height	UTM Zone	Coordinates (Geographic)		Accuracy	
	Easting	Northing			Latitude	Longitude	H	V
1	629581.679	7139801.673	1527.505	35S	-25.85440758	28.29315271	1	1
2	610787.24	7158649.929	1458.289	35S	-25.68578606	28.10404905	1	1
3	629691.94	7158772.17	1284.251	35S	-25.68313520	28.29239641	1	1
4	620748.943	7149146.143	1402.556	35S	-25.77080309	28.20416964	1	1
5	620354.913	7158978.25	1275.77	35S	-25.68206919	28.19934997	1	1
6	614590.54	7154449.11	1329.238	35S	-25.72342109	28.14230690	1	1
7	626106.521	7144871.115	1531.991	35S	-25.80894594	28.25799534	1	1
8	625004.879	7154260.968	1330.711	35S	-25.72426897	28.24612224	1	1
9	616815.37	7140615.775	1464.359	35S	-25.84813641	28.16570215	1	1
10	610634.665	7142848.078	1402.269	35S	-25.82846428	28.10384714	1	1

* **UTM**: Universal Transverse Mercator – easting (x-coordinate) and northing (y-coordinate) measured distance.

3.6.2.4 Vector layer

A road vector layer was self-created by driving a motor vehicle and capturing four separate GPS tracks using a Garmin ETrex GPS, covering the sample area. These four tracks were merged and converted to create a single polyline (i.e. *.shp – shapefile). This polyline was then split into four segments used to simulate various scenarios when GCPs are irregularly distributed (North, East, West and South) to cover only specific areas within an image scene. See Chapter 1, Figure 1.2 for distribution of vector layer across the sample area. The segmentation was done to test the use of a vector road layer as a source for collecting GCPs and the affect that these GCPs will have on the pointing accuracy of the resulting ortho-image.

For each scenario, GCPs were extracted from the various road segments to perform the required orthorectification. It is important to take note that vector layer capture using handheld ETrex will be less accurate than the GCPs captured by the GeoXH 3.5G handheld devices (see Paragraph 3.6.2.3.1). The reasons for this are:

- a) The ETrex device uses only L1 frequency which includes significant ionospheric error, which is described by Wang (2010) as refraction (caused by ionized gases that effects “*the velocity of propagation of the GPS radio signals*”).
- b) The nature of the data captured by the ETrex does not permit post-processed to the same level as the GCPs that were captured by the GeoXH 3.5G handheld GPS devices.

The ETrex handheld device was deliberately selected to capture less accurate vector road layers that could be used as a source of extracting GCPs. These GCPs could then be used to perform orthorectification for the purpose to test the influence of less accurate GCPs to the process of performing orthorectification. It was mentioned in Paragraph 1.2.1 that the collection of GCPs could become a problem when moving outside the South African borders and in such cases, only vector road layers (Tracks4Africa and OpenStreetMaps) are available as a source for extracting GCPs. For example, the primary navigation device of the South African National Defence Force (SANDF) is an ETrex handheld GPS. The SANDF only operates outside the South African borders and using ETrex handheld devices are the only means available to them for collecting ground control. It was therefore an important part of this study to include “*bad*” GCPs to perform orthorectification and measure the resulting ortho-image against the master image which was created from using very good GCPs. The results achieved from performing these orthorectification experiments would therefore assist the SANDF in determining the probable orthorectification accuracy that could be achieved from using ETrex vector road layers as a source of extracting GCPs.

3.7 DESIGN OF EXPERIMENTS

It was stated in Paragraph 3.5 that numerous orthorectification experiments were conducted during this study, which are presented in Chapter 4. This study comprised of three stages and each stage consisted of different orthorectification experiments:

- a) Stage 1: concluded with the identification of the master image, which was used as the benchmarked image for evaluating all ortho-images produced during stage 3.
- b) Stage 2: consists of two orthorectification experiments that were conducted. The first experiment utilised the TerraSAR-X GCPs and the 2 m DTM and the second

experiment followed the parametric approach without the use of GCPs, but also utilised the 2 m DTM.

- c) Stage 3: entails various orthorectification scenarios that were simulated using vector road layers as a means to extract GCPs. Only the 2 m DTM was used during each of these simulated orthorectification experiments.

These stages are discussed in more detail below.

3.7.1 Description of the stage 1 experiments

During stage 1, nine orthorectification experiments were performed where the number of GCPs in the image scene and the DEM quality were altered in each case. This design was briefly discussed in Chapter 1, Paragraph 1.2.1 and illustrated by Figure 1.1., where the Pléiades image was the backdrop for the desired number of uniformly distributed GCPs used in each experiment, as well as indicating the three DEMs used.

All experiments were conducted in the same manner, with only the number of GCPs utilised and quality of the DEMs that differed. This allowed for advertently testing the location accuracy of an ortho-image when the number of GCPs and the quality of an elevation source are altered. During stage 1, Hypothesis 1 (H_1) and research question 1 (presented in Paragraph 1.2.2) was tested and answered. The manually collected GCPs (described in Paragraph 3.6.2.3.1) were utilised during the stage 1 experiments.

These experiments are summarised as follows:

- a) Experiments 1(a), (b) and (c): the first experiments utilized five GCPs, which were evenly distributed to cover the entire image scene (Figure 1.1(a)). The elevation data used differed. Experiment 1(a) was performed by utilising the 30 m SRTM DEM, 1(b) the 12 m DTM and 1(c) utilised the 2 m DTM.
- b) Experiments 2(a), (b) and (c): the second experiments used 13 GCPs (Figure 1.1(b)) and the elevation sources were altered in the same manner as was done during the first experiments.
- c) Experiments 3(a), (b) and (c): during these three experiments, 25 evenly distributed GCPs were used (Figure 1.1(c)) and again the elevation sources were altered in the same fashion as done in the previous experiments.

3.7.2 Description of the stage 2 experiments

During stage 2, two independent orthorectification experiments were conducted which led to the testing of Hypotheses 3 and 4. Firstly, the TerraSAR-X GCPs acquired from Airbus Defence and Space and the 2 m DTM were utilised to create an ortho-image. This image was compared to the master image created during stage 1. This was done to determine the accuracy of ortho-images when using the TerraSAR-X GCPs compared to the ortho-images created from utilising accurate manually captured GCPs. This experiment allowed for answering research question 4. Secondly, one experiment was conducted by following the parametric approach without the use of GCPs. The specific rigorous sensor model (Pléiades Orbital Pushbroom) was selected and orthorectification was performed with the use of the 2 m DTM. The execution of this experiment allowed for answering research question 5 which was to determine if a geometrical sensor model used in isolation with a DEM could result in a comprehensive accurate ortho-image.

3.7.3 Description of the stage 3 experiments

The stage 3 orthorectification experiments were conducted to simulate various scenarios when GCPs are irregularly distributed and selected from vector road layers to cover only specific areas within an image scene (Figure 1.2). During stage 3, Hypothesis 2 (H₂) was tested and research questions 2 and 3 were answered (Paragraph 1.2.2). All ortho-images produced from these experiments were compared, measured and analysed against the master image to determine their accuracies.

Stage 3 consisted of six independent orthorectification experiments. Each experiment was performed by following the same procedural approach described earlier, utilising the parametric approach, adding GCPs and applying the 2 m DTM as the elevation source. However, for each experiment the distribution and cluster of GCPs differed:

- a) Experiment 01: represented a cluster of GCPs that were predominately distributed on the west side of the image;
- b) Experiment 02: was characterised by a cluster of GCPs that were distributed on the east side of the image;
- c) Experiment 03: signified a GCP distribution on the north side of the image;

- d) Experiment 04: was performed with a distribution of the GCPs on the south side of the image; and
- e) Experiment 05: had the GCPs distributed randomly across the entire image.

3.7.4 Validity and reliability of the data collected

Validity refers to the accuracy (Thomson, 2011) and manner a measurement actually measures what it is supposed to measure (Gravetter and Forzano, 2015; Thyer, 2009). Newman (1998) states that validity refers to the degree data analysis represents a true image of the phenomena that is researched. Alternatively, reliability refers to the degree of consistency, accuracy and stability demonstrated by an instrument or procedure, namely to consistently measure phenomena. Maree (2007) states that internal validity can be assured when the researcher exercises control over the dependable variables of a study. The variables over which control was exercised in this study were the selection of the locations of the GCPs that were manually collected with the use of two Trimble® GeoExplorer® 6000 series handheld (model: GeoXH 3.5G) GPS devices.

External validity has to do with the generalisation of results (Maree, 2007). The results of this study cannot be generalised to all types of satellite images, nor to all types of topographical layout, due to the following reasons:

- a) this study was limited to orthorectification experiments performed on only one type of satellite imagery, i.e. Pléiades-1B and
- b) the topographical layouts represented by the study area cannot simulate the vast variety of topographical physiognomies of the Earth's surface.

It is possible that the validity and reliability of the data collected during this study are influenced by the following factors:

- a) Location of GCPs that were manually collected.
- b) Number of GCPs used to perform all required orthorectification experiments.
- c) Type of image and elevation data used to conduct orthorectification experiments.
- d) Topographical layout of sample area.
- e) Image Processing System (IPS) used to conduct orthorectification experiments.

However, precautions were implemented to select good quality and a vast number of GCPs. The orthorectification experiments were conducted, utilising different quality types of elevation data. The sample area was characterized by differences in topographical layout, ranging from mountainous to relative flat plateaus. The ERDAS IMAGINE® 2015 (Version 15.00.0000, Build 212) image processing system, which is one of the world's leading IPSs was used to perform valid and reliable experiments.

3.8 DATA ANALYSIS

The data collected from all orthorectification experiments performed were descriptively analysed, contextualised and subjectively interpreted. Data results were supported by tables and charts that provided the necessary statistical analysis needed for comparison purposes. As was discussed in Chapter 1 (Paragraph 1.4.2.2), data analysis was performed by following two steps. The experiments performed during step 1 led to the creation of the master image that was used as the benchmarked image for comparing and evaluating the resulting ortho-images produced during step 2.

The accuracy assessment of each of the stage 1 ortho-images was done by considering the RMSE, utilising the ERDAS IMAGINE® 2015 Metric Accuracy Assessment tool and measuring specific image coordinates against the location accuracy of selected control points (CPs). The accuracy assessments performed were described in Chapter 2 (Paragraph 2.5). The CPs used during the accuracy assessments consisted of selected GCPs that were manually collected, as were described in Paragraph 3.6.2.3.1. During the stage 1 experiments, the manual GCPs collected and not used to perform orthorectification during the various experiments were utilised as checkpoints to compare the position of the orthorectified image pixels corresponding to the checkpoints. For all other experiments (stages 2 and 3), control points were derived from the master image created during stage 1.

During step 2, various scenarios were created to simulate the lack of GCPs that are irregularly distributed across an image scene. During these experiments, GCPs were extracted from a vector road layer. Each resulting ortho-image created from these experiments was measured against the master image to determine its accuracy deviation. Again, the ERDAS IMAGINE® 2015 Metric Accuracy Assessment tool was

utilised to perform accuracy assessments on each of these ortho-images. Ground control points used during step 2 were manually extracted from the master image. Accuracy was also determined by performing a visual assessment. Five features covering the corners and centre of each image were visually compared to the same features identified in the master image. Accuracy deviations were measured in distance and direction utilising the ERDAS IMAGINE® measurement tool. The deviations of all images were statistically analysed and descriptions were provided to assess the effect of each scenario. A methodological approach was developed once all step 1 and step 2 experiments were conducted and analysed.

In addition to the experiments performed during steps 1 and 2, two independent orthorectification experiments were conducted, as were described in Paragraph 3.7.2. These ortho-images were assessed in the same manner as was described above.

It is evident from the discussion above that numerous orthorectification experiments were conducted during this study. The challenge was to control and standardise the write-up of results, but great care was exercised to ensure that data results were precise and were accurately presented, for not to confuse readers. All experiments described in the foregoing Paragraphs were performed and the results achieved are presented in Chapter 4.

3.9 CHAPTER SUMMARY

In this chapter, the research methodology used during this study was discussed. Quantitative and qualitative research methods were used to collect and analyse data. The three stages of the empirical research, which constitute the various experiments conducted, were described in detail. This chapter concluded with a description of the ways the data were analysed and assessed. In Chapter 4, the various orthorectification experiments conducted are presented, analysed and assessed. The testing of the formulated hypotheses and answering of the various research questions are also presented.



CHAPTER 4 – EMPIRICAL RESEARCH: ORTHORECTIFICATION EXPERIMENTS AND METHODOLOGICAL CONTRIBUTION

4.1 INTRODUCTION

In this chapter, various orthorectification experiments which were conducted are reported on. These experiments were executed following the described three stages mentioned in Chapter 1 (Paragraph 1.4.2) and Chapter 3 (Paragraph 3.7) and were conducted to answer the research questions formulated in Chapter 1 (Paragraph 1.2.2). This allowed for achieving the aim of the research study.

The first part of this chapter highlights the orthorectification procedure followed to perform all experiments utilising the ERDAS IMAGINE® 2015 software. In the second part of this chapter, the 3 stages of this study (Paragraph 3.7, Chapter 3) were executed, described and analysed. All results achieved were analysed to test the hypotheses that were described in Chapter 1 (Paragraph 1.2.2) as well as to answer research questions 1 – 5. The third part of this chapter includes the developed methodological approach, described in Paragraph 3.8 (Chapter 3).

All experiments are analysed in terms of assessing the RMSE, utilising the ERDAS IMAGINE® 2015 Metric Accuracy Assessment (MAA) tool with a circular error probability of 90 (CE90) and manually measuring the deviation between image pixels and control point locations by means of performing visual inspections, as were described in Chapter 2 (Paragraph 2.5).

4.2 PROCESS FOLLOWED TO PERFORM ORTHORECTIFICATION

The image data utilised to perform all orthorectification experiments was a Pléiades-1B primary panchromatic image. The image specifications, derived from the image data are:

- a) Date
 - i. Start Time: 2013-06-22T08:21:47.7003965Z
 - ii. End Time: 2013-06-22T08:21:50.5745405Z
- b) Acquisition Angles
 - i. Azimuth angle: 179.9385215110322°

- ii. Viewing angle across track: -2.47742048688397°
 - iii. Viewing angle along track: $-0.8376857852077595^\circ$
 - iv. Viewing angle: 2.61487709853089°
 - v. Incidence angle along track: 1.21285896753351°
 - vi. Incidence angle across track: 2.566416535262453°
 - vii. Incidence angle: 2.83788480340555°
- c) Solar Incidences
- i. Sun azimuth: 30.41611649132131°
 - ii. Sun elevation: 34.45905749013301°
- d) Ground Sample Distance
- i. GSD across track: 0.6995724595875451 m
 - ii. GSD along track: 0.710156999626317 m

Various approaches and processes exist to conduct geometric correction (orthorectification) on high-resolution satellite images. The Pléiades primary image is no different. One of the processes, which can also be applied to the SPOT images, are highlighted below (steps 1 – 6).

These images are received from image vendors in a specific file format that requires a particular process to conduct parametric orthorectification (F. Ferreira 2010, personal communication, 11 May). The stage 1, 2 and 3 orthorectification experiments performed during this study followed the same process. However, the sensor models and elevation data were altered to match the various experiment parameters. All experiments were performed utilising the ERDAS IMAGINE® 2015 image processing software (IPS) and the illustrations and descriptions indicate the workflow of this specific software (Henrico, 2012).

- a) Step 1 – Confirmation of the file structure: the primary product is based on the DIMAP v2 structure as was explained in Paragraph 3.6.2.1 and illustrated by Figure 3.2.
- b) Step 2 – Convert the DIMAP file (primary data) to Image file
 - i. It is important to realise that when performing parametric orthorectification utilising the specific sensor model, which in this case is the Pléiades Orbital Pushbroom model, then the DIMAP XML Document file needs to be used. This

is done by opening the DIMAP XML Document file in ERDAS IMAGINE® and converts it to an image file.

- ii. Save the newly created image file as an IMAGINE Image (*.img) with exactly the same name as the DIMAP file and save it in the same folder and file location as the DIMAP XML Document file.
- c) Step 3 – Deleting the map model and projection information: a Pléiades primary image received from the image vendor is for all purposes a ‘raw’ image, but contains a map model and projection data, which is inherent in the image. These data are necessary for orientation purposes when viewing the image. However, to spatially correct these images, the embedded map model and projection information need to be deleted. In ERDAS IMAGINE®, this function is performed by utilising the ‘Image Info’ tab. When the data are deleted, the image needs to be closed and re–opened, before any spatial correction operations can take place.
- d) Step 4 – Selecting the geometric map model and add the elevation source
 - i. Select the Pléiades Orbital Pushbroom geometric model. This loads the metadata file and update the model solution.
 - ii. Select the elevation source. This allows the process to account for the Earth’s curvature when orthorectification is performed.
- e) Step 5 – Select input and reference points and run the orthorectification process by selecting an output format: place input points that correspond to reference points. Reference points can be selected from different reference data sources such as GPS points, reference images, reference maps, vector file, ASCII files, etc., which consists of points with x, y and z values. Select an output image format (e.g. JPEG2000, TIFF, IMG, etc.) and the resampling method (nearest neighbourhood, bilinear interpolation, cubic convolution or bicubic spline) and run the process to create an ortho–image.
- f) Step 6: Evaluate ortho-image: the last step entails the evaluation of the newly created ortho-image. Open the ortho-image and evaluate the projection information as correct. Individual pixels can also be evaluated for the presence of x, y and z values. An autonomous method to evaluate if orthorectification was correctly applied is to assess the edges of an image for signs of elevation. This is easily identifiable through rough irregular edges, especially along edges characterised by mountainous terrain (Figure 4.1).

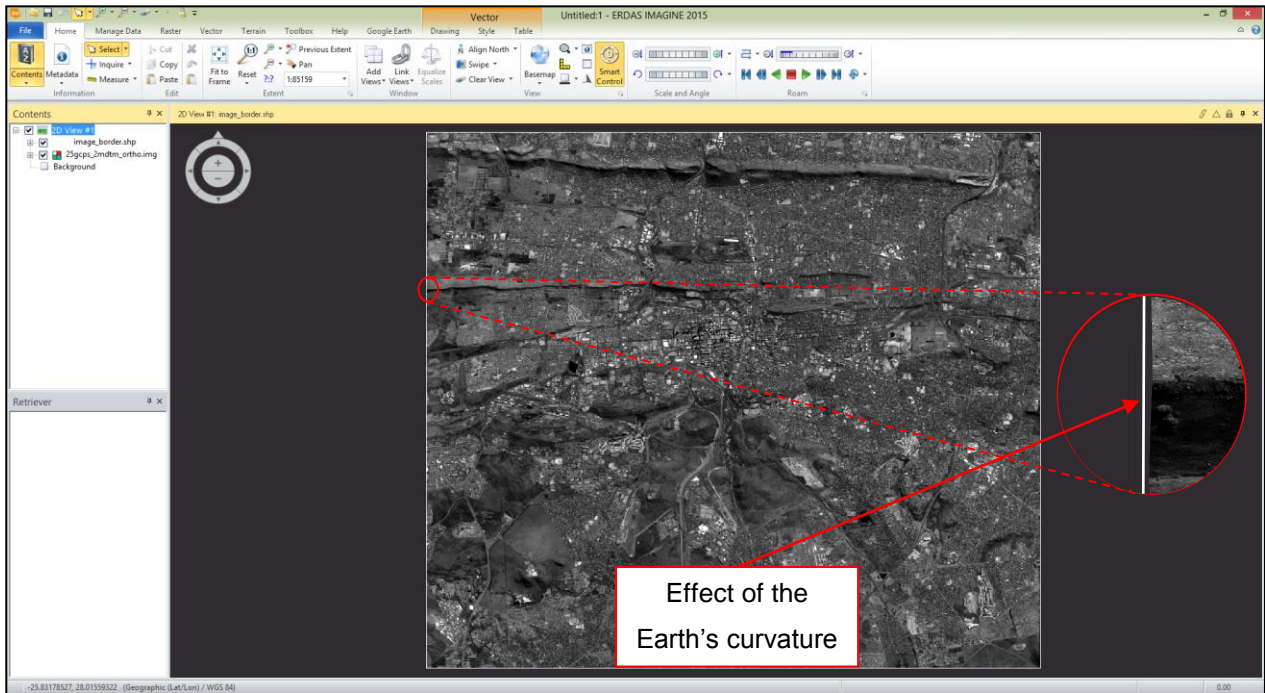


Figure 4.1: Evaluate rough irregular edges of ortho-image

4.2.1 Limitations of manually selecting and placing input GCPs

Absolute accuracy is very difficult to achieve when performing parametric orthorectification by selecting input and reference GCPs, because it is affected by variables such as the sensor orbital data and the elevation data. Another important factor that influences the accuracy of performing orthorectification is the involvement of the operator.

The operator will need to manually select and place input points (GCPs) to corresponding reference points on the primary image data. This can be a very daunting task, especially when working with HR and VHR satellite images even if the exact location of the reference points is known. The operator needs to identify the pixel location in the primary image that correspond to the specific reference point. This is achieved by zooming in to pixel scale on the primary image and identifying the location on the image to place an input point that corresponds to the reference point (Figure 4.2). It is advisable to place a backdrop image or map for orientation purposes to the reference data source viewing window.

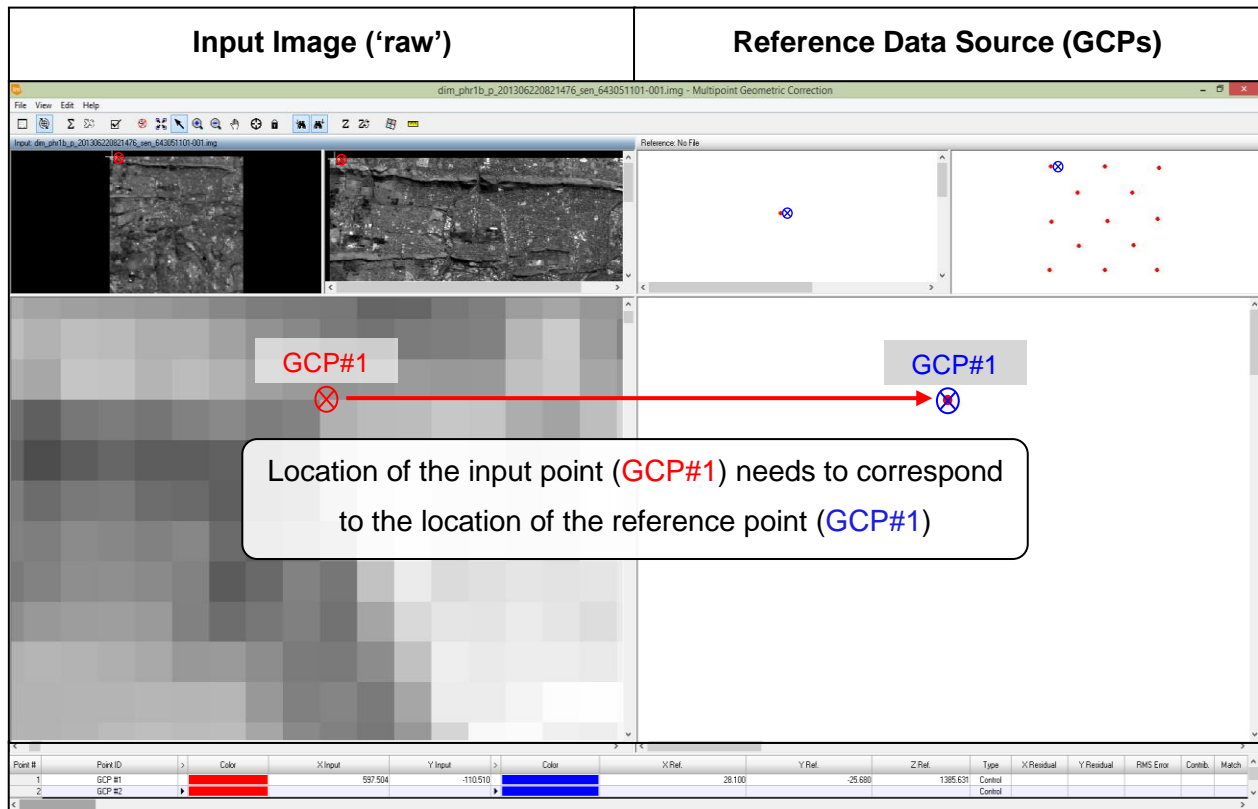


Figure 4.2: Placement of input point to correspond to reference points

From the aforementioned and by considering the literature study, it is evident that the accuracy of an ortho-image is dependent on the following factors, which need to be considered in preparing ortho products:

- a) The number, placement and accuracy of GCPs and the operators' ability to identify the locations on the primary image data to place input points that correspond to the locations of the reference points.
- b) The accuracy of the DEM.
- c) The sensor model used that corresponds to the approach applied: parametric (rigorous) or non-parametric (RPC).
- d) The inclination angle of the satellite.
- e) The capability of the IPS to implement the orthorectification mathematical model.

4.3 ORTHORECTIFICATION TESTS: STAGE 1 EXPERIMENTS

The experiments that encompass stage 1 of the empirical phase of this study are described in detail in Chapter 3 (Paragraph 3.7.1). All experiments are conducted in the same manner with only the number of GCPs utilised and quality of the DEM that differs.

The distribution of GCPs utilised to create each ortho-image is illustrated by Figure 1.1 (Chapter 1, Paragraph 1.2.1). In order to gauge the planimetric accuracy of the orthorectified image produced during these orthorectification tests, two commonly used statistical indicators and a manual measurement was recorded on each resulting image. The first statistic, the root mean square error, was calculated as (Equation 8):

$$RMSE_x = \frac{\sqrt{\sum(x_i - x_j)^2}}{n} \tag{8}$$

where : (x_i) is the x-coordinate in the ortho-image
 (x_j) is the control point's x-coordinate
 (n) is the total number of observations (GCPs)

The $RMSE_y$ was calculated in the same manner by substituting the x-coordinate values in Equation 8 with the respective y-values, shown by Equation 9:

$$RMSE_y = \frac{\sqrt{\sum(y_i - y_j)^2}}{n} \tag{9}$$

where : (y_i) is the y-coordinate in the ortho-image
 (y_j) is the control point's y-coordinate
 (n) is the total number of observations (GCPs)

To ultimately measure the radial distance ($RMSE_r$) from control (0, 0) to data point (x and y) – Equation 10 is used:

$$RMSE_r = \sqrt{RMSE_x^2 + RMSE_y^2} \tag{10}$$

where : $(RMSE_x^2)$ is the square root of $RMSE_x$
 $(RMSE_y^2)$ is the square root of $RMSE_y$

As mentioned in Paragraph 2.5.1, RMSE represents the pixel value a reference GCP is adrift from the input GCP. The pixel size of the Pléiades image is 0.5 m, therefore to express RMSE as a value of metres, the RMSE pixels value needs to be divided by the value 0.5. All experiments performed indicate either the RMSE pixel value, the converted value in metres or both values. Similarly, by using the image-identifiable GCPs, the second measure of accuracy was calculated using the Metric Accuracy

Assessment (MAA) tool available in ERDAS IMAGINE®. The GCPs, here referred to as Test and Evaluation (T&E) points, could simply be entered manually or read from the appropriate file (e.g. ASCII file). The manual measurement entails the process of measuring each T&E point to its correspondent pixel on the image utilising the ERDAS IMAGINE® measurement tool. After measuring each T&E point on the imagery, statistics were also calculated based on the error between the exact image coordinates and GCP coordinates, where after the MAA tool produced a report file containing individual point errors and statistics. Error computations are based on MIL-STD-600001, with bias taken into account. Using the calculated horizontal error as input, CE90 (circular error 90%) was then computed and recorded in each case. The MAA report for each experiment is attached as Appendices (Appendices G – O) at the back of this document.

Lastly, the manual measurements encompass visual inspections. All of the 25 collected GCPs are used as control points to physically measure the average directional deviation and distance error of corresponding image pixel locations. The ortho-image produced is used to zoom in to the exact pixel that represents each GCP. The centre of each pixel is used to measure the direction deviation and distance error using the ERDAS IMAGINE® measurement tool. The error deviations of each point are then illustrated using a PolarPlot diagram (see Figures 4.3 – 4.11).

Total accuracy of the ortho-images was ultimately calculated by dividing the sum of the values of the three accuracy measures/indicators (RMSE, MAA (CE90) and manual measurement) by three and then finally adding the GPS positional accuracy error of 50 cm, which was stated in Paragraph 3.6.2.3.1. The total accuracy achieved, for all stage 1 experiments, is indicated in Table 4.1. From the stage 1 experiments, the ortho-image with the highest level of accuracy was selected as the master image. This image was used as the benchmarked image for comparing and evaluating the accuracy all ortho-images produced from the stage 2 and 3 orthorectification experiments.

4.3.1 Experiment 1(a): Utilising 5 GCPs and 30 m SRTM DEM

Five GCPs were utilised to conduct the first orthorectification experiment. These GCPs were evenly distributed to cover the four corners and centre of the image scene and the

30 m SRTM DEM was used as the elevation source. The following accuracies were achieved:

- a) RMSE: the RMSE achieved was 4.6454 or 2.3227 m.
- b) MAA tool: the accuracy of the ortho-image created was measured against 25 CPs that were evenly distributed across the entire image scene. The CPs consisted of the GCPs that were manually collected during the data collection phase of this study (Paragraph 3.6.2.3.1). The accuracy assessment performed for this experiment show that the image has an accuracy of 2.371433 m (Appendix G).
- c) Manual measurements: these measurements show an average direction deviation of 202.91° and an average distance error of 1.46 m. This result is illustrated by the PolarPlot diagram below (Figure 4.3).

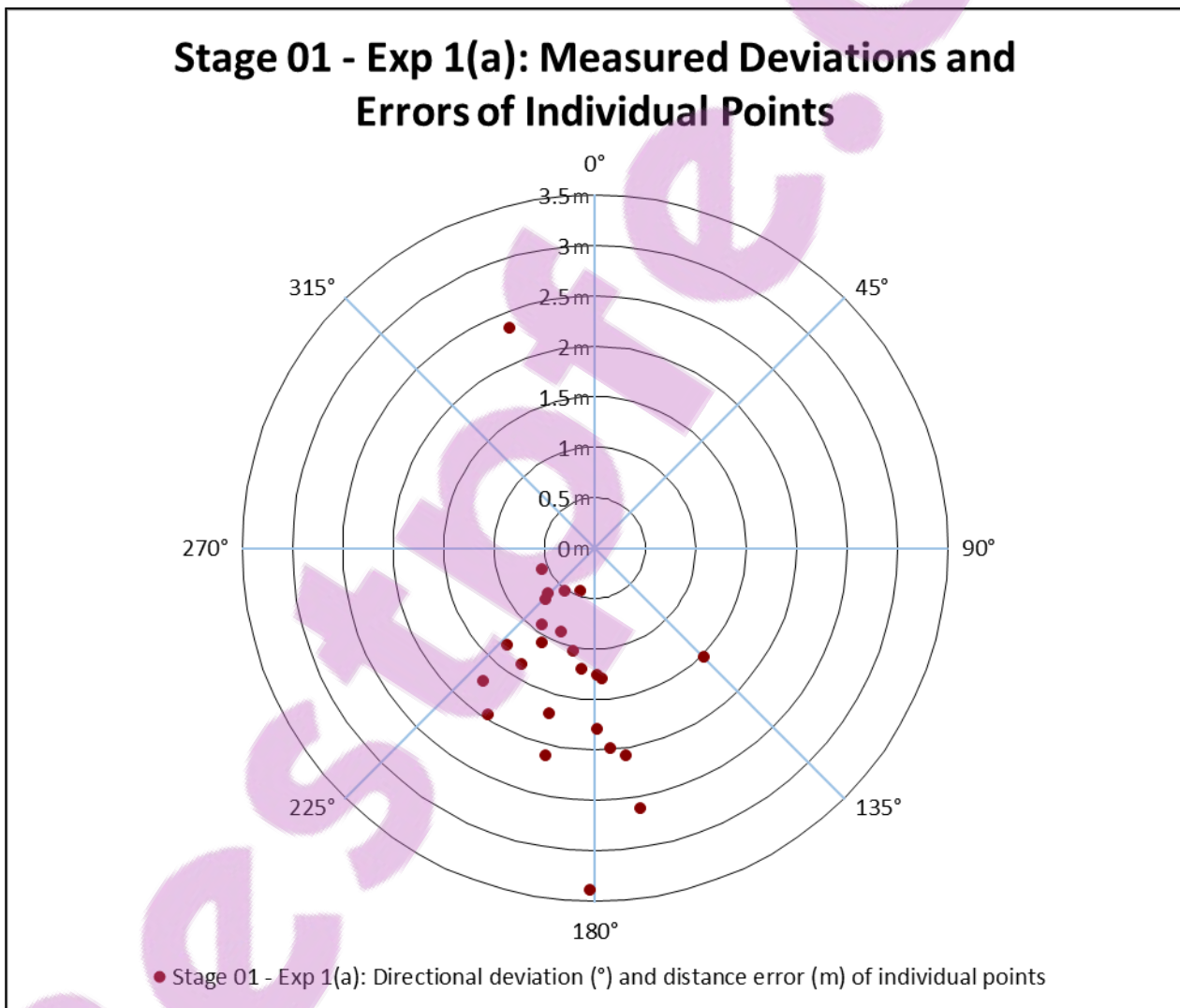


Figure 4.3: Stage 1 – Experiment 1(a): Measured deviations and errors against CPs

4.3.2 Experiment 1(b): Utilising 5 GCPs and 12 m DTM

This experiment was executed in the same manner as experiment 1(a). Five GCPs were utilised which covered the four corners and centre of the image scene. The only difference from the first experiment was that the 12 m DTM was used as the elevation source. The following accuracies were achieved:

- a) **RMSE**: the RMSE achieved from conducting this experiment, converted to metres, was 0.23 m. This is well within the normal guideline, which was determined to be 0.5 m (Paragraph 2.5).
- b) **MAA tool**: the MAA tool measured the accuracy at 2.338065 m (Appendix H).
- c) **Manual measurements**: the results achieved from utilising the ERDAS IMAGINE® measuring tool are illustrated below by Figure 4.4. The average direction deviation was 243.44° and the average distance error was 1.39 m.

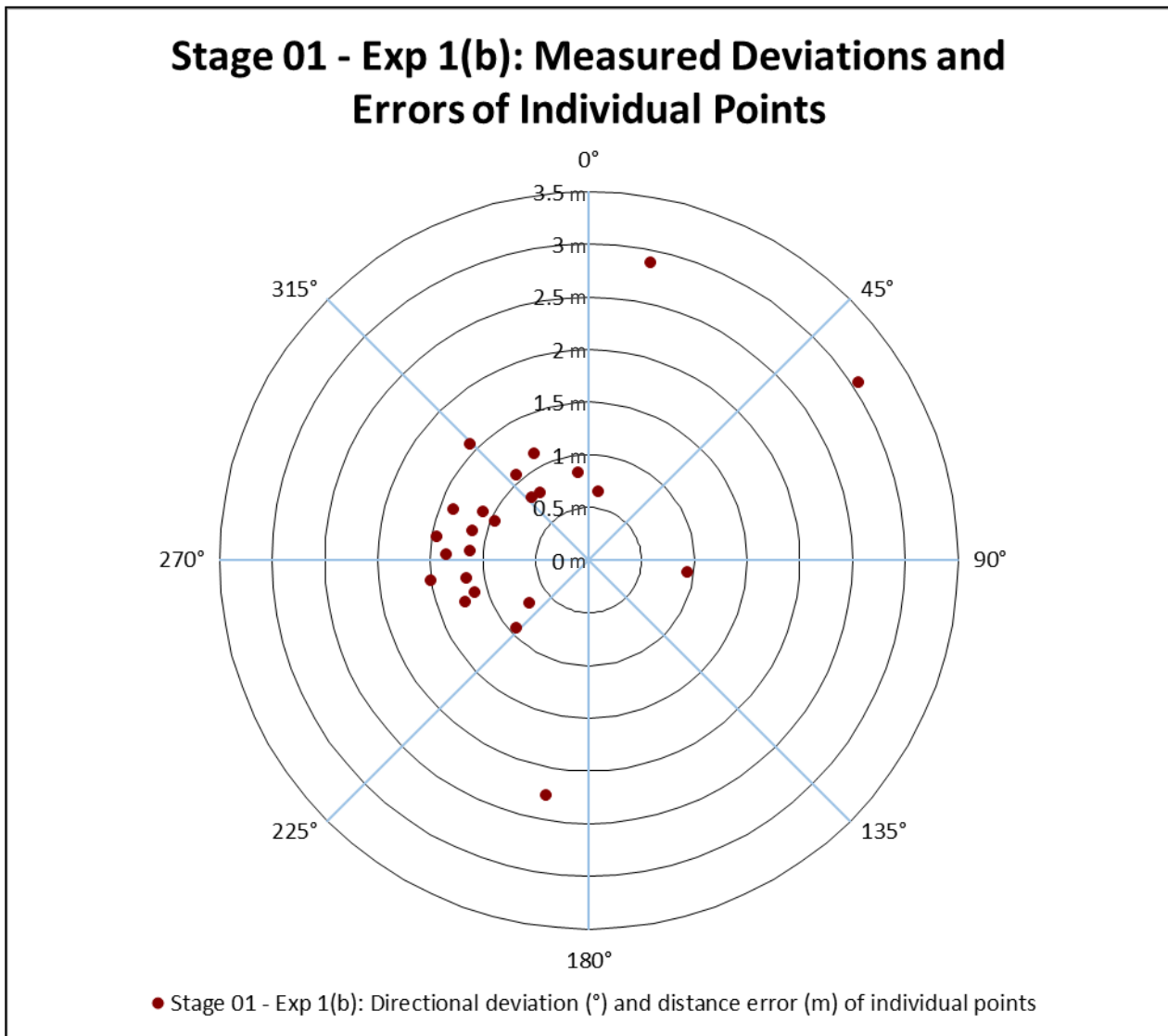


Figure 4.4: Stage 1 – Experiment 1(b): Measured deviations and errors against CPs

4.3.3 Experiment 1(c): Utilising 5 GCPs and 2 m DTM

This experiment was executed in the same manner as experiments 1(a) and (b), with only the elevation source that changed. For this experiment, the 2 m DTM was used. The following accuracies were measured:

- a) RMSE: the RMSE achieved from conducting this experiment was 0.4595, which is 0.22975 m (well within the 0.5 m normal guideline).
- b) MAA tool: the MAA tool measured the accuracy at 1.878747 m (Appendix I).
- c) Manual measurements: the results illustrated below by Figure 4.5, show the average direction deviation at 157.01° and the average distance error at 0.92 m.

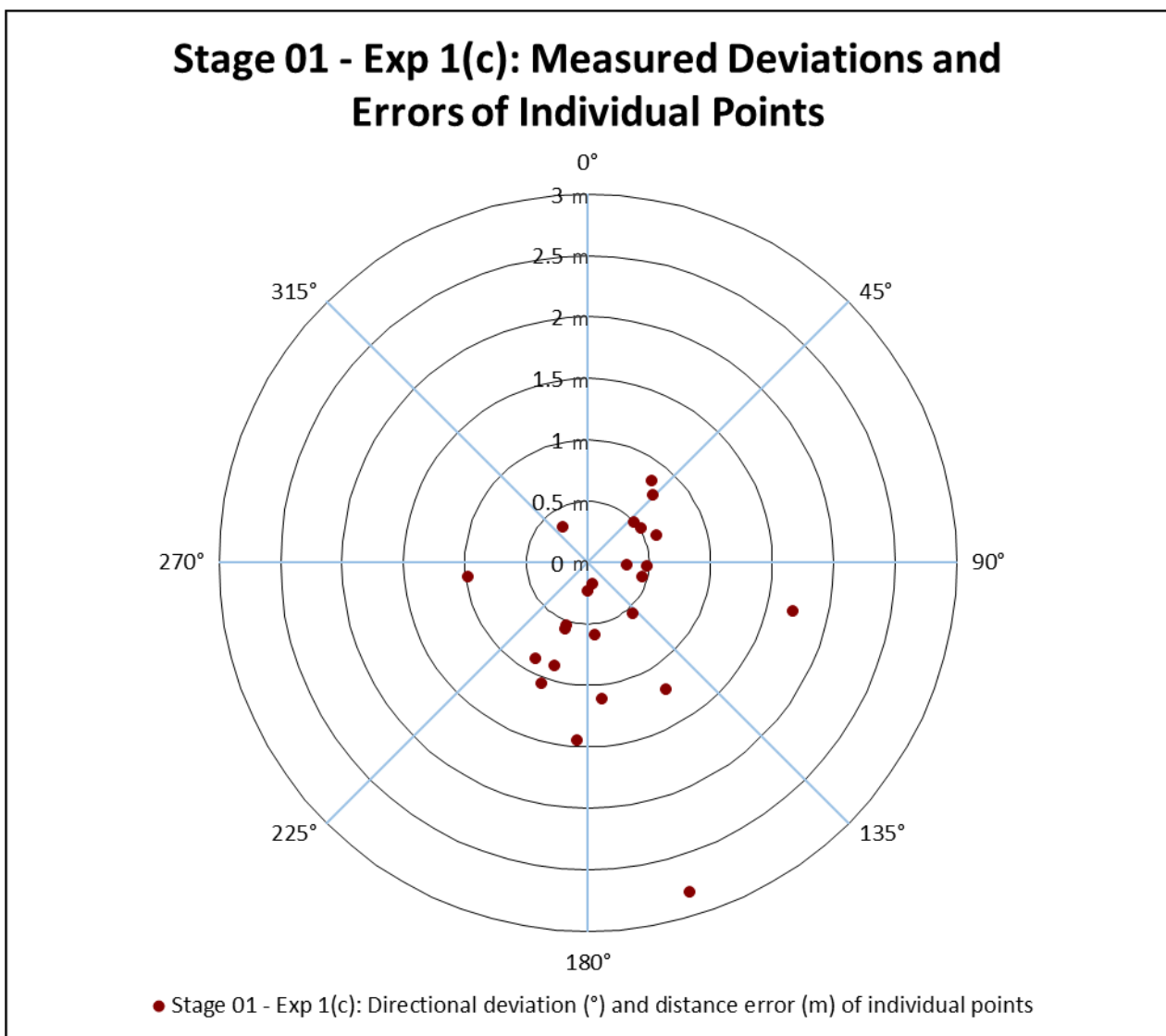


Figure 4.5: Stage 1 – Experiment 1(c): Measured deviations and errors against CPs



4.3.4 Experiment 2(a): Utilising 13 GCPs and 30 m SRTM DEM

Thirteen GCPs were utilised to conduct experiment 2(a). GCPs were evenly distributed to cover the entire image scene and the 30 m SRTM DEM was used as the elevation source. The following accuracies were measured:

- a) RMSE: the RMSE achieved from conducting this experiment was 2.0744 or 1.0372 m.
 - b) MAA tool: the MAA tool measured the accuracy at 1.552497 m (Appendix J).
 - c) Manual measurements: the measurement of each individual point shows an average direction deviation of 196.28° and an average distance error of 0.69 m.
- The distribution of measured points are illustrated by Figure 4.6.

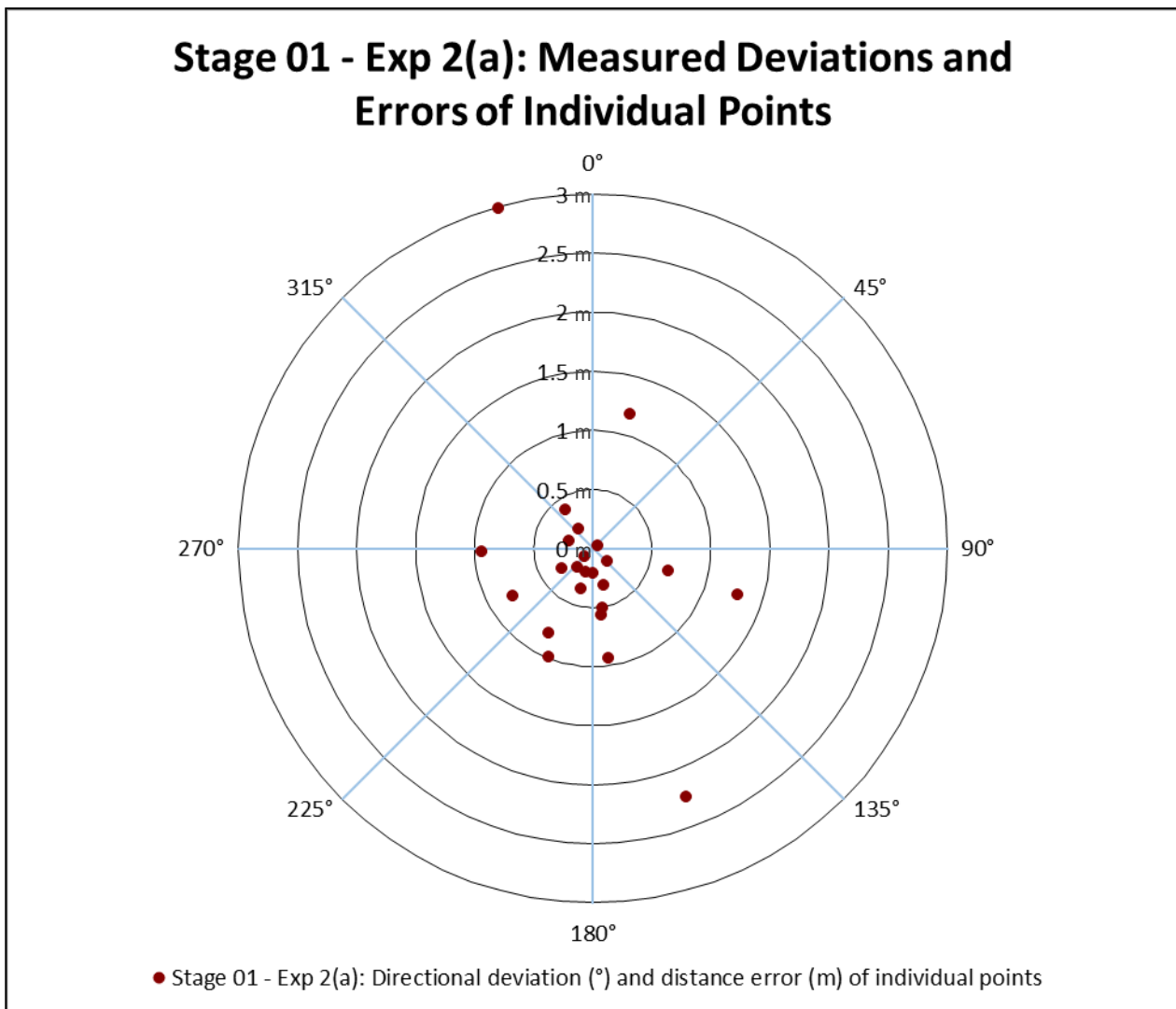


Figure 4.6: Stage 1 – Experiment 2(a): Measured deviations and errors against CPs

4.3.5 Experiment 2(b): Utilising 13 GCPs and 12 m DTM

As was the case with experiment 2(a), thirteen GCPs were utilised to conduct experiment 2(b). The 12 m DTM was used as the elevation source. The following accuracies were measured:

- a) RMSE: the RMSE achieved from conducting this experiment was 0.23 m, which is within the normal guideline of 0.5 m.
- b) MAA tool: this tool measured the accuracy at 1.546135 m (Appendix K).
- c) Manual measurements: the manual measurement indicates an average direction deviation of 244.07° and an average distance error of 1.00 m (Figure 4.7).

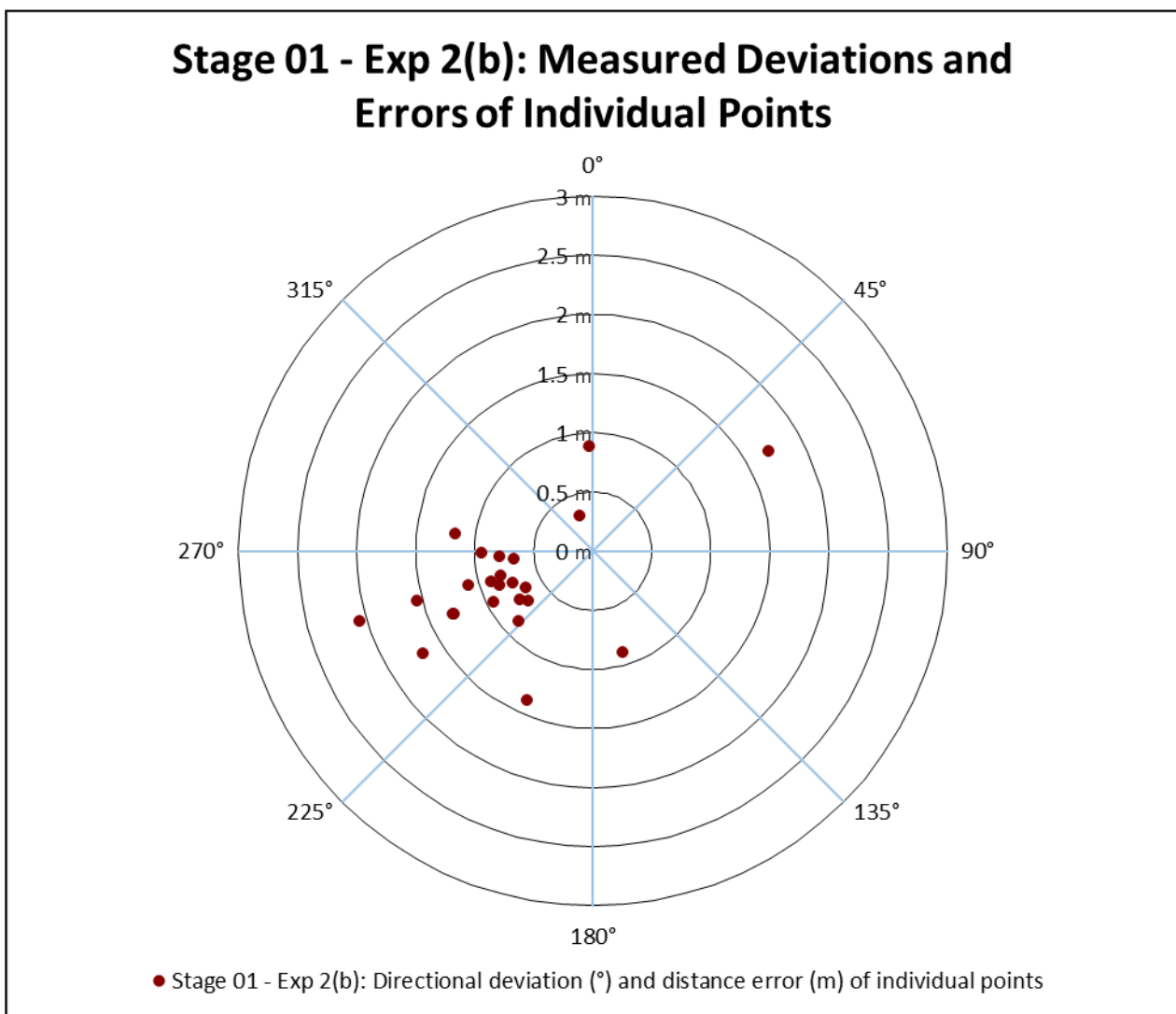


Figure 4.7: Stage 1 – Experiment 2(b): Measured deviations and errors against CPs

4.3.6 Experiment 2(c): Utilising 13 GCPs and 2 m DTM

Experiment 2(c) was executed in the same manner as was followed with experiments 2(a) and (b). Thirteen GCPs were utilised and the only difference was the use of the 2 m DTM. The following accuracies were measured:

- a) RMSE: the RMSE achieved from conducting this experiment was 1.2835, which is 0.64175 m.
- b) MAA tool: the accuracy assessment of this experiment showed the accuracy of the image to be 1.191322 m, as is indicated by the MAA report (Appendix L).
- c) Manual measurements: the average direction deviation was 158.83° and an average distance error of 0.59 m was measured (Figure 4.8).

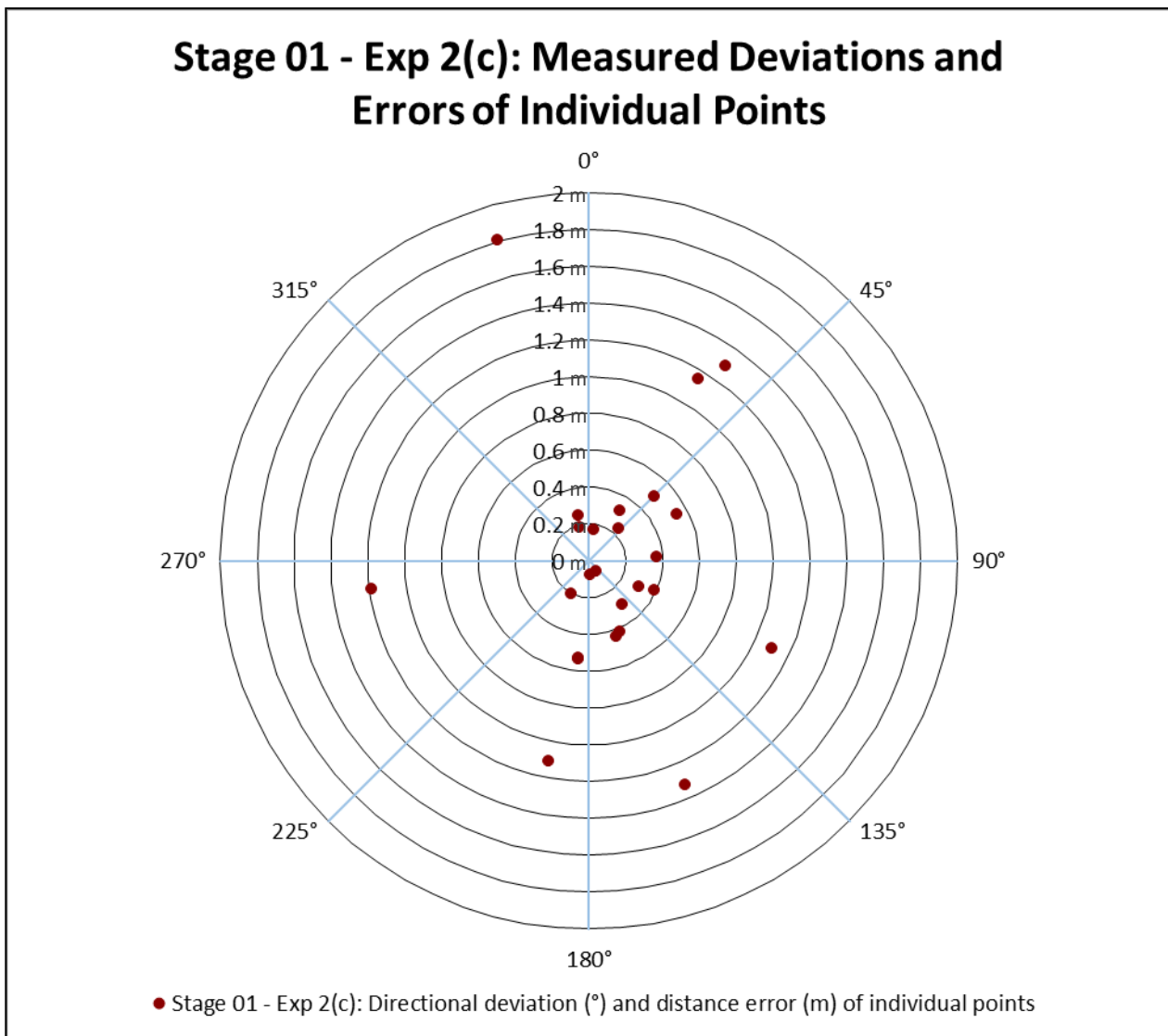


Figure 4.8: Stage 1 – Experiment 2(c): Measured deviations and errors against CPs

4.3.7 Experiment 3(a): Utilising 25 GCPs and 30 m SRTM DEM

Twenty-five GCPs that were evenly distributed across the image and the 30 m SRTM DEM encompass experiment 3(a). The following accuracies were measured:

- a) **RMSE**: the RMSE achieved from conducting this experiment was 1.439, which is 0.7195 m.
- b) **MAA tool**: the MAA tool measured the accuracy of the image to be 1.123205 m, as was derived from the MAA report (Appendix M).
- c) **Manual measurements**: the measurement of each individual point shows an average direction deviation of 229.36° and an average distance error of 0.58 m. Figure 4.9 illustrates the directional deviations and errors measured against the individual CPs.

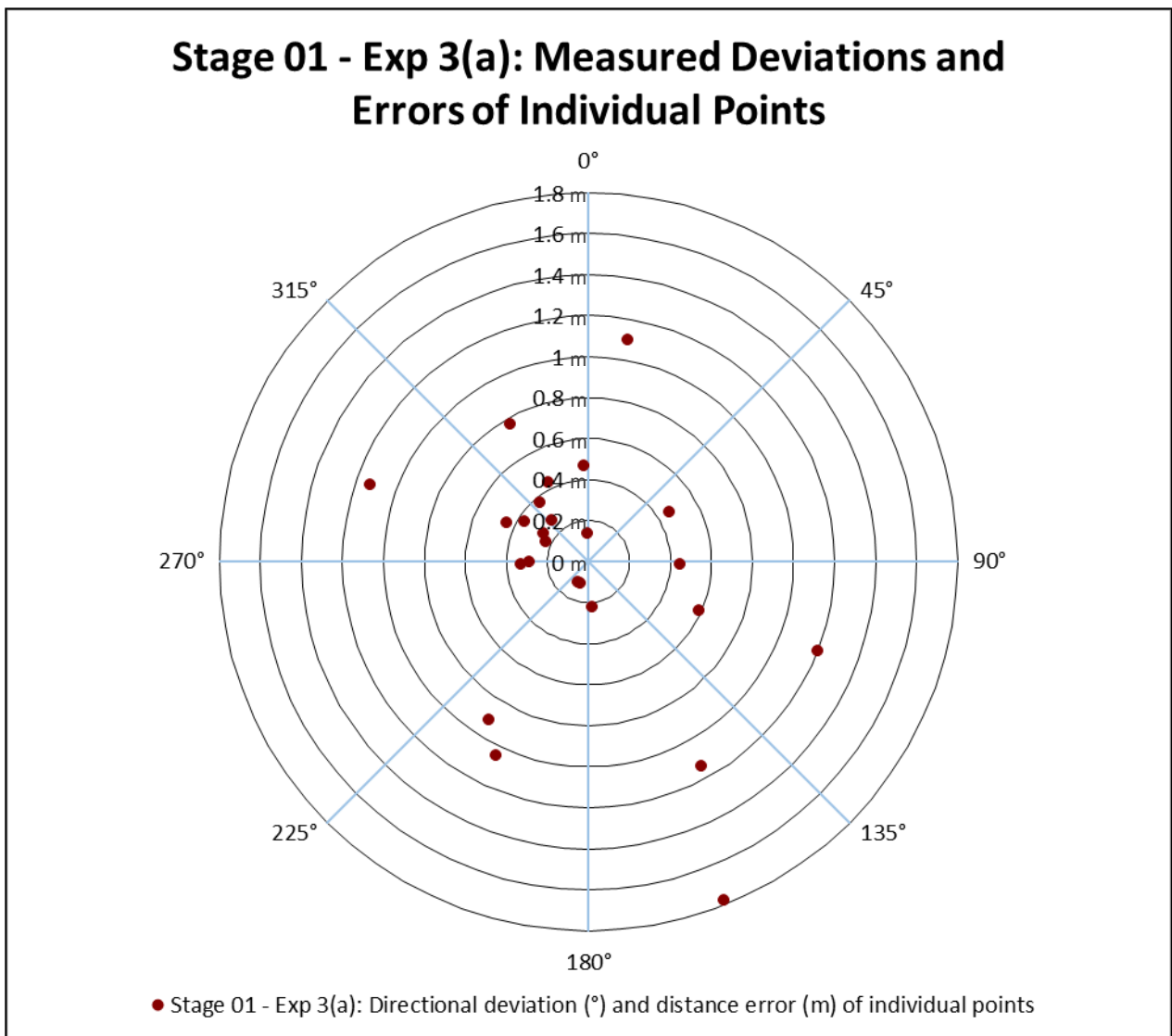


Figure 4.9: Stage 1 – Experiment 3(a): Measured deviations and errors against CPs

4.3.8 Experiment 3(b): Utilising 25 GCPs and 12 m DTM

Experiment 3(b) was executed in the same manner as experiment 3(a), with the only difference being that the 12 m DTM was used instead of the 30 m SRTM DEM. The following accuracies were measured:

- a) RMSE: the RMSE was 2.52, which is 1.26 m.
- b) MAA tool: the accuracy of this image is 0.854518 m. This is indicated by the MAA Report (Appendix N).
- c) Manual measurements: an average direction deviation of 226.53° and an average distance error of 0.45 m were measured. The distribution of the individual points measured is illustrated by Figure 4.10.

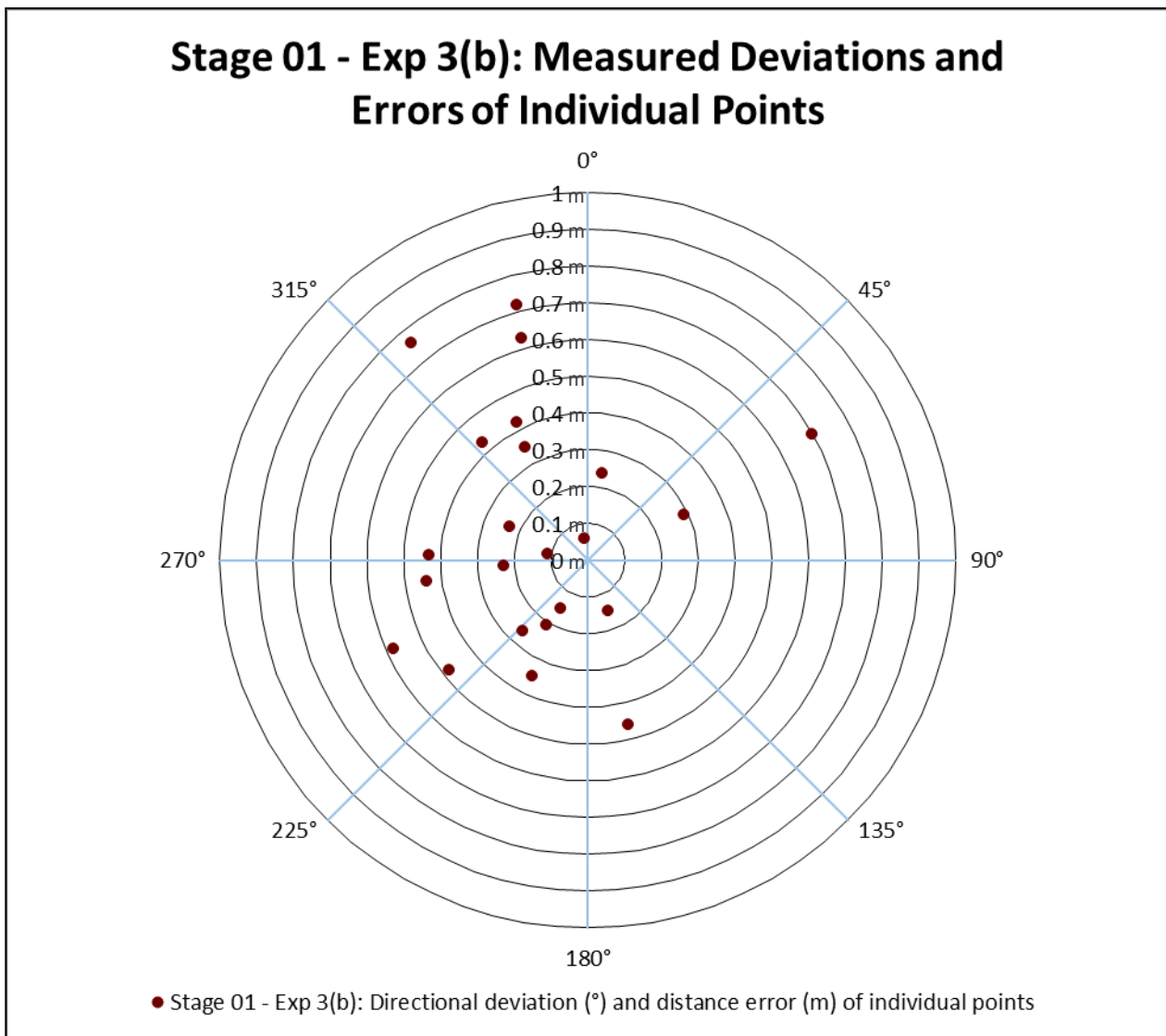


Figure 4.10: Stage 1 – Experiment 3(b): Measured deviations and errors against CPs

4.3.9 Experiment 3(c): Utilising 25 GCPs and 2 m DTM

Experiment 3(c) was executed in the same manner as experiments 3(a) and (b). Twenty-five GCPs were utilised and the higher accuracy 2 m DTM was used. The following accuracies were measured:

- a) RMSE: the RMSE was 1.264, which is 0.632 m.
- b) MAA tool: as indicated by the MAA Report, the accuracy of this image was measured at 0.718221 m (Appendix O).
- c) Manual measurements: an average direction deviation of 191.26° and an average distance error of 0.39 m were measured. The distribution of the individual points measured is illustrated by Figure 4.11.

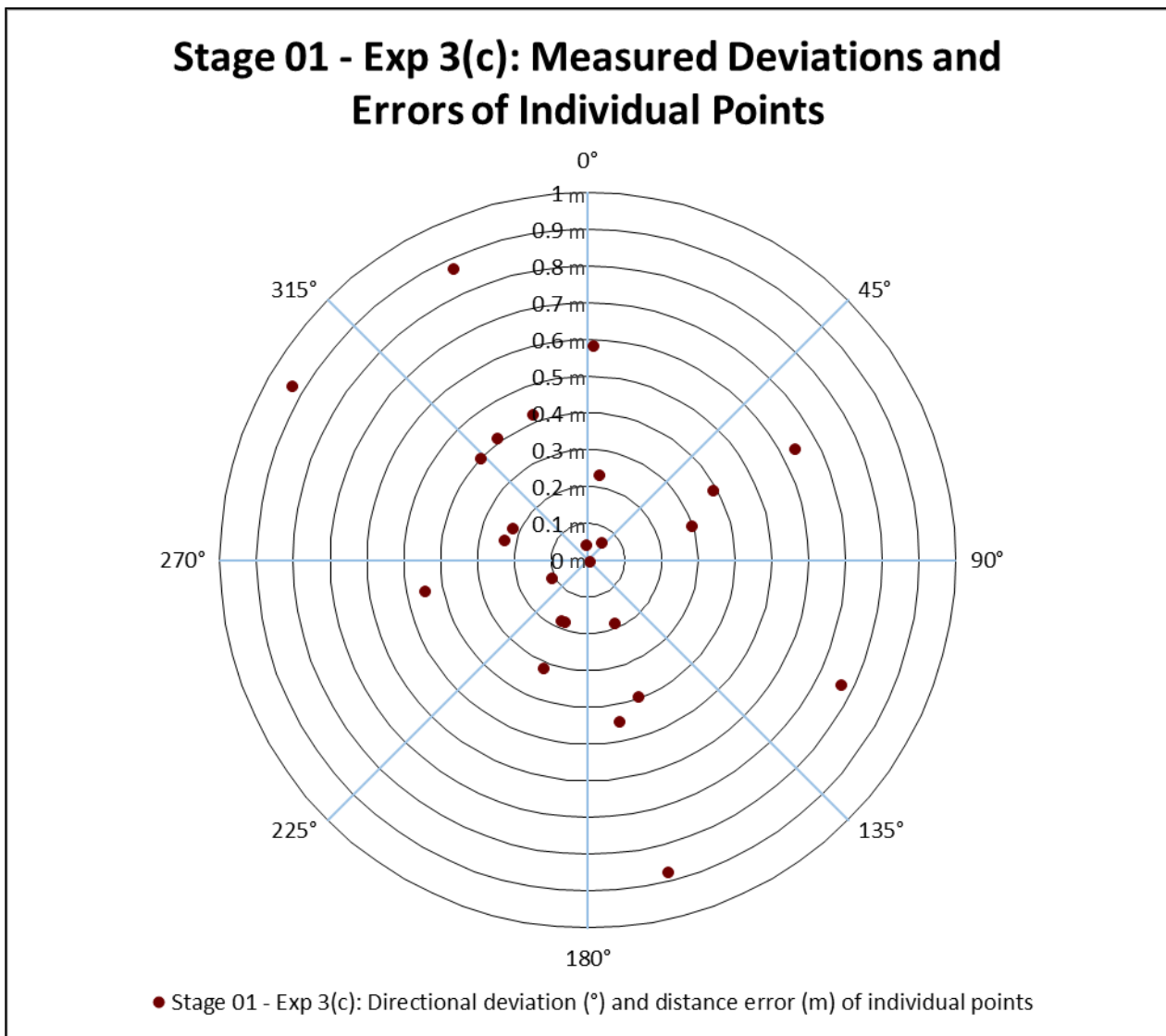


Figure 4.11: Stage 1 – Experiment 3(c): Measured deviations and errors against CPs

4.4 ANALYSIS OF STAGE 1 EXPERIMENTS

It is evident from the analysis performed during the stage 1 orthorectification experiments (Table 4.1) that an increase in uniformly distributed GCPs and utilising a higher quality elevation data source will render an increasingly accurate ortho-image. This table clearly indicates the increase of the overall accuracy when the number of GCPs are increased and higher quality DEMs are utilised.

Table 4.1: Overall accuracies achieved from the stage 1 experiments

Accuracy Indicators (m)	Number of GCPs								
	5			13			25		
	Exp 1(a)	Exp 1(b)	Exp 1(c)	Exp 2(a)	Exp 2(b)	Exp 2(c)	Exp 3(a)	Exp 3(b)	Exp 3(c)
	30 m SRTM	12 m DTM	2 m DTM	30 m SRTM	12 m DTM	2 m DTM	30 m SRTM	12 m DTM	2 m DTM
RMSE	2.32	0.23	0.23	1.04	0.23	0.64	0.72	1.26	0.63
MAA (CE90)	2.37	2.33	1.88	1.55	1.54	1.19	1.12	0.85	0.72
Manual Measurements	1.46	1.30	0.92	0.69	0.96	0.59	0.58	0.42	0.39
Accuracy	2.05	1.29	1.01	1.09	0.91	0.81	0.81	0.84	0.58
GPS error	+0.5								
Overall Accuracy	2.55	1.79	1.51	1.59	1.41	1.31	1.31	1.34	1.08

This increase in accuracy, measured by the three indicators, is illustrated by Figure 4.12 (below). Evident from this graph is the considerable lower RMSE for experiments 1(b), 1(c) and 2(b), compared to all other experiments. These three experiments produced RMSE values that are well within the normal guideline for the Pléiades image used (Paragraph 2.5). It was also stated in Paragraph 2.5 that RMSE can only be approximated (Smith, 2005). The bigger RMSE for the other experiments might be an indication that:

- a) Some GCPs might have been incorrectly captured by the GPS device in the field;
- b) The coordinate of a singular GCP was mistyped by the operator when the GCPs were imported into the GIS system;
- c) The GCP and the corresponding CP may have been placed in the incorrect location in the Input and Reference view during orthorectification, as was discussed in Paragraph 4.2; or

- d) The point is correct, but is in isolation compared to the distribution of all other active GCPs.

In such cases, it is always a good idea to test and verify the accuracy of GCPs to be able to identify defect points. Next, the question that needs to be considered: “*What considerations should be taken into account towards eliminating such anomalies?*” To answer this question, it is important to realise that RMSE provides only a guideline to which GCPs contribute to the overall accuracy of the image as well as the error value of GCPs. Four options to consider for achieving acceptable RMSE are:

- a) To eliminate the GCPs with high RMSE, which will provide a better-fit result;
- b) To tolerate the level of RMSE;
- c) Use a higher order transformation, but this option might result to a distorted image; and
- d) Utilise only high-confidence points and exclude all other points.

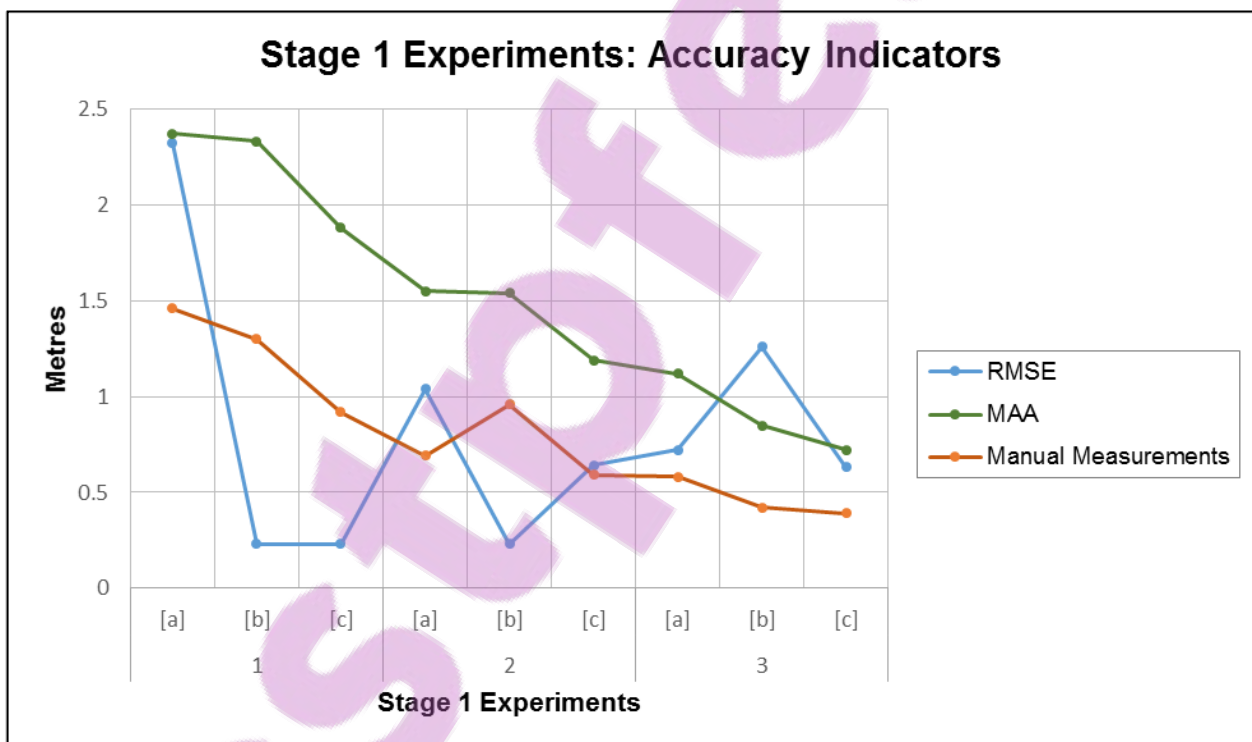


Figure 4.12: Stage 1 – Experiments: Accuracy assessments

In most cases, removing such anomalous GCPs will render a significantly improved overall RMSE. However, residuals are an indication of a best-fit scenario and the overall RMSE is influenced by all active GCPs. For the purpose of this study, no anomalous GCPs were removed from the orthorectification computations, for the reason to retain adequate and a uniform coverage over the entire image.

Determining the influence of the quality of an elevation source on orthorectification yielded the following results:

- a) Comparing experiments 1(a), (b) and (c): the difference between these three experiments was the quality of DEM utilised. The difference in accuracy between experiments 1(a) and (b) was 0.76 m, between experiments 1(b) and (c) was 0.28 and between experiments 1(a) and (c) was 1.04 m. This is an improvement in planimetric accuracy (percentage increase) of 40.78% between experiments 1(a) and (c), just by improving the elevation data sources from 30 m to 2 m spatial resolution.
- b) Comparing experiments 2(a), (b) and (c): the accuracy increased by 0.18 m between experiments 2(a) and 2(b), between experiments 2(b) and (c) was 0.10 and by 0.28 m between experiments 2(a) and 2(c). Although these increases might seem irrelevant and small, the accuracy increased by approximately 17.61% between experiments 2(a) and 2(c) when utilising a 2 m DEM instead of a 30 m DEM.
- c) Comparing experiments 3(a), (b) and (c): experiment 3(c) has an increase in accuracy of 0.23 m compared to experiment 3(a), which indicates that the accuracy of the ortho-image increased by 17.56%, through using a higher quality elevation source.

It is illustrated by Table 4.1 that experiment 3(b), utilising the 12 m DTM, yielded an overall accuracy that is 0.03 m worse than utilising the 30 m SRTM (indicated by experiment 3(a)). This does not fit in with the general trend of increase accuracy visible in Figure 4.13. This exception was due to the increased RMSE that was achieved from performing this ortho-experiment (Figure 4.12). However, as was mentioned earlier, RMSE is only a guideline as to which GCPs contribute to the overall accuracy. Important to note, is that the CE90 value and manual measurements for experiment 3(b) showed the expected accuracy increase when compared to experiment 3(a), see Figure 4.12.

It can be stated that the horizontal accuracy of an ortho-image can be considerably increased by utilising highly accurate elevation sources. Illustrated by Figure 4.13, in each case, the overall accuracy of the ortho-image increased by utilising the 12 m DTM (represented by the yellow bar) and 2 m DTM (green bar) respectively, compared to the 30 m SRTM DEM (red bar). However, also note that the more GCPs used, the lesser the

difference in accuracy was when higher quality elevation data sources were used. This is an indication that the use of GCPs and elevation data are intertwined when performing orthorectification. Both these sources have a direct influence on one another as well the accuracy of the ortho-image.

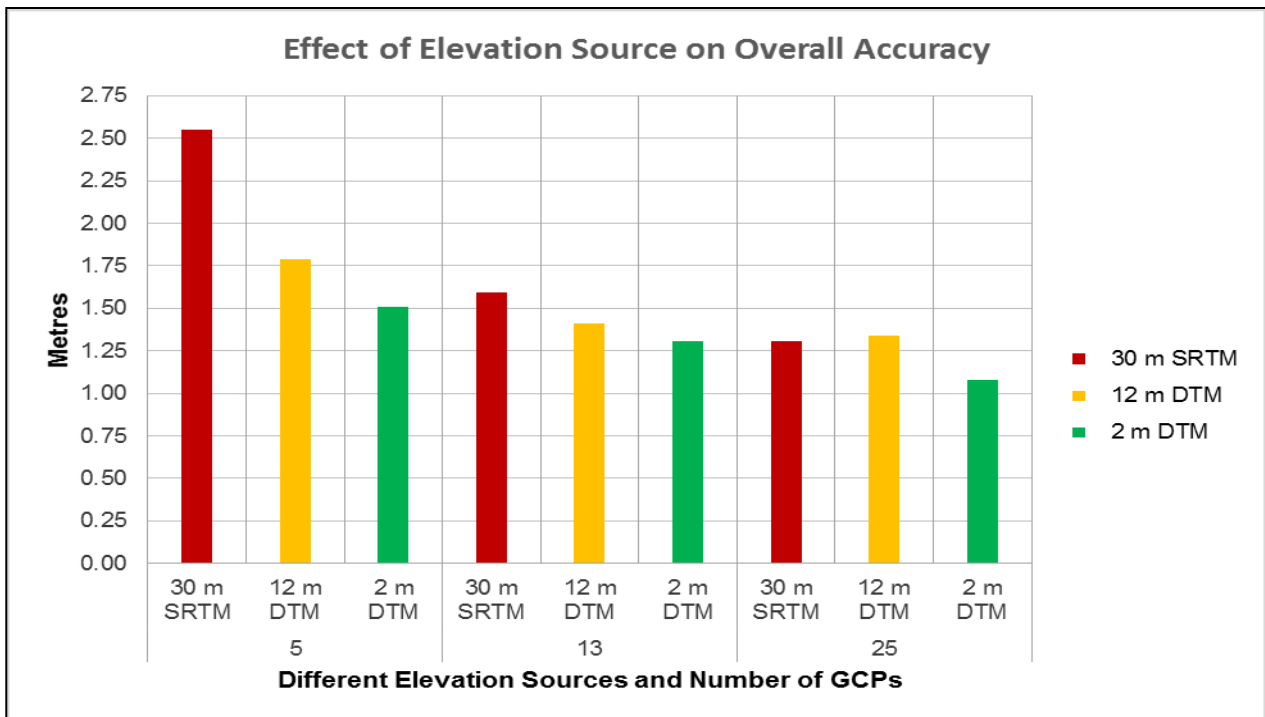
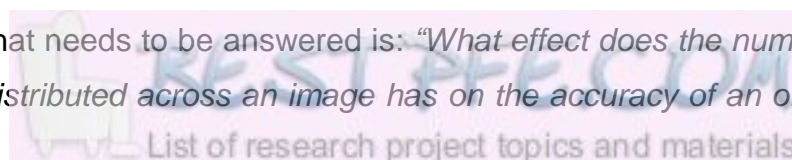


Figure 4.13: Effect of quality of elevation source on the overall accuracy of an ortho-image

It is evident from Figure 4.13 that utilising 25 GCPs combined with the use of the 2 m DEM yielded the most accurate ortho-image. This image had an overall positional accuracy of 1.08 m as opposed to 2.55 m, when only 5 GCPs and the 30 m DEM were used (Table 4.1). The difference in accuracy of 1.47 m between the best and worst ortho-image determined by the experiments, might be perceived as inconsequential or immaterial, which is true when using an ortho product for applications such as digital mapping (cartography), crime analysis, change detection, agricultural and environmental analysis, etc. However, it is a significant change that becomes a pivotal factor to consider when an ortho-image is used for applications such as military target acquisition, military intelligence analysis, navigation and civil engineering – when minute measurement deviations can have a catastrophic effect on the required result.

The next question that needs to be answered is: “What effect does the number of GCPs that are uniformly distributed across an image has on the accuracy of an ortho-image?”



This question has already been answered and is indicated by Figure 4.12 and 4.13 and confirmed by the following statistics when comparing experiments 1(c), 2(c) and 3(c). All three these experiments utilised the high quality 2 m DEM and the GCPs used were uniformly distributed, but the number of GCPs differed. The percentage difference in accuracy between experiments 1(c) and 2(c) is 19.80% and between experiments 2(c) and 3(c) is 28.40%. Therefore, utilising more GCPs yielded a more accurate ortho-image, but the difference becomes smaller and would continue to become smaller until too many GCPs are used (Paragraph 2.4.1), which will not render better quality ortho-images.

In Paragraph 1.4.2, it was stated that from the stage 1 experiments one ortho-image would be identified as the master image. The master image was identified as the ortho-image created from experiment 3(c), with an accuracy of 0.58 m. This image was used as the benchmarked image for comparing and evaluating all other ortho-images produced from the stage 2 and 3 experiments.

4.5 ORTHORECTIFICATION TESTS: STAGE 2 EXPERIMENTS

Two independent orthorectification experiments were conducted during stage 2. The first experiment consisted of the use of ten TerraSAR-X GCPs acquired from Airbus Defence and Space. The second experiment was conducted by following the parametric approach and characterised by the exclusion of GCPs. Both these experiments utilised the Pléiades Orbital Pushbroom geometric model and the 2 m DTM to orthorectify the Pléiades primary image. Comparisons were made between the resulting ortho-images and the master image to determine the accuracy of the images. These two experiments allowed for testing Hypotheses 3 and 4. The results also provided the answers to research questions 4 and 5.

4.5.1 Independent experiment 01: Using TerraSAR-X GCPs and 2 m DTM

This experiment was conducted to determine the accuracy of ortho-images when using the automated extracted GCPs from the TerraSAR-X satellites. Ten GCPs that are evenly distributed across the entire image scene were utilised as well as the 2 m DTM. The following accuracies were measured:

- a) RMSE: the RMSE was measured at 3.22, which is 1.61 m.
- b) MAA tool: the MAA tool indicated an accuracy of 1.820917 m (Appendix P).
- c) Manual measurements: an average direction deviation of 153.27° and an average distance error of 1.06 m were measured. The distribution of the individual points measured is illustrated by Figure 4.14.

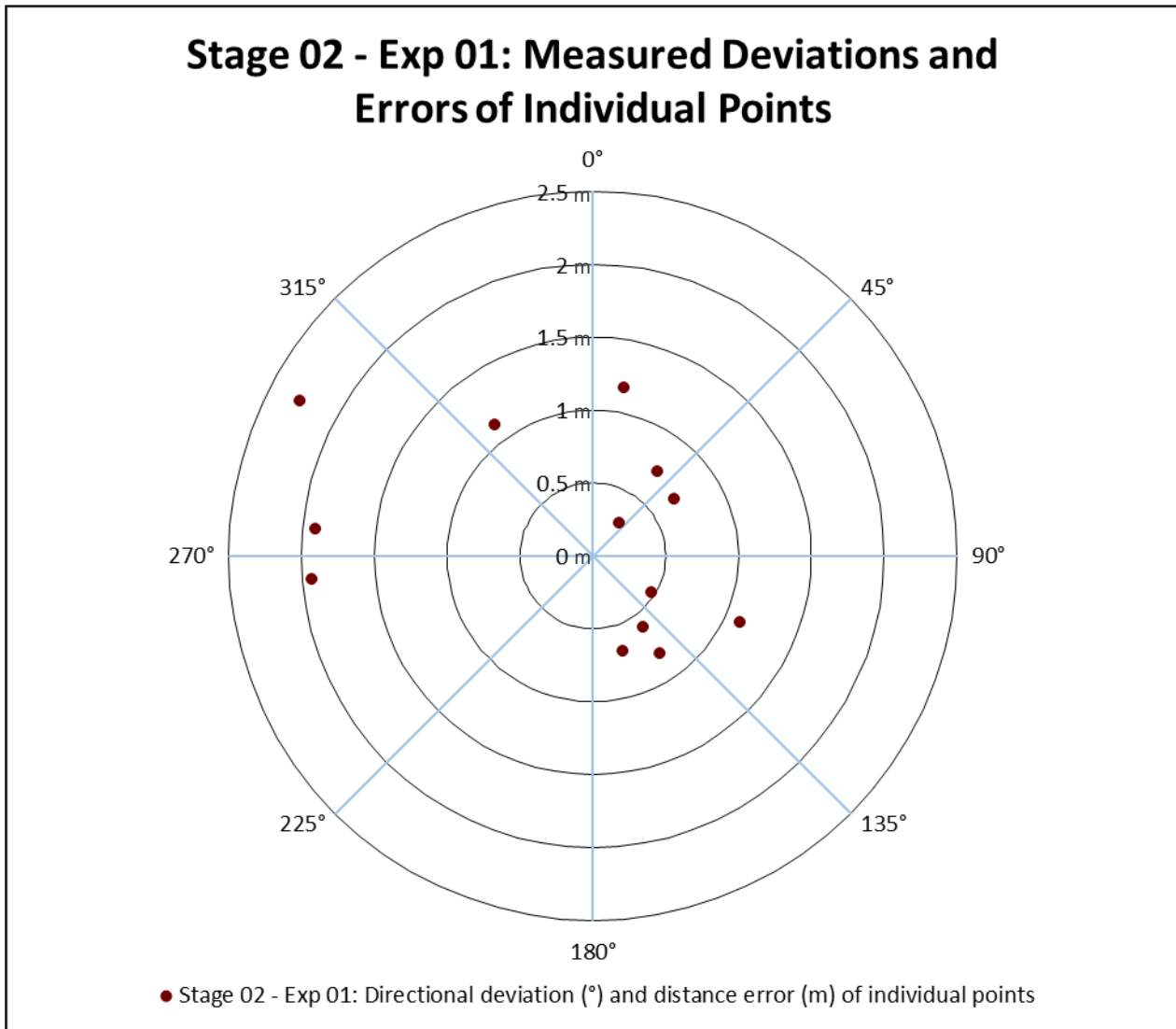


Figure 4.14: Stage 2 – Experiment 01: Measured deviations and errors against CPs

4.5.2 Independent experiment 02: Using sensor model and 2 m DTM

The parametric approach was followed to conduct this experiment. A rigorous sensor model, namely the Pléiades Orbital Pushbroom geometric model and the 2 m DTM was used to orthorectify the Pléiades primary image without the use of GCPs. This experiment was conducted to determine if a geometrical sensor model combined with a DEM and without the use of GCPs can create an accurate ortho-image that is of a

similar accuracy to an ortho-image create from utilising GCPs. The following accuracies were measured by the various accuracy assessments that were performed:

- a) RMSE: no RMSE, because no GCPs were used to produce this ortho-image.
- b) MAA tool: the MAA measurement (Appendix Q) was 6.542845 m.
- c) Manual measurements: an average direction deviation of 341.55° and an average distance error of 6.06 m were measured (Figure 4.15).

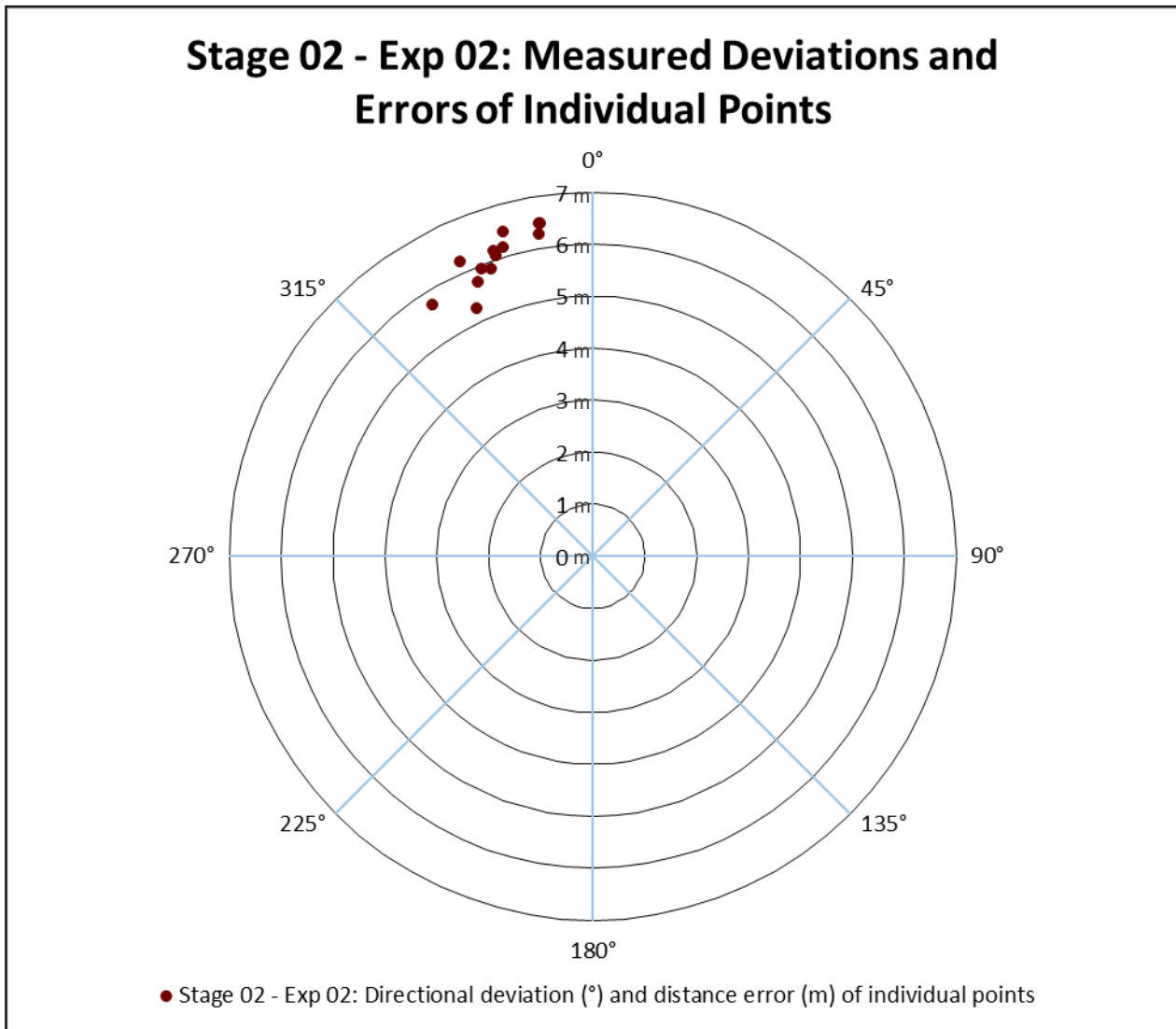


Figure 4.15: Stage 2 – Experiment 02: Measured deviations and errors against CPs

4.6 ANALYSIS OF STAGE 2 EXPERIMENTS

The first independent experiment produced an overall accuracy of 1.5 m, which is indicated below in Table 4.2. The use of the TerraSAR-X GCPs produced a consistent and high accurate ortho-image. The positional accuracy of this ortho-image is still less compared to the master image and most of the ortho-images produced during stage 1.

However, the high accuracy of this ortho-image is an indication that TerraSAR-X GCPs can be used as a source for reference ground control points to improvement the geometric orientation of HRSI. This space-borne approach to extract 3D GCPs and use them to georectify satellite images holds significant value in the field of orthorectification of satellite imagery. This is especially true due to significant problems posed by manually collecting suitable GCPs (Paragraph 1.2.1). It is very expensive to manually collect new GCPs for a specific area and in most cases such areas are inaccessible, due to environmental conditions and mobility restrictions.

Table 4.2: Overall accuracies achieved from the stage 2 experiments

Accuracy Indicators (m)	Stage 2 Experiments	
	Independent Experiment 01 (TerraSAR-X extracted GCPs)	Independent Experiment 02 (No GCPs)
<i>RMSE</i>	1.61	No RMSE
<i>MAA (CE90)</i>	1.82	6.54
<i>Manual Measurements</i>	1.06	6.06
Overall Accuracy	1.50	6.30

The second independent experiment produced an overall accuracy of 6.30 m. This is high value (worse accuracy) compared to all other accuracy tests already performed, which ranges between 2.55 m and 1.08 m. However, this accuracy is quite acceptable considering that only a DEM and the sensor model were used to create this ortho-image. As previously mentioned (Paragraphs 1.1, 3.2.1 and 4.4), many applications do not need highly accurate satellite images.

This experiment indicated that suitable location accuracy could be acquired when no GCPs exist and many applications will find such a solution acceptable. One important factor pertaining to the accuracy of this ortho-image that needs to be discussed is the conspicuous cluttered distribution of points, which is evident in Figure 4.15. All measured points are clustered together at approximately 340°. The points are precise in relation to one another, but not in terms of the overall absolute accuracy. There are a couple reasons why this distribution might occur, such as the use of an inaccurate elevation source, sensor model discrepancies and image data acquisition inconsistencies. One thing that is apparent though is the fact that this overall accuracy is

still well within the pointing accuracy (Table 4.3) of the Pléiades satellite sensor (Airbus Defence and Space, October 2012).

Table 4.3: Pléiades image quality performances

Image Quality Item	Design Specification	Up-to-Date Performance	Remark
GEOMETRY (Global)			
Pointing Accuracy (satellite tasking)	Across track: 500m LE99.7 Along track: 1000m LE99.7	320m CE99.7	
Dynamic Effect (high frequency jittering)	0.8 pixel Pan LE99.7	0.1 pixel Pan LE99.7	
GEOMETRY (Rigorous Geometric Model accuracy without GCP: all products)			
Location Accuracy	12m CE90 24m CE99.7	8.5m CE90 @ Nadir 10.5m within 30°	With refined attitudes
Length Distortion	0.5ppm CE90	0.31ppm CE90	Between 2 points distant of 1000 pixels Panchromatic
MS Registration	0.25 pixel MS CE90	0.18 pixel MS CE99.7	
MS and Pan Co-registration	0.5 pixel MS CE90	0.22 pixel MS CE99.7	
Global RPC Discrepancy vs. Rigorous Model	-	0.3 pixel PAN CE90	
GEOMETRY (Rigorous Geometric Model accuracy reset on (perfect) GCP and DEM)			
Planimetric Accuracy (Panchromatic)	0.5m CE90	0.30m CE90	
Planimetric Accuracy (Multispectral)	0.5m CE90	0.43m CE90	

Source: Airbus Defence and Space (October 2012)

It is indicated by Table 4.3 that the location accuracy of a rectified Pléiades image utilising the rigorous geometric model without the use of GCPs will have an accuracy of 12 m (CE90). This is exactly the process that was followed to conduct the second independent experiment. It is further stated that the up-to-date performance will deliver a location accuracy of 8.5 m (CE90) at Nadir.

It was indicated in Paragraph 4.2 that the incidence angle of the Pléiades image used to conduct all experiments of this study is 2.83788480340555°, hence a near-Nadir image and still the location accuracy achieved (6.3 m) is well within the design specifications. Therefore, this is an indication that the pointing accuracy of the Pléiades satellite sensor

is very good. Even though this result is acceptable in terms of the image data location accuracy, further research might be required to determine the exact cause to the conspicuous cluttered distribution of points.

4.7 ORTHORECTIFICATION TESTS: STAGE 3 EXPERIMENTS

The stage 3 experiments were conducted to simulate various scenarios when GCPs are irregularly distributed and varying in number. These GCPs were selected from vector road layers to cover only specific areas within an image scene (Paragraph 1.2.1). The different scenarios are illustrated by Figure 1.2 (Chapter 1) and are based on the following distribution settings, illustrated by Figure 4.16 (Jakubowicz and Jaszczak, 09 February 2005). GCPs were placed on the west side of the image (a) for the first experiment, on the east side (b) for the second experiment, on the north side (c) for the third experiment, on the south side (d) for the fourth experiment and GCPs had a random distribution across the entire image (e) for the fifth experiment.

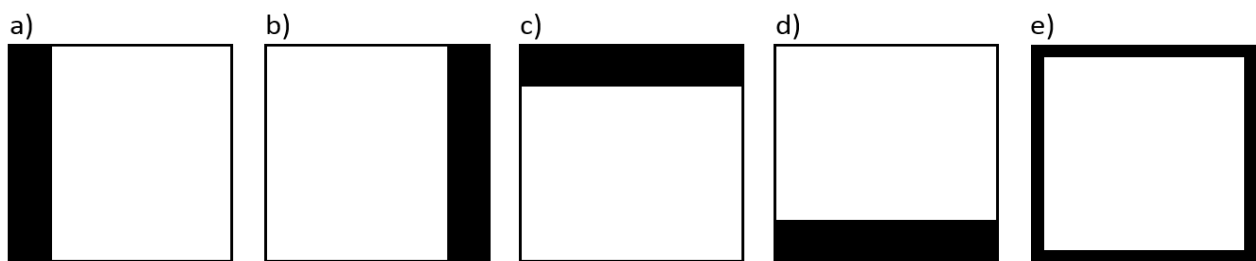


Figure 4.16: Stage 3 – Experiments GCP distribution settings

Adapted from Jakubowicz and Jaszczak (09 February 2005)

All ortho-images produced from these experiments were compared, measured and analysed against CPs extracted from the master image to determine their accuracies. The accuracy analysis is descriptively presented and states the results achieved from the assessment indicators, namely RMSE, MAA and manual measurements.

The overall accuracy of each experiment is presented in Table 4.4. As were the case for the stage 1 experiments, the overall accuracy of each ortho-image is calculated by dividing the sum of the values of the three indicators and adding the GPS positional accuracy of 50 cm. MAA reports were created for each experiment and are attached at the back of this study as addendums.

4.7.1 Experiment 01: GCPs concentrated on the west side of the image

The first experiments consisted of selecting 9 GCPs located on the west side of the image scene. An RMSE of 4.50 m was achieved. The MAA tool measured the accuracy of the image at 13.238588 m, as is indicated by the MAA report (Appendix R). The measurement of each individual point showed an average direction deviation of 229.28° and an average distance error of 8.41 m (Figure 4.17). An overall accuracy of 9.22 m was measured (Table 4.4).

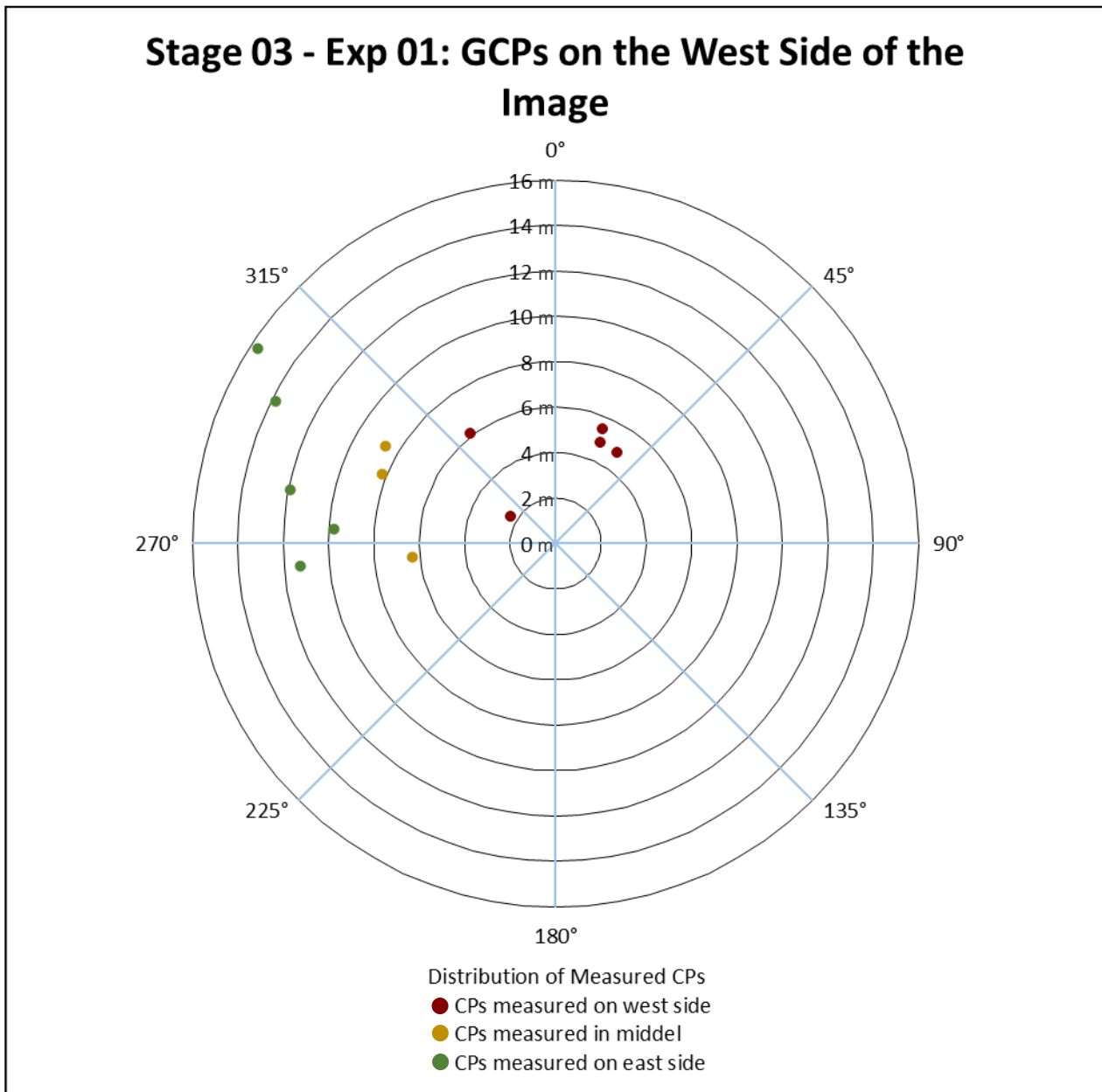


Figure 4.17: Stage 3 – Exp 01: GCPs distributed on the west side of the image

4.7.2 Experiment 02: GCPs concentrated on the east side of the image

Experiment 02 constitutes 12 GCPs which were selected on the east side of the image scene. The RMSE was 2.91 m and the MAA showed an accuracy of 13.980002 m (Appendix S). The average direction deviation was 219.64° and an average distance error of 7.93 m (Figure 4.18) was measured. The overall accuracy of this image was 8.77 m (Table 4.4).

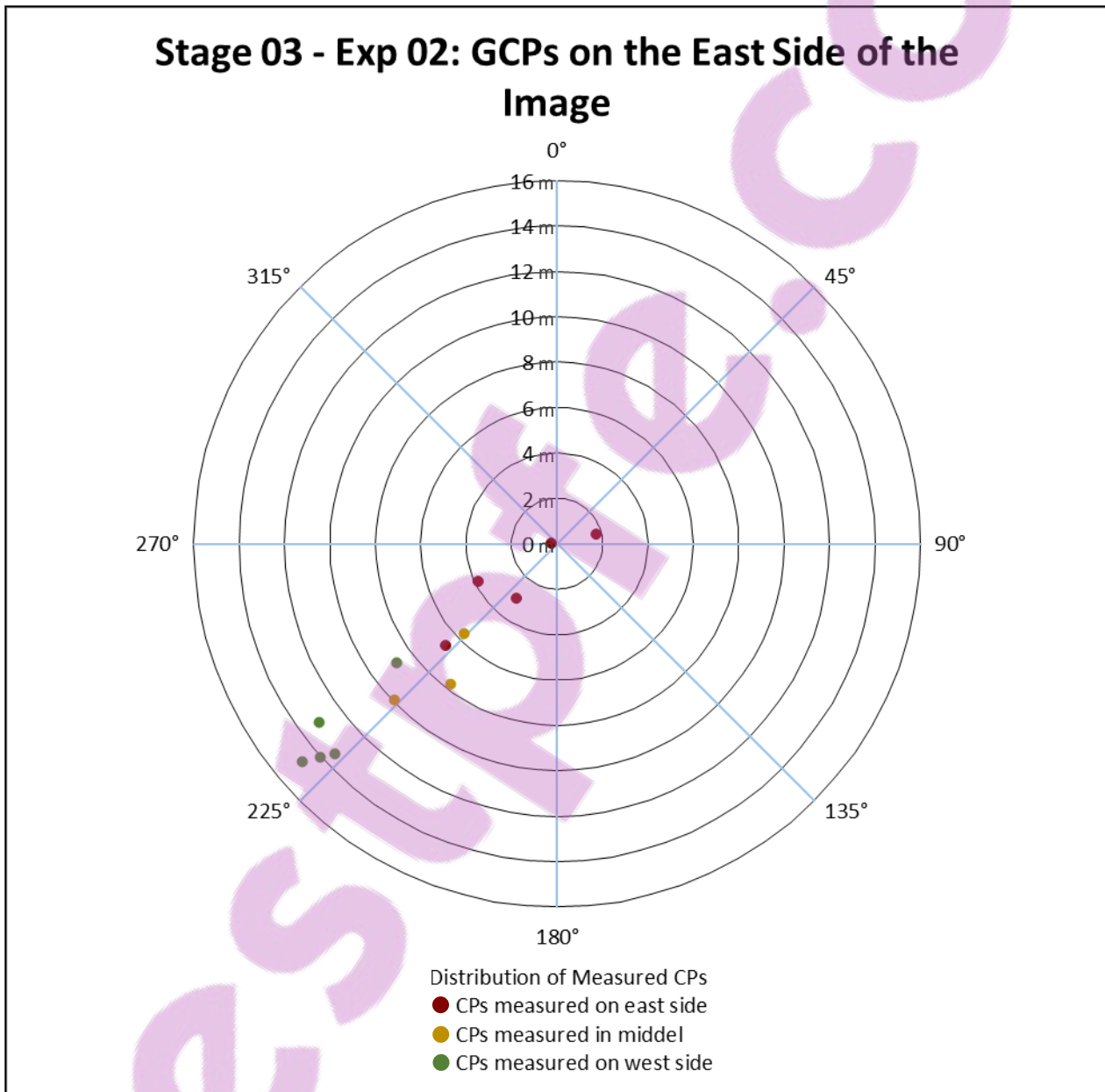


Figure 4.18: Stage 3 – Exp 02: GCPs distributed on the east side of the image

4.7.3 Experiment 03: GCPs concentrated on the north side of the image

This ortho-image was created by selecting 14 GCPs on the north side of the image. An RMSE of 3.15 m was achieved and an accuracy of 9.379670 m (Appendix T) was measured using the MAA tool. The average direction deviation was 58.27° and an average distance error of 5.27 m was attained using the measurement tool (Figure 4.19). For this experiment, the overall accuracy was 6.43 m (Table 4.4).

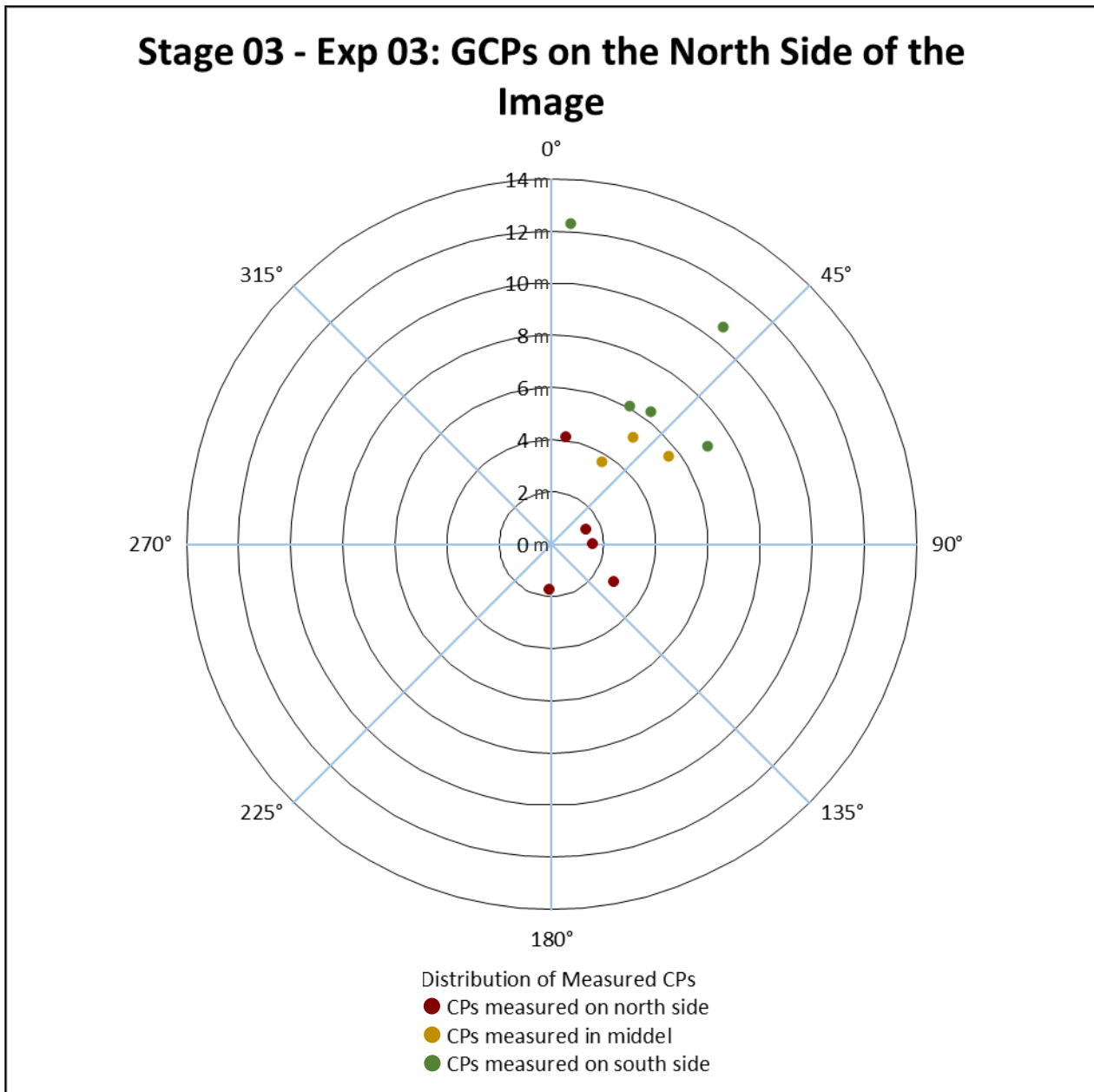


Figure 4.19: Stage 3 – Exp 03: GCPs distributed on the north side of the image

4.7.4 Experiment 04: GCPs concentrated on the south side of the image

Seventeen GCPs on the south side of the image was selected to perform this experiment. The RMSE was 2.03 m and using the MAA tool measured an accuracy of 5.047808 m (Appendix U). The average direction deviation was 115.90° and an average distance error of 3.38 m was measured (Figure 4.20). The overall accuracy was calculated at 3.99 m (Table 4.4).

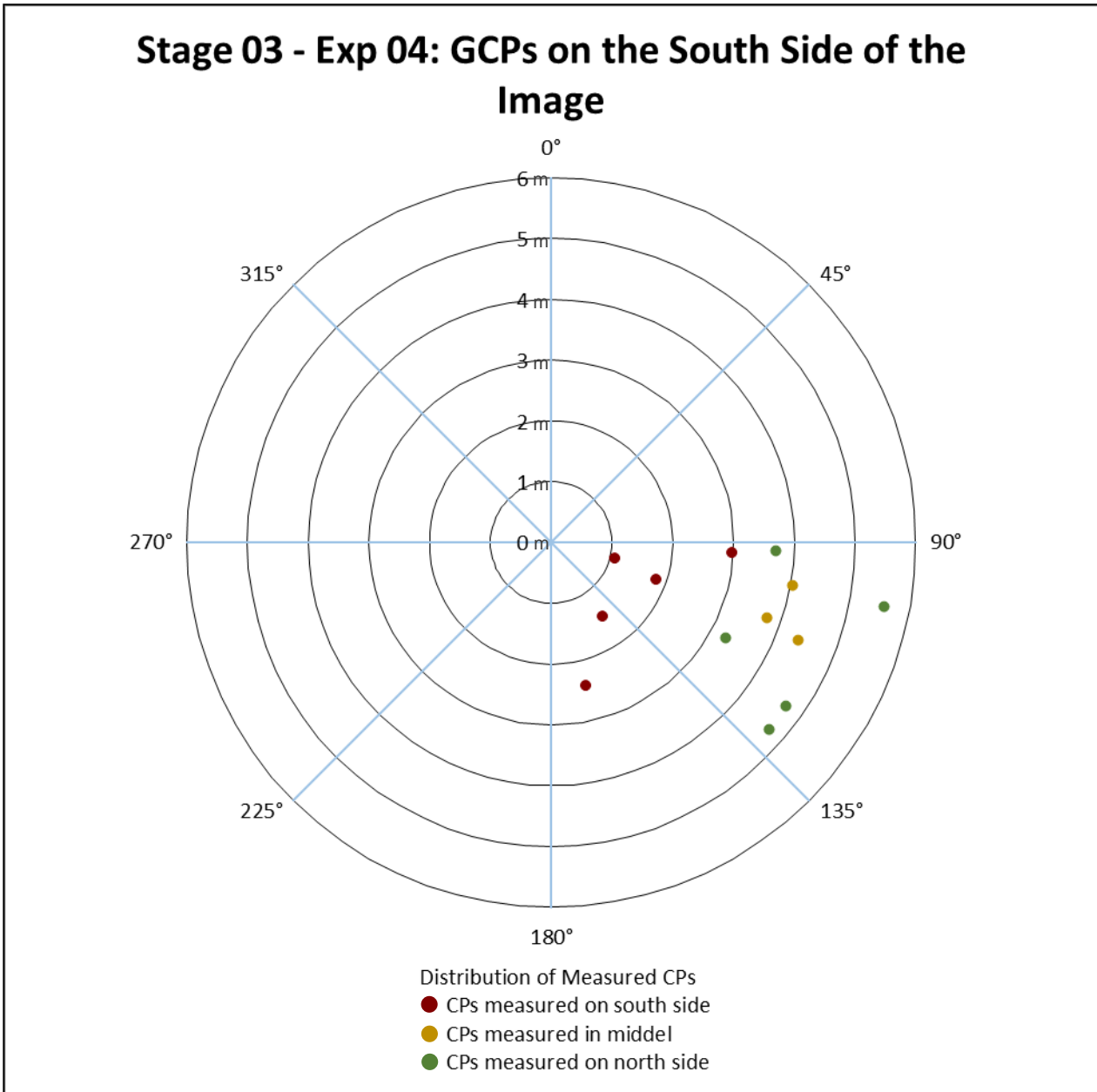


Figure 4.20: Stage 3 – Exp 04: GCPs distributed on the south side of the image



4.7.5 Experiment 05: Random distribution of GCPs covering the entire image

This experiment was executed through selecting 25 GCPs from the vector road layer to create a random distribution covering the entire image. From this experiment, a 2.00 m RMSE was achieved. The MAA report indicated that an accuracy of 1.517055 m was achieved (Appendix V). The average direction deviation was 200.56° and the average distance error was 0.85 m (Figure 4.21). The overall accuracy was calculated at 1.96 m (Table 4.4).

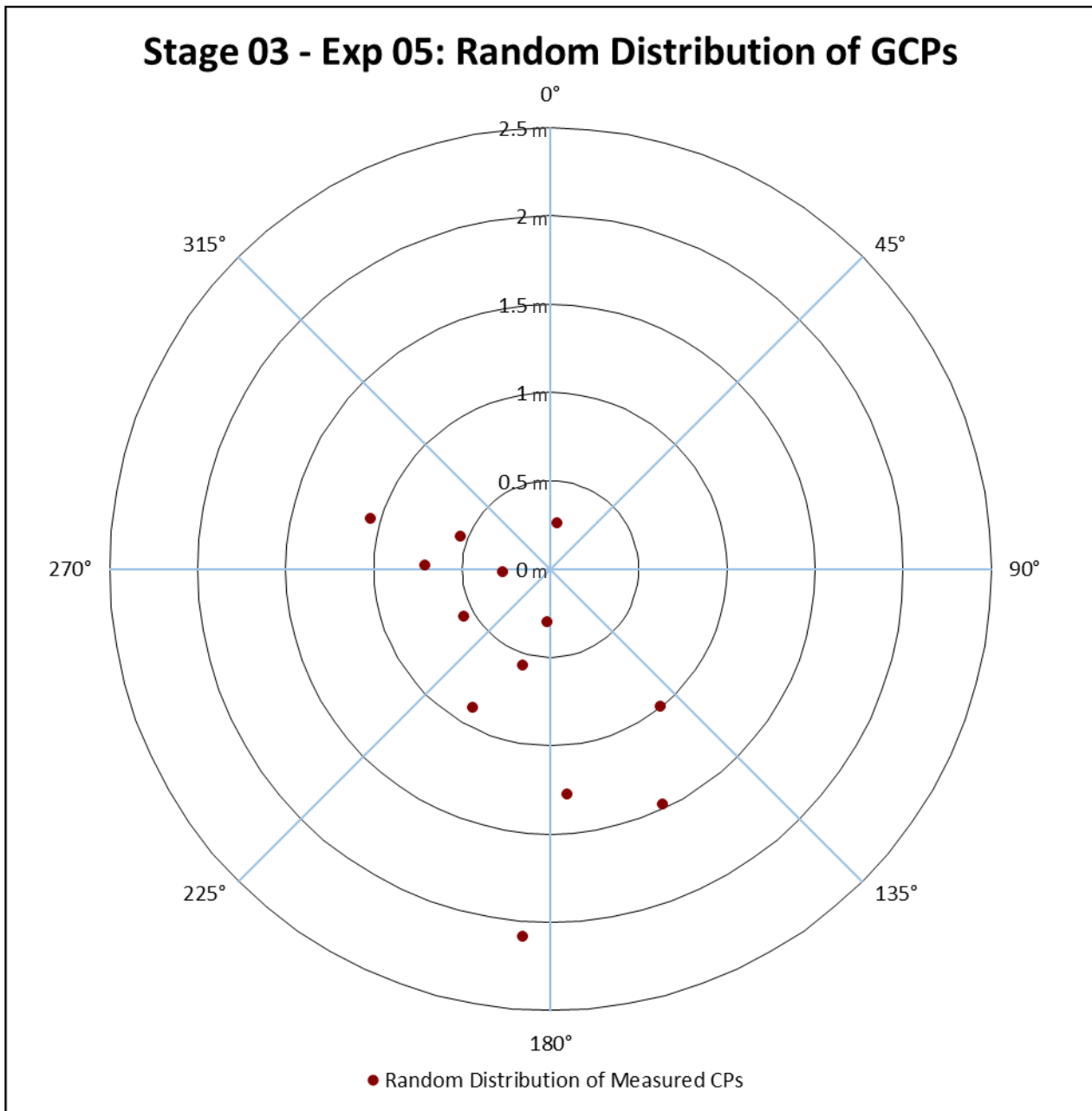


Figure 4.21: Stage 3 – Exp 05: Random distribution of GCPs

4.8 ANALYSIS OF STAGE 3 EXPERIMENTS

All the accuracies measured from the stage 3 experiments are summarised in Table 4.4, which indicates that the overall accuracy increased as the number of GCPs increased. The analysis of the stage 3 experiments also indicates that the accuracy of an ortho-image cannot be guaranteed without a uniform distribution of GCPs. It is evident by comparing the results of experiment 5 with the rest of the experiments that a random distribution produced a much better accuracy compared to when GCPs are only present in one area of the image.

Table 4.4: Overall accuracies achieved from the stage 3 experiments

Accuracy Indicators (m)	Stage 3 Experiments				
	Exp 01 (West)	Exp 02 (East)	Exp 03 (North)	Exp 04 (South)	Exp 05 (Random)
	Number of GCPs				
	09	12	14	17	25
RMSE	4.50	2.91	3.15	2.03	2.00
MAA (CE90)	13.24	13.98	9.38	5.05	1.52
Manual Measurements	8.41	7.93	5.27	3.38	0.85
Accuracy	8.72	8.27	5.93	3.49	1.46
GPS error	+0.5				
Overall Accuracy	9.22	8.77	6.43	3.99	1.96

Figure 4.22 illustrates the increase in accuracy measured by the assessment indicators. The numerical improvement of experiment 5 compared to the other experiments is evident by this Figure. The statistical analysis ascertained that increasing the number of GCPs that covers most of the image scene would render a more accurate image than using limited GCPs cluttered in one area.

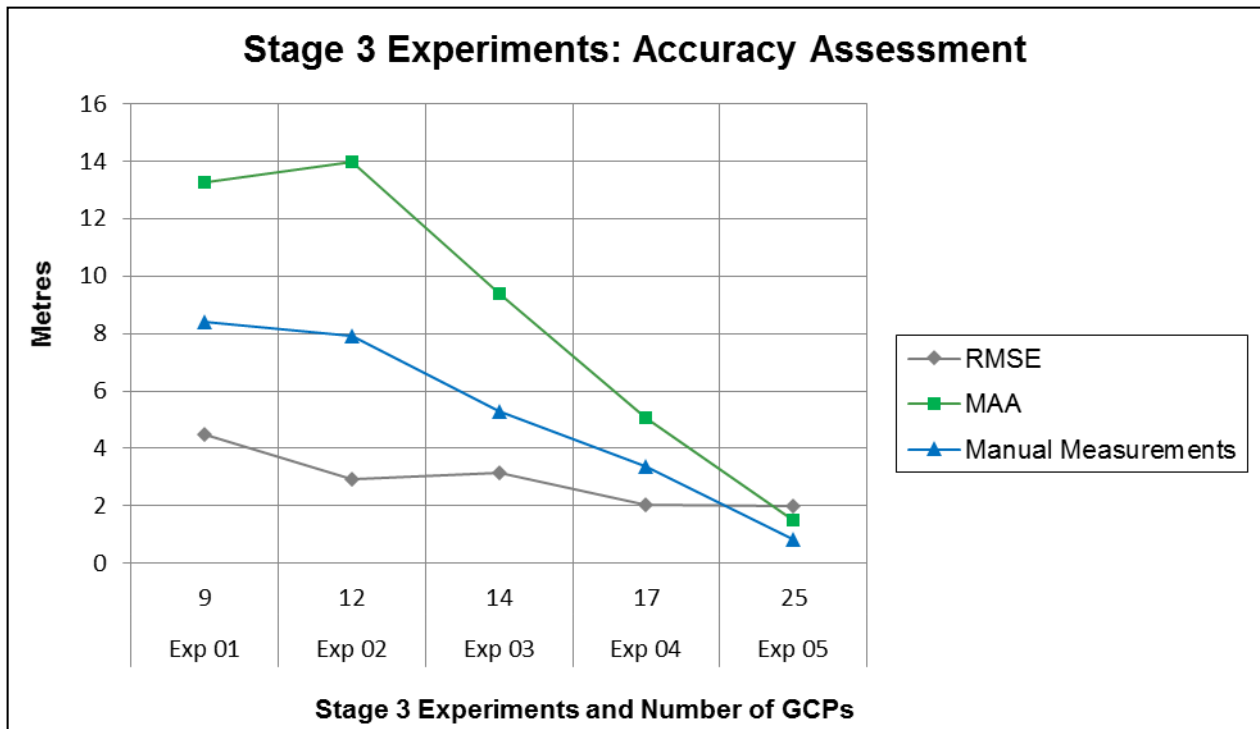


Figure 4.22: Stage 3 – Experiments: Accuracy assessments

When considering the distortion direction¹⁹ indicated by red circles in Figure 4.23, the following is observed:

- a) The accuracy of the ortho-images for each of the first four experiments is best in proximity of the clutter of GCPs used to orthorectify each image. The first experiment was performed with a cluster of GCPs only present on the west side of the image, the second experiment on the east side, the third experiment on the north of the image and the fourth experiment on the south side of the image. Each ortho-image has very high distortion in terms of the location accuracy furthest away from the input GCPs, indicated by control point 9 to 13 (Figure 4.23).
- b) However, the picture looks quite different for experiment 05. This experiment was performed, using 25 GCPs that were randomly distributed to cover most of the image scene. Very little accuracy distortions were measured across the image

¹⁹ Distortion direction (in this context) refers to the Control Point (CP) measurements taken in relation to the clutter distribution of GCPs for each experiment. Referring to Figure 4.23, CPs 1 to 5 were measured closest to the clutter of GCPs, CPs 6, 7 and 8 were measured in the centre of the image and CPs 9 to 13 were the furthest away from the clutter distribution of the GCPs used to orthorectify the specific image. This is an indication that the ortho-image is much less distorted in proximity of where the GCPs were placed as opposed to areas on the image that had no GCPs.

scene. This is confirmed by the linear orientation of the dark blue line illustrated by Figure 4.23.

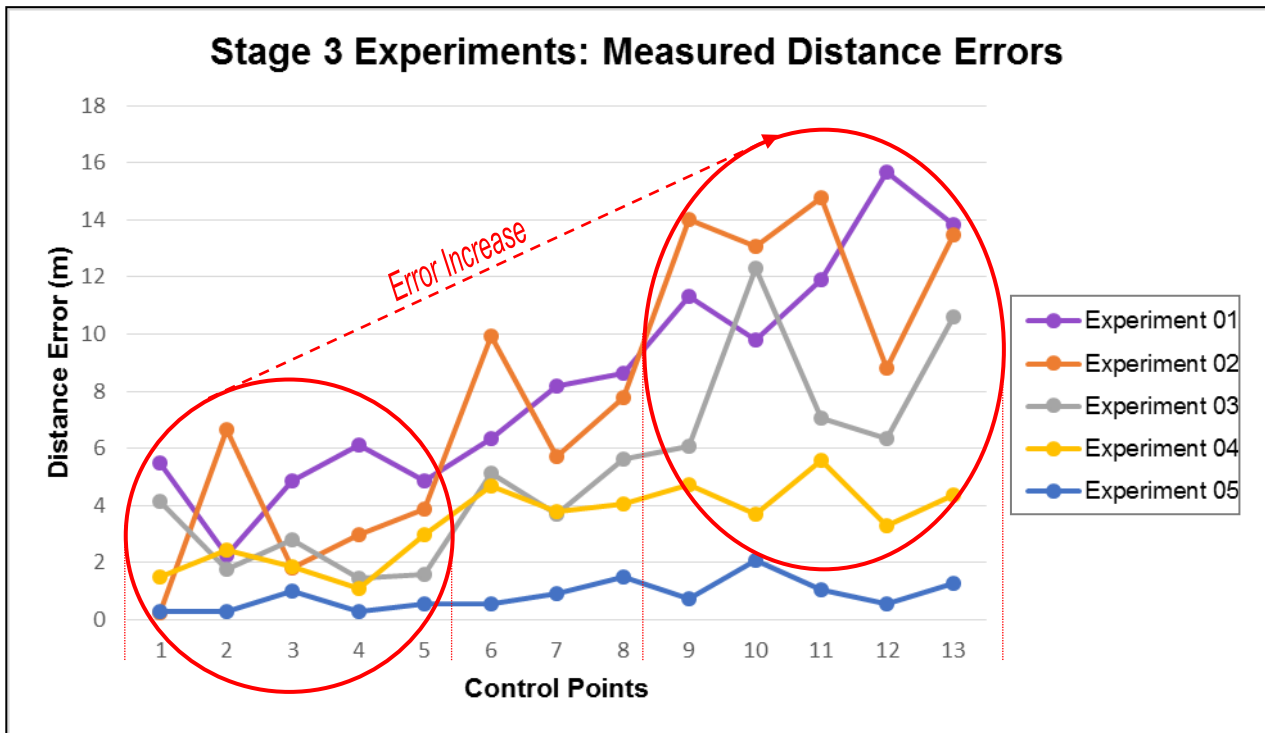


Figure 4.23: Stage 3 – Experiments: Measured distance errors

It should also be noted that when comparing the stage 3 results with the stage 1 results, only the ortho-image created from stage 3 experiment 5 produced an accuracy that can be compared with any of the stage 1 ortho-images. This should be seen in the light of the fact that only the 2 m DEM was utilised to perform the stage 3 experiments, compared to the 30 m SRTM DEM utilised during the stage 1 experiments. Considering the above, one should realise that the accuracy results achieved by the stage 3 experiments will decrease considerably if a lower accuracy DEM is used to conduct similar tests.

4.9 STUDY CONTRIBUTIONS

It was stated in Chapter 1 (Paragraph 1.6) that the contribution of this study would be three-fold. Firstly, to provide an overview (based on an exploration of scientific literature that was done in Chapter 2) of the input requirements necessary to achieve precise orthorectification of HR satellite imagery. Secondly, investigating the influence that the number of GCPs and the quality of DEMs has on the positional accuracy of an ortho-image.

Tests were conducted by increasing the number of uniformly distributed GCPs as well as various accurate DEMs. The results showed that when more GCPs were applied, the lesser the difference in accuracy was between the different DEMs utilised. Thirdly, to provide an answer to the question: *“To what extent an inadequate number of GCPs that are irregularly distributed across an image scene influence the accuracy of orthorectification of satellite imagery?”*

These contributions are methodological approaches that should be considered when performing orthorectification on HRSI. They provide clarity on the number of GCPs necessary, the distribution and placement of GCPs and the effect of the elevation data and quality DEM necessary to conduct orthorectification on HRSI.

4.9.1 Requirements necessary to create accurate ortho-images

In the literature study performed in Chapter 2, it was determined that the highest level of geometric accuracy could be achieved by following the parametric approach and utilising a physical sensor model. It was also stated that it is essential to utilise accurate GCPs that are uniformly distributed and high quality elevation data. These requirements were tested by performing the stage 1 experiments.

Ground control points need to be precise and have a uniform distribution across the entire image scene. Using a GPS device to collect GCPs will render exceptional results. The number of GCPs required to create high accurate ortho-images is dependent on the type of sensor model used and the mathematical function. However, it was determined by the experiments performed during the stage 1 experiments (Paragraph 4.4) that utilising 25 GCPs will render better accuracy results than utilising a small (relatively) number of GCPs.

The importance of utilising an elevation source to perform orthorectification is undisputed in the geospatial field. DEMs eliminate terrain distortions and transform an image into an orthogonal projection. As were described in Paragraph 4.4, it is evident that the better the elevation source, the better the positional accuracy will be. This is illustrated in Figure 4.13. The red bars represent the lower quality 30 m SRTM DEM, the orange bars the 12 m DTM and the green bars the 2 m DTM that were used during the

stage 1 experiments. It is easily recognisable that the 2 m DTM increased the overall accuracy of the ortho-images. Following on from this discussion, (Figure 4.24) illustrates the requirements necessary to create a high quality ortho-image.

It was determined through the stage 1 experiments that applying the approach illustrated in Figure 4.24 to a Pléiades HRSI with a spatial resolution of 50 cm would render the best positional accuracy results. This requires the use of the physical Pléiades Orbital Pushbroom model, using 25 accurate GCPs and applying a very high quality elevation source. A positional accuracy almost equivalent to the pixel size of the image can be expected (Table 4.1). This accuracy will however be degraded by incorporating the GPS device error determined when the GCPs were captured.

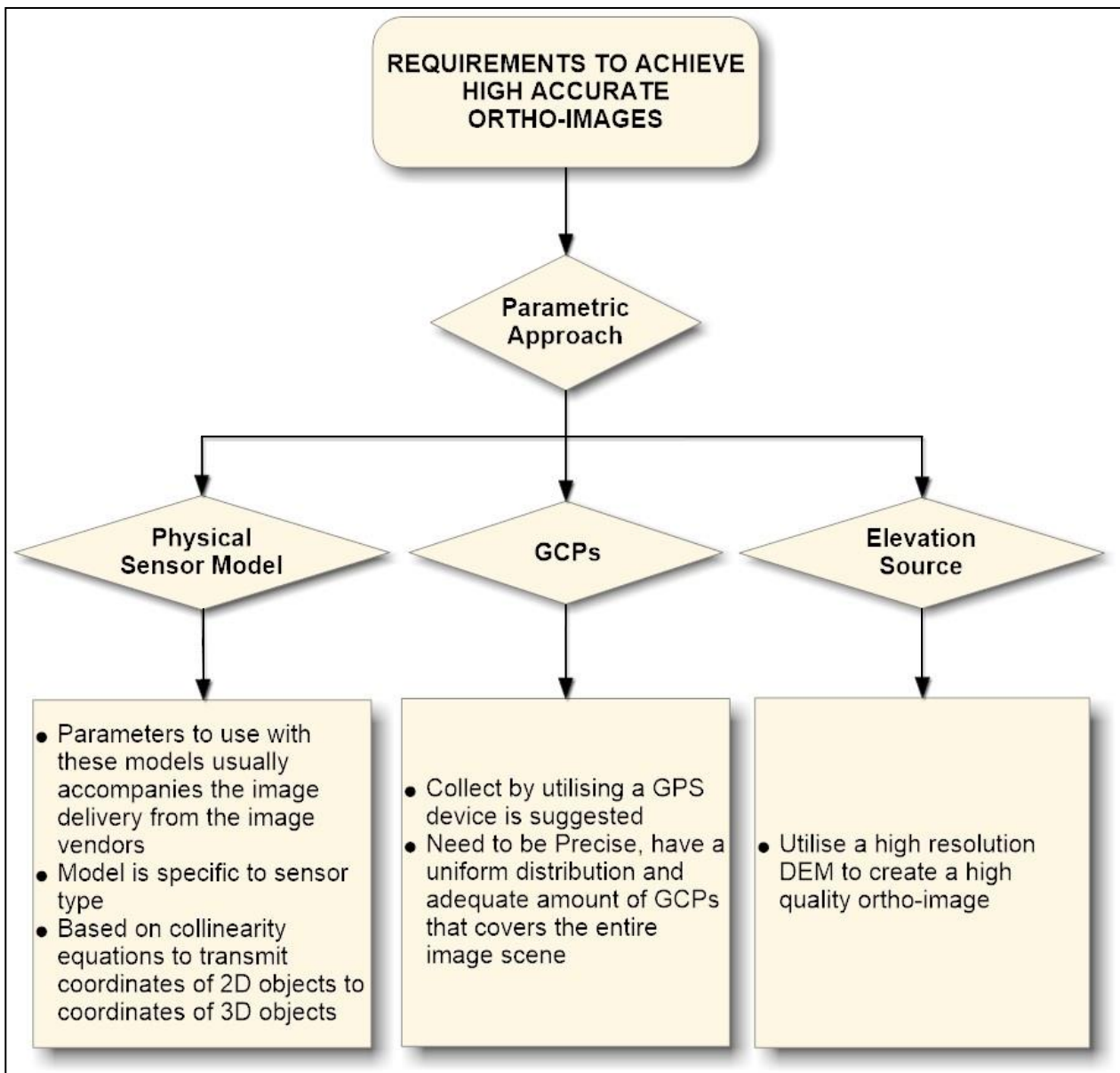


Figure 4.24: Requirements necessary to achieve high accurate ortho-images

4.9.2 Contributions derived from the stage 2 experiments

Two contributions are derived which relates to the two independent experiments that were performed during stage 2 of the empirical research:

- a) Utilising TerraSAR-X acquired GCPs as an alternative to using a limited number of GCPs that are irregular distributed in only one part of an image scene. As were described in Chapter 3 (Paragraph 3.6.2.3.3), TerraSAR-X produces unrivalled accuracies of 1 m and 3 m for the two GCP products available. During this study, the GCP-3 product was utilised and 10 GCPs were delivered with an accuracy of 1 m. The accuracy achieved from this experiment is described in Paragraph 4.5.1. It is therefore, the contribution of this study that the TerraSAR-X-based GCPs can certainly be used as an alternative to collecting manual GCPs using a GPS device, even more so when vector road layers are used to extract GCPs. However, it should be noted that acquiring these points could be very expensive. It is stated by Airbus Defence and Space on their website²⁰ that the price (May 2016) for the TerraSAR-X GCP-1 product is € 6,200.
- b) Considering not using GCPs as part of performing orthorectification and only use the physical sensor model and an elevation source. This approach can be considered as opposed to extracting GCPs from a vector road layer that are only located in a small area of the entire image scene. As was mentioned in Paragraph 4.6, the accuracy achievable from following this approach will not render accuracies as good as when GCPs are evenly distributed across the image scene. It is the contribution of this study to consider this approach for performing orthorectification before extracting GCPs from a vector road layer that have limited distribution.

4.9.3 The influence of inadequate and irregular GCPs on orthorectification

Executing the stage 3 experiments provided evidence that the relative orthorectification accuracy achieved were reasonably acceptable. Many applications can be performed with the accuracies that were achieved. However, with regards to the absolute accuracy that was achieved, the results are undesirable. Only experiment 5, using an irregular

²⁰ Airbus website: <http://www.intelligence-airbusds.com/en/122-price-lists>

distribution of GCPs that covers the entire image scene with a high-resolution DEM, delivered an acceptable accuracy result.

It can be expected that the overall positional accuracy of an ortho-image will be unsatisfactory when utilising an inadequate number of GCPs that are distributed only in a specific area of an image scene. It was illustrated by Figures 4.17 – 4.21 that the image will be more accurate in the vicinity where the GCPs are located. This is indicated by the red CPs that are closer to the centre of the PolarPlot diagrams for each experiment. Measurements taken further from the located GCPs show a decrease in positional accuracy, as is indicated by the yellow and green CPs. These accuracy drifts were measured for each experiment:

- a) closer to the cluster of the input GCPs (red CPs), the average positional accuracy was 3.04 m;
- b) in the middle section of the image (yellow CPs), the average accuracy was 6.13 m; and
- c) furthest away from the cluster of input GCPs (green CPs), the average accuracy was measured at 9.53 m.

It is also evident by examining Figures 4.17 – 4.21 that the accuracy drift for each experiment is in one direction, but not related to the placement of the input GCPs. Meaning that a placement of input GCPs on the west side of an image will not necessarily create an accuracy directional drift to the east side of the image, due to the influence of the elevation source. In some instances, this might be true as is the case in Figure 4.17, but Figure 4.18 shows a drift to the southwest for input GCPs that were on the east side of the image. Figure 4.19 illustrates input GCPs that were on the north side of the image, but indicates a drift to the northeast and Figure 4.20 shows a drift to the southeast, but the input GCPs were on the south side of the image. Therefore, the accuracy results of an ortho-image created from limited input GCPs that are distributed in a specific area of the entire image scene are unpredictable.

It is therefore the contribution of this study not to consider using a vector line layer (e.g. road layer) to extract GCPs to use as input points during orthorectification. However, when a vector line layer is the only source available for collecting input GCPs, ensure that GCPs are selected that covers the entire image scene. Although this approach is

not recommended, it will render acceptable results that can be applied for use in certain GIS related applications. This is evident in the distribution of measured CPs for Figure 4.21, which has a more random CP distribution compared to the other stage 3 experiments and delivered the best positional accuracy result. When using this approach, consider the application of GCPs discussed in Paragraph 2.4.1, that GCPs should have the characteristic to easily distinguish features on the image and corresponding features on the ground.

Consider the following factors when extracting GCPs from vector line features:

- a) If possible determine the direction of travelling as this will ensure that the GCP will be extracted on the correct side of a multi-lane road.
- b) The most feasible location for extracting GCPs will be where feature boundary outlines are clearly distinguishable, such as at road crossings, stop street road markings, centre points of traffic circles, etc.
- c) Always extract GCPs on a straight stretch of the road (e.g. just before the road turns) and never on curved roads or after a road turn. The predictive filter of a GPS device normally produces an off-the-road trajectory for curved roads, which provides a false representation of where the exact location is of the road.
- d) Never extract GCPs in a location with surrounding obstacles, such as high buildings, covered canopy of trees or electricity pylons. These obstacles interfere with the GPS signals and degrade the readings.

4.9.4 Concluding notes

The contributions of this study highlighted various considerations when performing orthorectification of HRSI. The use of precise data and reference sources were described, tested and analysed. It indicated that the location accuracy of ortho-images is influenced by utilising low quality elevation data sources and limited number of GCPs that are irregularly distributed.

Various orthorectification scenarios were tested and presented. These scenarios need consideration when conducting orthorectification to be able to contemplate all options available that can be applied to achieve a specific outcome. Considering these various

options will enable operators to produce a required ortho-image that is suitable for a specific application.

4.10 FINAL OUTCOME

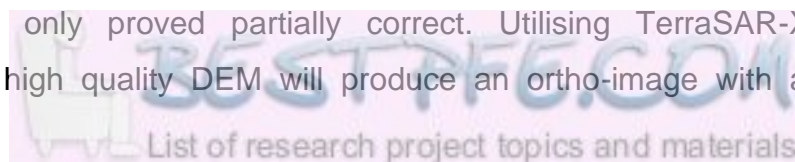
In the Paragraphs to follow, the Hypotheses which were identified in Paragraph 1.2.2 are discussed and proven correct or incorrect.

One of the purposes of the stage 1 experiments was to test Hypothesis 1. From these experiments, it was determined that there is an increase in the accuracy of ortho-images when accurate DEMs are used. This was illustrated in Figure 4.14. Therefore, Hypothesis 1 was proved correct. Also from comparing the stage 1 and 3 experiments, it was derived that the uniform distribution of GCPs influence the accuracy of an ortho-image and therefore research question 1, formulated in Chapter 1 (Paragraph 1.2.2), is answered. It was determined by the stage 1 experiments that the number of GCPs that are uniformly distributed across a single satellite image scene influence the accuracy of an ortho-image. This was proved by the results achieved from the experiments performed firstly with 5, then 13 and lastly with 25 GCPs (Table 4.1). Research question 2 is answered.

Hypothesis 2 was determined to be correct from the analysis performed on the stage 3 experiments. It was described in Paragraph 4.8 that there is a decrease in the accuracy of ortho-images when an inadequate number of GCPs are randomly distributed.

The answer to research question 3 is derived from the analyses that were performed on the stage 3 experiments (Paragraph 4.8). It was confirmed that the accuracy of an ortho-image is best in proximity to the cluster of input GCPs and poor accuracy furthest away from the input GCPs. It is also indicated in Paragraph 4.9.2 that the accuracy drift is in one direction and not related to the placement of the input GCPs. Accuracy of an ortho-image is therefore unpredictable when utilising limited GCPs that only covers a specific area in an image scene.

Hypothesis 3 was only proved partially correct. Utilising TerraSAR-X GCPs in conjunction with a high quality DEM will produce an ortho-image with an accuracy



equivalent to that of an ortho-image produced from utilising manually collected GCPs. This is only true when using 5 GCPs, which were manually collected. In the case where 13 and 25 manually collected GCPs are used, the accuracy of the ortho-image created from using TerraSAR-X GCPs is not as good. However, it should be noted that the accuracy difference between these two GCP collection methods is very small. It is therefore plausible to utilise TerraSAR-X GCPs instead of manually collected GCPs to create an accurate ortho-image – research question 4 is answered.

Hypothesis 4 was tested by the stage 2 independent experiment 2 that was performed. It was determined from analysing the results of this experiment that following the approach of utilising only a geometric sensor model and an elevation source to create an ortho-image should only be considered as opposed to extracting GCPs from a vector road layer that are only located in a small area of the entire image scene. This is also true for when using GCPs of which the accuracies cannot be proved. Hypothesis 4 is therefore proved correct. Utilising only a geometric sensor model and elevation source can substitute the process of acquiring GCPs to perform orthorectification. Nevertheless, it should be mentioned that the accuracy obtained from following this approach would not render accuracies as good as when utilising manually collected GCPs that are evenly distributed across the image scene. Consequently, research question 5 is answered. Following this approach would result in a comprehensive accurate ortho-image when compared to added GCP experiments, which can be applied to many GIS related applications as were described in Paragraph 4.6.

4.11 REALISING THE NEED FOR DEVELOPING AN AUTOMATIC GCP EXTRACTION SCRIPT (A-GCP-ES)

It should also be noted that whilst conducting the experiments described during this chapter, the challenge to accurately place/capture input GCPs was confirmed (Paragraph 4.2), especially when repeating orthorectification for the purpose to perform accuracy analysis. Capturing GCPs, through placing input points (GCPs) to corresponding reference points on the primary image data (Figure 4.1), is a daunting task. Therefore, one additional study contribution was developed which is the creation of an automatic GCP extraction script. The development, functioning and analysis of this script are described in Chapter 5.

4.12 CHAPTER SUMMARY

This chapter started by highlighting the procedure to follow when performing orthorectification on a HR Pléiades primary panchromatic image. Various orthorectification experiments were conducted utilising this procedure. Orthorectification experiments were performed in three stages. Firstly, utilising manually collected GCPs that were uniformly distributed across an entire image scene and various quality elevation sources. Secondly, performing two independent experiments related to alternative methods for creating ortho-images. Thirdly, performing numerous experiments using GCPs that were extracted from vector road layers. The results achieved from all these experiments were analysed, triangulated and compared to each other. This created the opportunities to test the hypotheses and answer the research questions that were formulated in Chapter 1. This empirical research also allowed for presenting four different study contributions, which were presented in this chapter.

CHAPTER 5 – DEVELOPMENT OF AN AUTOMATIC GCP EXTRACTION SCRIPT

5.1 INTRODUCTION

It was stated in Chapter 4 (Paragraph 4.2) that the involvement of an operator influences the accuracy of performing orthorectification on satellite imagery. This is especially true when the operator needs to manually select and place GCPs on primary image data to tie the image to a reference source. The operator needs to identify the pixel location in the primary image that correspond to the x, y and z values of the related reference point in the reference source. This is done by zooming in to pixel scale on the primary image and identifying the location on the image to place the input point that corresponds to the reference point (Figure 4.2).

The difficulty to perform this task was realised when the Stage 1 experiments were performed. During the Stage 1 experiments, 5, 13 and 25 GCPs had to be manually placed on the correct location of the primary image that corresponds to the GPS points that were collected for this study. Precautions were put in place and a manual verification process was followed to ensure that GCPs were placed in the correct location on the image for all experiments conducted. This manual verification process is described below in Paragraph 5.2.

This daunting task of accurately placing the GCPs on the image directed the need to develop a means to ease this process. Especially, when orthorectification of the same data sets is performed repetitively for testing parameter settings and accuracy assessments. After numerous attempts to resolve this issue, performing orthorectification on different image processing software (ERDAS IMAGINE® 2015 and PCI Geomatics 2015), the idea to develop a script to eliminate the possible human error when manually placing GCPs as well as to ease this process was conceived. An automatic GCP extraction script, which henceforth is referred to as the A-GCP-ES (Automatic Ground Control Point Extraction Script) was developed.

Although ERDAS IMAGINE® 2015 was the software of choice for performing the orthorectification experiments during this study, which has its own scripting language, namely ERDAS Macro Language (EML), the Python programming language was



selected for scripting. It is stated on the Python webpage (Python, 2016) that *“Python is an interpreted, object-oriented, high-level programming language with dynamic semantics. Its high-level built in data structures, combined with dynamic typing and dynamic binding, make it very attractive for Rapid Application Development, as well as for use as a scripting or glue language to connect existing components together. Python's simple, easy to learn syntax emphasizes readability and therefore reduces the cost of program maintenance. Python supports modules and packages, which encourages program modularity and code reuse. The Python interpreter and the extensive standard library are available in source or binary form without charge for all major platforms, and can be freely distributed.”*

Python is becoming more and more the programming language for most GIS and image processing software, because it can effortlessly be integrated into many operating systems and software programs. It supports multiple programming paradigms, is easy to work with and has many extensions, such as SciPython and Numerical Python.

The development of the A-GCP-ES, its functionality, ease of use and testing are described in the Paragraphs that follow.

5.2 MEASURES FOLLOWED TO VERIFY PLACEMENT OF GCPS

During the Stage 1 experiments (Paragraph 4.3), nine different experiments were performed utilising 5, 13 and 25 GCPs. Each of these experiments was performed numerous times to ensure the validity and reliability of the results achieved.

It was realised that whenever each of these experiments was repeated, the placement of GCPs had to not only correspond to the reference points, but also be placed in exactly the same location as when it was previously placed for the same GCP. To ensure that this was the case, a reference document (illustrated by Figure 5.1) was created that consisted of illustrations indicating the exact placement of GCPs. This document allowed for manually verifying that each GCP was placed on the precise location when experiments were repeated.

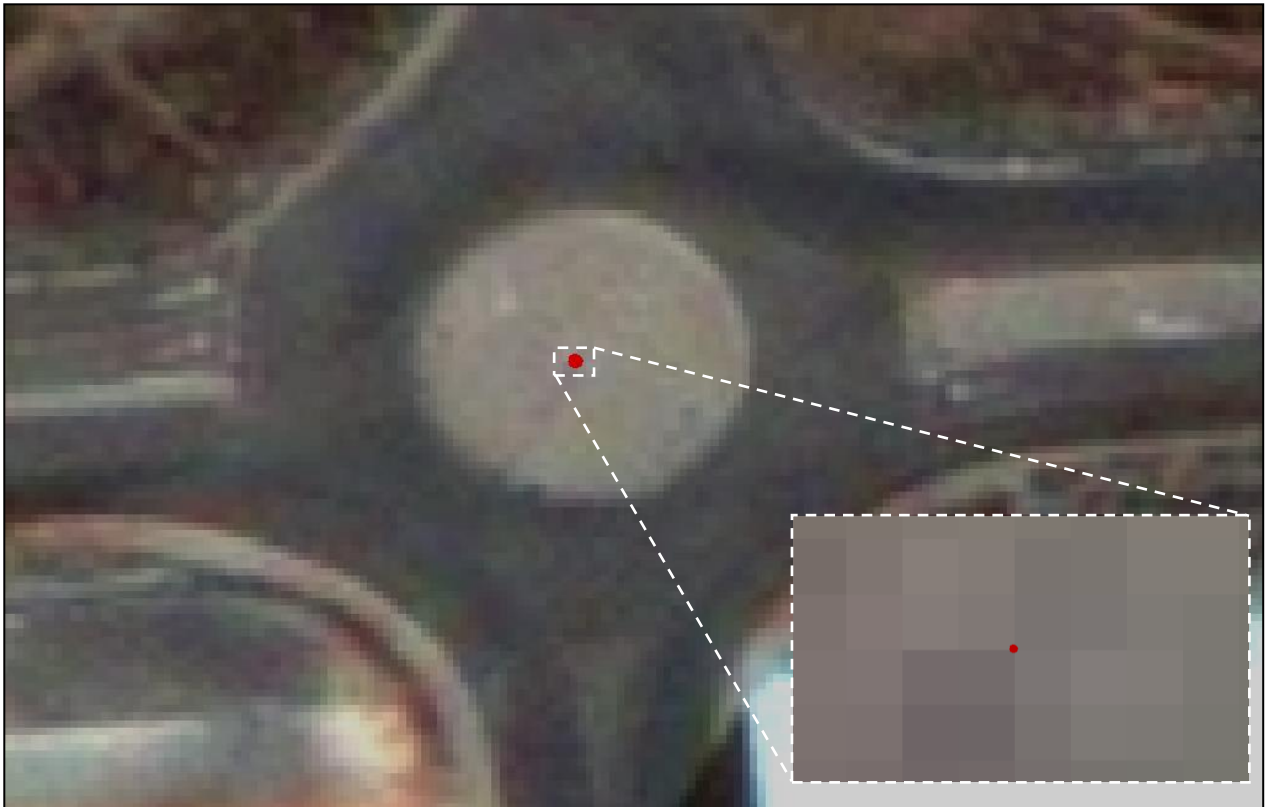


Figure 5.1: Screen capture of reference document used to verify the accurate placement of GCPs

As is indicated by the example, illustrated by Figure 5.1, the area where each collected GCP needed to be placed on the image was indicated by zooming in to pixel scale and identifying the exact location. In this example, the GCP represents the centre of a traffic circle. This was done for each of the GCPs that needed to be placed on the image. This ensured that each repeated experiment used GCPs that accurately represented its location placement.

However, this was a daunting and time-consuming process to follow every time experiments had to be repeated. Therefore, the A-GCP-ES was developed for the purpose to reduce the time it takes to perform repetitive single frame parametric orthorectification.

5.3 BACKGROUND CONCEPT OF THE A-GCP-ES

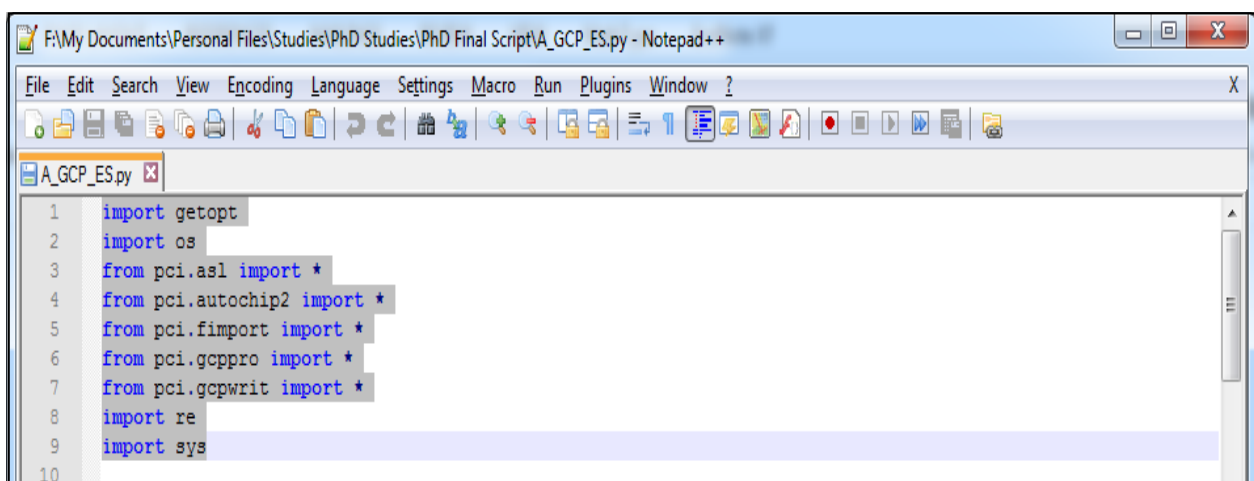
The concept of the A-GCP-ES was not conceived as a means to replace the capturing of GCPs when performing orthorectification, but rather to assist the operator that performs repeated orthorectification on the same dataset. This script extracts input GCPs from a

pre-created chip dataset consisting of the original GCPs (reference GCPs) that were collected by utilising the specified GPS devices, described in Paragraph 3.6.2.3.1. This script extracts the exact point coordinates (input GCPs) from the primary input image that corresponds to the reference GCPs. These input GCPs can then be used repeatedly to perform single frame orthorectification and it ensures that input GCPs would consistently represent the exact location as used before. This will reduce subjective errors that are operator dependent.

Due to the lack of experience in GIS software architect and engineering, assistance to develop the A-GCP-ES was sought from Mr. Chris Böhme (Solutions Architect at PinkMatter Solutions), Mrs. Sonja Goosen and Mr. Philip Boucher (see Appendix W for the A-GCP-ES Development Request Letter). The concept of the required script was explained, ideas were exchanged and it was decided to develop the Python script utilising PCI Pluggable Functions (PPF), see Appendix X. The reason for this was due to the vast geospatial processing and analysis algorithms available in PCI Geomatica®, especially relating to chip²¹ and GCP extraction and processing.

5.4 DEVELOPMENT OF THE A-GCP-ES

The A-GCP-ES utilises PCI Geomatica PPFs (Figure 5.2) to generate a *.txt document (ASCII) that consists of x, y and z coordinates in decimal degrees and representative pixel coordinates (x and y).



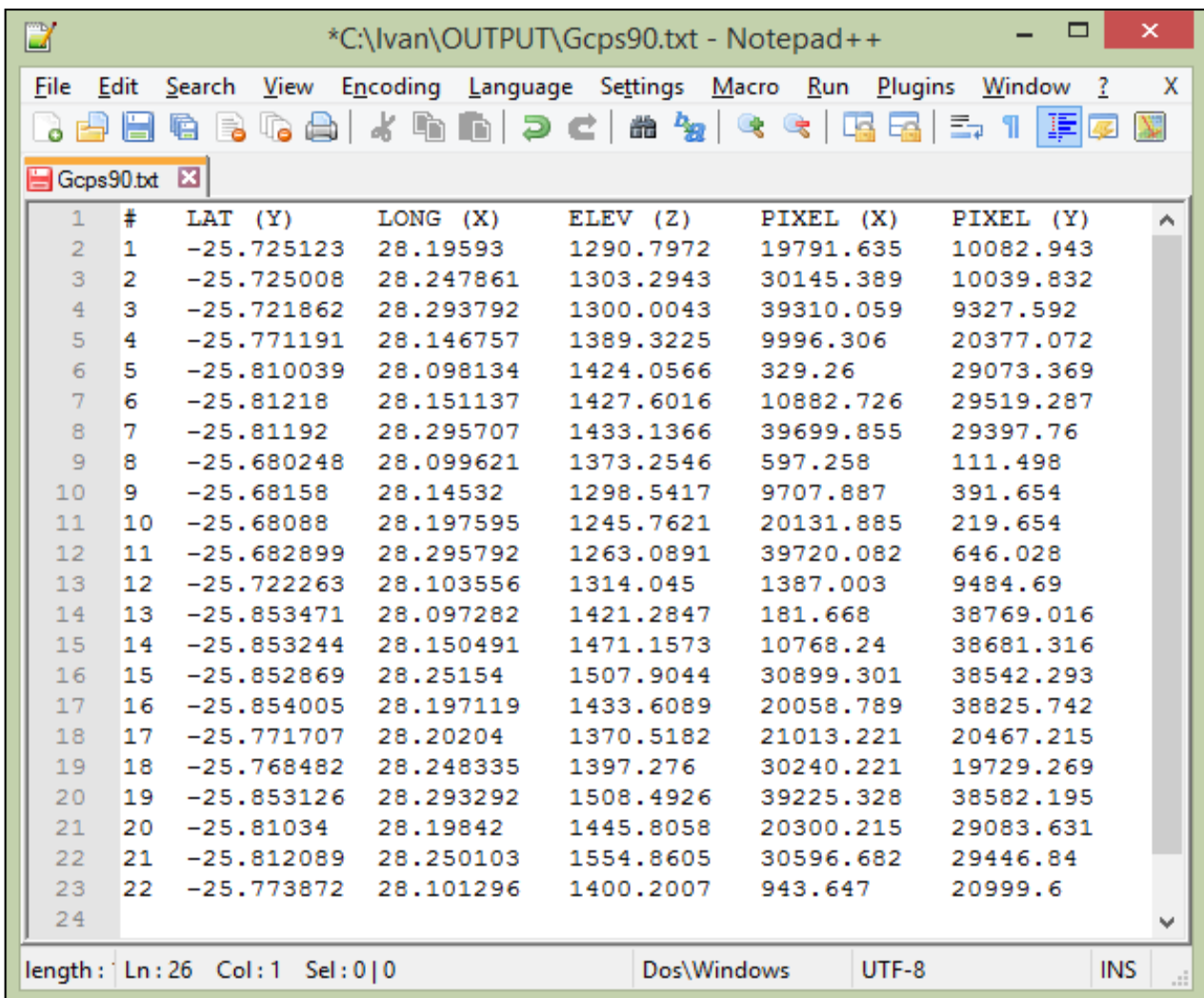
```
1 import getopt
2 import os
3 from pci.asl import *
4 from pci.autochip2 import *
5 from pci.fimport import *
6 from pci.gcpipro import *
7 from pci.gcpwrit import *
8 import re
9 import sys
10
```

Figure 5.2: The PPFs utilised by the A-GCP-ES

²¹ Chips are individual image samples or subsets that contains accurate geocoded locations and metadata extracted from a primary image source.

The GCP text document created by the A-GCP-ES indicates the representative GCPs (x, y and z coordinates) and pixel file values (x and y) extracted from a primary input image that correspond to the matching pixel locations of geocoded and highly accurate reference ground control. The reference source can be any highly accurate GPS points or an ortho-image. The PPFs (PCI Geomatics, 2016), as illustrated by Figure 5.2 to generate the output ASCII text document (Figure 5.3) are described as follows:

- a. AUTOCHIP2: “Registers a set of ground control points (GCPs) from a chip database file onto a raw image through chip matching and generates a GCP segment containing the successfully matched GCPs.”
- b. GCPPRO: “Converts the input segment or layer of Ground Control Points (GCPs) to GCPs in the specified output units and stores them in a second GCP segment or layer.”
- c. GCPWRIT: “Reads Ground Control Points (GCPs) from a specified GCP segment or layer and writes the GCP coordinates to a text file.”

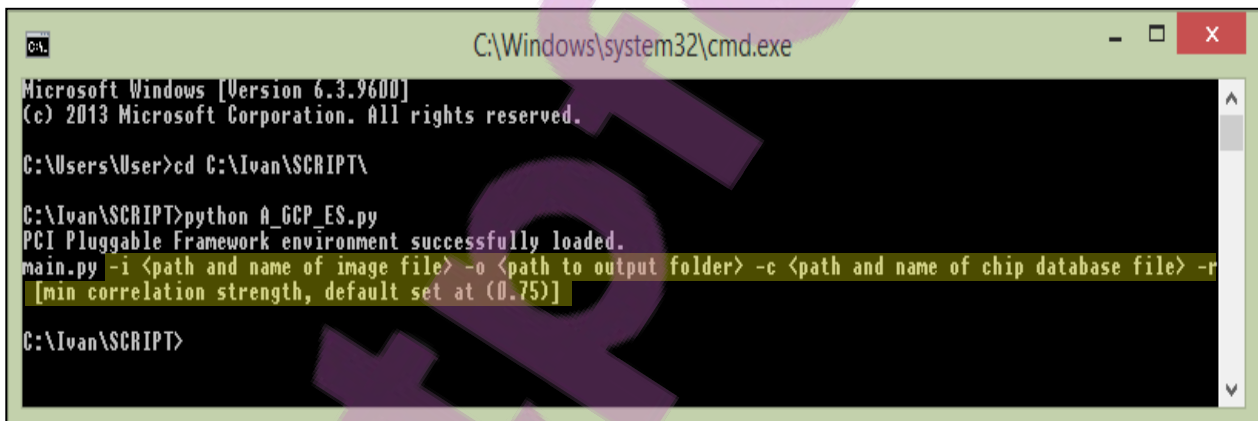


#	LAT (Y)	LONG (X)	ELEV (Z)	PIXEL (X)	PIXEL (Y)
1	-25.725123	28.19593	1290.7972	19791.635	10082.943
2	-25.725008	28.247861	1303.2943	30145.389	10039.832
3	-25.721862	28.293792	1300.0043	39310.059	9327.592
4	-25.771191	28.146757	1389.3225	9996.306	20377.072
5	-25.810039	28.098134	1424.0566	329.26	29073.369
6	-25.81218	28.151137	1427.6016	10882.726	29519.287
7	-25.81192	28.295707	1433.1366	39699.855	29397.76
8	-25.680248	28.099621	1373.2546	597.258	111.498
9	-25.68158	28.14532	1298.5417	9707.887	391.654
10	-25.68088	28.197595	1245.7621	20131.885	219.654
11	-25.682899	28.295792	1263.0891	39720.082	646.028
12	-25.722263	28.103556	1314.045	1387.003	9484.69
13	-25.853471	28.097282	1421.2847	181.668	38769.016
14	-25.853244	28.150491	1471.1573	10768.24	38681.316
15	-25.852869	28.25154	1507.9044	30899.301	38542.293
16	-25.854005	28.197119	1433.6089	20058.789	38825.742
17	-25.771707	28.20204	1370.5182	21013.221	20467.215
18	-25.768482	28.248335	1397.276	30240.221	19729.269
19	-25.853126	28.293292	1508.4926	39225.328	38582.195
20	-25.81034	28.19842	1445.8058	20300.215	29083.631
21	-25.812089	28.250103	1554.8605	30596.682	29446.84
22	-25.773872	28.101296	1400.2007	943.647	20999.6
23					
24					

Figure 5.3: The A-GCP-ES output ASCII text document

The A-GCP-ES can be executed on any computer that has an installed Python interpreter, as long as the PCI Geomatica® software is installed on that computer. However, it should be noted that executing this script requires four inputs (Figure 5.4), namely:

- a. Input image data: <-i "C:\Ivan\INPUT\INPUT_FILE_NAME.XML">
 - i. Specify the path (folder location) where the input image is saved on the computer as well as its name.
- b. Output location: <-o "C:\Ivan\OUTPUT">
 - i. Specify the path (folder location) where the output ASCII text document needs to be saved.
- c. Input chip database file: <-c "C:\Ivan\CHIP_DB\Chip_DataBase.cdb">
 - i. Specify the name and location of the chip database to use (Paragraph 5.4.1).
- d. Correlation strength: <-r "0.75">
 - i. The default value is set at 75%, but this can be changed as required. This script utilises the phase correlation method to match the relative correspondence between the input chips and the 'raw' input image pixels.



```
C:\Windows\system32\cmd.exe
Microsoft Windows [Version 6.3.9600]
(c) 2013 Microsoft Corporation. All rights reserved.

C:\Users\User>cd C:\Ivan\SCRIPT\

C:\Ivan\SCRIPT>python A_GCP_ES.py
PCI Pluggable Framework environment successfully loaded.
main.py -i <path and name of image file> -o <path to output folder> -c <path and name of chip database file> -r
[min correlation strength, default set at (0.75)]

C:\Ivan\SCRIPT>
```

Figure 5.4: Inputs required by the A-GCP-ES

5.4.1 Creating the required chip database utilising PCI Geomatica®

The chip database required by the script to be executed successfully is created by utilising the PCI Geomatica® 'PNT2CHIP' Module Control Panel. This module extracts "chips from a geocoded image using a point layer" (PCI Geomatics, 2016). The process to follow in creating the required chip database is explained as follows:

1. Open the PCI Geomatica® software and load the following reference sources (Figure 5.5). These sources should cover the same location on the Earth's surface to that of the input raster data that needs to be orthorectified:

- point layer (the GPS points captured for this study, see Paragraph 3.6.2.3.1);
- geocoded ortho-image (covering the study area); and
- elevation data source (the 2 m DTM used during this study was selected).

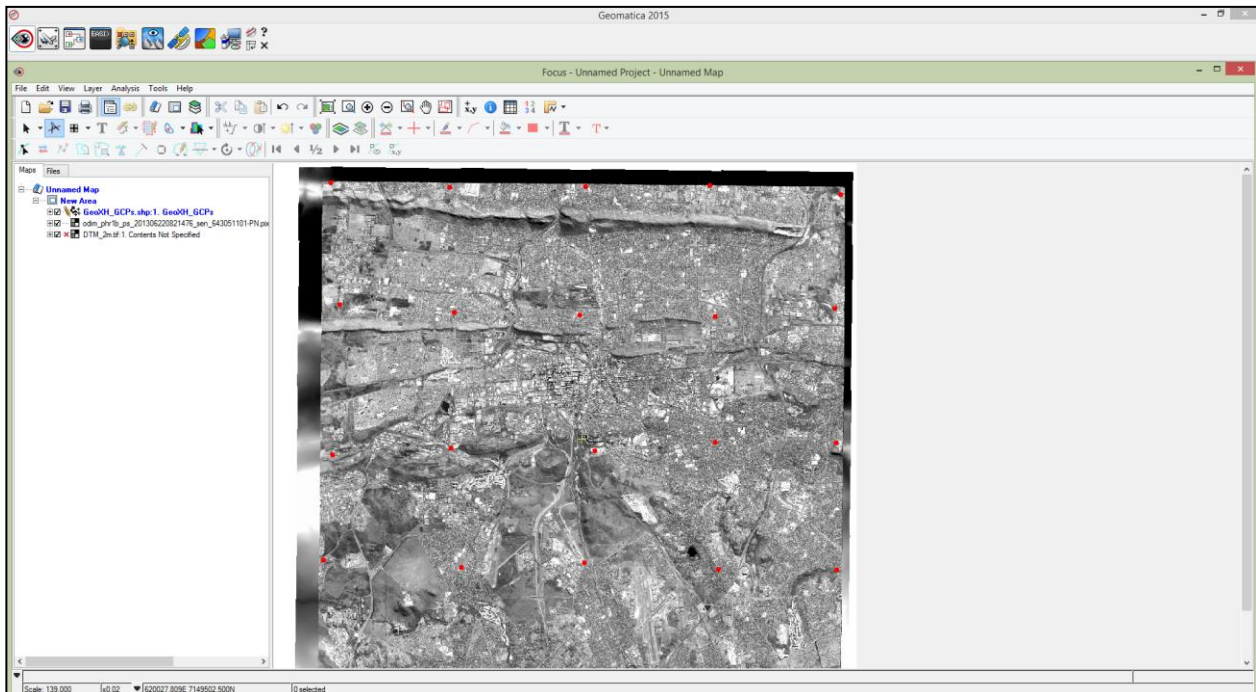


Figure 5.5: Creating Chip Database – Open the PCI Geomatica® software and load the reference sources

- Open the Algorithm Library window located in Focus on the Tools menu (Figure 5.6).

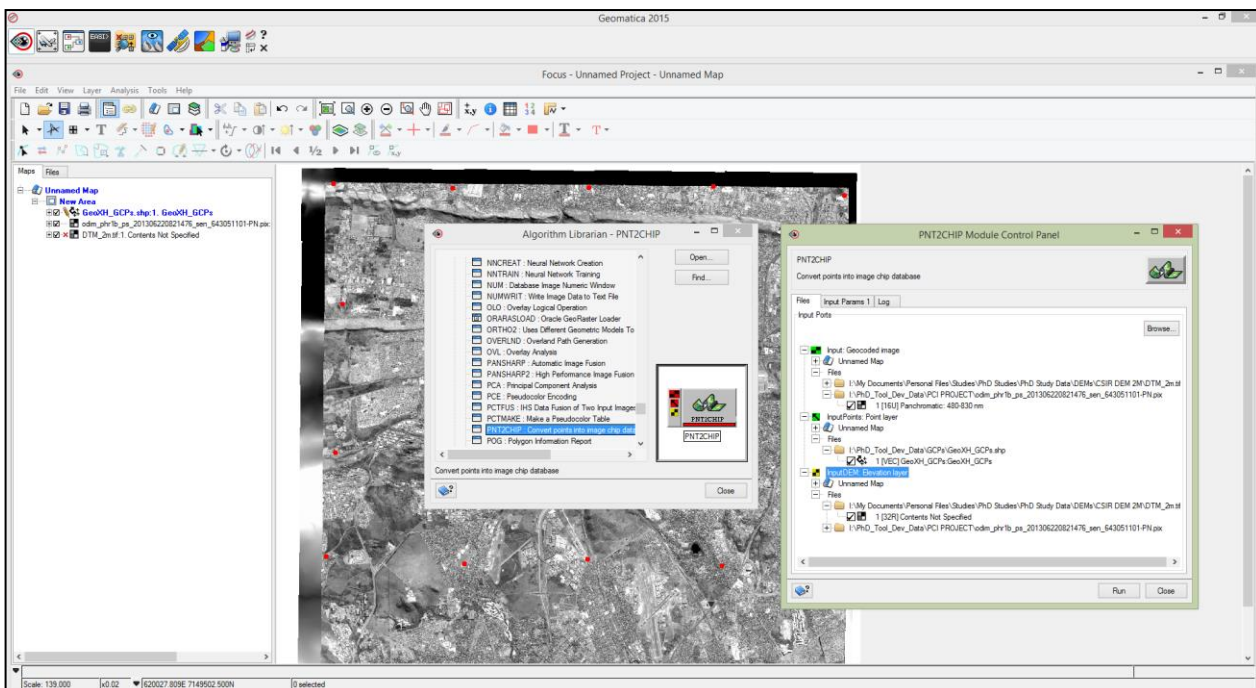


Figure 5.6: Creating Chip Database – Open the Algorithm Library window

- From the Algorithm Library window, find and open the PNT2CHIP algorithm (Figure 5.7) to extract chips from the loaded geocoded image using the point layer. Complete the parameters (Input Ports) located under the Files tab by selecting the reference sources for the Input (geocoded image), the Input Points (point layer) and the Input DEM (elevation layer).

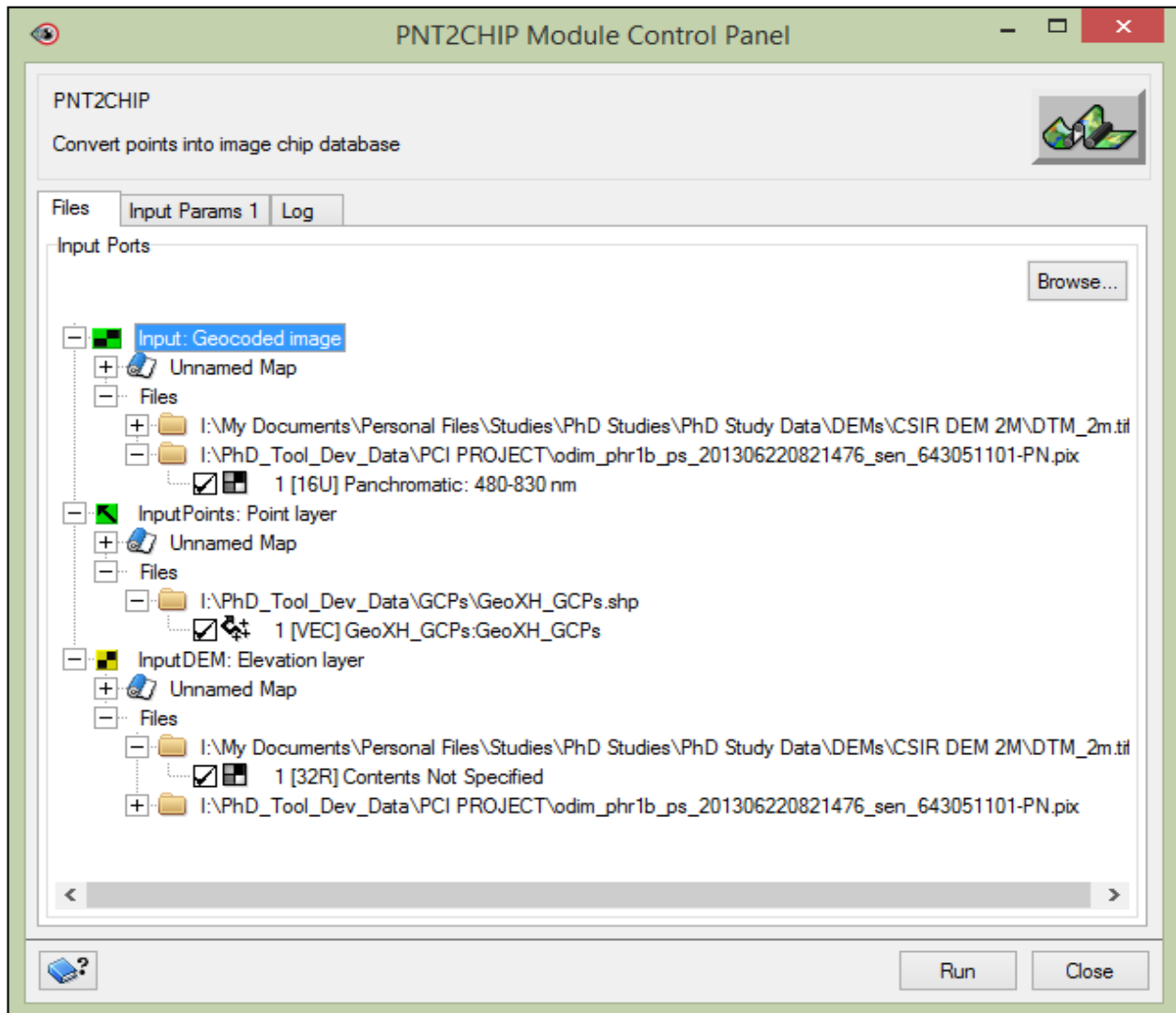


Figure 5.7: Creating Chip Database – Complete the PNT2CHIP parameters for the Input Ports

- Activate the Input Params 1 tab and provide the location and file name of the Chip Database to be created (Figure 5.8). The rest of the parameters are optional and can be completed if required. Take note that the default size for each extracted chip (in pixels and lines) is 64 and the maximum size allowed is 1024.



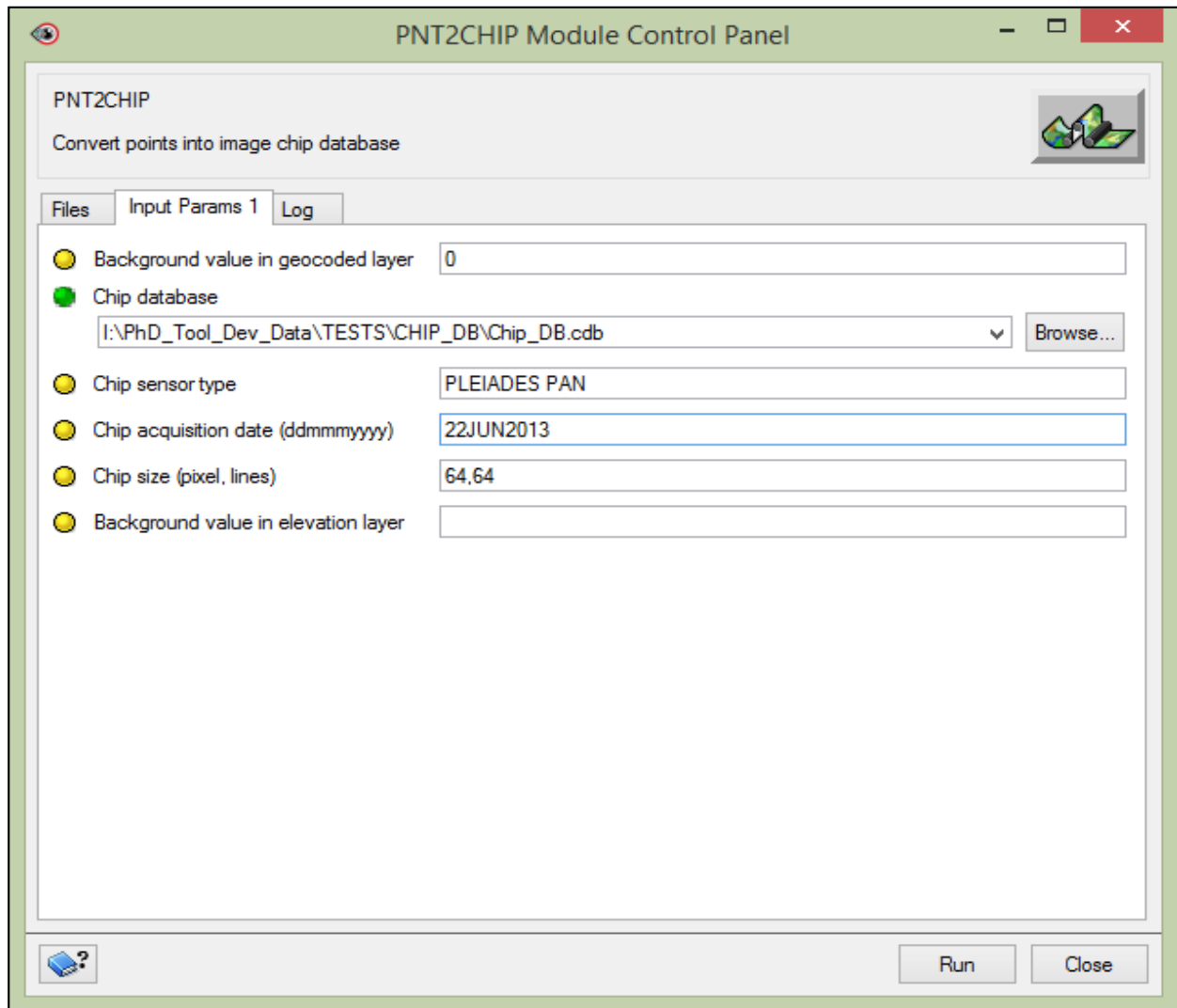


Figure 5.8: Creating Chip Database – Complete the PNT2CHIP parameters under the Input Params 1 tab

5. Lastly, run the algorithm to create the Chip Database. The chips created can now be evaluated by utilising the PCI Geomatica® Chip Manager (Figure 5.9). The Chip Manager can be opened from the PCI Geomatica® toolbar to manage image-chip libraries by adding, removing, and renaming chips from an existing database.
6. Once all the chips are evaluated, the chip database is ready and the A-GCP-ES can be executed.

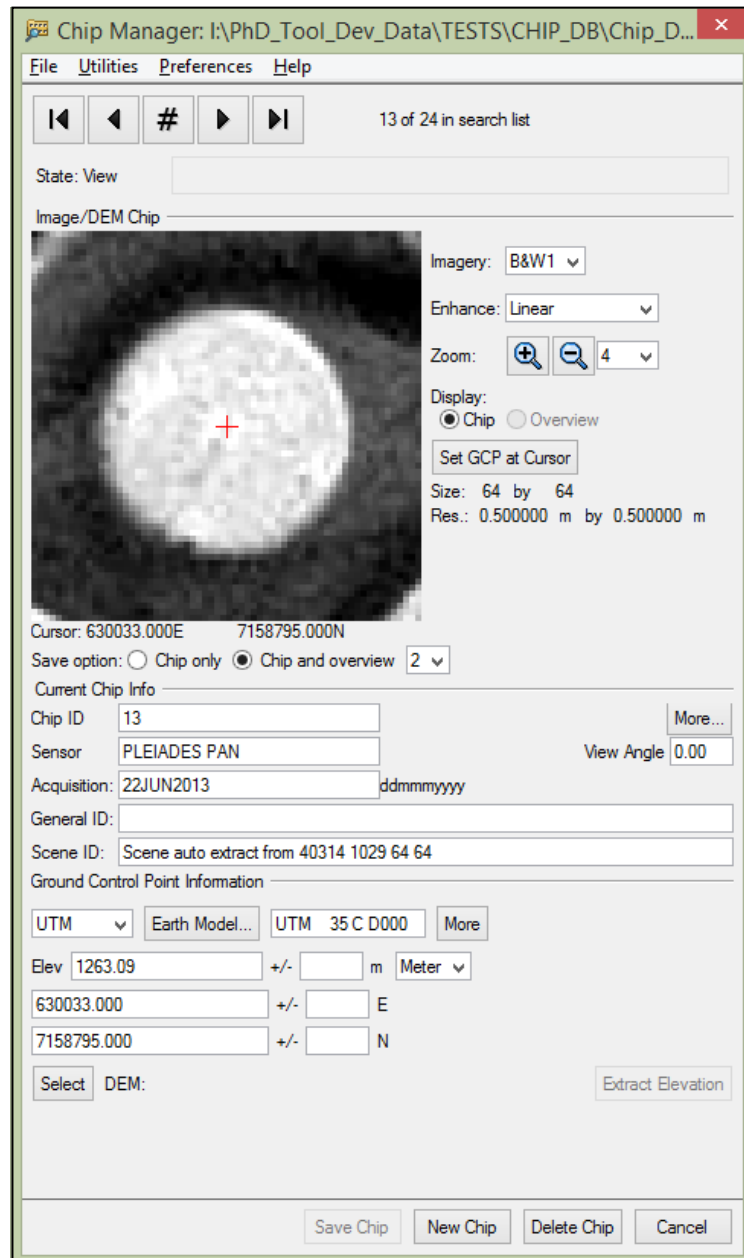


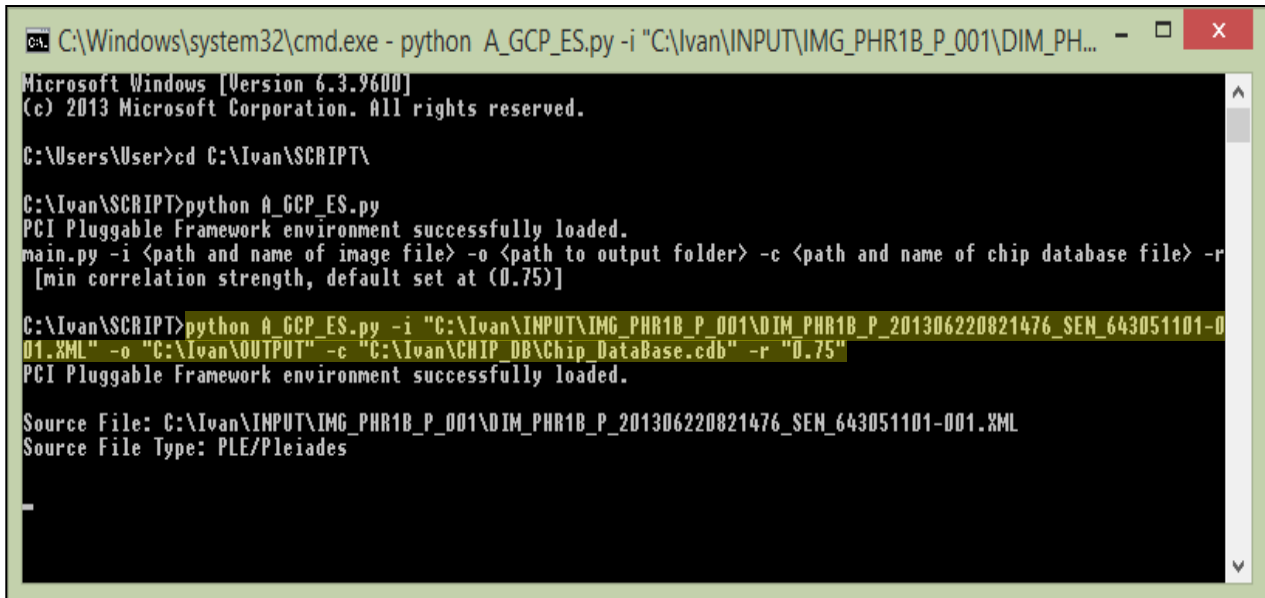
Figure 5.9: Evaluating chips by utilising the PCI Geomatica® Chip Manager

5.4.2 Executing the A-GCP-ES on Microsoft (MS) Windows operating system

As was mentioned in Paragraph 5.4, this Python script can be executed on any Python interpreter as long as the PCI Geomatica® software is installed on the same operating system. For this exercise, the MS Windows Command Prompt (CMD) interface was used to execute the A-GCP-ES. The process to run this script follows:

1. Open CMD from the MS Window start menu.
2. In CMD, navigate to the location where the script is saved. For this exercise it was saved in the folder 'SCRIPTS' with the following path: "c:\van\SCRIPTS\".

3. Type the following to load the script: “*python A-GCP-ES.py*”, and press Enter.
4. The script front-end indicates the required inputs. To successfully execute the script, run the script with the inputs provided (Figure 5.10), as described in Paragraph 5.4.



```
C:\Windows\system32\cmd.exe - python A_GCP_ES.py -i "C:\Ivan\INPUT\IMG_PHR1B_P_001\DIM_PH...
Microsoft Windows [Version 6.3.9600]
(c) 2013 Microsoft Corporation. All rights reserved.

C:\Users\User>cd C:\Ivan\SCRIPT\

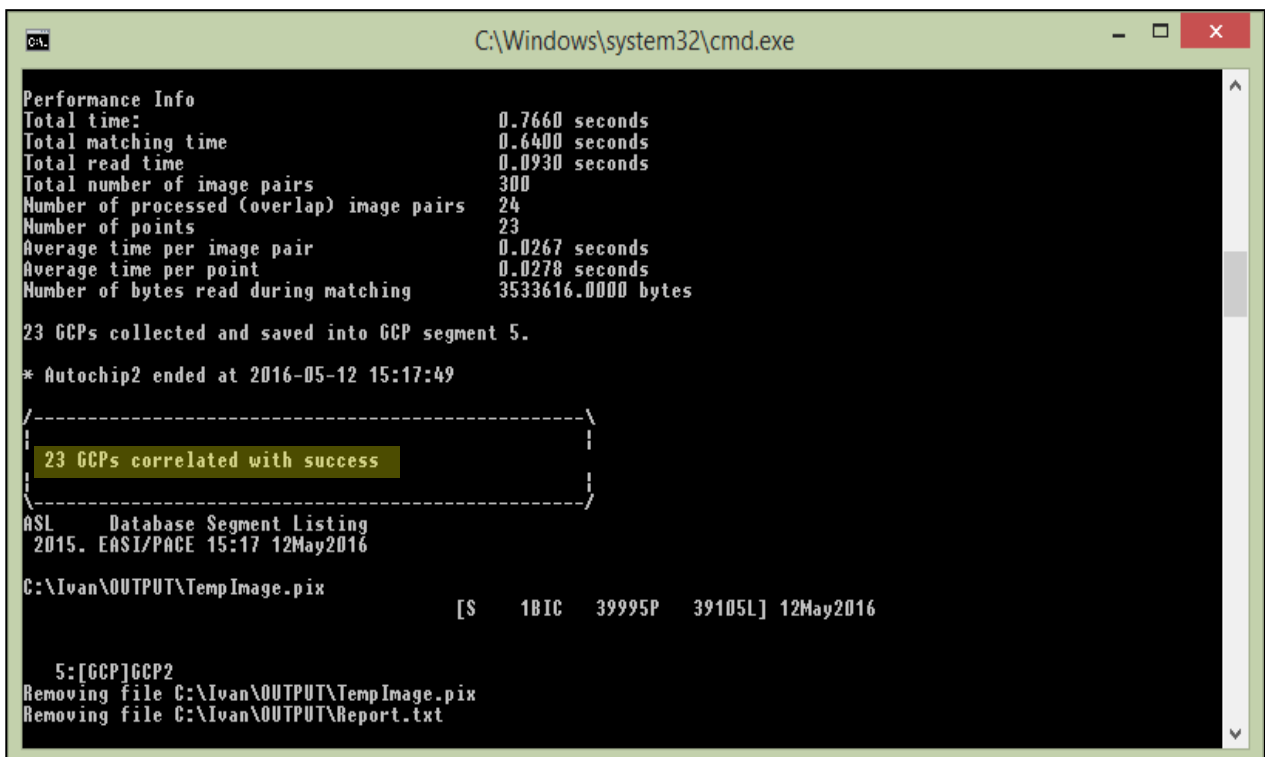
C:\Ivan\SCRIPT>python A_GCP_ES.py
PCI Pluggable Framework environment successfully loaded.
main.py -i <path and name of image file> -o <path to output folder> -c <path and name of chip database file> -r
[ min correlation strength, default set at (0.75) ]

C:\Ivan\SCRIPT>python A_GCP_ES.py -i "C:\Ivan\INPUT\IMG_PHR1B_P_001\DIM_PHR1B_P_201306220821476_SEN_643051101-001.XML" -o "C:\Ivan\OUTPUT" -c "C:\Ivan\CHIP_DB\Chip_Database.cdb" -r "0.75"
PCI Pluggable Framework environment successfully loaded.

Source File: C:\Ivan\INPUT\IMG_PHR1B_P_001\DIM_PHR1B_P_201306220821476_SEN_643051101-001.XML
Source File Type: PLE/Pleiades
```

Figure 5.10: Execute the A-GCP-ES with the required inputs provided

5. The script executes and once completed provides an executable summary with the number of GCPs that were successfully extracted (Figure 5.11).



```
C:\Windows\system32\cmd.exe

Performance Info
Total time: 0.7660 seconds
Total matching time 0.6400 seconds
Total read time 0.0930 seconds
Total number of image pairs 300
Number of processed (overlap) image pairs 24
Number of points 23
Average time per image pair 0.0267 seconds
Average time per point 0.0278 seconds
Number of bytes read during matching 3533616.0000 bytes

23 GCPs collected and saved into GCP segment 5.
* Autochip2 ended at 2016-05-12 15:17:49

-----\
| 23 GCPs correlated with success |
|-----/

ASL Database Segment Listing
2015. EASI/PAGE 15:17 12May2016

C:\Ivan\OUTPUT\TempImage.pix [S 1BIC 39995P 39105L] 12May2016

5:[GCP]GCP2
Removing file C:\Ivan\OUTPUT\TempImage.pix
Removing file C:\Ivan\OUTPUT\Report.txt
```

Figure 5.11: Executed script summary



6. Once the script is successfully executed, the output ASCII text document is created in the Output location specified (Figure 5.3). This text document created by the A-GCP-ES can now be used as the source for input points (x, y and z coordinates) to use when performing orthorectification. This point file can be used repetitively, every time the same orthorectification needs to be produced over the same input image and using the same reference sources.

On a concluding note, it should be mentioned that it might be required to convert this created ASCII text document to a physical vector point layer (e.g. ASCII GCP file with the file extension *.xml, *.shp or *.gcc) that can be loaded into a required image processing software.

5.5 TESTING AND EVALUATING THE A-GCP-ES

Testing the ASCII GCP file created by the A-GCP-ES entails the process of performing orthorectification on the same datasets and image processing software (ERDAS IMAGINE® 2015) used throughout this study. The ERDAS IMAGINE® software loads and stores input and reference ground control points in a *.gcc file, which comprises the map and projection information associated with the GCP coordinates. Therefore, the first step for testing the ASCII GCP file created by the A-GCP-ES is to convert this file (*.txt) to the ERDAS IMAGINE® GCP readable/native format (*.gcc). This process is described as follows:

1. Start the ERDAS IMAGINE® software and open the Coordinate Calculator from the Tools menu in the ERDAS IMAGINE® Icon Panel. The Coordinate Calculator is “*a utility that enables you to convert ground control coordinates from one map projection, spheroid, or datum to another*” (Hexagon Geospatial, 2015).
2. Once opened, define the input and output elevation and projection info parameters. It is important to define the output projection parameters to be representative of a map projection type such as Universal Transverse Mercator (UTM).
3. Select the Input Longitude, Input Latitude and Input Z columns and right click on the column headings to import the ASCII GCP file (Figure 5.12).

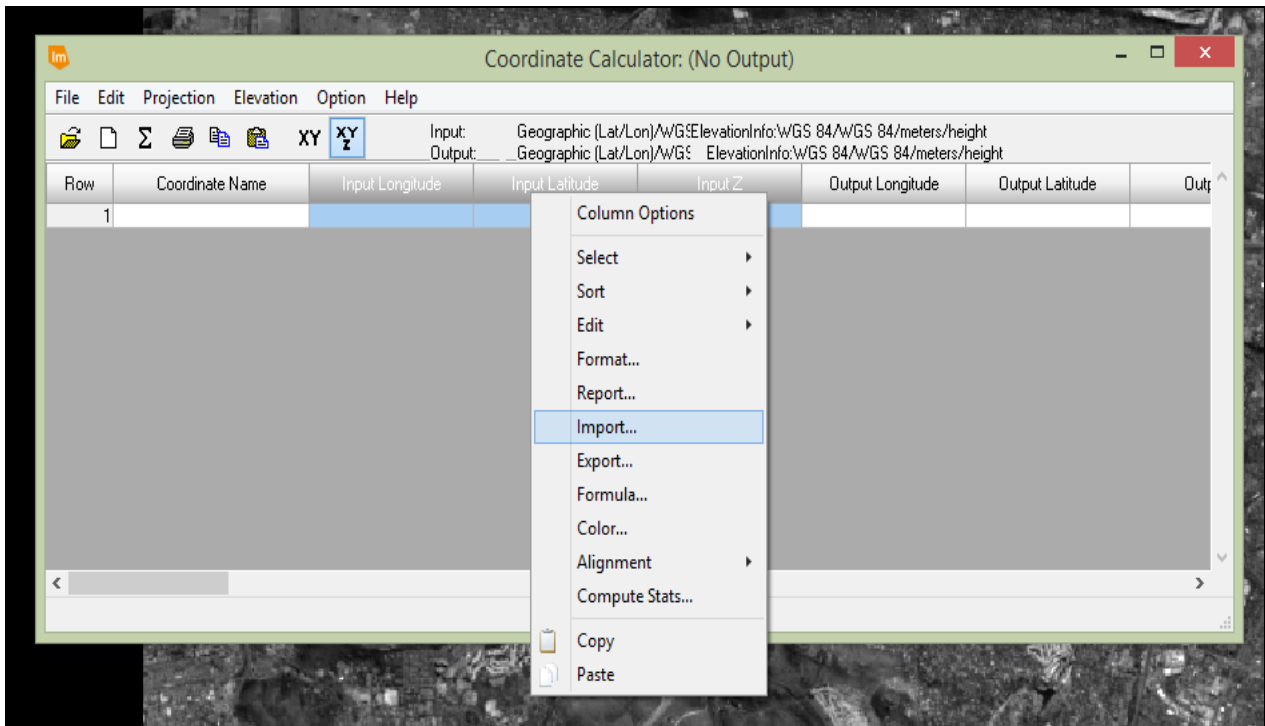


Figure 5.12: Import the ASCII GCP file into the ERDAS IMAGINE® Coordinate Calculator dialogue

- Next, the Import Data dialogue (Figure 5.13) opens and the parameters need to be formatted to correctly import the ASCII GCP file. Set the field or column in the Import Data dialogue to correspond to the ASCII file (x, y and z coordinates). For this exercise, the Field for the Input Longitude was set at “2”, the Input Latitude at “3” and the Input Z at “4”.

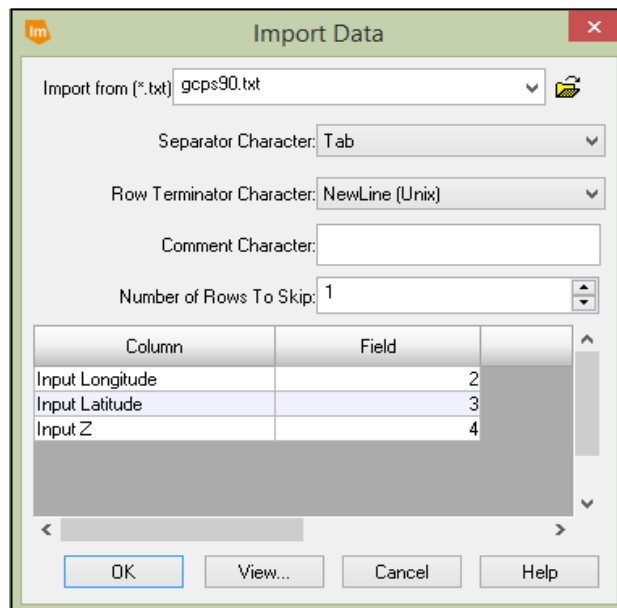


Figure 5.13: Settable fields to format the ERDAS IMAGINE® Import Data dialogue so as to correctly import the ASCII GCP file

5. The ASCII GCP file is then loaded into the Coordinate Calculator (Figure 5.14) from where it can be evaluated and edited if needed.

Coordinate Calculator: (No Output)

File Edit Projection Elevation Option Help

Input: Geographic (Lat/Lon)/WGS ElevationInfo:WGS 84/WGS 84/meters/height
Output: Geographic (Lat/Lon)/WGS ElevationInfo:WGS 84/WGS 84/meters/height

Row	Coordinate Name	Input X	Input Y	Input Z	Output X	Output Y	Output Z
1		-25.725122	28.195930	1290.797200	-25.725122	28.195930	1290.797200
2		-25.725008	28.247861	1303.294300	-25.725008	28.247861	1303.294300
3		-25.721862	28.293792	1300.004300	-25.721862	28.293792	1300.004300
4		-25.771191	28.146757	1389.322500	-25.771191	28.146757	1389.322500
5		-25.810039	28.098134	1424.056600	-25.810039	28.098134	1424.056600
6		-25.812180	28.151137	1427.601600	-25.812180	28.151137	1427.601600
7		-25.811920	28.295707	1433.136600	-25.811920	28.295707	1433.136600
8		-25.680248	28.099621	1373.254600	-25.680248	28.099621	1373.254600
9		-25.681580	28.145320	1298.541700	-25.681580	28.145320	1298.541700
10		-25.680880	28.197595	1245.762100	-25.680880	28.197595	1245.762100
11		-25.682899	28.295792	1263.089100	-25.682899	28.295792	1263.089100
12		-25.722263	28.103556	1314.045000	-25.722263	28.103556	1314.045000
13		-25.853471	28.097282	1421.284700	-25.853471	28.097282	1421.284700
14		-25.853244	28.150491	1471.157300	-25.853244	28.150491	1471.157300
15		-25.852869	28.251540	1507.904400	-25.852869	28.251540	1507.904400
16		-25.854005	28.197119	1433.608900	-25.854005	28.197119	1433.608900
17		-25.771707	28.202040	1370.518200	-25.771707	28.202040	1370.518200
18		-25.768482	28.248335	1397.276000	-25.768482	28.248335	1397.276000
19		-25.853126	28.293292	1508.492600	-25.853126	28.293292	1508.492600
20		-25.810340	28.198420	1445.805800	-25.810340	28.198420	1445.805800
21		-25.812089	28.250103	1554.860500	-25.812089	28.250103	1554.860500
22		-25.773872	28.101296	1400.200700	-25.773872	28.101296	1400.200700
23							

Figure 5.14: ASCII GCP file imported into the Coordinate Calculator

6. The next step is to save these GCP coordinates to the ERDAS IMAGINE® GCP coordinate format, namely *.gcc (Figure 5.15). This file is then saved in the specified output folder location, which can be verified.

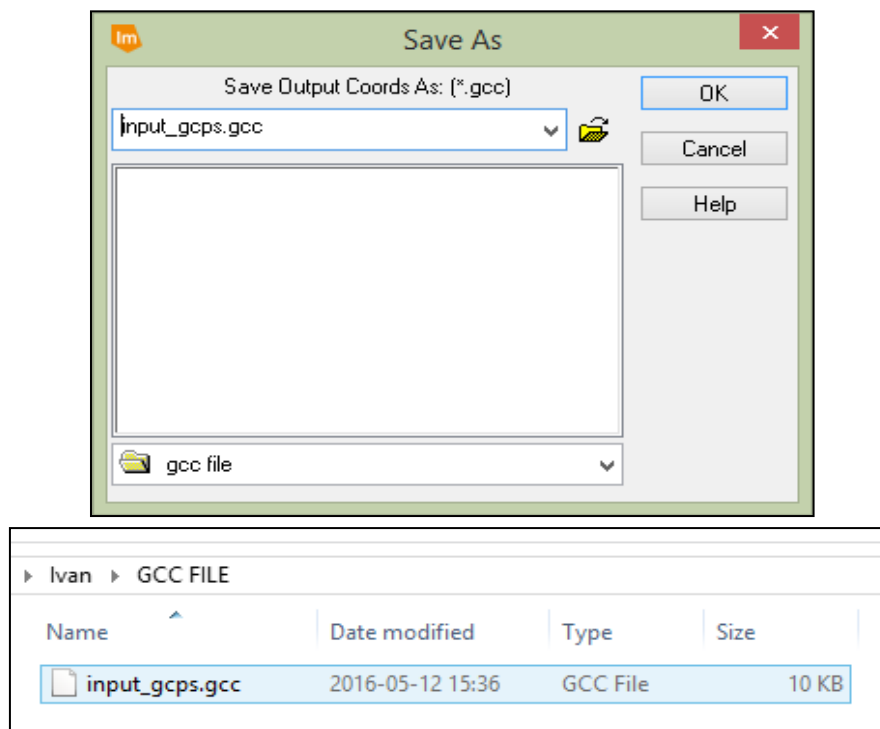


Figure 5.15: Verifying the saved *.gcc (GCP coordinate) file

7. Finally, before testing the ASCII GCP file created by the A-GCP-ES, the converted GCP coordinates need to be loaded into the ERDAS IMAGINE® Multipoint Geometric Correction workspace. This will allow for determining if the script executed successfully to extract GCPs utilising a geocoded point layer and ortho-image that corresponds to a 'raw' input image. From the File menu, select "Load Input GCPs" and navigate to the folder location of the converted GCPs created during the previous step. For this exercise, the GCPs loaded accurately and without any problems (Figure 5.16).

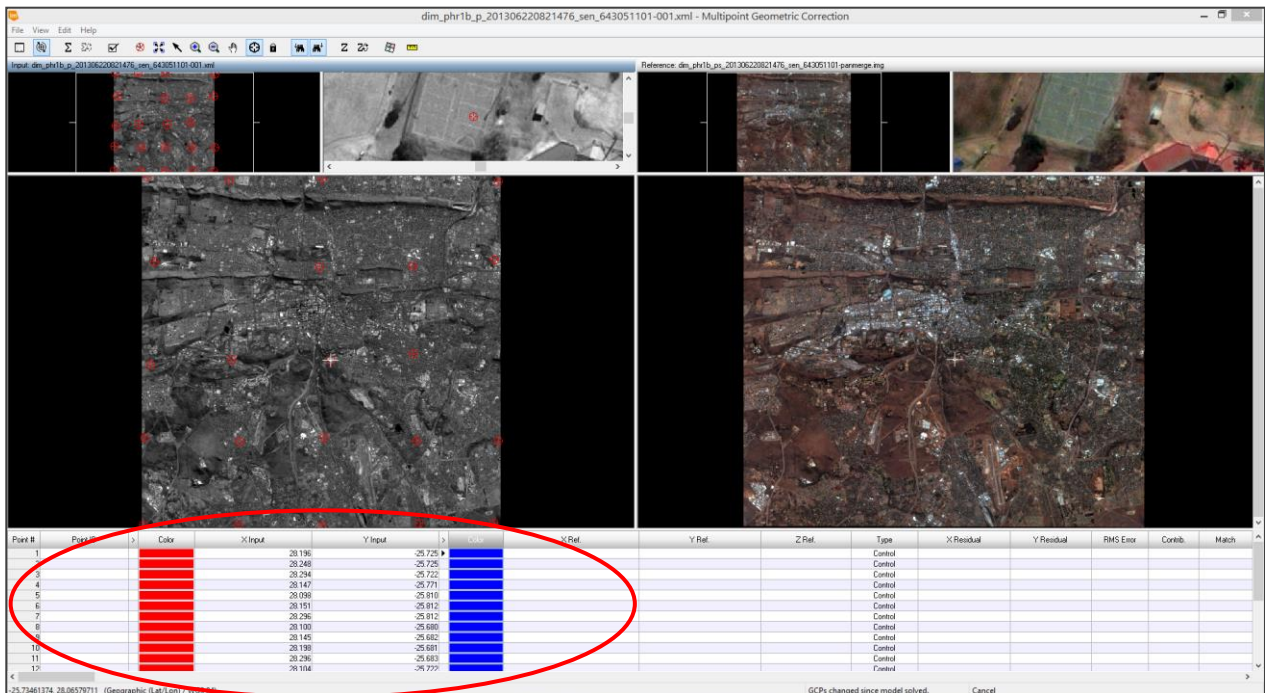


Figure 5.16: ASCII GCP file loaded into the ERDAS IMAGINE® Multipoint Geometric Correction workspace

These input GCPs can now be used repetitively to perform this specific orthorectification numerous times. In conclusion, it can be stated that the developed automatic ground control point extraction script does exactly what it was designed to do. The A-GCP-ES extracts GCPs from an input image utilising a reference point layer and geocoded image. These extracted GCPs can then be used continually to repeatedly perform orthorectification without subjective operator biases being introduced.

The next section evaluates the accuracy of the input GCPs that are manually placed by an operator and the accuracy of the GCPs extracted by the A-GCP-ES.

5.5.1 Comparing the accuracy of manually placed GCPs by an operator to the GCPs extracted by the A-GCP-ES

Comparing the accuracy of input GCPs placed by an operator and GCPs extracted by the A-GCP-ES, required numerous measurements of the positional placement of GCPs. This ensured statistical verification of subjective operator biases compared to the consistent GCP locations extracted by the A-GCP-ES. Six operators, with remote sensing and GIS experience from the Directorate Geospatial Information, were selected to each capture 5 input GCPs covering the four corners and centre of the primary image. This accounts for a total of 30 input GCPs which were manually placed by the operators. The locations of these five GCPs correspond to the locations of the five GCPs used to perform experiments 1(a), (b) and (c) of the stage 1 experiments (Paragraph 4.3), which were completed in Chapter 4. The location of the input GCPs was measured and compared to the locations of the reference GCPs, described in Paragraph 3.6.2.3.1. Measuring the 30 input GCPs provided a good statistical dimension for validating the manual placement accuracy of input GCPs captured by the operators. Figure 5.17 illustrates the standard deviation measurements (in metre) attained by the six operators. It is evident that the operators did not struggle to place input GCPs that corresponds to the locations of the reference GCPs. An average standard deviation of 10.92 cm at 90% CE was measured. The MAA report for each operator is attached as Appendix Y.

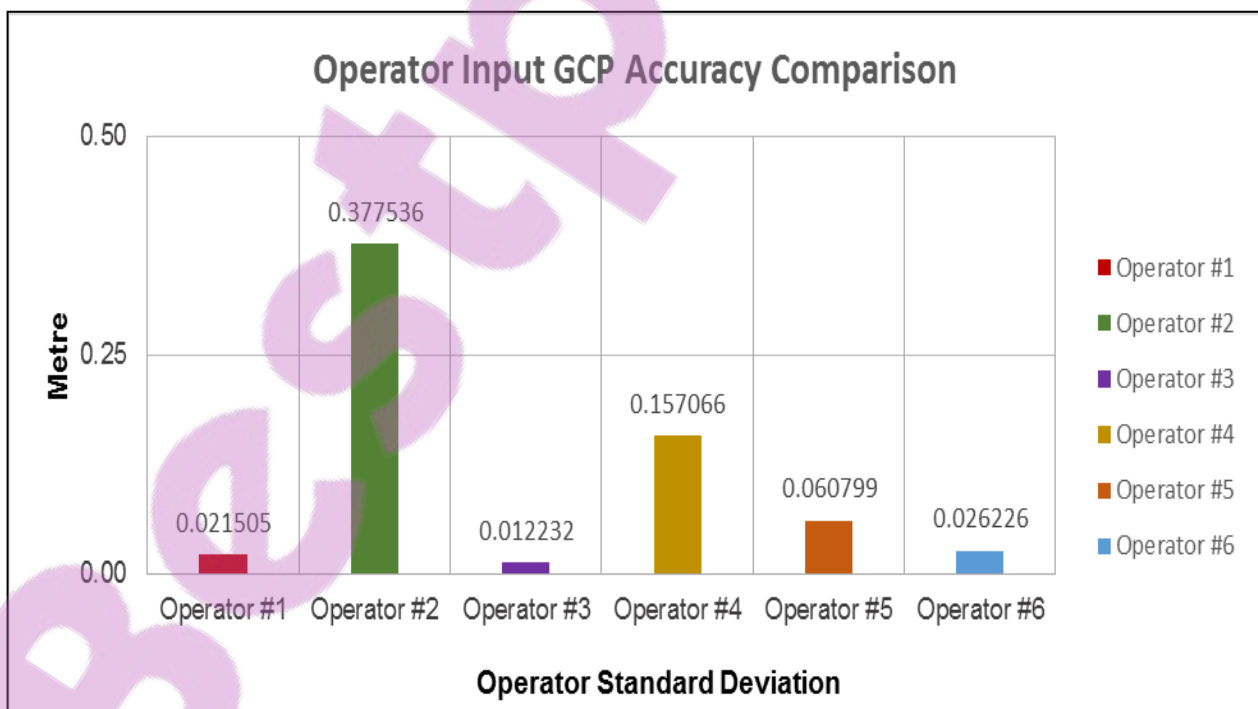


Figure 5.17: Operator input GCP accuracy comparison

However, the placement location of each GCP differs considerably (relatively) from operator to operator, which is mainly due to individual interpretations of where GCPs should be placed. Another determining factor to the accuracy of the GCPs placed by the operators relates to the zoom level utilised by each operator. Although all operators zoomed to pixel scale to place GCPs, differences in the zoom extent were still evident in the measurements. For example, Operator #2 delivered the highest standard deviation of 0.37754 m with a zoom scale of 1:200, while Operator #3 delivered the lowest standard deviation of 0.01223 m by utilising a zoom scale of 1:10. It is therefore evident that a better placement accuracy can be achieved when larger scale levels are used for capturing purposes.

The accuracy of the GCPs extracted by the A-GCP-ES was measured at 0.03943 m, compared to the locations of the reference GCPs. It was determined that this deviation is mainly due to the rounding down of coordinates from 6 decimal places to 4 decimal places by the ERDAS IMAGINE accuracy assessment tool. Figure 5.18 illustrates the standard deviations that were measured for the two input GCP placement methods described in this section.

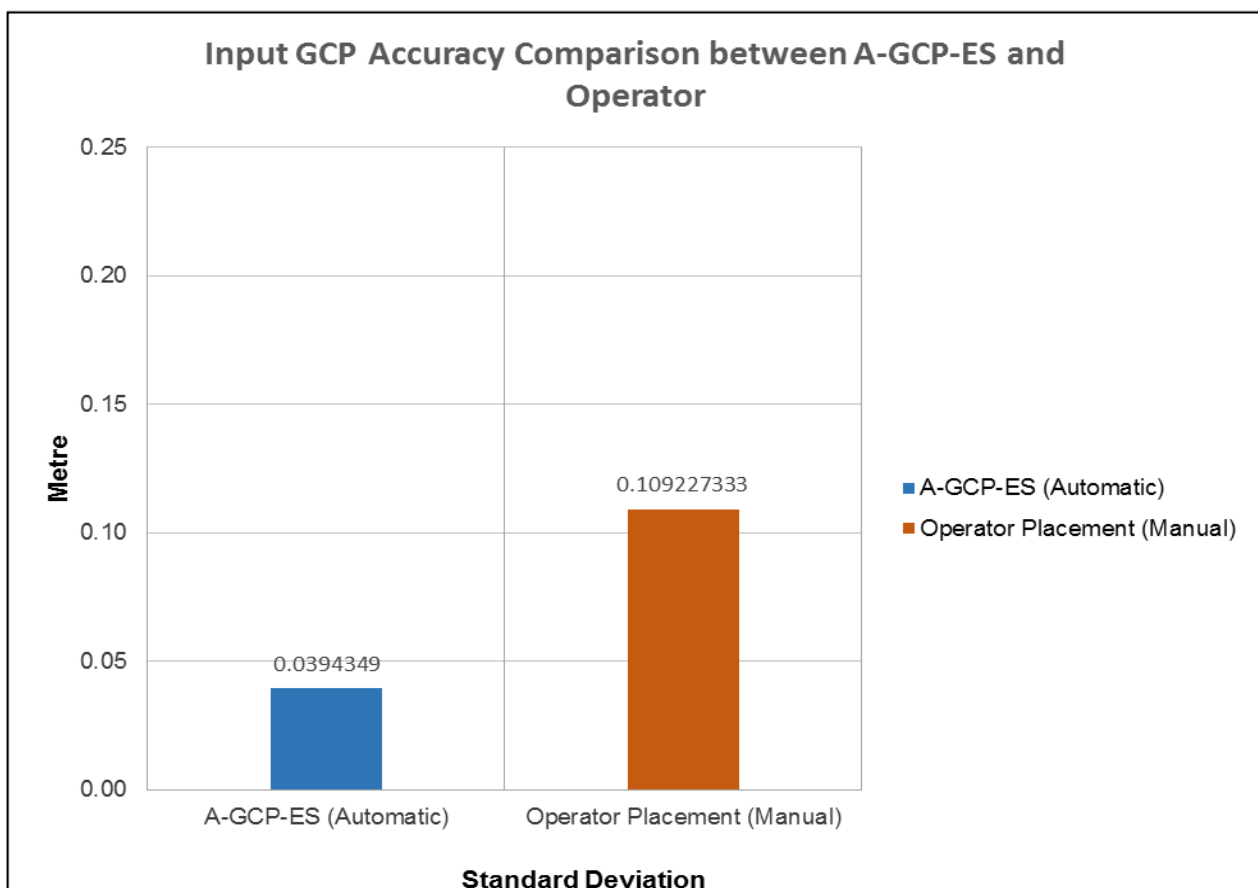


Figure 5.18: Input GCP accuracy comparison between A-GCP-ES and operator



Considering the above comparison, it can be stated that the A-GCP-ES will definitely ease the repeated process to manually place GCPs during orthorectification and inherently eliminates possible human error during this placement process.

5.6 CHAPTER SUMMARY

In this chapter the development, functioning and testing/evaluation of the A-GCP-ES were outlined. The accuracy of the input GCPs that are manually placed by an operator was compared to the accuracy of the GCPs extracted by the A-GCP-ES. Statistics were presented to indicate the findings of this comparison. It was concluded that this script definitely provides more accurate input GCPs compared to the subjective operator biases being introduced and would therefore ease the process to manually place input GCPs when performing orthorectification.

The next chapter, Chapter 6, encompass an overall conclusion to this study. Achievement of the study objectives are indicated, recommendations are made and future research possibilities are presented.



CHAPTER 6 – CONCLUSIONS AND RECOMMENDATIONS

6.1 INTRODUCTION

This study aimed to investigate and compare the positional accuracies of ortho-images under various orthorectification scenarios and provide improved geometric accuracies of VHR satellite imagery when diverse ground control and elevation data sources are available. The focus was to improve the geometric accuracy of satellite imagery during orthorectification procedures when there are inadequate GCPs available that are irregularly distributed in an entire image scene. To achieve the aim of this study, both a literature study and empirical research were conducted. The literature study (Chapter 2) identified the approach to follow to achieve the highest level of geometric accuracy performed on a HRSI. The empirical research comprised numerous experiments that were conducted as described in Chapter 4. All findings and results achieved and contributions derived were presented.

The literature study and empirical research conducted during this study are briefly described in this chapter as well as to which degree the study objectives and aim were achieved. Conclusions and recommendations are highlighted and this chapter concludes with future research to be considered, which is derived from the findings of this study.

6.2 STUDY REVIEW

6.2.1 Background

The theory to perform orthorectification on satellite imagery has been extensively tested and is well documented in the literature. Even the conditions and data sources to use when performing orthorectification are well known. However, there is a difference between what is written in theory and applying that in practice. Adhering to all conditional requirements to perform orthorectification can be a daunting task, such as the availability of a high-resolution DEM and acquiring good quality GCPs.

Sometimes, it will be necessary to depart from the best practice orthorectification method and find alternative methods to produce a high accuracy ortho-image. In such



cases, one must find the best procedural approach to deliver acceptable ortho-image products. When following such an approach, it will be important to understand the influence of auxiliary data (elevation source and ground control) on the accuracy of an ortho-image and consider other ways and means to deliver a more accurate ortho-image. At least be able to understand what input sources are required and parameters needed to achieve a specific accuracy result for a specific GIS application.

6.2.2 Literature study

Chapter 2 consists of the literature study that included a brief history to the evolution of satellite platforms and the characteristics of the most common HR and VHR observation satellite systems. Specific reference was made to the electromagnetic spectrum, converting recorded digital data into images, resolution capabilities and types of image distortion embedded in satellite imagery.

The later part of this chapter was devoted to the two approaches available when performing orthorectification. Great emphasis was put on the requirements and role of GCPs and DEMs as important sources in performing orthorectification. The literature study also investigated the importance of performing accuracy assessment as a final step during orthorectification.

6.2.3 Empirical research

The empirical component of this study consisted of three stages that were pragmatically executed. Various means and methods to perform orthorectification following the parametric approach were tested. In the end, results were achieved to confidently acknowledge the impact of various quality DEMs and GCPs on the accuracy of an ortho-image. This included the use of three different quality DEMs and different number of GCPs, collected from two different sources, namely utilising a GPS device and extraction from vector road layers. Two additional independent experiments were also executed to provide extra considerations when performing orthorectification.



6.3 ACHIEVEMENT OF STUDY OBJECTIVES AND AIM

In order to achieve the aim of this study, six study objectives were formulated (Chapter 1, Paragraph 1.3). Achievement of these objectives are presented below, as well as stating if the study aim was achieved. The findings below were derived from the empirical research performed and the results and analysis derived from the orthorectification experiments conducted, as described in Chapter 4.

- a) Reflection on Objective 1: objective 1 was achieved from the stage 1 experiments performed in Chapter 4. The master image was identified as the ortho-image created from experiment 3(c). This image had an overall accuracy of 1.08 m and was undoubtedly the image with the highest accuracy created from these experiments.
- b) Reflection on Objective 2: it is evident from the stage 1 experiments that the use of different quality DEMs plays a significant role in influencing the overall accuracy when creating an ortho-image. This fact was stated in Paragraph 4.4 (Chapter 4) and the effect of utilising different quality DEMs was illustrated by Figure 4.13. The grade of accuracy corresponding to the number of GCPs utilised were also described. Therefore, objective 2 was achieved successfully.
- c) Reflection on Objective 3: one of the important considerations during the stage 1 experiments was to test the effect of GCPs during the orthorectification process, with specific reference to the manipulation of the number of uniformly distributed GCPs covering an image scene. This was executed successfully and the results were described in Chapter 4 (Paragraph 4.4 and Table 4.1). Consequently, objective 3 was achieved.
- d) Reflection on Objective 4: this objective was achieved. The main purpose of the stage 3 experiments was to investigate and examine the influence of an inadequate number of GCPs that are only distributed in a specific area of an image scene. This was performed successfully, of which the results were captured in Paragraph 4.8.
- e) Reflection on Objective 5: it was determined from the first independent experiment performed during the stage 2 experiments that the TerraSAR-X GCP products can be used as a source of information for orientation improvement of HRSI (Chapter 4, Paragraph 4.6). This was done by comparing the positional



accuracy of this ortho-image with the master image created during the stage 1 experiments. Therefore, objective 5 was successfully achieved.

- f) Reflection on Objective 6: objective 6 was achieved by performing the second independent experiment (stage 2). This ortho-image produced an overall accuracy of 6.30 m and it was suggested that this accuracy is quite acceptable considering that only a DEM and the sensor model were used to create the ortho-image. Utilising this method will produce a feasible alternative as opposed to utilising GCPs that have a cluttered distribution.

It is evident from the above discussions that all objectives formulated during this study were achieved. Therefore, it is conclusive that the study aim was accomplished.

6.4 CONCLUSIONS

The literature study conducted during this study should not be underestimated. It provided the theoretical framework that needs consideration when geometrically correcting satellite imagery. The various approaches available to conduct orthorectification were addressed. It is important to understand these theoretical descriptions, because it will allow one to understand the parameters required to achieve a specific outcome. During this study, the research methodology and design (described in Chapter 3) laid the foundation for the successful execution of the empirical phase of this study.

The empirical research was divided into three stages to test various approaches to perform orthorectification on HRSI. Numerous results were achieved, which were presented in Chapter 4 and four study contributions were formulated (Chapter 4, Paragraph 4.9), which were derived from these results. These study contributions as well as some limitations identified while conducting the empirical research allowed for the compilation of study recommendations and considerations for future research. These recommendations and future research are highlighted in the next two sections.

This study also presented the development of the automatic ground control point extraction script (A-GCP-ES). This GCP extraction function was developed as a Python script with the assistance of the highly skilled computer scientists and electronic



engineers at PinkMatter Solutions. Nowadays, most image processing software can load a Python script to perform a specific task and the function of the A-GCP-ES was demonstrated and proved by utilising both PCI Geomatica® 2015 and ERDAS IMAGINE® 2015 software.

6.5 RECOMMENDATIONS

The following recommendations are formulated concerning the orthorectification of HRSI. Some of these recommendations were touched on in Chapter 4, especially in Paragraphs 4.9 and 4.10.

The highest accuracy that can be achieved during orthorectifying HRSI is by following the parametric approach. This approach requires the use of a physical sensor model, a high quality elevation source and high quality GCPs that are uniformly distributed. From this statement, the following recommendations are derived:

- a) Recommendation 1: it is recommended to follow the parametric approach as oppose to the non-parametric approach to be able to achieve the best possible and most accurate ortho-image. This is however dependent on the availability of GCPs.
- b) Recommendation 2: it is recommended to utilise the highest possible resolution elevation source when conducting orthorectification. It was indicated by this study that an accurate elevation source would render better accuracy results than utilising a lower resolution elevation source. Therefore, the quality of an elevation source plays a significant role during the orthorectification process.
- c) Recommendation 3: the use of GCPs during the orthorectification process play an important role and it is recommended to utilise as many GCPs as possible that are spread over the entire image, covering the centre and four corners of the image when the terrain variation and geometric distortion are great. However, the number of GCPs to utilise is dependent on the sensor model and order of transformation (Paragraph 2.4.1) utilised to perform orthorectification.

The accuracy of an ortho-image is greatly degraded by GCPs that are extracted from a vector road layer. This is especially true when few GCPs are available as well as



clustered together in a specific area within the entire image scene. The following recommendations are made, relating to the above statement:

- a) Recommendation 4: when utilising GCPs that are extracted from a vector road layer, ensure that as many as possible GCPs are extracted and distributed across the entire image scene.
- b) Recommendation 5: it is recommended that GCPs be extracted accurately by considering:
 - i. the correct side of a multi-lane road;
 - ii. extract GCPs at road crossings, stop street road markings, centre points of traffic circles, etc.;
 - iii. never extract GCPs on curved roads; and
 - iv. disregard locations with high surrounding obstacles, such as buildings and electricity pylons.

It was stated in Chapter 4 (Paragraph 4.9.2) that TerraSAR-X produces an unrivalled accuracy of 1 m and 3 m for the two GCP products available. This study showed that an overall positional accuracy of 1.5 m is achievable by utilising the TerraSAR-X GCP-3 product (Table 4.2).

- a) Recommendation 6: it is recommended that the TerraSAR-X-based GCPs can certainly be used as an alternative to collecting manual GCPs using a GPS device and should definitely be considered before utilising GCPs that were extracted from a vector road layer.

It was determined from the second independent experiment performed during stage 2 of the empirical research that utilising only a geometric sensor model and an elevation source does not produce a favourable accuracy result when compared to performing orthorectification with highly accurate GCPs. However, it still produced better results than utilising few GCPs that were extracted from a vector road layer and are clustered to cover only a specific area in an image scene.

- a) Recommendation 7: it is recommended to follow this approach as opposed to performing orthorectification with the use of low quality ground control. In this case, low quality ground control refers to GCPs that are located in a small area of the entire image scene and that were extracted from a vector road.



It was stated in Chapter 2 (Paragraph 2.1) and re-emphasised in Chapter 4 (Paragraph 4.6) that various GIS applications require different imagery positional accuracies. Certain military applications, such as target acquisition will require a very high accuracy ortho-image to extract targets from, whereas drafting a 1:50 000 topographic map will require a lesser accurate ortho-image for digitizing purposes.

- a) Recommendation 8: it is recommended that specific GIS applications be identified and corresponding imagery positional accuracies be determined to evaluate the feasibility of the accuracies achieved from this study. This will serve the purpose to differentiate between which approaches (indicated by the various orthorectification experiments performed during this study) need to be followed when utilising satellite imagery to successfully execute specific GIS applications.

6.6 FUTURE RESEARCH

This study was limited to the use of the ERDAS IMAGINE® 2015 software. Conducting the same experiments with the use of additional software might pose different accuracy results. Software such as PCI Geomatica® and ENVI® has additional functions and mathematical formulas for use to orthorectify HRSI. Exploring different ways and means to conduct the experiments performed during this study could be of value for future research.

Another important consideration for future research is a comparison between the parametric approach, which was the approach followed during this study and the non-parametric approach. This will allow for determining the accuracy differences between these two approaches.

This study had the limitation that it only performed the orthorectification tests on a single Pléiades-1B primary image, utilising 5, 13 and 25 GCPs. In order to substantiate this study's findings, future research can consider a similar test design where the number of GCPs are increased beyond the maximum 25 used. This will allow for determining the threshold of the maximum number of GCPs to use before the quality of the ortho-image is degraded (see Chapter 2, Paragraph 2.4.1).

It is also proposed to apply this study design on a variety of current HR and/or VHR satellite imagery, not only a Pléiades primary image.

It may also prove to be worth investigating the quality of an ortho-image when using a DSM versus a DTM.

It was indicated in Paragraph 4.6 that three reasons might be the cause to the conspicuous cluttered distribution of points showed for the second independent experiment. It was stated that even though the distribution is noticeable, it was expected due to the pointing accuracy offset of the Pléiades satellite sensor. However, it is suggested that further research be conducted to determine the exact cause to the conspicuous cluttered distribution of points. Research should be conducted by considering the influence of the elevation source, sensor model and image data and possibly to test this experiment with the use of other image processing software and determine if the same conspicuous cluttered distribution of points is obtained.

Next, it might be interesting to determine the impact on the positional accuracy of an ortho-image by utilising high quality GCPs (i.e. GPS collected points) that are random and scattered as opposed to the uniformly distributed GCPs that were used in this study.

Lastly, it may be advantageous to further improve the A-GCP-ES and develop a toolbar to be software specific that can perform the function of this script.

6.7 CHAPTER SUMMARY

This chapter provided a background review on the literature study and the empirical research that comprise this study. Brief conclusions were presented, where after specific recommendations were formulated for considerations when orthorectifying HRSI. This chapter concluded with suggestions for future research. These suggestions were derived from the study contributions formulated in Chapter 4, as well as limitations that were identified while executing the empirical research component of this study.

The most important offerings of this chapter were the conclusion that all study objectives were achieved successfully, which ultimately means that the study aim was attained.

REFERENCES

- AGUILAR, M., AGÜERA, F., AGUILAR, F. and CARVAJAL, F. 2008. Geometric accuracy assessment of the orthorectification process from very high resolution satellite imagery for Common Agricultural Policy purposes. *International journal of remote sensing*, 29, 7181-7197.
- AIRBUS DEFENCE AND SPACE. 2017. *Pléiades Products* [Online]. Available: <http://www.intelligence-airbusds.com/en/3027-pléiades-50-cm-resolution-product> [Accessed 18 January 2017].
- AIRBUS DEFENCE AND SPACE. August 2014. TerraSAR-X Services Image Product Guide: Basic and enhanced radar satellite imagery. Available: http://www2.geo-airbusds.com/files/pmedia/public/r459_9_201408_tsxx-itd-ma-0009_tsx-product-guide_i2.00.pdf.
- AIRBUS DEFENCE AND SPACE. October 2012. Pleiades Technical Documents: Pleiades User Guide. 2.0. Available: <http://geo-airbusds.com/en/4572-pleiades-technical-documents> [Accessed 26 March 2015].
- ALLISON, L. J., WEXLER, R., LAUGHLIN, C. and BANDEEN, W. 1978. Remote sensing of the atmosphere from environmental satellites. *Air quality meteorology and atmospheric ozone*, 83-155.
- AVERY, T. E. and BERLIN, G. L. 1992. *Fundamentals of remote sensing and airphoto interpretation*, New York, Macmillan.
- BECKER, K., DETSIS, E., NWOOSA, C. C., PALEVSKA, V., RATHNASABAPATHY, M. and TAHERAN, M. 2012. Space situation awareness. *SSS Educational Series 2012. Space generation advisory council*. [Online]. Available: https://www.agi.com/resources/educational-alliance-program/curriculum_exercises_labs/SGAC_Space%20Generation%20Advisory%20Council/space_situational_awareness.pdf [Accessed 23 June 2014].
- BERG, B. L. 2004. *Qualitative research methods for the social sciences*, Boston, MA, Pearson Education Ltd.
- BERGMAN, M. M. 2008. *Advances in mixed methods research: Theories and applications*, London, Sage.
- BONNEVAL, H. 1972. Levés topographiques par photogrammétrie aérienne, dans *Photogrammétrie générale: Tome 3, Collection scientifique de l'Institut Géographique National. Paris, France: Eyrolles Editeur*.
- BROVELLI, M. A., CRESPI, M., FRATARCANGELI, F., GIANNONE, F. and REALINI, E. Accuracy assessment of high resolution satellite imagery by leave-one-out method. Proceedings of the 7th International Symposium on Spatial Accuracy

- Assessment in Natural Resources and Environmental Sciences, 2006. Citeseer, 533-542.
- CALOZ, R. and COLLET, C. 2001. Précis de télédétection Transformations géométriques. *Traitements numériques d'images de télédétection, Volume 3 (Ste Foy, Québec, Canada: Presse de l'Université du Québec)*, 76-105.
- CHMIEL, J., KAY, S. and SPRUYT, P. Orthorectification and geometric quality assessment of very high spatial resolution satellite imagery for Common Agricultural Policy purposes. Proceedings of XXth ISPRS Congress, 2004. 12-23.
- COHEN, L., MANION, L. and MORRISON, K. 2004. *A guide to teaching practice*, London, Routledge Psychology Press.
- COMBRINCK, W. L. 2009. Products of Space Geodesy and links to Earth Science and Astronomy. *11th SAGA Biennial Technical Meeting and Exhibition, 16 - 18 September 2009*. Swaziland.
- COSTLOW, T. 21 March 2014. The future of satellites: What are the options? *Defense Systems: Knowledge Technology and Net-Enabled Warfare* [Online]. Available: <http://defensesystems.com/articles/2014/03/21/satellite-communications-future-options.aspx> [Accessed 04 July 2014].
- CRESWELL, J. W. 2012. *Qualitative inquiry and research design: Choosing among five approaches*, London, Sage.
- DE VOS, A., SCHURINK, E. and STRYDOM, H. 1998. The nature of research in the caring professions. *Research at grass roots: A primer for the caring professions*. Pretoria: JL van Schaik Publishers, 3-22.
- DIAL, G. and GRODECKI, J. 2005. RPC replacement camera models. *The International Archives of the Photogrammetry, Remote Sensing and Spatial Information Sciences*, 34.
- DOLL, R. C. 1970. *Curriculum improvement: Decision making and process*, California, United States of America, Allyn and Bacon.
- DREYER, J. S. 1998. The researcher and the researched: Methodological challenges for practical theology. *Practical theology in South Africa*, 13, 14-27.
- FARR, T. G., HENSLEY, S., RODRIGUEZ, E., MARTIN, J. and KOBRICK, M. 2000. The shuttle radar topography mission. *EUROPEAN SPACE AGENCY-PUBLICATIONS-ESA SP*, 450, 361-364.
- FEDERAL GEOGRAPHIC DATA COMMITTEE. 1998. Geospatial Positioning Accuracy Standards Part 3: National Standard for Spatial Data Accuracy. Available: <https://www.fgdc.gov/standards/projects/FGDC-standards-projects/accuracy/part-3/chapter3> [Accessed 07 May 2014].

- FOX, E. 2015. *CMOS TDI image sensor with rolling shutter pixels*. U.S. Patent 9,148,601.
- GAO, J. 2008. *Digital analysis of remotely sensed imagery*, New York, McGraw-Hill Professional.
- GELO, O., BRAAKMANN, D. and BENETKA, G. 2008. Quantitative and qualitative research: Beyond the debate. *Integrative psychological and behavioural science*, 42, 266-290.
- GEOCONNECT. 2016. *GPS signals (L1, L2, L5)* [Online]. Available: <http://geoconnect.com.au/gps-signals-l1-l2-l5/> [Accessed 03 September 2015].
- GLEYZES, M., PERRET, L. and KUBIK, P. 2012. Pleiades system architecture and main performances. *International Archives of the Photogrammetry, Remote Sensing and Spatial Information Sciences*, 39, B1.
- GRAVETTER, F. and FORZANO, L. A. 2015. *Research methods for the behavioural sciences*, Boston, Massachusetts, United States, Cengage Learning.
- GRODECKI, J. and DIAL, G. 2002. IKONOS geometric accuracy validation. *International archives of photogrammetry remote sensing and spatial information sciences*, 34, 50-55.
- HAAS, I. and SHAPIRO, R. 1982. The Nimbus Satellite System-Remote Sensing R&D platform of the 70's. *Meteorological Satellites - Past, Present and Future*. (p.17).
- HARRISON, B. A. and JUPP, D. L. B. 1989. *Introduction to remotely sensed data: Part one of the microBrian resource manual*, Clayton, Australia, CSIRO Publications.
- HARRISON, G. W. and LIST, J. A. 2004. Field experiments. *Journal of Economic Literature*, 1009-1055.
- HEMMLEB, M. and WIEDEMANN, A. 1997. Digital rectification and generation of orthoimages in architectural photogrammetry. *The CIPA International Symposium '97, Photogrammetry in Architecture, Archaeology and Urban Conservation*. International Archives for Photogrammetry and Remote Sensing. Band XXXII, Part 5C1B.
- HENRICO, I. 2012. An analysis of applied methods to satellite image interpretation as performed by image analysts in the SANDF. MSc. Unpublished Thesis. University of South Africa.
- HENRICO, I., COMBRINCK, L. and ELOFF, C. 2016. Orthorectification accuracy comparison applied on Pléiades imagery using GPS collected GCPs and TerraSAR-X based GCPs. *South African Journal of Geomatics*, 5, 358-372.

- HEXAGON GEOSPATIAL. 2015. *ERDAS Imagine Help Guide* [Online]. Available: <https://hexagongeospatial.fluidtopics.net/book#!book;uri=f2790e0ca81311531f1a57c6b7bc80b2;breadcrumb=463fdbd554b442e712f3960796bf66ca> [Accessed 08 March 2016].
- HEXAGON GEOSPATIAL. October 2013. ERDAS IMAGINE Field Guide. Available: http://www.hexagon-solutions.com.cn/Libraries/Misc_Docs/ERDAS_Field-Guide_PDF_Intergraph_brand.sflb.pdf [Accessed 28 April 2014].
- HOJA, D., SCHNEIDER, M., MÜLLER, R., LEHNER, M. and REINARTZ, P. 2008. Comparison of orthorectification methods suitable for rapid mapping using direct georeferencing and RPC for optical satellite data. *The International Archives of the Photogrammetry, Remote Sensing and Spatial Information Sciences*, 37, 1617-1624.
- HORN, B. K. and WOODHAM, R. J. 1978. Destriping satellite images. DTIC Document (No. AI-M-467). Massachusetts Int of Tech Cambridge Artificial Intelligence Lab.
- HOWE, K. R. 2003. *Closing methodological divides: Toward democratic educational research*, Vol. 11, New York, Springer Science & Business Media.
- HUTCHINSON, M. F. 2011. ANUDEM Version 5.3. *User Guide, (Revision: 09 August 2011), The Australian National University, Centre for Resource and Environmental Studies, Canberra.*
- JACOBSEN, K. 2002. Geometric aspects of the handling of space images. *International Archives of Photogrammetry Remote Sensing and Spatial Information Sciences*, 34, 89-93.
- JACOBSEN, K. 2003. DEM generation from satellite data. *EARSeL Ghent*, 273-276.
- JAKUBOWICZ, D. and JASZCZAK, P. 09 February 2005. GCP accuracy requirements for Quickbird orthorectification. *6th Geomatic Week*. Barcelona, Spain: International Society for Photogrammetry and Remote Sensing.
- JOHNSON, B. and CHRISTENSEN, L. 2008. *Educational research: Quantitative, qualitative, and mixed approaches*, MA, United States, Sage.
- JOHNSON, R. B. and ONWUEGBUZIE, A. J. 2004. Mixed methods research: A research paradigm whose time has come. *Educational researcher*, 33, 14-26.
- KAICHANG, D., RUIJIN, M. and RONG XING, L. 2003. Rational functions and potential for rigorous sensor model recovery. *Photogrammetric Engineering & Remote Sensing*, 69, 33-41.
- KE, L. C. 2006. Orthorectification accuracies of VHRS imagery under the characteristics of ground control points. *International Symposium on Geoinformatics for Spatial Infrastructure Development in Earth and Allied Sciences*. Ho Chi Minh, Vietnam.

- KEEVES, J. P. 1988. *Educational research, methodology, and measurement: An international handbook*, Oxford, Pergamon Press.
- KRAMER, H. J. 2002. *Observation of the Earth and its Environment: Survey of Missions and Sensors*, New York, Springer Science & Business Media.
- KUMAR, M. Digital image processing. *In*: HARMSEN, K., SAHA, S. K., ROY, P. S. and SIVAKUMAR, M. V. K., eds. *Satellite remote sensing and GIS applications in agricultural meteorology*, 2004 Dehra Dun, India. World Meteorological Organisation, Switzerland.
- LEPRINCE, S., BARBOT, S., AYOUB, F. and AVOUAC, J. P. 2007. Automatic and precise orthorectification, coregistration, and subpixel correlation of satellite images, application to ground deformation measurements. *Geoscience and Remote Sensing, IEEE Transactions on*, 45, 1529-1558.
- LIEW, S. C. 2001. *What is remote sensing? Tutorial 01. CRISP (Centre for Remote Imaging, Sensing & Processing)*. [Online]. Available: <http://www.crisp.nus.edu.sg/research/tutorial/intro.htm> [Accessed 18 January 2017].
- LILLESAND, T., KIEFER, R. and CHIPMAN, J. 2008. *Remote sensing and image interpretation*, Chichester (UK), John Wiley & Sons Ltd.
- LIU, X., ZHANG, Z., PETERSON, J. and CHANDRA, S. 2007. LiDAR-derived high quality ground control information and DEM for image orthorectification. *GeoInformatic*, 11, 37-53.
- MAREE, K. 2007. *First steps in research*, Pretoria, Van Schaik Publishers.
- MAXWELL, A., STRAGER, M., WARNER, T., ZEGRE, N. and YUILL, C. 2014. Comparison of NAIP orthophotography and RapidEye satellite imagery for mapping of mining and mine reclamation. *GIScience & Remote Sensing*, 51, 301-320.
- MOBASHERYA, M. and DASTFARD, M. 2013. Separation of IKONOS sensor's electronic noise from atmospheric induced effects. *ISPRS-International Archives of the Photogrammetry, Remote Sensing and Spatial Information Sciences*, 1, 117-121.
- MOFFITT, F. and MIKHAIL, E. 1980. *Photogrammetry*. Happer & Row Publisher, 648.
- NATIONAL GEOSPATIAL INFORMATION. 2014. *Trignet Web Application: Sensor Map* [Online]. Available: www.trignet.co.za/Map/SensorMap.aspx [Accessed 17 July 2014].
- NATIONAL IMAGERY AND MAPPING AGENCY [NIMA]. 16 November 2000. The compendium of controlled extensions for the National Imagery Transmission

- Format (NITF). Available: http://geotiff.maptools.org?STDI-0002_v2.1.pdf [Accessed 30 June 2014].
- NATURAL RESOURCES CANADA: CANADA CENTRE FOR REMOTE SENSING. 2015. *Fundamentals of Remote Sensing*. Available: http://www.nrcan.gc.ca/files-/earthsciences/pdf/resource/tutor/fundam/pdf/fundamentals_e.pdf [Accessed 30 June 2015].
- NEWMAN, I. 1998. *Qualitative-quantitative research methodology: Exploring the interactive continuum*, Southern Illinois University Press.
- NIAZ, M. 2008. A rationale for mixed methods (integrative) research programmes in education. *Journal of Philosophy of Education*, 42, 287-305.
- OLSEN, R. C. 2007. *Remote sensing from air and space*, (Vol. 229), Bellingham, WA, USA, SPIE Press.
- ONWUEGBUZIE, A. J., JOHNSON, R. B. and COLLINS, K. M. 2009. Call for mixed analysis: A philosophical framework for combining qualitative and quantitative approaches. *International journal of multiple research approaches*, 3, 114-139.
- PANEM, C., BIGNALET-CAZALET, F. and BAILLARIN, S. 2012. Pleiades-HR system products performance after in-orbit commissioning phase. *International Archives of the Photogrammetry, Remote Sensing and Spatial Information Sciences*, 39, 567-572.
- PCI GEOMATICS. 2016. *Geomatica 2016 Online Help* [Online]. Available: <http://www.pcigeomatics.com/geomatica-help/> [Accessed 14 May 2016].
- PETRAT, L. and ELOFF, C. 2014. Integrated use of optical and radar satellite constellations: A new era for remote sensing. Available: <http://geospatial-world.net/Paper/Technology/ArticleView.aspx?aid=30793> [Accessed 01 July 2014].
- POLITECNICO. 2017. The colinearity equations and the basic photogrammetric problems. Available: http://geomatica.como.polimi.it/corsi/rs_ia/Class_Notes_01.pdf [Accessed 19 January 2017].
- POWELL, D. 2013. Laser boost space communications: Optical systems set to handle planetary science's big data. *Nature: International weekly journal of science*, 499, 266 – 267.
- PURPLEMATH. 2014. *Polynomials: Definitions / Evaluation* [Online]. Available: www.purplemath.com/modules/polydefs.htm [Accessed 23 February 2014].
- PYTHON. 2016. *What is Python? Executive Summary* [Online]. Available: <https://www.python.org/doc/essays/blurb/> [Accessed 13 May 2016].


- REXES, M. and HIRT, C. 2014. Comparison of free high resolution digital elevation data sets (ASTER GDEM2, SRTM v2.1/4.1) and validation against accurate heights from the Australian National Gravity Database. *Australian Journal of Earth Sciences*, 61, 213-226.
- RICHARDS, J. A. 2012. *Remote Sensing Digital Image Analysis: An Introduction*, Springer-Verlag Berlin Heidelberg.
- RICHARDS, J. A. and XIUPING, J. 2006. *Remote sensing digital image analysis: an introduction*, Heidelberg, Germany, Springer-Verlag Berlin.
- SATELLITE IMAGE CORPORATION. 2016. Available: <http://www.satimaging-corp.com/satellites-sensors> [Accessed 18 September 2016].
- SHORT, N. M. 2000. Technical and Historical Perspectives of Remote Sensing. Available from <http://rst.gsfc.nasa.gov/Intro/Part2>, Vol. 24.
- SMITH, R. 2005. Tutorial: Orthorectification using Rational Polynomials with TNTmips. Available: <http://gisteam.de/ftp/Tutorial/rpcortho.pdf> [Accessed 27 September 2015].
- STALLMANN, C., MEYER, J., PRETORIUS, L. and MAASS, F. 30 July 2015. An Open Source Implementation of Automated Orthorectification using a Rational Polynomial Coefficients Model.
- STAMPOULIDIS, L. 2014. G&H optical fibre amplifiers for next generation satellite communications robust against ionizing radiation. Available: http://goochand-housego.com/press_release/rad-edfas/ [Accessed 01 July 2014].
- STRYDOM, D. 2009. *Die implementering van 'n voorkomingsprogram teen die psigiese uitbrandingsindroom by hoëprofiel adolessente*. D.Litt. et Phil. (Psychology) D.Litt. et Phil., UNISA.
- TAHAR, K. N. An evaluation on different number of ground control points in unmanned aerial vehicle photogrammetric block. International Archives of the Photogrammetry, Remote Sensing and Spatial Information Sciences, ISPRS 8th 3DGeoInfo Conference & WG II/2 Workshop, 27-29 November 2013 Istanbul, Turkey.
- TAO, C. V. and HU, Y. 2001. A comprehensive study of the rational function model for photogrammetric processing. *Photogrammetric Engineering & Remote Sensing*, 67, 1347-1358.
- TEMPFLI, K., HUURNEMAN, G., BAKKER, W., JANSSEN, L., BAKKER, W., FERINGA, W., GIESKE, A., GRABMAIER, K., HECKER, C. and HORN, J. 2009. Principles of remote sensing: an introductory textbook. *ITC, the Netherlands*.

- THOMSON, B. 2011. Qualitative research: Validity. *Journal of Administration & Governance (JOAAG)*, 6, 77-82.
- THYER, B. 2009. *The handbook of social work research methods*, London, Sage.
- TIGHE, M. L., AHLRICHS, J. S. and XIAOPENG, L. Orthorectification and pansharpen RAPIDEYE, IKONOS and ALOS optical imagery using high resolution NextMap® data. ASPRS Conference, San Antonia, Texas, 2009. 16-19.
- TOUTIN, T. 2003. Geometric correction of remotely sensed images. *Remote Sensing of Forest Environments*. United States: Springer.
- TOUTIN, T. 2004. Review article: Geometric processing of remote sensing images: models, algorithms and methods. *International Journal of Remote Sensing*, 25, 1893-1924.
- TOUTIN, T. Sensor orientation and ortho-rectification of high resolution satellite images: Review and application with FERMOSAT-2. Map Middle East 2006 conference proceeding, 2006.
- TOUTIN, T. and CHÉNIER, R. GCP requirement for high-resolution satellite mapping. International Society for Photogrammetry and Remote Sensing Congress, July 2004 Istanbul, Turkey. 836-839.
- TOUTIN, T., CHÉNIER, R. and CARBONNEAU, Y. 2002. 3D models for high resolution images: examples with QuickBird, IKONOS and EROS. *International archives of photogrammetry remote sensing and spatial information sciences*, 34, 547-551.
- TRIMBLE. August 2014. Student Guide: Trimble TerraSync Software and GPS Pathfinder Office Software. Available: [https://training.fws.gov/courses/references/tutorials/geospatial/CSP7304/2016documents/HandsOn_Afternoon/TerraSync_PFO/TS_PFO_Student_Guide_v5_60%20\(1\).pdf](https://training.fws.gov/courses/references/tutorials/geospatial/CSP7304/2016documents/HandsOn_Afternoon/TerraSync_PFO/TS_PFO_Student_Guide_v5_60%20(1).pdf) [Accessed 03 June 2016].
- TRIMBLE. February 2011. User Guide: GeoExplorer 6000 Series. Available: http://sendai.hmdc.harvard.edu/cga_website_files/PDF_misc/GPS/GeoExpl6000_UserGde_ENG.pdf [Accessed 04 July 2014].
- US ARMY CORPS OF ENGINEERS. October 2003. Engineering and Design: Remote Sensing. Engineering Manual. Available: www.publications.usace.army.mil/Portals/76/Publications/EngineerManuals/EM_1110-2-2907.pdf [Accessed 22 December 2014].
- US DEPARTMENT OF DEFENSE. 26 February 1990. Department of Defense Standard Practice: Mapping, Charting and Geodesy Accuracy. Available: http://earth-info.nga.mil/publications/specs/printed/600001/600001_Accuracy.pdf [Accessed 26 March 2015].

- USGA. 2016. *Atmosphere and Target Interactions - Solar Radiation and the Earth's Atmosphere*. U.S. Geological Survey [Online]. Available: <https://landsat.usgs.gov/atmosphere-and-target-interactions-solar-radiation-and-earths-atmosphere> [Accessed 18 January 2017].
- WANG, D. 2010. *Performance evaluation of GPS L1/L2 positioning with partial availability of the L2C signals*. Master Thesis. University of Calgary.
- WEBBER, W. F. 1973. Techniques for image registration. *The Laboratory for Applications of Remote Sensing (LARS) Symposia*. Purdue University Libraries.
- WONG, K. 1980. Basic mathematics of photogrammetry. *Manual of photogrammetry*, 4, 37-101.
- YANG, X. 1997. *Georeferencing CAMS Data: Polynomial rectification and beyond*. Ph.D., University of South Carolina.
- YANG, X. and WILLIAMS, D. 1997. The effect of DEM data uncertainty on the quality of orthoimage generation. *Geographic Information Systems/Land Information Systems (GIS/LIS)*. Cincinnati, Ohio: American Congress on Surveying and Mapping & American Society for Photogrammetry and Remote Sensing.
- ZHANG, J. and CHENG, B. Distribution optimization of ground control points in remote sensing image geometric rectification based on cluster analysis. Sixth International Symposium on Multispectral Image Processing and Pattern Recognition, 2009. International Society for Optics and Photonics, 749707-749707-7.

APPENDICES

APPENDIX A: SRTM DEM METADATA AND IDENTIFICATION INFORMATION



USGS Home
Contact USGS
Search USGS

EarthExplorer

Identification_Information:

Citation:

Citation_Information:

Originator: U.S. Geological Survey (USGS)
Originator: National Geospatial-Intelligence Agency (NGA)
Originator: National Aeronautics and Space Administration (NASA)

Publication_Date:

Title: Shuttle Radar Topography Mission 1 Arc-Second Global: SRTM1S26E028V3
Geospatial_Data_Presentation_Form: Elevation data in raster format

Series_Information:

Series_Name: SRTM 1 Arc-Second Global
Issue_Identification: Digital elevation data

Publication_Information:

Publication_Place: Sioux Falls, South Dakota
Publisher: USGS Earth Resources Observations and Science (EROS) Center
Online_Linkage: <http://earthexplorer.usgs.gov>

Description:

Abstract: The Shuttle Radar Topography Mission (SRTM) was a partnership between NASA and the National Geospatial-Intelligence Agency (NGA). Flown aboard the NASA Space Shuttle Endeavour (11-22 February 2000), SRTM fulfilled its mission to map the world in three dimensions. The USGS is under agreement with NGA and NASA's Jet Propulsion Laboratory to distribute SRTM elevation products derived from the C-band radar data. SRTM utilized interferometric C-band Spaceborne Imaging Radar to generate elevation data over 80 percent of the Earth's land surface.

Global SRTM data at a resolution of 1 arc-second have been edited to delineate and flatten water bodies, better define coastlines, remove spikes and wells, and fill small voids. Larger areas of missing data or voids were filled by the NGA using interpolation algorithms in conjunction with other sources of elevation data. The SRTM 1 Arc-Second Global data offer worldwide coverage of void filled data at a resolution of 1 arc-second (30 meters) and provide open distribution of this high-resolution global data set.

Purpose: SRTM elevation data of the Earth's land surface are available with data points posted every 1 arc second for global coverage.

Supplemental_Information: Global coverage is between 60 degrees North and 56 degrees South latitude. Raster size is 1 degree tiles. The data are expressed in geographic coordinates (latitude/longitude) and is horizontally referenced to WGS84 and vertically referenced to EGM96 Geoid.

Formats:

1. DTED - Digital Terrain Elevation Data is a standard mapping format designed by the NGA. Each file or cell contains a matrix of vertical elevation values spaced at regular horizontal intervals measured in geographic latitude and longitude units. DTED is a trademark of NGA.
2. BIL - Band interleaved by line is a simple binary raster format with accompanying ASCII descriptor files. The BIL integer format is recommended for software packages that do not support floating-point data.
3. GeoTIFF - Georeferenced Tagged Image File Format is a TIFF file with embedded geographic information. This is standard image format for GIS applications.

Time_Period_of_Content:

Time_Period_Information:

Single_Date/Time:

Calendar_Date: 11-FEB-00

Spatial_Domain:

Data_Set_G-Polygon:
Data_Set_G-Polygon_Outer_G-Ring:



G-Ring_Latitude: -25
G-Ring_Longitude: 28

G-Ring_Latitude: -25
G-Ring_Longitude: 29

G-Ring_Latitude: -26
G-Ring_Longitude: 29

G-Ring_Latitude: -26
G-Ring_Longitude:

Keywords:

Theme:

Theme_Keyword: 30 meter
Theme_Keyword: Global
Theme_Keyword: Shuttle Radar Topography Mission
Theme_Keyword: NGA
Theme_Keyword: NASA
Theme_Keyword: C-band
Theme_Keyword: Elevation
Theme_Keyword: SRTM
Theme_Keyword: Mapping
Theme_Keyword: Topography
Theme_Keyword: Imaging Radar
Theme_Keyword: DTED

Place:

Place_Keyword_Thesaurus: U.S. Department of Commerce, 1995, Countries, dependencies, areas of special sovereignty, and their principal administrative divisions, Federal Information Processing Standard 10-4, Washington, D.C., National Institute of Standards and Technology

Place_Keyword: Global

Access_Constraints: Any downloading and use of these data signifies a user's agreement to comprehension and compliance of the USGS Standard Disclaimer. Insure all portions of metadata are read and clearly understood before using these data in order to protect both user and USGS interests.

Use_Constraints: There is no guarantee of warranty concerning the accuracy of these data. Users should be aware that temporal changes may have occurred since the data was collected and that some parts of these data may no longer represent actual surface conditions. Users should not use these data for critical applications without a full awareness of their limitations. Acknowledgement of NASA, NGA and the USGS would be appreciated in products derived from these data. Any user who modifies the data set is obligated to describe the types of modifications they perform. User specifically agrees not to misrepresent the data set, nor to imply that changes made were approved or endorsed by the originating agencies. Please refer to <http://www.usgs.gov/privacy.html> for the USGS disclaimer.

Point_of_Contact:

Contact_Information:

Contact_Person_Primary:

Contact_Person: lta@usgs.gov

Contact_Organization_Primary:

Contact_Organization: U.S. Geological Survey Earth Resources Observation and Science (EROS) Center

Contact_Person: lta@usgs.gov

Contact_Position: Long Term Archive (LTA) Representative

Contact_Address:

Address_Type: mailing and physical address

Address: Long Term Archive (LTA), U.S. Geological Survey (USGS)

Earth Resources Observation and Science (EROS) Center

47914 252nd Street

City: Sioux Falls

State_or_Province: SD

Postal_Code: 57198-0001

Country: USA

Contact_Electronic_Mail_Address: lta@usgs.gov

Hours_of_Service: 0800 - 1600 CT, M-F, -6 h GMT

Contact_Instructions:

Browse_Graphic:



Browse_Graphic_File_Name: browse graphic
for:http://earthexplorer.usgs.gov/browse/srtm_v3/1arc/e028/s26_e028_1arc_v3.jpg
Browse_Graphic_File_Description: This is a resampled version of the data cell to help validate area of interest and quality.
Browse_Graphic_File_Type: JPEG
Security_Information:
Security_Classification_System: none
Security_Classification: unclassified
Security_Handling_Description: none
Native_Data_Set_Environment: Oracle
Data_Quality_Information:
Attribute_Accuracy:
Attribute_Accuracy_Report: The SRTM data meet the absolute horizontal and vertical accuracies of 20 meters (circular error at 90% confidence) and 16 meters (linear error at 90% confidence), respectively, as specified for the mission.
Lineage:
Process_Step:
Process_Contact:
Contact_Information:
Contact_Person_Primary:
Contact_Person: lta@usgs.gov
Contact_Organization_Primary:
Contact_Person: lta@usgs.gov
Contact_Position: Long Term Archive (LTA) Representative
Contact_Address:
Address: Long Term Archive (LTA), U.S. Geological Survey (USGS)
Earth Resources Observation and Science (EROS) Center
47914 252nd Street
Contact_Electronic_Mail_Address: lta@usgs.gov
Contact_Instructions: lta@usgs.gov
Distribution_Information:
Distributor:
Contact_Information:
Contact_Person_Primary:
Contact_Person: lta@usgs.gov
Contact_Organization_Primary:
Contact_Organization: U.S. Geological Survey Earth Resources Observation and Science (EROS) Center
Contact_Person: lta@usgs.gov
Contact_Position: Long Term Archive (LTA) Representative
Contact_Address:
Address_Type: mailing and physical address
Address: Long Term Archive (LTA), U.S. Geological Survey (USGS)
Earth Resources Observation and Science (EROS) Center
47914 252nd Street
City: Sioux Falls
State_or_Province: SD
Postal_Code: 57198-0001
Country: USA
Contact_Electronic_Mail_Address: lta@usgs.gov
Hours_of_Service: 0800 - 1600 CT, M-F, -6 h GMT
Contact_Instructions: lta@usgs.gov
Distribution_Liability: Although these data have been processed successfully on a computer system at the U.S. Geological Survey, no warranty expressed or implied is made by the USGS regarding the use of the data on any other system, nor does the act of distribution constitute any such warranty.
Standard_Order_Process:
Digital_Form:
Digital_Transfer_Information:
Format_Name: DTED, BIL, or GeoTIFF
Fees: SRTM data are available from the USGS EROS Center at no cost to the user.
Ordering_Instructions: SRTM products are available via download through EarthExplorer (<http://earthexplorer.usgs.gov>).

Turnaround: The Global SRTM 1 Arc-Second (30 meters) data set will be released in phases. Users should check the coverage map in EarthExplorer to verify if their area of interest is available. Existing data are available for immediate download.

Technical_Prerequisites: SRTM data are intended for scientific use with Geographic Information System (GIS) or other special application software that is compatible with the DTED, BIL, or GeoTIFF format.

Metadata_Reference_Information:

Metadata_Review_Date: as needed

Metadata_Contact:

Contact_Information:

Contact_Person_Primary:

Contact_Person: lta@usgs.gov

Contact_Organization_Primary:

Contact_Organization: U.S. Geological Survey Earth Resources Observation and Science (EROS) Center

Contact_Person: lta@usgs.gov

Contact_Position: Long Term Archive (LTA) Representative

Contact_Address:

Address_Type: mailing and physical address

Address: Long Term Archive (LTA), U.S. Geological Survey (USGS)

Earth Resources Observation and Science (EROS) Center

47914 252nd Street

City: Sioux Falls

State_or_Province: South Dakota

Postal_Code: 57198-0001

Country: USA

Contact_Electronic_Mail_Address: lta.usgs.gov

Hours_of_Service: 0800 - 1600 CT, M-F, -6 h GMT

Contact_Instructions: lta@usgs.gov

Metadata_Standard_Name: Content Standard for Digital Geospatial Metadata

Metadata_Standard_Version: FGDC-STD-001-1998, Version 2

Metadata_Time_Convention: local time

Metadata_Access_Constraints: None

Metadata_Use_Constraints: None

Metadata_Security_Information:

Metadata_Security_Classification_System: None

Metadata_Security_Classification: Unclassified

Metadata_Security_Handling_Description: None

Table Format

[Accessibility](#)

[FOIA](#)

[Privacy](#)

[Policies and Notices](#)

[Google Maps API Disclaimer](#)

[U.S. Department of the Interior U.S. Geological Survey](#)

URL: <http://earthexplorer.usgs.gov>

Page Contact Information: lta@usgs.gov

Page Last Modified: 11/03/2014





APPENDIX B: LETTER OF REQUEST TO UTILISE DTM TO PERFORM ORTHORECTIFICATION EXPERIMENTS

LETTER OF REQUEST

20 January 2015

To: Mr Derick O'Brien
Geo-Spatial Integrated Management (DerickO@tshwane.gov.za)
City of Tshwane – Corporate GIS / City Planning and Development Department

From: Ivan Henrico (ivan.henrico@sita.co.za)
PhD Registered Student: University of Pretoria

PERMISSION TO UTILISE DERIVATIVE DTM CREATED BY CSIR FOR PHD IN GEOINFORMATICA STUDIES

1. I am currently registered at the University of Pretoria for my PhD in Geoinformatica, student number = 15025901. As part of my studies, I need to utilise a high quality digital elevation model for performing various orthorectification experiments. In September 2014, I had a discussion with Mr André Breytenbach (CSIR) and he informed that he is busy to derive a 2 m resolution DTM from LiDAR Point Cloud, which covers my PhD study area. The LiDAR Point Cloud data is the property of the City of Tshwane. Earlier this week Mr Breytenbach contacted me and informed me that he has finished the derived DTM product.

2. I request permission from the City of Tshwane (Corporate GIS / City Planning and Development Department) to utilise the derived DTM product for my PhD studies. This product will only be used for my studies and will not be distributed for use to any other person, department or party.

Regards


Ivan Henrico

APPROVED / NOT APPROVED


(DERICK O'BRIEN)
Geo-Spatial Integrated Management
City of Tshwane – Corporate GIS / City Planning and Development Department



APPENDIX C: LETTER OF REQUEST TO UTILISE GPS DEVICES FOR CAPTURING GCPS

LETTER OF REQUEST

To: Mr Russell Meyer (RMeyer@optron.com)
Key Account Manager MGIS

10 June 2014

From: Ivan Henrico (ivan.henrico@sita.co.za)
PhD Registered Student: University of Pretoria

Mr Russell Meyer

PERMISSION TO ACQUIRE AND UTILISE TWO TRIMBLE GEOEXPLORER 6000 SERIES GEOXH HANDHELD DEVICES FOR CAPTURING GROUND CONTROL POINTS

1. I am currently registered at the University of Pretoria for my PhD in Geoinformatica. As part of my studies, I need to capture ground control points for performing various orthorectification experiments. For this purpose, it was decided to utilise the Trimble GeoExplorer 6000 Series GeoXH handheld device, as it can deliver high-accuracy fieldwork at ~10 cm positional accuracy.

2. This fieldwork exercise will be executed on 19 June 2014 in cooperation with members of the Directorate Geospatial Information and Prof. Ludwig Combrinck (Associate Director: Space Geodesy HartRAO). Permission is requested to acquire and utilise two Trimble GeoExplorer 6000 Series GeoXH handheld devices from Optron (Pty) Ltd for the period 18 June 2014 to 23 June 2014.

Regards



Ivan Henrico

APPROVED / NOT APPROVED



(RUSSELL MEYER)
Key Account Manager: Mapping and GIS



APPENDIX D: GPS POST-PROCESSING LOG FILES

POST PROCESSING LOG FILES

-----Base Data Details:-----

Using reference position from base data

Name: TrigNet Pretoria

Source: PRET170A.14o, PRET171L.14o, PRET174E.14o, PRET175k.zip, PRET175l.zip, PRET175m.zip, PRET175n.zip

-----Differentially correcting...-----

Differential correction settings:

Use smart automatic filtering: On

Re-correct real-time positions: On

Output positions: Corrected only

-----Coverage Details:-----

Rover file: GCP#1.SSF

Local time: 2014/06/24 13:38:01 to 2014/06/24 13:42:36

100% total coverage

100% coverage by PRET175l.zip

Rover file: GCP#2.SSF

Local time: 2014/06/24 13:06:54 to 2014/06/24 13:28:24

100% total coverage

100% coverage by PRET175l.zip

Rover file: GCP#3.SSF

Local time: 2014/06/24 13:02:37 to 2014/06/24 13:06:50

100% total coverage

100% coverage by PRET175l.zip

Rover file: GCP#4.SSF

Local time: 2014/06/24 12:37:05 to 2014/06/24 12:52:56

100% total coverage

100% coverage by PRET175k.zip

Rover file: GCP#5.SSF

Local time: 2014/06/24 12:32:33 to 2014/06/24 12:37:00

100% total coverage

100% coverage by PRET175k.zip

Rover file: GCP#6.SSF

Local time: 2014/06/24 14:07:34 to 2014/06/24 14:12:00

100% total coverage

100% coverage by PRET175m.zip

Rover file: GCP#7.SSF

Local time: 2014/06/19 12:41:25 to 2014/06/19 12:47:53

100% total coverage

100% coverage by PRET170A.14o

Rover file: GCP#8.SSF

Local time: 2014/06/19 13:09:45 to 2014/06/19 13:15:06

100% total coverage

100% coverage by PRET170A.14o

Rover file: GCP#9.SSF

Local time: 2014/06/19 13:29:45 to 2014/06/19 13:35:01

100% total coverage

100% coverage by PRET170A.14o

Rover file: GCP#10.SSF

Local time: 2014/06/20 11:21:10 to 2014/06/20 11:21:59

100% total coverage

100% coverage by PRET171E.14o

Rover file: GCP#11.SSF

Local time: 2014/06/19 13:56:45 to 2014/06/19 14:02:09

100% total coverage

100% coverage by PRET170A.14o

Rover file: GCP#12.SSF

Local time: 2014/06/20 10:21:14 to 2014/06/20 10:26:48

100% total coverage

100% coverage by PRET171E.14o



Rover file: GCP#13.SSF
Local time: 2014/06/20 11:20:15 to 2014/06/20 11:29:58
100% total coverage
100% coverage by PRET171I.14o

Rover file: GCP#14.SSF
Local time: 2014/06/20 11:38:06 to 2014/06/20 11:56:02
100% total coverage
100% coverage by PRET171I.14o

Rover file: GCP#15.SSF
Local time: 2014/06/20 09:42:35 to 2014/06/20 09:47:52
100% total coverage
100% coverage by PRET171E.14o

Rover file: GCP#16.SSF
Local time: 2014/06/20 10:47:20 to 2014/06/20 10:53:31
100% total coverage
100% coverage by PRET171E.14o

Rover file: GCP#17.SSF
Local time: 2014/06/20 11:15:45 to 2014/06/20 11:21:00
100% total coverage
100% coverage by PRET171E.14o

Rover file: GCP#18.SSF
Local time: 2014/06/20 12:18:44 to 2014/06/20 12:22:49
100% total coverage
100% coverage by PRET171I.14o

Rover file: GCP#19.SSF
Local time: 2014/06/20 12:44:42 to 2014/06/20 12:48:23
100% total coverage
100% coverage by PRET171I.14o

Rover file: GCP#20.SSF
Local time: 2014/06/20 09:24:20 to 2014/06/20 09:29:41
100% total coverage
100% coverage by PRET171E.14o

Rover file: GCP#21.SSF
Local time: 2014/06/24 14:48:45 to 2014/06/24 14:51:38
100% total coverage
100% coverage by PRET175m.zip

Rover file: GCP#22.SSF
Local time: 2014/06/24 14:51:42 to 2014/06/24 15:08:57
100% total coverage
100% coverage by PRET175n.zip

Rover file: GCP#23.SSF
Local time: 2014/06/20 13:10:39 to 2014/06/20 13:15:55
100% total coverage
100% coverage by PRET171I.14o

Rover file: GCP#24.SSF
Local time: 2014/06/24 15:42:29 to 2014/06/24 15:49:15
100% total coverage
100% coverage by PRET175n.zip

Rover file: GCP#25.SSF
Local time: 2014/06/23 09:46:39 to 2014/06/23 09:54:06
100% total coverage
100% coverage by PRET174E.14o



Processing rover file, GCP#1.SSF ...
Carrier processing...
Selected 217 positions for post-processing
Corrected 184 positions
Failed to correct 33 positions
32 of these were due to insufficient satellites for position fix
Code processing...
Selected 217 positions for post-processing
Corrected 209 positions
Failed to correct 8 positions
Chose 89 code solutions over the carrier solutions
89 code solutions were of higher quality
Filtered out 8 uncorrected positions
(only "Corrected" positions selected for output)

Processing rover file, GCP#2.SSF ...
Carrier processing...
Selected 219 positions for post-processing
Corrected 198 positions
Failed to correct 21 positions
21 of these were due to insufficient satellites for position fix
Code processing...
Selected 219 positions for post-processing
Corrected 198 positions
Failed to correct 21 positions
Filtered out 21 uncorrected positions
(only "Corrected" positions selected for output)

Processing rover file, GCP#3.SSF ...
Carrier processing...
Selected 211 positions for post-processing
Corrected 207 positions
Failed to correct 4 positions
4 of these were due to insufficient satellites for position fix
Code processing...
Selected 211 positions for post-processing
Corrected 207 positions
Failed to correct 4 positions
Filtered out 4 uncorrected positions
(only "Corrected" positions selected for output)

Processing rover file, GCP#4.SSF ...
Carrier processing...
Selected 259 positions for post-processing
Corrected 231 positions
Failed to correct 28 positions
28 of these were due to insufficient satellites for position fix
Code processing...
Selected 259 positions for post-processing
Corrected 259 positions
Chose 4 code solutions over the carrier solutions
4 code solutions were of higher quality

Processing rover file, GCP#5.SSF ...
Carrier processing...
Selected 214 positions for post-processing
Corrected 186 positions
Failed to correct 28 positions
28 of these were due to insufficient satellites for position fix
Code processing...
Selected 214 positions for post-processing
Corrected 204 positions
Failed to correct 10 positions
Filtered out 10 uncorrected positions
(only "Corrected" positions selected for output)



Processing rover file, GCP#6.SSF ...
Carrier processing...
Selected 215 positions for post-processing
Corrected 175 positions
Failed to correct 40 positions
40 of these were due to insufficient satellites for position fix
Code processing...
Selected 215 positions for post-processing
Corrected 213 positions
Failed to correct 2 positions
Filtered out 2 uncorrected positions
(only "Corrected" positions selected for output)

Processing rover file, GCP#7.SSF ...
Carrier processing...
Selected 309 positions for post-processing
Corrected 277 positions
Failed to correct 32 positions
32 of these were due to insufficient satellites for position fix
Code processing...
Selected 309 positions for post-processing
Corrected 309 positions
Chose 277 code solutions over the carrier solutions
277 code solutions were of higher quality

Processing rover file, GCP#8.SSF ...
Carrier processing...
Selected 313 positions for post-processing
Corrected 255 positions
Failed to correct 58 positions
58 of these were due to insufficient satellites for position fix
Code processing...
Selected 313 positions for post-processing
Corrected 313 positions
Chose 255 code solutions over the carrier solutions
255 code solutions were of higher quality

Processing rover file, GCP#9.SSF ...
Carrier processing...
Selected 306 positions for post-processing
Corrected 0 positions
Failed to correct 306 positions
306 of these were due to insufficient satellites for position fix
Code processing...
Selected 306 positions for post-processing
Corrected 306 positions
Filtered out 1 uncorrected positions
(only "Corrected" positions selected for output)

Processing rover file, GCP#10.SSF ...
Carrier processing...
Selected 43 positions for post-processing
Corrected 6 positions
Failed to correct 37 positions
20 of these were due to insufficient satellites for position fix
Code processing...
Selected 43 positions for post-processing
Corrected 43 positions
Chose 6 code solutions over the carrier solutions
6 code solutions were of higher quality
Filtered out 1 uncorrected positions
(only "Corrected" positions selected for output)



Processing rover file, GCP#11.SSF ...
Carrier processing...
Selected 305 positions for post-processing
Corrected 125 positions
Failed to correct 180 positions
173 of these were due to insufficient satellites for position fix
Code processing...
Selected 305 positions for post-processing
Corrected 305 positions
Chose 125 code solutions over the carrier solutions
125 code solutions were of higher quality

Processing rover file, GCP#12.SSF ...
Carrier processing...
Selected 306 positions for post-processing
Corrected 281 positions
Failed to correct 25 positions
25 of these were due to insufficient satellites for position fix
Code processing...
Selected 306 positions for post-processing
Corrected 306 positions
Chose 281 code solutions over the carrier solutions
281 code solutions were of higher quality

Processing rover file, GCP#13.SSF ...
Carrier processing...
Selected 546 positions for post-processing
Corrected 451 positions
Failed to correct 95 positions
95 of these were due to insufficient satellites for position fix
Code processing...
Selected 546 positions for post-processing
Corrected 546 positions
Chose 451 code solutions over the carrier solutions
451 code solutions were of higher quality

Processing rover file, GCP#14.SSF ...
Carrier processing...
Selected 218 positions for post-processing
Corrected 89 positions
Failed to correct 129 positions
129 of these were due to insufficient satellites for position fix
Code processing...
Selected 218 positions for post-processing
Corrected 218 positions
Chose 89 code solutions over the carrier solutions
89 code solutions were of higher quality

Processing rover file, GCP#15.SSF ...
Carrier processing...
Selected 306 positions for post-processing
Corrected 0 positions
Failed to correct 306 positions
306 of these were due to insufficient satellites for position fix
Code processing...
Selected 306 positions for post-processing
Corrected 306 positions

Processing rover file, GCP#16.SSF ...
Carrier processing...
Selected 335 positions for post-processing
Corrected 221 positions
Failed to correct 114 positions
114 of these were due to insufficient satellites for position fix
Code processing...
Selected 335 positions for post-processing
Corrected 335 positions
Chose 218 code solutions over the carrier solutions
218 code solutions were of higher quality



Processing rover file, GCP#17.SSF ...

Carrier processing...
Selected 311 positions for post-processing
Corrected 231 positions
Failed to correct 80 positions
80 of these were due to insufficient satellites for position fix
Code processing...
Selected 311 positions for post-processing
Corrected 311 positions
Chose 231 code solutions over the carrier solutions
231 code solutions were of higher quality

Processing rover file, GCP#18.SSF ...

Carrier processing...
Selected 178 positions for post-processing
Corrected 145 positions
Failed to correct 33 positions
33 of these were due to insufficient satellites for position fix
Code processing...
Selected 178 positions for post-processing
Corrected 178 positions
Chose 133 code solutions over the carrier solutions
133 code solutions were of higher quality

Processing rover file, GCP#19.SSF ...

Carrier processing...
Selected 184 positions for post-processing
Corrected 167 positions
Failed to correct 17 positions
17 of these were due to insufficient satellites for position fix
Code processing...
Selected 184 positions for post-processing
Corrected 184 positions
Chose 166 code solutions over the carrier solutions
166 code solutions were of higher quality

Processing rover file, GCP#20.SSF ...

Carrier processing...
Selected 313 positions for post-processing
Corrected 289 positions
Failed to correct 24 positions
24 of these were due to insufficient satellites for position fix
Code processing...
Selected 313 positions for post-processing
Corrected 313 positions
Chose 289 code solutions over the carrier solutions
289 code solutions were of higher quality

Processing rover file, GCP#21.SSF ...

Carrier processing...
Selected 137 positions for post-processing
Corrected 129 positions
Failed to correct 8 positions
8 of these were due to insufficient satellites for position fix
Code processing...
Selected 137 positions for post-processing
Corrected 130 positions
Failed to correct 7 positions
Chose 59 code solutions over the carrier solutions
59 code solutions were of higher quality
Filtered out 7 uncorrected positions
(only "Corrected" positions selected for output)



Processing rover file, GCP#22.SSF ...

Carrier processing...
Selected 209 positions for post-processing
Corrected 194 positions
Failed to correct 15 positions
14 of these were due to insufficient satellites for position fix
Code processing...
Selected 209 positions for post-processing
Corrected 208 positions
Failed to correct 1 positions
Chose 66 code solutions over the carrier solutions
66 code solutions were of higher quality
Filtered out 1 uncorrected positions
(only "Corrected" positions selected for output)

Processing rover file, GCP#23.SSF ...

Carrier processing...
Selected 255 positions for post-processing
Corrected 252 positions
Failed to correct 3 positions
3 of these were due to insufficient satellites for position fix
Code processing...
Selected 255 positions for post-processing
Corrected 255 positions
Chose 220 code solutions over the carrier solutions
220 code solutions were of higher quality

Processing rover file, GCP#24.SSF ...

Carrier processing...
Selected 227 positions for post-processing
Corrected 176 positions
Failed to correct 51 positions
47 of these were due to insufficient satellites for position fix
Code processing...
Selected 227 positions for post-processing
Corrected 220 positions
Failed to correct 7 positions
Chose 108 code solutions over the carrier solutions
108 code solutions were of higher quality
Filtered out 7 uncorrected positions
(only "Corrected" positions selected for output)

Processing rover file, GCP#25.SSF ...

Carrier processing...
Selected 431 positions for post-processing
Corrected 27 positions
Failed to correct 404 positions
399 of these were due to insufficient satellites for position fix
Code processing...
Selected 431 positions for post-processing
Corrected 431 positions
Chose 27 code solutions over the carrier solutions
27 code solutions were of higher quality

Differential Correction Summary:

25 files processed. In these files:
7152 (100.00%) of 7152 selected positions were code corrected by post-processing
4986 (69.71%) of 4986 selected positions were carrier corrected by post-processing
3411 (47.69%) of code positions chosen over carrier, as they were of higher quality

Estimated accuracies for 7152 corrected positions are as follows:



Range	Percentage
0-5cm	-
5-15cm	17.04% (1219)
15-30cm	1.86% (133)
30-50cm	66.73% (4773)
0.5-1m	14.37% (1027)
>1m	-

Differential correction complete.





APPENDIX E: GCP COLLECTION CHECKLISTS



GCP #1

GCP #	GCP #1	
GCP Coordinates (Lat & Long)	25° 40' 48.836" S 28° 05' 58.629" E	
GPS Altitude (above sea level)	1378.64 m MSL	
Position Error Estimation	27 cm	
No. Of Satellites	13	
Description of Feature	Corner of Residential Perimeter Fence	
	<i><u>Photo</u></i>	<i><u>Satellite Image</u></i>
		
Terrain Type	Hilly surroundings and grass surface	
Remarks	This feature is clearly visible and identifiable on the satellite image	



GCP #2

GCP #	GCP #2	
GCP Coordinates (Lat & Long)	25° 40' 53.644" S 28° 08' 43.157" E	
GPS Altitude (above sea level)	1302.82 m MSL	
Position Error Estimation	19 cm	
No. Of Satellites	14	
Description of Feature	Concrete of Man-Hole	
	<i><u>Photo</u></i>	<i><u>Satellite Image</u></i>
		
Terrain Type	Flat surroundings with hard cement surface	
Remarks	This feature is clearly visible and identifiable on the satellite image	



GCP #3

GCP #	GCP #3	
GCP Coordinates (Lat & Long)	25° 40' 51.168" S 28° 11' 51.342" E	
GPS Altitude (above sea level)	1251.13 m MSL	
Position Error Estimation	18 cm	
No. Of Satellites	17	
Description of Feature	Corner of Stop Street White Line	
	<i>Photo</i>	<i>Satellite Image</i>
		
Terrain Type	Flat residential surroundings with hard tar surface	
Remarks	This feature is clearly visible and identifiable on the satellite image	



GCP #4

GCP #	GCP #4	
GCP Coordinates (Lat & Long)	25° 40' 48.360" S 28° 14' 43.376" E	
GPS Altitude (above sea level)	1283.27 m MSL	
Position Error Estimation	17 cm	
No. Of Satellites	16	
Description of Feature	Centre of Traffic Circle	
	<i>Photo</i>	<i>Satellite Image</i>
		
Terrain Type	Flat surroundings with hard paved surface	
Remarks	This feature is clearly visible and identifiable on the satellite image	



GCP #5

GCP #	GCP #5	
GCP Coordinates (Lat & Long)	25° 40' 58.428" S 28° 17' 44.839" E	
GPS Altitude (above sea level)	1268.35 m MSL	
Position Error Estimation	19 cm	
No. Of Satellites	17	
Description of Feature	Centre of Traffic Circle	
	<i>Photo</i>	<i>Satellite Image</i>
		
Terrain Type	Flat open surroundings with hard paved surface	
Remarks	This feature is clearly visible and identifiable on the satellite image	



GCP #6

GCP #	GCP #6	
GCP Coordinates (Lat & Long)	25° 43' 20.093" S 28° 06' 12.828" E	
GPS Altitude (above sea level)	1319.67 m MSL	
Position Error Estimation	21 cm	
No. Of Satellites	15	
Description of Feature	Corner of Race Track Perimeter Wall	
	<i>Photo</i>	<i>Satellite Image</i>
		
Terrain Type	Relatively flat surroundings with ground surface	
Remarks	This feature is clearly visible and identifiable on the satellite image	



GCP #7

GCP #	GCP #7	
GCP Coordinates (Lat & Long)	25° 43' 28.505" S 28° 08' 51.186" E	
GPS Altitude (above sea level)	1315.20 m MSL	
Position Error Estimation	34 cm	
No. Of Satellites	10	
Description of Feature	Centre of Traffic Circle	
	<i>Photo</i>	<i>Satellite Image</i>
		
Terrain Type	Flat residential surroundings with hard tar surface	
Remarks	This feature is clearly visible and identifiable on the satellite image	



GCP #8

GCP #	GCP #8	
GCP Coordinates (Lat & Long)	25° 43' 30.456" S 28° 11' 45.337" E	
GPS Altitude (above sea level)	1303.45 m MSL	
Position Error Estimation	22 cm	
No. Of Satellites	16	
Description of Feature	Eastern Corner of School Parking Cement Pavement	
	<i>Photo</i>	<i>Satellite Image</i>
		
Terrain Type	Flat residential surroundings hard cement surface	
Remarks	This feature is clearly visible and identifiable on the satellite image	



GCP #9

GCP #	GCP #9	
GCP Coordinates (Lat & Long)	25° 43' 30.08" S 28° 14' 52.284" E	
GPS Altitude (above sea level)	1380.2 m MSL	
Position Error Estimation	24 cm	
No. Of Satellites	14	
Description of Feature	Corner of Northern Stop Street White Line	
	<i>Photo</i>	<i>Satellite Image</i>
		
Terrain Type	Flat residential surroundings with hard tar surface	
Remarks	This feature is clearly visible and identifiable on the satellite image	



GCP #10

GCP #	GCP #10	
GCP Coordinates (Lat & Long)	25° 43' 18.66" S 28° 17' 37.7" E	
GPS Altitude (above sea level)	1326.5 m MSL	
Position Error Estimation	27 cm	
No. Of Satellites	11	
Description of Feature	Where Stop Street White Line and Pavement Meet	
	<i>Photo</i>	<i>Satellite Image</i>
		
Terrain Type	Flat industrial surroundings with hard cement surface	
Remarks	This feature is clearly visible and identifiable on the satellite image	



GCP #11

GCP #	GCP #11	
GCP Coordinates (Lat & Long)	25° 46' 25.891" S 28° 06' 04.717" E	
GPS Altitude (above sea level)	1417.43 m MSL	
Position Error Estimation	25 cm	
No. Of Satellites	14	
Description of Feature	North-Eastern Corner of Concrete Block	
	<u>Photo</u>	<u>Satellite Image</u>
		
Terrain Type	Flat surroundings with hard cement surface	
Remarks	This feature is clearly visible and identifiable on the satellite image	

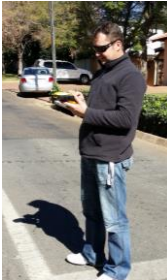
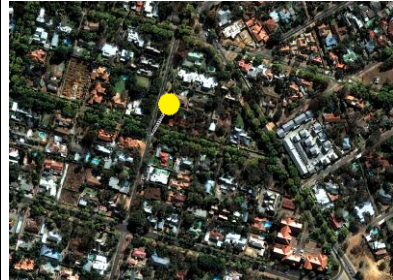
GCP #12

GCP #	GCP #12	
GCP Coordinates (Lat & Long)	25° 46' 16.295" S 28° 08' 48.31" E	
GPS Altitude (above sea level)	1402 m MSL	
Position Error Estimation	23 cm	
No. Of Satellites	13	
Description of Feature	South Corner of Traffic Pavement Corner	
	<u>Photo</u>	<u>Satellite Image</u>
		
Terrain Type	Relatively hilly surroundings with hard cement surface	
Remarks	This feature is clearly visible and identifiable on the satellite image	



GCP #13

GCP #	GCP #13	
GCP Coordinates (Lat & Long)	25° 46' 18.182" S 28° 12' 07.370" E	
GPS Altitude (above sea level)	1355.07 m MSL	
Position Error Estimation	14 cm	
No. Of Satellites	13	
Description of Feature	Centre Circle of South-West Netball Court	
	<i>Photo</i>	<i>Satellite Image</i>
		
Terrain Type	Flat surroundings with plexipave tennis court surface	
Remarks	This feature is clearly visible and identifiable on the satellite image	



GCP #14

GCP #	GCP #14	
GCP Coordinates (Lat & Long)	25° 46' 06.509" S 28° 14' 54.0" E	
GPS Altitude (above sea level)	1400.29 m MSL	
Position Error Estimation	20 cm	
No. Of Satellites	14	
Description of Feature	Corner of Stop Street White Line	
	<i>Photo</i>	<i>Satellite Image</i>
		
Terrain Type	Relatively flat residential surroundings with hard tar surface	
Remarks	This feature is clearly visible and identifiable on the satellite image	



GCP #15

GCP #	GCP #15	
GCP Coordinates (Lat & Long)	25° 48' 36.111" S 28° 05' 53.237" E	
GPS Altitude (above sea level)	1398 m MSL	
Position Error Estimation	18 cm	
No. Of Satellites	15	
Description of Feature	South-Eastern Stone Monument in Centre of Traffic Circle	
	<u>Photo</u>	<u>Satellite Image</u>
		
Terrain Type	Flat surroundings with sandstone rock surface	
Remarks	This feature is clearly visible and identifiable on the satellite image	



GCP #16

GCP #	GCP #16	
GCP Coordinates (Lat & Long)	25° 46' 05.440" S 28° 17' 41.234" E	
GPS Altitude (above sea level)	1438.2 m MSL	
Position Error Estimation	24 cm	
No. Of Satellites	14	
Description of Feature	Corner of Stop Street White Line	
	<u>Photo</u>	<u>Satellite Image</u>
		
Terrain Type	Relatively flat surroundings with hard tar surface	
Remarks	This feature is clearly visible and identifiable on the satellite image	



GCP #17

GCP #	GCP #17	
GCP Coordinates (Lat & Long)	25° 48' 43.697" S 28° 09' 05.420" E	
GPS Altitude (above sea level)	1444 m MSL	
Position Error Estimation	16 cm	
No. Of Satellites	16	
Description of Feature	Southern T-Connection of the 3 rd Tennis Court from the Right	
	<u>Photo</u>	<u>Satellite Image</u>
		
Terrain Type	Flat open surroundings with plexipave tennis court surface	
Remarks	This feature is clearly visible and identifiable on the satellite image	



GCP #18

GCP #	GCP #18	
GCP Coordinates (Lat & Long)	25° 48' 37.286" S 28° 11' 54.264" E	
GPS Altitude (above sea level)	1454.62 m MSL	
Position Error Estimation	16 cm	
No. Of Satellites	17	
Description of Feature	Cement Pavement	
	<u>Photo</u>	<u>Satellite Image</u>
		
Terrain Type	Flat surroundings with hard cement pavement surface	
Remarks	This feature is clearly visible and identifiable on the satellite image	



GCP #19

GCP #	GCP #19	
GCP Coordinates (Lat & Long)	25° 48' 43.557" S 28° 15' 00.373" E	
GPS Altitude (above sea level)	1559.96 m MSL	
Position Error Estimation	18 cm	
No. Of Satellites	17	
Description of Feature	Corner of Stop Street White Line	
	<u>Photo</u> 	<u>Satellite Image</u> 
Terrain Type	Relatively steep surroundings with hard tar surface	
Remarks	This feature is clearly visible and identifiable on the satellite image	


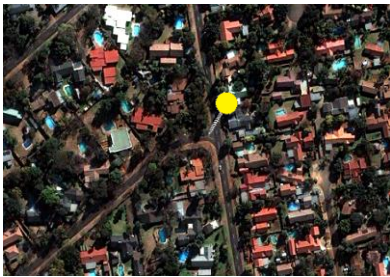
GCP #20

GCP #	GCP #20	
GCP Coordinates (Lat & Long)	25° 48' 42.95" S 28° 17' 44.5" E	
GPS Altitude (above sea level)	1446.5 m MSL	
Position Error Estimation	26 cm	
No. Of Satellites	13	
Description of Feature	Centre of Traffic Circle	
	<u>Photo</u> 	<u>Satellite Image</u> 
Terrain Type	Relatively steep open surroundings with hard tar surface	
Remarks	This feature is clearly visible and identifiable on the satellite image	



GCP #21

GCP #	GCP #21	
GCP Coordinates (Lat & Long)	25° 51' 12.428" S 28° 05' 50.236" E	
GPS Altitude (above sea level)	1428.11 m MSL	
Position Error Estimation	24 cm	
No. Of Satellites	16	
Description of Feature	Corner of the Southern Part of the Ruin Building	
	<i>Photo</i>	<i>Satellite Image</i>
		
Terrain Type	Flat open surroundings with grass surface	
Remarks	This feature is clearly visible and identifiable on the satellite image	



GCP #22

GCP #	GCP #22	
GCP Coordinates (Lat & Long)	25° 51' 11.646" S 28° 09' 01.775" E	
GPS Altitude (above sea level)	1476.53 m MSL	
Position Error Estimation	22 cm	
No. Of Satellites	14	
Description of Feature	Corner of Stop Street White Line	
	<i>Photo</i>	<i>Satellite Image</i>
		
Terrain Type	Flat residential surroundings with hard tar surface	
Remarks	This feature is clearly visible and identifiable on the satellite image	



GCP #23

GCP #	GCP #23	
GCP Coordinates (Lat & Long)	25° 51' 13.382" S 28° 11' 49.657" E	
GPS Altitude (above sea level)	1440.47 m MSL	
Position Error Estimation	25 cm	
No. Of Satellites	14	
Description of Feature	Corner of Stop Street White Line	
	<i>Photo</i>	<i>Satellite Image</i>
		
Terrain Type	Flat residential surroundings with hard tar surface	
Remarks	This feature is clearly visible and identifiable on the satellite image	

GCP #24


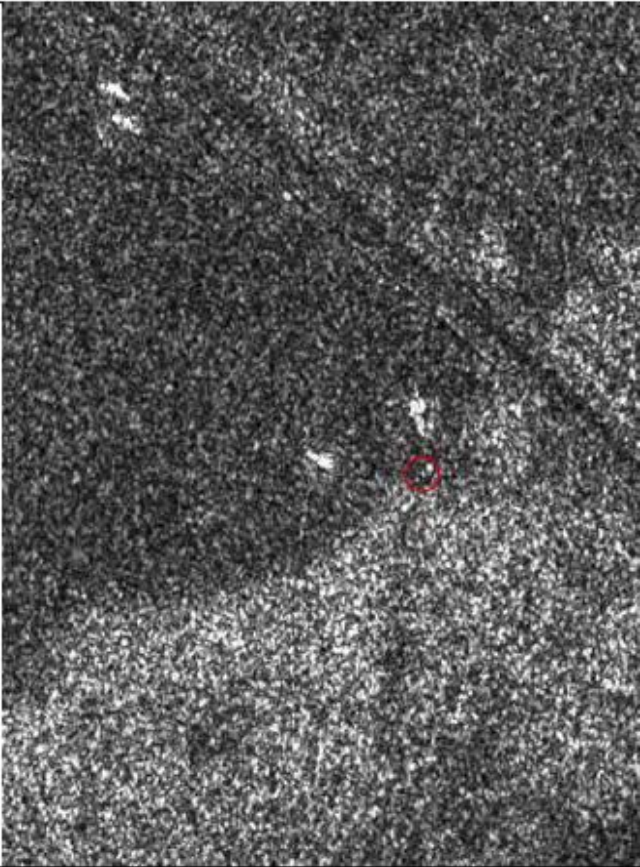
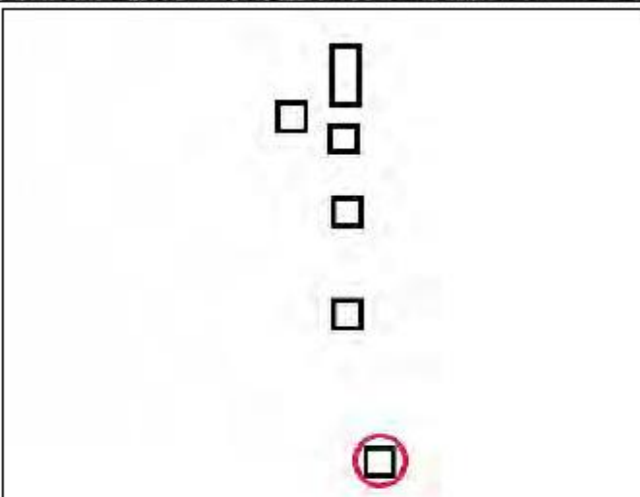
GCP #	GCP #24	
GCP Coordinates (Lat & Long)	25° 51' 10.288" S 28° 15' 05.542" E	
GPS Altitude (above sea level)	1514.10 m MSL	
Position Error Estimation	29 cm	
No. Of Satellites	18	
Description of Feature	South-West Corner of Concrete Block	
	<i>Photo</i>	<i>Satellite Image</i>
		
Terrain Type	Flat open surroundings with hard cement surface	
Remarks	This feature is clearly visible and identifiable on the satellite image	

GCP #25

GCP #	GCP #25	
GCP Coordinates (Lat & Long)	25° 51' 11.271" S 28° 17' 35.862" E	
GPS Altitude (above sea level)	1507.58 m MSL	
Position Error Estimation	71 cm	
No. Of Satellites	14	
Description of Feature	West Side of Steel Gate.	
	<u>Photo</u> 	<u>Satellite Image</u> 
Terrain Type	Flat open surroundings with grass surface	
Remarks	This feature is clearly visible and identifiable on the satellite image	



APPENDIX F: TERRASAR-X GCP LOCATION SHEETS

	Infoterra GmbH	TerraSAR-X GCP location sheet	Date: 18.08.2014
Customer Mr. Ivan Henrico			No.of Sheets: 10 Sheet: 1
Point ID: 1	Inputtype: SM	Input Images: 4	
Point East: 629581.679	Point North: 7139801.673	Point Height: 1527.505	
AOI: Pretoria	ITRF 2008 Ellipsoid	Projection: UTM zone 35S	
Remarks / Description Object on ground			
Radar Image Overview			
Sketch			

	Infoterra GmbH	TerraSAR-X GCP location sheet	Date: 18.08.2014
Customer Mr. Ivan Henrico			No. of Sheets: 10 Sheet: 2
Point ID: 2	Inputtype: SM	Input Images: 4	
Point East: 610787.240	Point North: 7158649.929	Point Height: 1458.289	
AOI: Pretoria	ITRF 2008 Ellipsoid	Projection: UTM zone 35S	
Remarks / Description Bottom of pole			
Radar Image Overview			
Sketch			

	Infoterra GmbH	TerraSAR-X GCP location sheet	Date: 18.08.2014
Customer Mr. Ivan Henrico			No. of Sheets: 10 Sheet: 3
Point ID: 3	Inputtype: SM	Input Images: 4	
Point East: 629691.940	Point North: 7158772.170	Point Height: 1284.251	
AOI: Pretoria	ITRF 2008 Ellipsoid	Projection: UTM zone 35S	
Remarks / Description Object on ground			
Radar Image Overview			
Sketch			

	Infoterra GmbH	TerraSAR-X GCP location sheet	Date: 18.08.2014
Customer Mr. Ivan Henrico			No.of Sheets: 10 Sheet: 4
Point ID: 4	Inputtype: SM	Input Images: 4	
Point East: 620748.943	Point North: 7149146.143	Point Height: 1402.556	
AOI: Pretoria	ITRF 2008 Ellipsoid	Projection: UTM zone 35S	
Remarks / Description Bottom of pole or lantern			
Radar Image Overview			
Sketch			

	Infoterra GmbH	TerraSAR-X GCP location sheet	Date: 18.08.2014
Customer Mr. Ivan Henrico			No.of Sheets: 10 Sheet: 5
Point ID: 5	Inputtype: SM	Input Images: 4	
Point East: 620354.913	Point North: 7158978.250	Point Height: 1275.770	
AOI: Pretoria	ITRF 2008 Ellipsoid	Projection: UTM zone 35S	
Remarks / Description Bottom of pole or lantern			
Radar Image Overview			
Sketch			

	Infoterra GmbH	TerraSAR-X GCP location sheet	Date: 18.08.2014
Customer Mr. Ivan Henrico			No. of Sheets: 10 Sheet: 6
Point ID: 6		Inputtype: SM	Input Images: 4
Point East: 614590.540		Point North: 7154449.110	Point Height: 1329.238
AOI: Pretoria		ITRF 2008 Ellipsoid	Projection: UTM zone 35S
Remarks / Description Bottom of pole or lantern			
Radar Image Overview			
Sketch			

	Infoterra GmbH	TerraSAR-X GCP location sheet	Date: 18.08.2014
Customer Mr. Ivan Henrico			No. of Sheets: 10 Sheet: 7
Point ID: 7	Inputtype: SM	Input Images: 4	
Point East: 626106.521	Point North: 7144871.115	Point Height: 1531.991	
AOI: Pretoria	ITRF 2008 Ellipsoid	Projection: UTM zone 35S	
Remarks / Description Bottom of pole or lantern			
Radar Image Overview			
Sketch			

	Infoterra GmbH	TerraSAR-X GCP location sheet	Date: 18.08.2014
Customer Mr. Ivan Henrico			No. of Sheets: 10 Sheet: 8
Point ID: 8	Inputtype: SM	Input Images: 4	
Point East: 625004.879	Point North: 7154260.968	Point Height: 1330.711	
AOI: Pretoria	ITRF 2008 Ellipsoid	Projection: UTM zone 35S	
Remarks / Description Object on ground			
Radar Image Overview			
Sketch			

	Infoterra GmbH	TerraSAR-X GCP location sheet	Date: 18.08.2014
Customer Mr. Ivan Henrico			No.of Sheets: 10 Sheet: 9
Point ID: 9	Inputtype: SM	Input Images: 4	
Point East: 616815.370	Point North: 7140615.775	Point Height: 1464.359	
AOI: Pretoria	ITRF 2008 Ellipsoid	Projection: UTM zone 35S	
Remarks / Description Bottom of pole or lantern			
Radar Image Overview			
Sketch			

	Infoterra GmbH	TerraSAR-X GCP location sheet	Date: 18.08.2014
Customer Mr. Ivan Henrico			No. of Sheets: 10 Sheet: 10
Point ID: 10	Inputtype: SM	Input Images: 4	
Point East: 610634.665	Point North: 7142848.078	Point Height: 1402.269	
AOI: Pretoria	ITRF 2008 Ellipsoid	Projection: UTM zone 35S	
Remarks / Description Bottom of pole or lantern			
Radar Image Overview			
Sketch			



APPENDIX G: MAA REPORT FOR STAGE 1 – EXPERIMENT 1(a) (ORTHO-IMAGE USING 5 GCPS AND THE 30 M SRTM DEM)

MAA Report for 5gcps_strm_ortho						
Distance values are in meters						
Mean latitude error: 1.171999						
Mean longitude error: 0.255882						
Mean horizontal error (average HE): 1.461420						
Standard deviation latitude error: 0.998900						
Standard deviation longitude error: 0.450726						
Standard deviation horizontal error: 0.710115						
90% Circular Error (against T&E): 2.371433						
90% Circular Error (T&E and mensuration error included): 2.371433						

ID	T&E Latitude	T&E Longitude	T&E Elevation	T&E CE90	T&E LE90	
1	-25 40 48.898	+28 05 58.648	1378.640	0.000	0.000	
						T&E Description
						CP #1

Measured Latitude		Measured Longitude		Measured Elevation		
-25 40 48.873		+28 05 58.666		1378.640		

Delta Latitude	Delta Longitude	Delta Elevation	Mensuration Error			
0.788	0.479	0.000	0.000			
						Individual HE
						0.923
						Individual VE
						0.000

ID	T&E Latitude	T&E Longitude	T&E Elevation	T&E CE90	T&E LE90	
2	-25 40 53.691	+28 08 43.169	1302.820	0.000	0.000	
						T&E Description
						CP #2

Measured Latitude		Measured Longitude		Measured Elevation		
-25 40 53.684		+28 08 43.188		1302.820		

Delta Latitude	Delta Longitude	Delta Elevation	Mensuration Error			
0.226	0.509	0.000	0.000			
						Individual HE
						0.557
						Individual VE
						0.000

ID	T&E Latitude	T&E Longitude	T&E Elevation	T&E CE90	T&E LE90	
3	-25 40 51.185	+28 11 51.353	1251.130	0.000	0.000	
						T&E Description
						CP #3

Measured Latitude		Measured Longitude		Measured Elevation		
-25 40 51.171		+28 11 51.363		1251.130		

Delta Latitude	Delta Longitude	Delta Elevation	Mensuration Error			
0.434	0.272	0.000	0.000			
						Individual HE
						0.512
						Individual VE
						0.000



ID	T&E Latitude	T&E Longitude	T&E Elevation	T&E CE90	T&E LE90
4	-25 40 48.373	+28 14 43.374	1283.270	0.000	0.000
					T&E Description
					CP #4
Measured Latitude		Measured Longitude		Measured Elevation	
-25 40 48.358		+28 14 43.389		1283.270	
Delta Latitude	Delta Longitude	Delta Elevation	Mensuration Error		
0.471	0.426	0.000	0.000		
Individual HE			Individual VE		
0.635			0.000		
ID	T&E Latitude	T&E Longitude	T&E Elevation	T&E CE90	T&E LE90
5	-25 40 58.441	+28 17 44.854	1268.350	0.000	0.000
					T&E Description
					CP #5
Measured Latitude		Measured Longitude		Measured Elevation	
-25 40 58.408		+28 17 44.883		1268.350	
Delta Latitude	Delta Longitude	Delta Elevation	Mensuration Error		
1.006	0.808	0.000	0.000		
Individual HE			Individual VE		
1.290			0.000		
ID	T&E Latitude	T&E Longitude	T&E Elevation	T&E CE90	T&E LE90
6	-25 43 20.146	+28 06 12.816	1319.670	0.000	0.000
					T&E Description
					CP #6
Measured Latitude		Measured Longitude		Measured Elevation	
-25 43 20.129		+28 06 12.832		1319.670	
Delta Latitude	Delta Longitude	Delta Elevation	Mensuration Error		
0.542	0.453	0.000	0.000		
Individual HE			Individual VE		
0.706			0.000		
ID	T&E Latitude	T&E Longitude	T&E Elevation	T&E CE90	T&E LE90
7	-25 43 28.495	+28 08 51.254	1315.200	0.000	0.000
					T&E Description
					CP #7
Measured Latitude		Measured Longitude		Measured Elevation	
-25 43 28.481		+28 08 51.258		1315.200	
Delta Latitude	Delta Longitude	Delta Elevation	Mensuration Error		
0.423	0.129	0.000	0.000		
Individual HE			Individual VE		
0.442			0.000		



ID	T&E Latitude	T&E Longitude	T&E Elevation	T&E CE90	T&E LE90
8	-25 43 30.456	+28 11 45.362	1303.450	0.000	0.000
					T&E Description
					CP #8
Measured Latitude		Measured Longitude		Measured Elevation	
-25 43 30.420		+28 11 45.325		1303.450	
Delta Latitude	Delta Longitude	Delta Elevation	Mensuration Error		
1.126	-1.035	0.000	0.000		
Individual HE			Individual VE		
1.529			0.000		
ID	T&E Latitude	T&E Longitude	T&E Elevation	T&E CE90	T&E LE90
9	-25 43 30.035	+28 14 52.315	1380.200	0.000	0.000
					T&E Description
					CP #9
Measured Latitude		Measured Longitude		Measured Elevation	
-25 43 30.007		+28 14 52.325		1380.200	
Delta Latitude	Delta Longitude	Delta Elevation	Mensuration Error		
0.841	0.296	0.000	0.000		
Individual HE			Individual VE		
0.892			0.000		
ID	T&E Latitude	T&E Longitude	T&E Elevation	T&E CE90	T&E LE90
10	-25 43 18.712	+28 17 37.661	1326.500	0.000	0.000
					T&E Description
					CP #10
Measured Latitude		Measured Longitude		Measured Elevation	
-25 43 18.602		+28 17 37.663		1326.500	
Delta Latitude	Delta Longitude	Delta Elevation	Mensuration Error		
3.403	0.037	0.000	0.000		
Individual HE			Individual VE		
3.403			0.000		
ID	T&E Latitude	T&E Longitude	T&E Elevation	T&E CE90	T&E LE90
11	-25 46 25.942	+28 06 4.674	1417.430	0.000	0.000
					T&E Description
					CP #11
Measured Latitude		Measured Longitude		Measured Elevation	
-25 46 26.013		+28 06 4.701		1417.430	
Delta Latitude	Delta Longitude	Delta Elevation	Mensuration Error		
-2.211	0.766	0.000	0.000		
Individual HE			Individual VE		
2.340			0.000		



ID	T&E Latitude	T&E Longitude	T&E Elevation	T&E CE90	T&E LE90
12	-25 46 16.305	+28 08 48.334	1402.000	0.000	0.000
					T&E Description
					CP #12
Measured Latitude		Measured Longitude		Measured Elevation	
-25 46 16.271		+28 08 48.341		1402.000	
Delta Latitude	Delta Longitude	Delta Elevation	Mensuration Error		
1.040	0.196	0.000	0.000		
Individual HE			Individual VE		
1.059			0.000		
ID	T&E Latitude	T&E Longitude	T&E Elevation	T&E CE90	T&E LE90
13	-25 46 18.155	+28 12 7.352	1355.070	0.000	0.000
					T&E Description
					CP #13
Measured Latitude		Measured Longitude		Measured Elevation	
-25 46 18.115		+28 12 7.356		1355.070	
Delta Latitude	Delta Longitude	Delta Elevation	Mensuration Error		
1.210	0.128	0.000	0.000		
Individual HE			Individual VE		
1.217			0.000		
ID	T&E Latitude	T&E Longitude	T&E Elevation	T&E CE90	T&E LE90
14	-25 46 6.549	+28 14 54.009	1400.290	0.000	0.000
					T&E Description
					CP #14
Measured Latitude		Measured Longitude		Measured Elevation	
-25 46 6.496		+28 14 54.023		1400.290	
Delta Latitude	Delta Longitude	Delta Elevation	Mensuration Error		
1.654	0.390	0.000	0.000		
Individual HE			Individual VE		
1.699			0.000		
ID	T&E Latitude	T&E Longitude	T&E Elevation	T&E CE90	T&E LE90
15	-25 46 5.504	+28 17 41.246	1398.000	0.000	0.000
					T&E Description
					CP #15
Measured Latitude		Measured Longitude		Measured Elevation	
-25 46 5.449		+28 17 41.281		1398.000	
Delta Latitude	Delta Longitude	Delta Elevation	Mensuration Error		
1.707	0.969	0.000	0.000		
Individual HE			Individual VE		
1.962			0.000		



ID	T&E Latitude	T&E Longitude	T&E Elevation	T&E CE90	T&E LE90
16	-25 48 36.146	+28 05 53.281	1438.200	0.000	0.000
					T&E Description
					CP #16
Measured Latitude		Measured Longitude		Measured Elevation	
-25 48 36.105		+28 05 53.280		1438.200	
Delta Latitude	Delta Longitude	Delta Elevation	Mensuration Error		
1.263	-0.049	0.000	0.000		
Individual HE				Individual VE	
1.264				0.000	
ID	T&E Latitude	T&E Longitude	T&E Elevation	T&E CE90	T&E LE90
17	-25 48 43.856	+28 09 4.106	1444.000	0.000	0.000
					T&E Description
					CP #17
Measured Latitude		Measured Longitude		Measured Elevation	
-25 48 43.789		+28 09 4.122		1444.000	
Delta Latitude	Delta Longitude	Delta Elevation	Mensuration Error		
2.055	0.435	0.000	0.000		
Individual HE				Individual VE	
2.101				0.000	
ID	T&E Latitude	T&E Longitude	T&E Elevation	T&E CE90	T&E LE90
18	-25 48 37.225	+28 11 54.324	1454.620	0.000	0.000
					T&E Description
					CP #18
Measured Latitude		Measured Longitude		Measured Elevation	
-25 48 37.186		+28 11 54.347		1454.620	
Delta Latitude	Delta Longitude	Delta Elevation	Mensuration Error		
1.200	0.649	0.000	0.000		
Individual HE				Individual VE	
1.365				0.000	
ID	T&E Latitude	T&E Longitude	T&E Elevation	T&E CE90	T&E LE90
19	-25 48 43.528	+28 15 0.374	1559.960	0.000	0.000
					T&E Description
					CP #19
Measured Latitude		Measured Longitude		Measured Elevation	
-25 48 43.464		+28 15 0.369		1559.960	
Delta Latitude	Delta Longitude	Delta Elevation	Mensuration Error		
1.993	-0.140	0.000	0.000		
Individual HE				Individual VE	
1.998				0.000	



ID	T&E Latitude	T&E Longitude	T&E Elevation	T&E CE90	T&E LE90
20	-25 48 42.925	+28 17 44.555	1446.500	0.000	0.000
					T&E Description
					CP #20
Measured Latitude		Measured Longitude		Measured Elevation	
-25 48 42.880		+28 17 44.592		1446.500	
Delta Latitude	Delta Longitude	Delta Elevation	Mensuration Error		
1.378	1.033	0.000	0.000		
Individual HE			Individual VE		
1.722			0.000		
ID	T&E Latitude	T&E Longitude	T&E Elevation	T&E CE90	T&E LE90
21	-25 51 12.497	+28 05 50.230	1428.110	0.000	0.000
					T&E Description
					CP #21
Measured Latitude		Measured Longitude		Measured Elevation	
-25 51 12.456		+28 05 50.227		1428.110	
Delta Latitude	Delta Longitude	Delta Elevation	Mensuration Error		
1.290	-0.083	0.000	0.000		
Individual HE			Individual VE		
1.293			0.000		
ID	T&E Latitude	T&E Longitude	T&E Elevation	T&E CE90	T&E LE90
22	-25 51 11.691	+28 09 1.772	1476.530	0.000	0.000
					T&E Description
					CP #22
Measured Latitude		Measured Longitude		Measured Elevation	
-25 51 11.633		+28 09 1.771		1476.530	
Delta Latitude	Delta Longitude	Delta Elevation	Mensuration Error		
1.804	-0.025	0.000	0.000		
Individual HE			Individual VE		
1.804			0.000		
ID	T&E Latitude	T&E Longitude	T&E Elevation	T&E CE90	T&E LE90
23	-25 51 14.426	+28 11 49.629	1440.470	0.000	0.000
					T&E Description
					CP #23
Measured Latitude		Measured Longitude		Measured Elevation	
-25 51 14.342		+28 11 49.613		1440.470	
Delta Latitude	Delta Longitude	Delta Elevation	Mensuration Error		
2.599	-0.431	0.000	0.000		
Individual HE			Individual VE		
2.634			0.000		



ID	T&E Latitude	T&E Longitude	T&E Elevation	T&E CE90	T&E LE90
24	-25 51 10.328	+28 15 5.543	1514.100	0.000	0.000
					T&E Description
					CP #24
Measured Latitude		Measured Longitude		Measured Elevation	
-25 51 10.261		+28 15 5.533		1514.100	
Delta Latitude	Delta Longitude	Delta Elevation	Mensuration Error		
2.076	-0.291	0.000	0.000		
Individual HE			Individual VE		
2.096			0.000		
ID	T&E Latitude	T&E Longitude	T&E Elevation	T&E CE90	T&E LE90
25	-25 51 11.253	+28 17 35.862	1507.580	0.000	0.000
					T&E Description
					CP #25
Measured Latitude		Measured Longitude		Measured Elevation	
-25 51 11.222		+28 17 35.879		1507.580	
Delta Latitude	Delta Longitude	Delta Elevation	Mensuration Error		
0.982	0.475	0.000	0.000		
Individual HE			Individual VE		
1.091			0.000		





APPENDIX H: MAA REPORT FOR STAGE 1 – EXPERIMENT 1(b) (ORTHO-IMAGE USING 5 GCPS AND THE 12 M DTM)

MAA Report for exp01b_5gcps_12mdtm_ortho						
Distance values are in meters						
Mean latitude error: -0.346076						
Mean longitude error: 0.680250						
Mean horizontal error (average HE): 1.376624						
Standard deviation latitude error: 0.912757						
Standard deviation longitude error: 1.020946						
Standard deviation horizontal error: 0.750246						
90% Circular Error (against T&E): 2.338065						
90% Circular Error (T&E and mensuration error included): 2.338065						
ID	T&E Latitude	T&E Longitude	T&E Elevation	T&E CE90	T&E LE90	
1	-25 40 48.898	+28 05 58.648	1378.640	0.000	0.000	
						T&E Description

Measured Latitude		Measured Longitude		Measured Elevation		
-25 40 48.924		+28 05 58.652		1378.640		

Delta Latitude	Delta Longitude	Delta Elevation	Mensuration Error			
-0.803	0.090	0.000	0.000			

Individual HE			Individual VE			
0.808			0.000			

ID	T&E Latitude	T&E Longitude	T&E Elevation	T&E CE90	T&E LE90	
2	-25 40 53.691	+28 08 43.169	1302.820	0.000	0.000	
						T&E Description

Measured Latitude		Measured Longitude		Measured Elevation		
-25 40 53.718		+28 08 43.193		1302.820		

Delta Latitude	Delta Longitude	Delta Elevation	Mensuration Error			
-0.842	0.649	0.000	0.000			

Individual HE			Individual VE			
1.063			0.000			

ID	T&E Latitude	T&E Longitude	T&E Elevation	T&E CE90	T&E LE90	
3	-25 40 51.185	+28 11 51.353	1251.130	0.000	0.000	
						T&E Description

Measured Latitude		Measured Longitude		Measured Elevation		
-25 40 51.202		+28 11 51.386		1251.130		

Delta Latitude	Delta Longitude	Delta Elevation	Mensuration Error			
-0.529	0.924	0.000	0.000			

Individual HE			Individual VE			
1.064			0.000			

ID	T&E Latitude	T&E Longitude	T&E Elevation	T&E CE90	T&E LE90
4	-25 40 48.373	+28 14 43.374	1283.270	0.000	0.000
T&E Description					
Measured Latitude		Measured Longitude		Measured Elevation	
-25 40 48.391		+28 14 43.418		1283.270	
Delta Latitude	Delta Longitude	Delta Elevation	Mensuration Error		
-0.535	1.235	0.000	0.000		
Individual HE			Individual VE		
1.346			0.000		
ID	T&E Latitude	T&E Longitude	T&E Elevation	T&E CE90	T&E LE90
5	-25 40 58.441	+28 17 44.854	1268.350	0.000	0.000
T&E Description					
Measured Latitude		Measured Longitude		Measured Elevation	
-25 40 58.428		+28 17 44.898		1268.350	
Delta Latitude	Delta Longitude	Delta Elevation	Mensuration Error		
0.406	1.211	0.000	0.000		
Individual HE			Individual VE		
1.278			0.000		
ID	T&E Latitude	T&E Longitude	T&E Elevation	T&E CE90	T&E LE90
6	-25 43 20.146	+28 06 12.816	1319.670	0.000	0.000
T&E Description					
Measured Latitude		Measured Longitude		Measured Elevation	
-25 43 20.180		+28 06 12.833		1319.670	
Delta Latitude	Delta Longitude	Delta Elevation	Mensuration Error		
-1.042	0.493	0.000	0.000		
Individual HE			Individual VE		
1.153			0.000		
ID	T&E Latitude	T&E Longitude	T&E Elevation	T&E CE90	T&E LE90
7	-25 43 28.495	+28 08 51.254	1315.200	0.000	0.000
T&E Description					
Measured Latitude		Measured Longitude		Measured Elevation	
-25 43 28.515		+28 08 51.270		1315.200	
Delta Latitude	Delta Longitude	Delta Elevation	Mensuration Error		
-0.629	0.451	0.000	0.000		
Individual HE			Individual VE		
0.774			0.000		

ID	T&E Latitude	T&E Longitude	T&E Elevation	T&E CE90	T&E LE90
8	-25 43 30.456	+28 11 45.362	1303.450	0.000	0.000
T&E Description					
Measured Latitude		Measured Longitude	Measured Elevation		
-25 43 30.452		+28 11 45.330	1303.450		
Delta Latitude	Delta Longitude	Delta Elevation	Mensuration Error		
0.123	-0.885	0.000	0.000		
Individual HE			Individual VE		
0.894			0.000		
ID	T&E Latitude	T&E Longitude	T&E Elevation	T&E CE90	T&E LE90
9	-25 43 30.035	+28 14 52.315	1380.200	0.000	0.000
T&E Description					
Measured Latitude		Measured Longitude	Measured Elevation		
-25 43 30.063		+28 14 52.439	1380.200		
Delta Latitude	Delta Longitude	Delta Elevation	Mensuration Error		
-0.868	3.470	0.000	0.000		
Individual HE			Individual VE		
3.577			0.000		
ID	T&E Latitude	T&E Longitude	T&E Elevation	T&E CE90	T&E LE90
10	-25 43 18.712	+28 17 37.661	1326.500	0.000	0.000
T&E Description					
Measured Latitude		Measured Longitude	Measured Elevation		
-25 43 18.639		+28 17 37.675	1326.500		
Delta Latitude	Delta Longitude	Delta Elevation	Mensuration Error		
2.260	0.391	0.000	0.000		
Individual HE			Individual VE		
2.293			0.000		
ID	T&E Latitude	T&E Longitude	T&E Elevation	T&E CE90	T&E LE90
11	-25 46 25.942	+28 06 4.674	1417.430	0.000	0.000
T&E Description					
Measured Latitude		Measured Longitude	Measured Elevation		
-25 46 26.001		+28 06 4.584	1417.430		
Delta Latitude	Delta Longitude	Delta Elevation	Mensuration Error		
-1.834	-2.485	0.000	0.000		
Individual HE			Individual VE		
3.089			0.000		

ID	T&E Latitude	T&E Longitude	T&E Elevation	T&E CE90	T&E LE90
12	-25 46 16.305	+28 08 48.334	1402.000	0.000	0.000
T&E Description					
Measured Latitude		Measured Longitude		Measured Elevation	
-25 46 16.395		+28 08 48.315		1402.000	
Delta Latitude	Delta Longitude	Delta Elevation	Mensuration Error		
-2.798	-0.545	0.000	0.000		
Individual HE			Individual VE		
2.850			0.000		
ID	T&E Latitude	T&E Longitude	T&E Elevation	T&E CE90	T&E LE90
13	-25 46 18.155	+28 12 7.352	1355.070	0.000	0.000
T&E Description					
Measured Latitude		Measured Longitude		Measured Elevation	
-25 46 18.164		+28 12 7.389		1355.070	
Delta Latitude	Delta Longitude	Delta Elevation	Mensuration Error		
-0.296	1.051	0.000	0.000		
Individual HE			Individual VE		
1.092			0.000		
ID	T&E Latitude	T&E Longitude	T&E Elevation	T&E CE90	T&E LE90
14	-25 46 6.549	+28 14 54.009	1400.290	0.000	0.000
T&E Description					
Measured Latitude		Measured Longitude		Measured Elevation	
-25 46 6.553		+28 14 54.047		1400.290	
Delta Latitude	Delta Longitude	Delta Elevation	Mensuration Error		
-0.123	1.056	0.000	0.000		
Individual HE			Individual VE		
1.063			0.000		
ID	T&E Latitude	T&E Longitude	T&E Elevation	T&E CE90	T&E LE90
15	-25 46 5.504	+28 17 41.246	1398.000	0.000	0.000
T&E Description					
Measured Latitude		Measured Longitude		Measured Elevation	
-25 46 5.505		+28 17 41.295		1398.000	
Delta Latitude	Delta Longitude	Delta Elevation	Mensuration Error		
-0.042	1.359	0.000	0.000		
Individual HE			Individual VE		
1.360			0.000		

ID	T&E Latitude	T&E Longitude	T&E Elevation	T&E CE90	T&E LE90
16	-25 48 36.146	+28 05 53.281	1438.200	0.000	0.000
T&E Description					
Measured Latitude		Measured Longitude	Measured Elevation		
-25 48 36.166		+28 05 53.298	1438.200		
Delta Latitude	Delta Longitude	Delta Elevation	Mensuration Error		
-0.628	0.454	0.000	0.000		
Individual HE			Individual VE		
0.775			0.000		
ID	T&E Latitude	T&E Longitude	T&E Elevation	T&E CE90	T&E LE90
17	-25 48 43.856	+28 09 4.106	1444.000	0.000	0.000
T&E Description					
Measured Latitude		Measured Longitude	Measured Elevation		
-25 48 43.844		+28 09 4.146	1444.000		
Delta Latitude	Delta Longitude	Delta Elevation	Mensuration Error		
0.373	1.116	0.000	0.000		
Individual HE			Individual VE		
1.177			0.000		
ID	T&E Latitude	T&E Longitude	T&E Elevation	T&E CE90	T&E LE90
18	-25 48 37.225	+28 11 54.324	1454.620	0.000	0.000
T&E Description					
Measured Latitude		Measured Longitude	Measured Elevation		
-25 48 37.211		+28 11 54.341	1454.620		
Delta Latitude	Delta Longitude	Delta Elevation	Mensuration Error		
0.437	0.486	0.000	0.000		
Individual HE			Individual VE		
0.653			0.000		
ID	T&E Latitude	T&E Longitude	T&E Elevation	T&E CE90	T&E LE90
19	-25 48 43.528	+28 15 0.374	1559.960	0.000	0.000
T&E Description					
Measured Latitude		Measured Longitude	Measured Elevation		
-25 48 43.522		+28 15 0.416	1559.960		
Delta Latitude	Delta Longitude	Delta Elevation	Mensuration Error		
0.179	1.164	0.000	0.000		
Individual HE			Individual VE		
1.178			0.000		

ID	T&E Latitude	T&E Longitude	T&E Elevation	T&E CE90	T&E LE90
20	-25 48 42.925	+28 17 44.555	1446.500	0.000	0.000
T&E Description					
Measured Latitude		Measured Longitude		Measured Elevation	
-25 48 42.933		+28 17 44.605		1446.500	
Delta Latitude	Delta Longitude	Delta Elevation	Mensuration Error		
-0.240	1.397	0.000	0.000		
Individual HE			Individual VE		
1.418			0.000		
ID	T&E Latitude	T&E Longitude	T&E Elevation	T&E CE90	T&E LE90
21	-25 51 12.497	+28 05 50.230	1428.110	0.000	0.000
T&E Description					
Measured Latitude		Measured Longitude		Measured Elevation	
-25 51 12.518		+28 05 50.227		1428.110	
Delta Latitude	Delta Longitude	Delta Elevation	Mensuration Error		
-0.642	-0.081	0.000	0.000		
Individual HE			Individual VE		
0.647			0.000		
ID	T&E Latitude	T&E Longitude	T&E Elevation	T&E CE90	T&E LE90
22	-25 51 11.691	+28 09 1.772	1476.530	0.000	0.000
T&E Description					
Measured Latitude		Measured Longitude		Measured Elevation	
-25 51 11.727		+28 09 1.809		1476.530	
Delta Latitude	Delta Longitude	Delta Elevation	Mensuration Error		
-1.107	1.023	0.000	0.000		
Individual HE			Individual VE		
1.507			0.000		
ID	T&E Latitude	T&E Longitude	T&E Elevation	T&E CE90	T&E LE90
23	-25 51 14.426	+28 11 49.629	1440.470	0.000	0.000
T&E Description					
Measured Latitude		Measured Longitude		Measured Elevation	
-25 51 14.405		+28 11 49.652		1440.470	
Delta Latitude	Delta Longitude	Delta Elevation	Mensuration Error		
0.672	0.651	0.000	0.000		
Individual HE			Individual VE		
0.936			0.000		

ID	T&E Latitude	T&E Longitude	T&E Elevation	T&E CE90	T&E LE90
24	-25 51 10.328	+28 15 5.543	1514.100	0.000	0.000
T&E Description					
Measured Latitude		Measured Longitude		Measured Elevation	
-25 51 10.321		+28 15 5.596		1514.100	
Delta Latitude	Delta Longitude	Delta Elevation	Mensuration Error		
0.222	1.482	0.000	0.000		
Individual HE			Individual VE		
1.498			0.000		
ID	T&E Latitude	T&E Longitude	T&E Elevation	T&E CE90	T&E LE90
25	-25 51 11.253	+28 17 35.862	1507.580	0.000	0.000
T&E Description					
Measured Latitude		Measured Longitude		Measured Elevation	
-25 51 11.265		+28 17 35.892		1507.580	
Delta Latitude	Delta Longitude	Delta Elevation	Mensuration Error		
-0.366	0.848	0.000	0.000		
Individual HE			Individual VE		
0.923			0.000		



APPENDIX I: MAA REPORT FOR STAGE 1 – EXPERIMENT 1(c) (ORTHO-IMAGE USING 5 GCPS AND THE 2 M DTM)

MAA Report for 5gcps_2mdtm_ortho

Distance values are in meters

Mean latitude error: 0.259856
 Mean longitude error: -0.171402
 Mean horizontal error (average HE): 0.921935
 Standard deviation latitude error: 1.029433
 Standard deviation longitude error: 0.497789
 Standard deviation horizontal error: 0.744624
 90% Circular Error (against T&E): 1.878747
 90% Circular Error (T&E and mensuration error included): 1.878747

ID	T&E Latitude	T&E Longitude	T&E Elevation	T&E CE90	T&E LE90
1	-25 40 48.898	+28 05 58.648	1378.640	0.000	0.000
T&E Description CP #1					
Measured Latitude		Measured Longitude		Measured Elevation	
-25 40 48.897		+28 05 58.631		1378.640	
Delta Latitude	Delta Longitude	Delta Elevation	Mensuration Error		
0.032	-0.483	0.000	0.000		
Individual HE			Individual VE		
0.484			0.000		
ID	T&E Latitude	T&E Longitude	T&E Elevation	T&E CE90	T&E LE90
2	-25 40 53.691	+28 08 43.169	1302.820	0.000	0.000
T&E Description CP #2					
Measured Latitude		Measured Longitude		Measured Elevation	
-25 40 53.709		+28 08 43.151		1302.820	
Delta Latitude	Delta Longitude	Delta Elevation	Mensuration Error		
-0.564	-0.502	0.000	0.000		
Individual HE			Individual VE		
0.755			0.000		
ID	T&E Latitude	T&E Longitude	T&E Elevation	T&E CE90	T&E LE90
3	-25 40 51.185	+28 11 51.353	1251.130	0.000	0.000
T&E Description CP #3					
Measured Latitude		Measured Longitude		Measured Elevation	
-25 40 51.196		+28 11 51.340		1251.130	
Delta Latitude	Delta Longitude	Delta Elevation	Mensuration Error		
-0.354	-0.356	0.000	0.000		
Individual HE			Individual VE		
0.502			0.000		

ID	T&E Latitude	T&E Longitude	T&E Elevation	T&E CE90	T&E LE90
4	-25 40 48.373	+28 14 43.374	1283.270	0.000	0.000
					T&E Description
					CP #4
Measured Latitude		Measured Longitude		Measured Elevation	
-25 40 48.383		+28 14 43.380		1283.270	
Delta Latitude	Delta Longitude	Delta Elevation	Mensuration Error		
-0.288	0.186	0.000	0.000		
Individual HE			Individual VE		
0.343			0.000		
ID	T&E Latitude	T&E Longitude	T&E Elevation	T&E CE90	T&E LE90
5	-25 40 58.441	+28 17 44.854	1268.350	0.000	0.000
					T&E Description
					CP #5
Measured Latitude		Measured Longitude		Measured Elevation	
-25 40 58.434		+28 17 44.854		1268.350	
Delta Latitude	Delta Longitude	Delta Elevation	Mensuration Error		
0.228	-0.000	0.000	0.000		
Individual HE			Individual VE		
0.228			0.000		
ID	T&E Latitude	T&E Longitude	T&E Elevation	T&E CE90	T&E LE90
6	-25 43 20.146	+28 06 12.816	1319.670	0.000	0.000
					T&E Description
					CP #6
Measured Latitude		Measured Longitude		Measured Elevation	
-25 43 20.169		+28 06 12.798		1319.670	
Delta Latitude	Delta Longitude	Delta Elevation	Mensuration Error		
-0.692	-0.490	0.000	0.000		
Individual HE			Individual VE		
0.848			0.000		
ID	T&E Latitude	T&E Longitude	T&E Elevation	T&E CE90	T&E LE90
7	-25 43 28.495	+28 08 51.254	1315.200	0.000	0.000
					T&E Description
					CP #7
Measured Latitude		Measured Longitude		Measured Elevation	
-25 43 28.504		+28 08 51.238		1315.200	
Delta Latitude	Delta Longitude	Delta Elevation	Mensuration Error		
-0.296	-0.428	0.000	0.000		
Individual HE			Individual VE		
0.520			0.000		

ID	T&E Latitude	T&E Longitude	T&E Elevation	T&E CE90	T&E LE90
8	-25 43 30.456	+28 11 45.362	1303.450	0.000	0.000
					T&E Description
					CP #8
Measured Latitude		Measured Longitude		Measured Elevation	
-25 43 30.442		+28 11 45.302		1303.450	
Delta Latitude	Delta Longitude	Delta Elevation	Mensuration Error		
0.439	-1.667	0.000	0.000		
Individual HE				Individual VE	
1.723				0.000	
ID	T&E Latitude	T&E Longitude	T&E Elevation	T&E CE90	T&E LE90
9	-25 43 30.035	+28 14 52.315	1380.200	0.000	0.000
					T&E Description
					CP #9
Measured Latitude		Measured Longitude		Measured Elevation	
-25 43 30.030		+28 14 52.299		1380.200	
Delta Latitude	Delta Longitude	Delta Elevation	Mensuration Error		
0.131	-0.436	0.000	0.000		
Individual HE				Individual VE	
0.455				0.000	
ID	T&E Latitude	T&E Longitude	T&E Elevation	T&E CE90	T&E LE90
10	-25 43 18.712	+28 17 37.661	1326.500	0.000	0.000
					T&E Description
					CP #10
Measured Latitude		Measured Longitude		Measured Elevation	
-25 43 18.625		+28 17 37.634		1326.500	
Delta Latitude	Delta Longitude	Delta Elevation	Mensuration Error		
2.711	-0.767	0.000	0.000		
Individual HE				Individual VE	
2.817				0.000	
ID	T&E Latitude	T&E Longitude	T&E Elevation	T&E CE90	T&E LE90
11	-25 46 25.942	+28 06 4.674	1417.430	0.000	0.000
					T&E Description
					CP #11
Measured Latitude		Measured Longitude		Measured Elevation	
-25 46 26.051		+28 06 4.686		1417.430	
Delta Latitude	Delta Longitude	Delta Elevation	Mensuration Error		
-3.367	0.332	0.000	0.000		
Individual HE				Individual VE	
3.383				0.000	



 List of research project topics and materials

ID	T&E Latitude	T&E Longitude	T&E Elevation	T&E CE90	T&E LE90
12	-25 46 16.305	+28 08 48.334	1402.000	0.000	0.000
					T&E Description
					CP #12
Measured Latitude		Measured Longitude		Measured Elevation	
-25 46 16.291		+28 08 48.322		1402.000	
Delta Latitude	Delta Longitude	Delta Elevation	Mensuration Error		
0.426	-0.338	0.000	0.000		
Individual HE				Individual VE	
0.544				0.000	
ID	T&E Latitude	T&E Longitude	T&E Elevation	T&E CE90	T&E LE90
13	-25 46 18.155	+28 12 7.352	1355.070	0.000	0.000
					T&E Description
					CP #13
Measured Latitude		Measured Longitude		Measured Elevation	
-25 46 18.135		+28 12 7.350		1355.070	
Delta Latitude	Delta Longitude	Delta Elevation	Mensuration Error		
0.594	-0.047	0.000	0.000		
Individual HE				Individual VE	
0.596				0.000	
ID	T&E Latitude	T&E Longitude	T&E Elevation	T&E CE90	T&E LE90
14	-25 46 6.549	+28 14 54.009	1400.290	0.000	0.000
					T&E Description
					CP #14
Measured Latitude		Measured Longitude		Measured Elevation	
-25 46 6.533		+28 14 54.014		1400.290	
Delta Latitude	Delta Longitude	Delta Elevation	Mensuration Error		
0.508	0.153	0.000	0.000		
Individual HE				Individual VE	
0.530				0.000	
ID	T&E Latitude	T&E Longitude	T&E Elevation	T&E CE90	T&E LE90
15	-25 46 5.504	+28 17 41.246	1398.000	0.000	0.000
					T&E Description
					CP #15
Measured Latitude		Measured Longitude		Measured Elevation	
-25 46 5.486		+28 17 41.253		1398.000	
Delta Latitude	Delta Longitude	Delta Elevation	Mensuration Error		
0.552	0.171	0.000	0.000		
Individual HE				Individual VE	
0.578				0.000	

ID	T&E Latitude	T&E Longitude	T&E Elevation	T&E CE90	T&E LE90
16	-25 48 36.146	+28 05 53.281	1438.200	0.000	0.000
					T&E Description
					CP #16
Measured Latitude		Measured Longitude		Measured Elevation	
-25 48 36.140		+28 05 53.280		1438.200	
Delta Latitude	Delta Longitude	Delta Elevation	Mensuration Error		
0.193	-0.029	0.000	0.000		
Individual HE			Individual VE		
0.195			0.000		
ID	T&E Latitude	T&E Longitude	T&E Elevation	T&E CE90	T&E LE90
17	-25 48 43.856	+28 09 4.106	1444.000	0.000	0.000
					T&E Description
					CP #17
Measured Latitude		Measured Longitude		Measured Elevation	
-25 48 43.823		+28 09 4.118		1444.000	
Delta Latitude	Delta Longitude	Delta Elevation	Mensuration Error		
1.001	0.339	0.000	0.000		
Individual HE			Individual VE		
1.057			0.000		
ID	T&E Latitude	T&E Longitude	T&E Elevation	T&E CE90	T&E LE90
18	-25 48 37.225	+28 11 54.324	1454.620	0.000	0.000
					T&E Description
					CP #18
Measured Latitude		Measured Longitude		Measured Elevation	
-25 48 37.220		+28 11 54.358		1454.620	
Delta Latitude	Delta Longitude	Delta Elevation	Mensuration Error		
0.132	0.967	0.000	0.000		
Individual HE			Individual VE		
0.976			0.000		
ID	T&E Latitude	T&E Longitude	T&E Elevation	T&E CE90	T&E LE90
19	-25 48 43.528	+28 15 0.374	1559.960	0.000	0.000
					T&E Description
					CP #19
Measured Latitude		Measured Longitude		Measured Elevation	
-25 48 43.481		+28 15 0.377		1559.960	
Delta Latitude	Delta Longitude	Delta Elevation	Mensuration Error		
1.467	0.067	0.000	0.000		
Individual HE			Individual VE		
1.468			0.000		

ID	T&E Latitude	T&E Longitude	T&E Elevation	T&E CE90	T&E LE90
20	-25 48 42.925	+28 17 44.555	1446.500	0.000	0.000
					T&E Description
					CP #20
Measured Latitude		Measured Longitude		Measured Elevation	
-25 48 42.897		+28 17 44.563		1446.500	
Delta Latitude	Delta Longitude	Delta Elevation	Mensuration Error		
0.853	0.230	0.000	0.000		
Individual HE			Individual VE		
0.883			0.000		
ID	T&E Latitude	T&E Longitude	T&E Elevation	T&E CE90	T&E LE90
21	-25 51 12.497	+28 05 50.230	1428.110	0.000	0.000
					T&E Description
					CP #21
Measured Latitude		Measured Longitude		Measured Elevation	
-25 51 12.505		+28 05 50.210		1428.110	
Delta Latitude	Delta Longitude	Delta Elevation	Mensuration Error		
-0.232	-0.549	0.000	0.000		
Individual HE			Individual VE		
0.596			0.000		
ID	T&E Latitude	T&E Longitude	T&E Elevation	T&E CE90	T&E LE90
22	-25 51 11.691	+28 09 1.772	1476.530	0.000	0.000
					T&E Description
					CP #22
Measured Latitude		Measured Longitude		Measured Elevation	
-25 51 11.665		+28 09 1.786		1476.530	
Delta Latitude	Delta Longitude	Delta Elevation	Mensuration Error		
0.808	0.381	0.000	0.000		
Individual HE			Individual VE		
0.894			0.000		
ID	T&E Latitude	T&E Longitude	T&E Elevation	T&E CE90	T&E LE90
23	-25 51 14.426	+28 11 49.629	1440.470	0.000	0.000
					T&E Description
					CP #23
Measured Latitude		Measured Longitude		Measured Elevation	
-25 51 14.391		+28 11 49.607		1440.470	
Delta Latitude	Delta Longitude	Delta Elevation	Mensuration Error		
1.084	-0.597	0.000	0.000		
Individual HE			Individual VE		
1.237			0.000		

ID	T&E Latitude	T&E Longitude	T&E Elevation	T&E CE90	T&E LE90
24	-25 51 10.328	+28 15 5.543	1514.100	0.000	0.000
					T&E Description
					CP #24
Measured Latitude		Measured Longitude		Measured Elevation	
-25 51 10.292		+28 15 5.539		1514.100	
Delta Latitude	Delta Longitude	Delta Elevation	Mensuration Error		
1.109	-0.100	0.000	0.000		
Individual HE			Individual VE		
1.113			0.000		
ID	T&E Latitude	T&E Longitude	T&E Elevation	T&E CE90	T&E LE90
25	-25 51 11.253	+28 17 35.862	1507.580	0.000	0.000
					T&E Description
					CP #25
Measured Latitude		Measured Longitude		Measured Elevation	
-25 51 11.253		+28 17 35.850		1507.580	
Delta Latitude	Delta Longitude	Delta Elevation	Mensuration Error		
0.023	-0.323	0.000	0.000		
Individual HE			Individual VE		
0.323			0.000		



APPENDIX J: MAA REPORT FOR STAGE 1 – EXPERIMENT 2(a) (ORTHO-IMAGE USING 13 GCPS AND THE 30 M SRTM DEM)

MAA Report for 13gcps_srtm_ortho

Distance values are in meters

Mean latitude error: 0.177333
 Mean longitude error: 0.023905
 Mean horizontal error (average HE): 0.688425
 Standard deviation latitude error: 0.839613
 Standard deviation longitude error: 0.435148
 Standard deviation horizontal error: 0.672603
 90% Circular Error (against T&E): 1.552497
 90% Circular Error (T&E and mensuration error included): 1.552497

ID	T&E Latitude	T&E Longitude	T&E Elevation	T&E CE90	T&E LE90
1	-25 40 48.898	+28 05 58.648	1378.640	0.000	0.000
					T&E Description
					CP #1
Measured Latitude		Measured Longitude		Measured Elevation	
-25 40 48.881		+28 05 58.646		1378.640	
Delta Latitude	Delta Longitude	Delta Elevation	Mensuration Error		
0.531	-0.074	0.000	0.000		
Individual HE			Individual VE		
0.536			0.000		

ID	T&E Latitude	T&E Longitude	T&E Elevation	T&E CE90	T&E LE90
2	-25 40 53.691	+28 08 43.169	1302.820	0.000	0.000
					T&E Description
					CP #2
Measured Latitude		Measured Longitude		Measured Elevation	
-25 40 53.691		+28 08 43.167		1302.820	
Delta Latitude	Delta Longitude	Delta Elevation	Mensuration Error		
-0.012	-0.052	0.000	0.000		
Individual HE			Individual VE		
0.053			0.000		

ID	T&E Latitude	T&E Longitude	T&E Elevation	T&E CE90	T&E LE90
3	-25 40 51.185	+28 11 51.353	1251.130	0.000	0.000
					T&E Description
					CP #3
Measured Latitude		Measured Longitude		Measured Elevation	
-25 40 51.179		+28 11 51.357		1251.130	
Delta Latitude	Delta Longitude	Delta Elevation	Mensuration Error		
0.162	0.115	0.000	0.000		
Individual HE			Individual VE		
0.199			0.000		



ID	T&E Latitude	T&E Longitude	T&E Elevation	T&E CE90	T&E LE90
4	-25 40 48.373	+28 14 43.374	1283.270	0.000	0.000
					T&E Description
					CP #4
Measured Latitude		Measured Longitude		Measured Elevation	
-25 40 48.384		+28 14 43.382		1283.270	
Delta Latitude	Delta Longitude	Delta Elevation	Mensuration Error		
-0.334	0.216	0.000	0.000		
Individual HE			Individual VE		
0.398			0.000		
ID	T&E Latitude	T&E Longitude	T&E Elevation	T&E CE90	T&E LE90
5	-25 40 58.441	+28 17 44.854	1268.350	0.000	0.000
					T&E Description
					CP #5
Measured Latitude		Measured Longitude		Measured Elevation	
-25 40 58.435		+28 17 44.856		1268.350	
Delta Latitude	Delta Longitude	Delta Elevation	Mensuration Error		
0.197	0.054	0.000	0.000		
Individual HE			Individual VE		
0.204			0.000		
ID	T&E Latitude	T&E Longitude	T&E Elevation	T&E CE90	T&E LE90
6	-25 43 20.146	+28 06 12.816	1319.670	0.000	0.000
					T&E Description
					CP #6
Measured Latitude		Measured Longitude		Measured Elevation	
-25 43 20.136		+28 06 12.813		1319.670	
Delta Latitude	Delta Longitude	Delta Elevation	Mensuration Error		
0.324	-0.085	0.000	0.000		
Individual HE			Individual VE		
0.335			0.000		
ID	T&E Latitude	T&E Longitude	T&E Elevation	T&E CE90	T&E LE90
7	-25 43 28.495	+28 08 51.254	1315.200	0.000	0.000
					T&E Description
					CP #7
Measured Latitude		Measured Longitude		Measured Elevation	
-25 43 28.488		+28 08 51.253		1315.200	
Delta Latitude	Delta Longitude	Delta Elevation	Mensuration Error		
0.206	-0.003	0.000	0.000		
Individual HE			Individual VE		
0.206			0.000		



ID	T&E Latitude	T&E Longitude	T&E Elevation	T&E CE90	T&E LE90
8	-25 43 30.456	+28 11 45.362	1303.450	0.000	0.000
					T&E Description
					CP #8
Measured Latitude		Measured Longitude		Measured Elevation	
-25 43 30.442		+28 11 45.319		1303.450	
Delta Latitude	Delta Longitude	Delta Elevation	Mensuration Error		
0.429	-1.208	0.000	0.000		
Individual HE			Individual VE		
1.282			0.000		
ID	T&E Latitude	T&E Longitude	T&E Elevation	T&E CE90	T&E LE90
9	-25 43 30.035	+28 14 52.315	1380.200	0.000	0.000
					T&E Description
					CP #9
Measured Latitude		Measured Longitude		Measured Elevation	
-25 43 30.032		+28 14 52.317		1380.200	
Delta Latitude	Delta Longitude	Delta Elevation	Mensuration Error		
0.080	0.067	0.000	0.000		
Individual HE			Individual VE		
0.104			0.000		
ID	T&E Latitude	T&E Longitude	T&E Elevation	T&E CE90	T&E LE90
10	-25 43 18.712	+28 17 37.661	1326.500	0.000	0.000
					T&E Description
					CP #10
Measured Latitude		Measured Longitude		Measured Elevation	
-25 43 18.643		+28 17 37.635		1326.500	
Delta Latitude	Delta Longitude	Delta Elevation	Mensuration Error		
2.141	-0.721	0.000	0.000		
Individual HE			Individual VE		
2.259			0.000		
ID	T&E Latitude	T&E Longitude	T&E Elevation	T&E CE90	T&E LE90
11	-25 46 25.942	+28 06 4.674	1417.430	0.000	0.000
					T&E Description
					CP #11
Measured Latitude		Measured Longitude		Measured Elevation	
-25 46 26.035		+28 06 4.699		1417.430	
Delta Latitude	Delta Longitude	Delta Elevation	Mensuration Error		
-2.898	0.716	0.000	0.000		
Individual HE			Individual VE		
2.985			0.000		



ID	T&E Latitude	T&E Longitude	T&E Elevation	T&E CE90	T&E LE90
12	-25 46 16.305	+28 08 48.334	1402.000	0.000	0.000
					T&E Description
					CP #12
Measured Latitude		Measured Longitude		Measured Elevation	
-25 46 16.310		+28 08 48.338		1402.000	
Delta Latitude	Delta Longitude	Delta Elevation	Mensuration Error		
-0.171	0.109	0.000	0.000		
Individual HE			Individual VE		
0.203			0.000		
ID	T&E Latitude	T&E Longitude	T&E Elevation	T&E CE90	T&E LE90
13	-25 46 18.155	+28 12 7.352	1355.070	0.000	0.000
					T&E Description
					CP #13
Measured Latitude		Measured Longitude		Measured Elevation	
-25 46 18.136		+28 12 7.349		1355.070	
Delta Latitude	Delta Longitude	Delta Elevation	Mensuration Error		
0.568	-0.069	0.000	0.000		
Individual HE			Individual VE		
0.572			0.000		
ID	T&E Latitude	T&E Longitude	T&E Elevation	T&E CE90	T&E LE90
14	-25 46 6.549	+28 14 54.009	1400.290	0.000	0.000
					T&E Description
					CP #14
Measured Latitude		Measured Longitude		Measured Elevation	
-25 46 6.535		+28 14 54.032		1400.290	
Delta Latitude	Delta Longitude	Delta Elevation	Mensuration Error		
0.440	0.657	0.000	0.000		
Individual HE			Individual VE		
0.791			0.000		
ID	T&E Latitude	T&E Longitude	T&E Elevation	T&E CE90	T&E LE90
15	-25 46 5.504	+28 17 41.246	1398.000	0.000	0.000
					T&E Description
					CP #15
Measured Latitude		Measured Longitude		Measured Elevation	
-25 46 5.506		+28 17 41.254		1398.000	
Delta Latitude	Delta Longitude	Delta Elevation	Mensuration Error		
-0.066	0.197	0.000	0.000		
Individual HE			Individual VE		
0.208			0.000		



ID	T&E Latitude	T&E Longitude	T&E Elevation	T&E CE90	T&E LE90
16	-25 48 36.146	+28 05 53.281	1438.200	0.000	0.000
					T&E Description
					CP #16
Measured Latitude		Measured Longitude		Measured Elevation	
-25 48 36.142		+28 05 53.277		1438.200	
Delta Latitude	Delta Longitude	Delta Elevation	Mensuration Error		
0.125	-0.123	0.000	0.000		
Individual HE			Individual VE		
0.175			0.000		
ID	T&E Latitude	T&E Longitude	T&E Elevation	T&E CE90	T&E LE90
17	-25 48 43.856	+28 09 4.106	1444.000	0.000	0.000
					T&E Description
					CP #17
Measured Latitude		Measured Longitude		Measured Elevation	
-25 48 43.826		+28 09 4.118		1444.000	
Delta Latitude	Delta Longitude	Delta Elevation	Mensuration Error		
0.928	0.329	0.000	0.000		
Individual HE			Individual VE		
0.985			0.000		
ID	T&E Latitude	T&E Longitude	T&E Elevation	T&E CE90	T&E LE90
18	-25 48 37.225	+28 11 54.324	1454.620	0.000	0.000
					T&E Description
					CP #18
Measured Latitude		Measured Longitude		Measured Elevation	
-25 48 37.224		+28 11 54.357		1454.620	
Delta Latitude	Delta Longitude	Delta Elevation	Mensuration Error		
0.034	0.930	0.000	0.000		
Individual HE			Individual VE		
0.931			0.000		
ID	T&E Latitude	T&E Longitude	T&E Elevation	T&E CE90	T&E LE90
19	-25 48 43.528	+28 15 0.374	1559.960	0.000	0.000
					T&E Description
					CP #19
Measured Latitude		Measured Longitude		Measured Elevation	
-25 48 43.517		+28 15 0.377		1559.960	
Delta Latitude	Delta Longitude	Delta Elevation	Mensuration Error		
0.340	0.077	0.000	0.000		
Individual HE			Individual VE		
0.348			0.000		



ID	T&E Latitude	T&E Longitude	T&E Elevation	T&E CE90	T&E LE90
20	-25 48 42.925	+28 17 44.555	1446.500	0.000	0.000
					T&E Description
					CP #20
Measured Latitude		Measured Longitude		Measured Elevation	
-25 48 42.919		+28 17 44.563		1446.500	
Delta Latitude	Delta Longitude	Delta Elevation	Mensuration Error		
0.180	0.249	0.000	0.000		
Individual HE			Individual VE		
0.307			0.000		
ID	T&E Latitude	T&E Longitude	T&E Elevation	T&E CE90	T&E LE90
21	-25 51 12.497	+28 05 50.230	1428.110	0.000	0.000
					T&E Description
					CP #21
Measured Latitude		Measured Longitude		Measured Elevation	
-25 51 12.491		+28 05 50.207		1428.110	
Delta Latitude	Delta Longitude	Delta Elevation	Mensuration Error		
0.206	-0.637	0.000	0.000		
Individual HE			Individual VE		
0.670			0.000		
ID	T&E Latitude	T&E Longitude	T&E Elevation	T&E CE90	T&E LE90
22	-25 51 11.691	+28 09 1.772	1476.530	0.000	0.000
					T&E Description
					CP #22
Measured Latitude		Measured Longitude		Measured Elevation	
-25 51 11.667		+28 09 1.784		1476.530	
Delta Latitude	Delta Longitude	Delta Elevation	Mensuration Error		
0.742	0.342	0.000	0.000		
Individual HE			Individual VE		
0.817			0.000		
ID	T&E Latitude	T&E Longitude	T&E Elevation	T&E CE90	T&E LE90
23	-25 51 14.426	+28 11 49.629	1440.470	0.000	0.000
					T&E Description
					CP #23
Measured Latitude		Measured Longitude		Measured Elevation	
-25 51 14.396		+28 11 49.625		1440.470	
Delta Latitude	Delta Longitude	Delta Elevation	Mensuration Error		
0.935	-0.121	0.000	0.000		
Individual HE			Individual VE		
0.943			0.000		



ID	T&E Latitude	T&E Longitude	T&E Elevation	T&E CE90	T&E LE90
24	-25 51 10.328	+28 15 5.543	1514.100	0.000	0.000
					T&E Description
					CP #24
Measured Latitude		Measured Longitude		Measured Elevation	
-25 51 10.312		+28 15 5.540		1514.100	
Delta Latitude	Delta Longitude	Delta Elevation	Mensuration Error		
0.503	-0.077	0.000	0.000		
Individual HE			Individual VE		
0.508			0.000		
ID	T&E Latitude	T&E Longitude	T&E Elevation	T&E CE90	T&E LE90
25	-25 51 11.253	+28 17 35.862	1507.580	0.000	0.000
					T&E Description
					CP #25
Measured Latitude		Measured Longitude		Measured Elevation	
-25 51 11.291		+28 17 35.851		1507.580	
Delta Latitude	Delta Longitude	Delta Elevation	Mensuration Error		
-1.156	-0.291	0.000	0.000		
Individual HE			Individual VE		
1.192			0.000		

APPENDIX K: MAA REPORT FOR STAGE 1 – EXPERIMENT 2(b) (ORTHO-IMAGE USING 13 GCPS AND THE 12 M DTM)

MAA Report for exp02b_13gcps_12mdtm_ortho						
Distance values are in meters						
Mean latitude error: 0.292000						
Mean longitude error: 0.674538						
Mean horizontal error (average HE): 1.002887						
Standard deviation latitude error: 0.486141						
Standard deviation longitude error: 0.639444						
Standard deviation horizontal error: 0.423916						
90% Circular Error (against T&E): 1.546135						
90% Circular Error (T&E and mensuration error included): 1.546135						
ID	T&E Latitude	T&E Longitude	T&E Elevation	T&E CE90	T&E LE90	T&E Description
1	-25 40 48.898	+28 05 58.648	1378.640	0.000	0.000	
Measured Latitude		Measured Longitude		Measured Elevation		
-25 40 48.892		+28 05 58.654		1378.640		
Delta Latitude	Delta Longitude	Delta Elevation	Mensuration Error			
0.178	0.151	0.000	0.000			
Individual HE			Individual VE			
0.234			0.000			
ID	T&E Latitude	T&E Longitude	T&E Elevation	T&E CE90	T&E LE90	T&E Description
2	-25 40 53.691	+28 08 43.169	1302.820	0.000	0.000	
Measured Latitude		Measured Longitude		Measured Elevation		
-25 40 53.689		+28 08 43.197		1302.820		
Delta Latitude	Delta Longitude	Delta Elevation	Mensuration Error			
0.055	0.784	0.000	0.000			
Individual HE			Individual VE			
0.786			0.000			
ID	T&E Latitude	T&E Longitude	T&E Elevation	T&E CE90	T&E LE90	T&E Description
3	-25 40 51.185	+28 11 51.353	1251.130	0.000	0.000	
Measured Latitude		Measured Longitude		Measured Elevation		
-25 40 51.174		+28 11 51.390		1251.130		
Delta Latitude	Delta Longitude	Delta Elevation	Mensuration Error			
0.334	1.039	0.000	0.000			
Individual HE			Individual VE			
1.091			0.000			



ID	T&E Latitude	T&E Longitude	T&E Elevation	T&E CE90	T&E LE90
4	-25 40 48.373	+28 14 43.374	1283.270	0.000	0.000
T&E Description					
Measured Latitude		Measured Longitude		Measured Elevation	
-25 40 48.364		+28 14 43.405		1283.270	
Delta Latitude	Delta Longitude	Delta Elevation	Mensuration Error		
0.277	0.863	0.000	0.000		
Individual HE			Individual VE		
0.906			0.000		
ID	T&E Latitude	T&E Longitude	T&E Elevation	T&E CE90	T&E LE90
5	-25 40 58.441	+28 17 44.854	1268.350	0.000	0.000
T&E Description					
Measured Latitude		Measured Longitude		Measured Elevation	
-25 40 58.434		+28 17 44.881		1268.350	
Delta Latitude	Delta Longitude	Delta Elevation	Mensuration Error		
0.229	0.746	0.000	0.000		
Individual HE			Individual VE		
0.780			0.000		
ID	T&E Latitude	T&E Longitude	T&E Elevation	T&E CE90	T&E LE90
6	-25 43 20.146	+28 06 12.816	1319.670	0.000	0.000
T&E Description					
Measured Latitude		Measured Longitude		Measured Elevation	
-25 43 20.136		+28 06 12.840		1319.670	
Delta Latitude	Delta Longitude	Delta Elevation	Mensuration Error		
0.309	0.670	0.000	0.000		
Individual HE			Individual VE		
0.738			0.000		
ID	T&E Latitude	T&E Longitude	T&E Elevation	T&E CE90	T&E LE90
7	-25 43 28.495	+28 08 51.254	1315.200	0.000	0.000
T&E Description					
Measured Latitude		Measured Longitude		Measured Elevation	
-25 43 28.480		+28 08 51.275		1315.200	
Delta Latitude	Delta Longitude	Delta Elevation	Mensuration Error		
0.443	0.587	0.000	0.000		
Individual HE			Individual VE		
0.735			0.000		



ID	T&E Latitude	T&E Longitude	T&E Elevation	T&E CE90	T&E LE90
8	-25 43 30.456	+28 11 45.362	1303.450	0.000	0.000
T&E Description					
Measured Latitude		Measured Longitude		Measured Elevation	
-25 43 30.427		+28 11 45.354		1303.450	
Delta Latitude	Delta Longitude	Delta Elevation	Mensuration Error		
0.895	-0.238	0.000	0.000		
Individual HE			Individual VE		
0.926			0.000		
ID	T&E Latitude	T&E Longitude	T&E Elevation	T&E CE90	T&E LE90
9	-25 43 30.035	+28 14 52.315	1380.200	0.000	0.000
T&E Description					
Measured Latitude		Measured Longitude		Measured Elevation	
-25 43 30.032		+28 14 52.339		1380.200	
Delta Latitude	Delta Longitude	Delta Elevation	Mensuration Error		
0.075	0.666	0.000	0.000		
Individual HE			Individual VE		
0.670			0.000		
ID	T&E Latitude	T&E Longitude	T&E Elevation	T&E CE90	T&E LE90
10	-25 43 18.712	+28 17 37.661	1326.500	0.000	0.000
T&E Description					
Measured Latitude		Measured Longitude		Measured Elevation	
-25 43 18.698		+28 17 37.680		1326.500	
Delta Latitude	Delta Longitude	Delta Elevation	Mensuration Error		
0.437	0.509	0.000	0.000		
Individual HE			Individual VE		
0.671			0.000		
ID	T&E Latitude	T&E Longitude	T&E Elevation	T&E CE90	T&E LE90
11	-25 46 25.942	+28 06 4.674	1417.430	0.000	0.000
T&E Description					
Measured Latitude		Measured Longitude		Measured Elevation	
-25 46 25.972		+28 06 4.621		1417.430	
Delta Latitude	Delta Longitude	Delta Elevation	Mensuration Error		
-0.926	-1.453	0.000	0.000		
Individual HE			Individual VE		
1.723			0.000		



ID	T&E Latitude	T&E Longitude	T&E Elevation	T&E CE90	T&E LE90
12	-25 46 16.305	+28 08 48.334	1402.000	0.000	0.000
T&E Description					
Measured Latitude		Measured Longitude		Measured Elevation	
-25 46 16.333		+28 08 48.335		1402.000	
Delta Latitude	Delta Longitude	Delta Elevation	Mensuration Error		
-0.870	0.009	0.000	0.000		
Individual HE			Individual VE		
0.870			0.000		
ID	T&E Latitude	T&E Longitude	T&E Elevation	T&E CE90	T&E LE90
13	-25 46 18.155	+28 12 7.352	1355.070	0.000	0.000
T&E Description					
Measured Latitude		Measured Longitude		Measured Elevation	
-25 46 18.134		+28 12 7.372		1355.070	
Delta Latitude	Delta Longitude	Delta Elevation	Mensuration Error		
0.637	0.581	0.000	0.000		
Individual HE			Individual VE		
0.862			0.000		
ID	T&E Latitude	T&E Longitude	T&E Elevation	T&E CE90	T&E LE90
14	-25 46 6.549	+28 14 54.009	1400.290	0.000	0.000
T&E Description					
Measured Latitude		Measured Longitude		Measured Elevation	
-25 46 6.539		+28 14 54.036		1400.290	
Delta Latitude	Delta Longitude	Delta Elevation	Mensuration Error		
0.308	0.768	0.000	0.000		
Individual HE			Individual VE		
0.827			0.000		
ID	T&E Latitude	T&E Longitude	T&E Elevation	T&E CE90	T&E LE90
15	-25 46 5.504	+28 17 41.246	1398.000	0.000	0.000
T&E Description					
Measured Latitude		Measured Longitude		Measured Elevation	
-25 46 5.474		+28 17 41.297		1398.000	
Delta Latitude	Delta Longitude	Delta Elevation	Mensuration Error		
0.939	1.403	0.000	0.000		
Individual HE			Individual VE		
1.689			0.000		



ID	T&E Latitude	T&E Longitude	T&E Elevation	T&E CE90	T&E LE90
16	-25 48 36.146	+28 05 53.281	1438.200	0.000	0.000
T&E Description					
Measured Latitude		Measured Longitude		Measured Elevation	
-25 48 36.135		+28 05 53.302		1438.200	
Delta Latitude	Delta Longitude	Delta Elevation	Mensuration Error		
0.341	0.564	0.000	0.000		
Individual HE			Individual VE		
0.660			0.000		
ID	T&E Latitude	T&E Longitude	T&E Elevation	T&E CE90	T&E LE90
17	-25 48 43.856	+28 09 4.106	1444.000	0.000	0.000
T&E Description					
Measured Latitude		Measured Longitude		Measured Elevation	
-25 48 43.836		+28 09 4.147		1444.000	
Delta Latitude	Delta Longitude	Delta Elevation	Mensuration Error		
0.600	1.150	0.000	0.000		
Individual HE			Individual VE		
1.297			0.000		
ID	T&E Latitude	T&E Longitude	T&E Elevation	T&E CE90	T&E LE90
18	-25 48 37.225	+28 11 54.324	1454.620	0.000	0.000
T&E Description					
Measured Latitude		Measured Longitude		Measured Elevation	
-25 48 37.183		+28 11 54.342		1454.620	
Delta Latitude	Delta Longitude	Delta Elevation	Mensuration Error		
1.298	0.512	0.000	0.000		
Individual HE			Individual VE		
1.395			0.000		
ID	T&E Latitude	T&E Longitude	T&E Elevation	T&E CE90	T&E LE90
19	-25 48 43.528	+28 15 0.374	1559.960	0.000	0.000
T&E Description					
Measured Latitude		Measured Longitude		Measured Elevation	
-25 48 43.510		+28 15 0.416		1559.960	
Delta Latitude	Delta Longitude	Delta Elevation	Mensuration Error		
0.566	1.145	0.000	0.000		
Individual HE			Individual VE		
1.277			0.000		



ID	T&E Latitude	T&E Longitude	T&E Elevation	T&E CE90	T&E LE90
20	-25 48 42.925	+28 17 44.555	1446.500	0.000	0.000
T&E Description					
Measured Latitude		Measured Longitude		Measured Elevation	
-25 48 42.910		+28 17 44.607		1446.500	
Delta Latitude	Delta Longitude	Delta Elevation	Mensuration Error		
0.478	1.460	0.000	0.000		
Individual HE			Individual VE		
1.536			0.000		
ID	T&E Latitude	T&E Longitude	T&E Elevation	T&E CE90	T&E LE90
21	-25 51 12.497	+28 05 50.230	1428.110	0.000	0.000
T&E Description					
Measured Latitude		Measured Longitude		Measured Elevation	
-25 51 12.507		+28 05 50.234		1428.110	
Delta Latitude	Delta Longitude	Delta Elevation	Mensuration Error		
-0.289	0.105	0.000	0.000		
Individual HE			Individual VE		
0.308			0.000		
ID	T&E Latitude	T&E Longitude	T&E Elevation	T&E CE90	T&E LE90
22	-25 51 11.691	+28 09 1.772	1476.530	0.000	0.000
T&E Description					
Measured Latitude		Measured Longitude		Measured Elevation	
-25 51 11.696		+28 09 1.814		1476.530	
Delta Latitude	Delta Longitude	Delta Elevation	Mensuration Error		
-0.169	1.158	0.000	0.000		
Individual HE			Individual VE		
1.170			0.000		
ID	T&E Latitude	T&E Longitude	T&E Elevation	T&E CE90	T&E LE90
23	-25 51 14.426	+28 11 49.629	1440.470	0.000	0.000
T&E Description					
Measured Latitude		Measured Longitude		Measured Elevation	
-25 51 14.411		+28 11 49.658		1440.470	
Delta Latitude	Delta Longitude	Delta Elevation	Mensuration Error		
0.474	0.808	0.000	0.000		
Individual HE			Individual VE		
0.937			0.000		

ID	T&E Latitude	T&E Longitude	T&E Elevation	T&E CE90	T&E LE90
24	-25 51 10.328	+28 15 5.543	1514.100	0.000	0.000
T&E Description					
Measured Latitude		Measured Longitude		Measured Elevation	
-25 51 10.307		+28 15 5.613		1514.100	
Delta Latitude	Delta Longitude	Delta Elevation	Mensuration Error		
0.658	1.954	0.000	0.000		
Individual HE				Individual VE	
2.062				0.000	
ID	T&E Latitude	T&E Longitude	T&E Elevation	T&E CE90	T&E LE90
25	-25 51 11.253	+28 17 35.862	1507.580	0.000	0.000
T&E Description					
Measured Latitude		Measured Longitude		Measured Elevation	
-25 51 11.253		+28 17 35.895		1507.580	
Delta Latitude	Delta Longitude	Delta Elevation	Mensuration Error		
0.023	0.923	0.000	0.000		
Individual HE				Individual VE	
0.923				0.000	

APPENDIX L: MAA REPORT FOR STAGE 1 – EXPERIMENT 2(c) (ORTHO-IMAGE USING 13 GCPS AND THE 2 M DTM)

MAA Report for 13gcps_2mdtm_ortho						
Distance values are in meters						
Mean latitude error: 0.014387						
Mean longitude error: -0.131851						
Mean horizontal error (average HE): 0.592703						
Standard deviation latitude error: 0.628287						
Standard deviation longitude error: 0.395205						
Standard deviation horizontal error: 0.466076						
90% Circular Error (against T&E): 1.191322						
90% Circular Error (T&E and mensuration error included): 1.191322						
ID	T&E Latitude	T&E Longitude	T&E Elevation	T&E CE90	T&E LE90	
1	-25 40 48.898	+28 05 58.648	1378.640	0.000	0.000	
						T&E Description
						CP #1
Measured Latitude		Measured Longitude		Measured Elevation		
-25 40 48.892		+28 05 58.636		1378.640		
Delta Latitude	Delta Longitude	Delta Elevation	Mensuration Error			
0.173	-0.352	0.000	0.000			
Individual HE			Individual VE			
0.392			0.000			
ID	T&E Latitude	T&E Longitude	T&E Elevation	T&E CE90	T&E LE90	
2	-25 40 53.691	+28 08 43.169	1302.820	0.000	0.000	
						T&E Description
						CP #2
Measured Latitude		Measured Longitude		Measured Elevation		
-25 40 53.703		+28 08 43.157		1302.820		
Delta Latitude	Delta Longitude	Delta Elevation	Mensuration Error			
-0.372	-0.336	0.000	0.000			
Individual HE			Individual VE			
0.501			0.000			
ID	T&E Latitude	T&E Longitude	T&E Elevation	T&E CE90	T&E LE90	
3	-25 40 51.185	+28 11 51.353	1251.130	0.000	0.000	
						T&E Description
						CP #3
Measured Latitude		Measured Longitude		Measured Elevation		
-25 40 51.190		+28 11 51.347		1251.130		
Delta Latitude	Delta Longitude	Delta Elevation	Mensuration Error			
-0.180	-0.151	0.000	0.000			
Individual HE			Individual VE			
0.235			0.000			

ID	T&E Latitude	T&E Longitude	T&E Elevation	T&E CE90	T&E LE90
4	-25 40 48.373	+28 14 43.374	1283.270	0.000	0.000
					T&E Description
					CP #4
Measured Latitude		Measured Longitude		Measured Elevation	
-25 40 48.379		+28 14 43.373		1283.270	
Delta Latitude	Delta Longitude	Delta Elevation	Mensuration Error		
-0.160	-0.024	0.000	0.000		
Individual HE			Individual VE		
0.162			0.000		
ID	T&E Latitude	T&E Longitude	T&E Elevation	T&E CE90	T&E LE90
5	-25 40 58.441	+28 17 44.854	1268.350	0.000	0.000
					T&E Description
					CP #5
Measured Latitude		Measured Longitude		Measured Elevation	
-25 40 58.428		+28 17 44.849		1268.350	
Delta Latitude	Delta Longitude	Delta Elevation	Mensuration Error		
0.388	-0.154	0.000	0.000		
Individual HE			Individual VE		
0.417			0.000		
ID	T&E Latitude	T&E Longitude	T&E Elevation	T&E CE90	T&E LE90
6	-25 43 20.146	+28 06 12.816	1319.670	0.000	0.000
					T&E Description
					CP #6
Measured Latitude		Measured Longitude		Measured Elevation	
-25 43 20.147		+28 06 12.803		1319.670	
Delta Latitude	Delta Longitude	Delta Elevation	Mensuration Error		
-0.022	-0.363	0.000	0.000		
Individual HE			Individual VE		
0.363			0.000		
ID	T&E Latitude	T&E Longitude	T&E Elevation	T&E CE90	T&E LE90
7	-25 43 28.495	+28 08 51.254	1315.200	0.000	0.000
					T&E Description
					CP #7
Measured Latitude		Measured Longitude		Measured Elevation	
-25 43 28.500		+28 08 51.244		1315.200	
Delta Latitude	Delta Longitude	Delta Elevation	Mensuration Error		
-0.174	-0.260	0.000	0.000		
Individual HE			Individual VE		
0.313			0.000		

ID	T&E Latitude	T&E Longitude	T&E Elevation	T&E CE90	T&E LE90
8	-25 43 30.456	+28 11 45.362	1303.450	0.000	0.000
					T&E Description
					CP #8
Measured Latitude		Measured Longitude		Measured Elevation	
-25 43 30.439		+28 11 45.327		1303.450	
Delta Latitude	Delta Longitude	Delta Elevation	Mensuration Error		
0.533	-0.965	0.000	0.000		
Individual HE				Individual VE	
1.103				0.000	
ID	T&E Latitude	T&E Longitude	T&E Elevation	T&E CE90	T&E LE90
9	-25 43 30.035	+28 14 52.315	1380.200	0.000	0.000
					T&E Description
					CP #9
Measured Latitude		Measured Longitude		Measured Elevation	
-25 43 30.027		+28 14 52.308		1380.200	
Delta Latitude	Delta Longitude	Delta Elevation	Mensuration Error		
0.241	-0.169	0.000	0.000		
Individual HE				Individual VE	
0.295				0.000	
ID	T&E Latitude	T&E Longitude	T&E Elevation	T&E CE90	T&E LE90
10	-25 43 18.712	+28 17 37.661	1326.500	0.000	0.000
					T&E Description
					CP #10
Measured Latitude		Measured Longitude		Measured Elevation	
-25 43 18.672		+28 17 37.644		1326.500	
Delta Latitude	Delta Longitude	Delta Elevation	Mensuration Error		
1.251	-0.479	0.000	0.000		
Individual HE				Individual VE	
1.340				0.000	
ID	T&E Latitude	T&E Longitude	T&E Elevation	T&E CE90	T&E LE90
11	-25 46 25.942	+28 06 4.674	1417.430	0.000	0.000
					T&E Description
					CP #11
Measured Latitude		Measured Longitude		Measured Elevation	
-25 46 25.998		+28 06 4.690		1417.430	
Delta Latitude	Delta Longitude	Delta Elevation	Mensuration Error		
-1.754	0.443	0.000	0.000		
Individual HE				Individual VE	
1.809				0.000	

ID	T&E Latitude	T&E Longitude	T&E Elevation	T&E CE90	T&E LE90
12	-25 46 16.305	+28 08 48.334	1402.000	0.000	0.000
T&E Description					
CP #12					
Measured Latitude		Measured Longitude		Measured Elevation	
-25 46 16.340		+28 08 48.310		1402.000	
Delta Latitude	Delta Longitude	Delta Elevation	Mensuration Error		
-1.091	-0.681	0.000	0.000		
Individual HE			Individual VE		
1.287			0.000		
ID	T&E Latitude	T&E Longitude	T&E Elevation	T&E CE90	T&E LE90
13	-25 46 18.155	+28 12 7.352	1355.070	0.000	0.000
T&E Description					
CP #13					
Measured Latitude		Measured Longitude		Measured Elevation	
-25 46 18.150		+28 12 7.342		1355.070	
Delta Latitude	Delta Longitude	Delta Elevation	Mensuration Error		
0.138	-0.259	0.000	0.000		
Individual HE			Individual VE		
0.294			0.000		
ID	T&E Latitude	T&E Longitude	T&E Elevation	T&E CE90	T&E LE90
14	-25 46 6.549	+28 14 54.009	1400.290	0.000	0.000
T&E Description					
CP #14					
Measured Latitude		Measured Longitude		Measured Elevation	
-25 46 6.547		+28 14 54.007		1400.290	
Delta Latitude	Delta Longitude	Delta Elevation	Mensuration Error		
0.053	-0.043	0.000	0.000		
Individual HE			Individual VE		
0.068			0.000		
ID	T&E Latitude	T&E Longitude	T&E Elevation	T&E CE90	T&E LE90
15	-25 46 5.504	+28 17 41.246	1398.000	0.000	0.000
T&E Description					
CP #15					
Measured Latitude		Measured Longitude		Measured Elevation	
-25 46 5.501		+28 17 41.246		1398.000	
Delta Latitude	Delta Longitude	Delta Elevation	Mensuration Error		
0.098	-0.000	0.000	0.000		
Individual HE			Individual VE		
0.098			0.000		

ID	T&E Latitude	T&E Longitude	T&E Elevation	T&E CE90	T&E LE90
16	-25 48 36.146	+28 05 53.281	1438.200	0.000	0.000
					T&E Description
					CP #16
Measured Latitude		Measured Longitude		Measured Elevation	
-25 48 36.140		+28 05 53.284		1438.200	
Delta Latitude	Delta Longitude	Delta Elevation	Mensuration Error		
0.183	0.071	0.000	0.000		
Individual HE			Individual VE		
0.197			0.000		
ID	T&E Latitude	T&E Longitude	T&E Elevation	T&E CE90	T&E LE90
17	-25 48 43.856	+28 09 4.106	1444.000	0.000	0.000
					T&E Description
					CP #17
Measured Latitude		Measured Longitude		Measured Elevation	
-25 48 43.839		+28 09 4.108		1444.000	
Delta Latitude	Delta Longitude	Delta Elevation	Mensuration Error		
0.508	0.044	0.000	0.000		
Individual HE			Individual VE		
0.510			0.000		
ID	T&E Latitude	T&E Longitude	T&E Elevation	T&E CE90	T&E LE90
18	-25 48 37.225	+28 11 54.324	1454.620	0.000	0.000
					T&E Description
					CP #18
Measured Latitude		Measured Longitude		Measured Elevation	
-25 48 37.219		+28 11 54.366		1454.620	
Delta Latitude	Delta Longitude	Delta Elevation	Mensuration Error		
0.182	1.177	0.000	0.000		
Individual HE			Individual VE		
1.190			0.000		
ID	T&E Latitude	T&E Longitude	T&E Elevation	T&E CE90	T&E LE90
19	-25 48 43.528	+28 15 0.374	1559.960	0.000	0.000
					T&E Description
					CP #19
Measured Latitude		Measured Longitude		Measured Elevation	
-25 48 43.514		+28 15 0.369		1559.960	
Delta Latitude	Delta Longitude	Delta Elevation	Mensuration Error		
0.435	-0.148	0.000	0.000		
Individual HE			Individual VE		
0.459			0.000		

ID	T&E Latitude	T&E Longitude	T&E Elevation	T&E CE90	T&E LE90
20	-25 48 42.925	+28 17 44.555	1446.500	0.000	0.000
					T&E Description
					CP #20
Measured Latitude		Measured Longitude		Measured Elevation	
-25 48 42.931		+28 17 44.556		1446.500	
Delta Latitude	Delta Longitude	Delta Elevation	Mensuration Error		
-0.187	0.037	0.000	0.000		
Individual HE			Individual VE		
0.191			0.000		
ID	T&E Latitude	T&E Longitude	T&E Elevation	T&E CE90	T&E LE90
21	-25 51 12.497	+28 05 50.230	1428.110	0.000	0.000
					T&E Description
					CP #21
Measured Latitude		Measured Longitude		Measured Elevation	
-25 51 12.506		+28 05 50.215		1428.110	
Delta Latitude	Delta Longitude	Delta Elevation	Mensuration Error		
-0.254	-0.425	0.000	0.000		
Individual HE			Individual VE		
0.495			0.000		
ID	T&E Latitude	T&E Longitude	T&E Elevation	T&E CE90	T&E LE90
22	-25 51 11.691	+28 09 1.772	1476.530	0.000	0.000
					T&E Description
					CP #22
Measured Latitude		Measured Longitude		Measured Elevation	
-25 51 11.699		+28 09 1.774		1476.530	
Delta Latitude	Delta Longitude	Delta Elevation	Mensuration Error		
-0.260	0.059	0.000	0.000		
Individual HE			Individual VE		
0.267			0.000		
ID	T&E Latitude	T&E Longitude	T&E Elevation	T&E CE90	T&E LE90
23	-25 51 14.426	+28 11 49.629	1440.470	0.000	0.000
					T&E Description
					CP #23
Measured Latitude		Measured Longitude		Measured Elevation	
-25 51 14.409		+28 11 49.631		1440.470	
Delta Latitude	Delta Longitude	Delta Elevation	Mensuration Error		
0.537	0.056	0.000	0.000		
Individual HE			Individual VE		
0.540			0.000		

ID	T&E Latitude	T&E Longitude	T&E Elevation	T&E CE90	T&E LE90
24	-25 51 10.328	+28 15 5.543	1514.100	0.000	0.000
					T&E Description
					CP #24
Measured Latitude		Measured Longitude		Measured Elevation	
-25 51 10.292		+28 15 5.549		1514.100	
Delta Latitude	Delta Longitude	Delta Elevation	Mensuration Error		
1.116	0.177	0.000	0.000		
Individual HE				Individual VE	
1.130				0.000	
ID	T&E Latitude	T&E Longitude	T&E Elevation	T&E CE90	T&E LE90
25	-25 51 11.253	+28 17 35.862	1507.580	0.000	0.000
					T&E Description
					CP #25
Measured Latitude		Measured Longitude		Measured Elevation	
-25 51 11.287		+28 17 35.842		1507.580	
Delta Latitude	Delta Longitude	Delta Elevation	Mensuration Error		
-1.022	-0.550	0.000	0.000		
Individual HE				Individual VE	
1.161				0.000	



APPENDIX M: MAA REPORT FOR STAGE 1 – EXPERIMENT 3(a) (ORTHO-IMAGE USING 25 GCPS AND THE 30 M SRTM DEM)

MAA Report for 25gcps_srtmdem_ortho						
Distance values are in meters						
Mean latitude error: 0.042255						
Mean longitude error: 0.035083						
Mean horizontal error (average HE): 0.582111						
Standard deviation latitude error: 0.571638						
Standard deviation longitude error: 0.433321						
Standard deviation horizontal error: 0.422729						
90% Circular Error (against T&E): 1.123205						
90% Circular Error (T&E and mensuration error included): 1.123205						

ID	T&E Latitude	T&E Longitude	T&E Elevation	T&E CE90	T&E LE90	
1	-25 40 48.898	+28 05 58.648	1378.640	0.000	0.000	
						T&E Description
						CP #1

Measured Latitude		Measured Longitude		Measured Elevation		
-25 40 48.895		+28 05 58.650		1378.640		

Delta Latitude	Delta Longitude	Delta Elevation	Mensuration Error			
0.102	0.038	0.000	0.000			

Individual HE			Individual VE			
0.108			0.000			

ID	T&E Latitude	T&E Longitude	T&E Elevation	T&E CE90	T&E LE90	
2	-25 40 53.691	+28 08 43.169	1302.820	0.000	0.000	
						T&E Description
						CP #2

Measured Latitude		Measured Longitude		Measured Elevation		
-25 40 53.706		+28 08 43.170		1302.820		

Delta Latitude	Delta Longitude	Delta Elevation	Mensuration Error			
-0.471	0.027	0.000	0.000			

Individual HE			Individual VE			
0.472			0.000			

ID	T&E Latitude	T&E Longitude	T&E Elevation	T&E CE90	T&E LE90	
3	-25 40 51.185	+28 11 51.353	1251.130	0.000	0.000	
						T&E Description
						CP #3

Measured Latitude		Measured Longitude		Measured Elevation		
-25 40 51.194		+28 11 51.361		1251.130		

Delta Latitude	Delta Longitude	Delta Elevation	Mensuration Error			
-0.294	0.217	0.000	0.000			

Individual HE			Individual VE			
0.365			0.000			



ID	T&E Latitude	T&E Longitude	T&E Elevation	T&E CE90	T&E LE90
4	-25 40 48.373	+28 14 43.374	1283.270	0.000	0.000
					T&E Description
					CP #4
Measured Latitude		Measured Longitude		Measured Elevation	
-25 40 48.380		+28 14 43.385		1283.270	
Delta Latitude	Delta Longitude	Delta Elevation	Mensuration Error		
-0.219	0.315	0.000	0.000		
Individual HE			Individual VE		
0.384			0.000		
ID	T&E Latitude	T&E Longitude	T&E Elevation	T&E CE90	T&E LE90
5	-25 40 58.441	+28 17 44.854	1268.350	0.000	0.000
					T&E Description
					CP #5
Measured Latitude		Measured Longitude		Measured Elevation	
-25 40 58.448		+28 17 44.860		1268.350	
Delta Latitude	Delta Longitude	Delta Elevation	Mensuration Error		
-0.216	0.166	0.000	0.000		
Individual HE			Individual VE		
0.273			0.000		
ID	T&E Latitude	T&E Longitude	T&E Elevation	T&E CE90	T&E LE90
6	-25 43 20.146	+28 06 12.816	1319.670	0.000	0.000
					T&E Description
					CP #6
Measured Latitude		Measured Longitude		Measured Elevation	
-25 43 20.150		+28 06 12.816		1319.670	
Delta Latitude	Delta Longitude	Delta Elevation	Mensuration Error		
-0.124	0.003	0.000	0.000		
Individual HE			Individual VE		
0.124			0.000		
ID	T&E Latitude	T&E Longitude	T&E Elevation	T&E CE90	T&E LE90
7	-25 43 28.495	+28 08 51.254	1315.200	0.000	0.000
					T&E Description
					CP #7
Measured Latitude		Measured Longitude		Measured Elevation	
-25 43 28.503		+28 08 51.240		1315.200	
Delta Latitude	Delta Longitude	Delta Elevation	Mensuration Error		
-0.251	-0.384	0.000	0.000		
Individual HE			Individual VE		
0.459			0.000		



ID	T&E Latitude	T&E Longitude	T&E Elevation	T&E CE90	T&E LE90
8	-25 43 30.456	+28 11 45.362	1303.450	0.000	0.000
T&E Description CP #8					
Measured Latitude		Measured Longitude		Measured Elevation	
-25 43 30.441		+28 11 45.323		1303.450	
Delta Latitude	Delta Longitude	Delta Elevation	Mensuration Error		
0.475	-1.094	0.000	0.000		
Individual HE				Individual VE	
1.193				0.000	
ID	T&E Latitude	T&E Longitude	T&E Elevation	T&E CE90	T&E LE90
9	-25 43 30.035	+28 14 52.315	1380.200	0.000	0.000
T&E Description CP #9					
Measured Latitude		Measured Longitude		Measured Elevation	
-25 43 30.047		+28 14 52.321		1380.200	
Delta Latitude	Delta Longitude	Delta Elevation	Mensuration Error		
-0.385	0.175	0.000	0.000		
Individual HE				Individual VE	
0.423				0.000	
ID	T&E Latitude	T&E Longitude	T&E Elevation	T&E CE90	T&E LE90
10	-25 43 18.712	+28 17 37.661	1326.500	0.000	0.000
T&E Description CP #10					
Measured Latitude		Measured Longitude		Measured Elevation	
-25 43 18.658		+28 17 37.639		1326.500	
Delta Latitude	Delta Longitude	Delta Elevation	Mensuration Error		
1.673	-0.605	0.000	0.000		
Individual HE				Individual VE	
1.779				0.000	
ID	T&E Latitude	T&E Longitude	T&E Elevation	T&E CE90	T&E LE90
11	-25 46 25.942	+28 06 4.674	1417.430	0.000	0.000
T&E Description CP #11					
Measured Latitude		Measured Longitude		Measured Elevation	
-25 46 25.964		+28 06 4.686		1417.430	
Delta Latitude	Delta Longitude	Delta Elevation	Mensuration Error		
-0.683	0.352	0.000	0.000		
Individual HE				Individual VE	
0.768				0.000	



ID	T&E Latitude	T&E Longitude	T&E Elevation	T&E CE90	T&E LE90
12	-25 46 16.305	+28 08 48.334	1402.000	0.000	0.000
					T&E Description
					CP #12
Measured Latitude		Measured Longitude		Measured Elevation	
-25 46 16.309		+28 08 48.342		1402.000	
Delta Latitude	Delta Longitude	Delta Elevation	Mensuration Error		
-0.116	0.206	0.000	0.000		
Individual HE			Individual VE		
0.236			0.000		
ID	T&E Latitude	T&E Longitude	T&E Elevation	T&E CE90	T&E LE90
13	-25 46 18.155	+28 12 7.352	1355.070	0.000	0.000
					T&E Description
					CP #13
Measured Latitude		Measured Longitude		Measured Elevation	
-25 46 18.151		+28 12 7.353		1355.070	
Delta Latitude	Delta Longitude	Delta Elevation	Mensuration Error		
0.101	0.042	0.000	0.000		
Individual HE			Individual VE		
0.109			0.000		
ID	T&E Latitude	T&E Longitude	T&E Elevation	T&E CE90	T&E LE90
14	-25 46 6.549	+28 14 54.009	1400.290	0.000	0.000
					T&E Description
					CP #14
Measured Latitude		Measured Longitude		Measured Elevation	
-25 46 6.549		+28 14 54.019		1400.290	
Delta Latitude	Delta Longitude	Delta Elevation	Mensuration Error		
0.004	0.281	0.000	0.000		
Individual HE			Individual VE		
0.281			0.000		
ID	T&E Latitude	T&E Longitude	T&E Elevation	T&E CE90	T&E LE90
15	-25 46 5.504	+28 17 41.246	1398.000	0.000	0.000
					T&E Description
					CP #15
Measured Latitude		Measured Longitude		Measured Elevation	
-25 46 5.503		+28 17 41.258		1398.000	
Delta Latitude	Delta Longitude	Delta Elevation	Mensuration Error		
0.032	0.332	0.000	0.000		
Individual HE			Individual VE		
0.334			0.000		



ID	T&E Latitude	T&E Longitude	T&E Elevation	T&E CE90	T&E LE90
16	-25 48 36.146	+28 05 53.281	1438.200	0.000	0.000
					T&E Description CP #16
Measured Latitude		Measured Longitude		Measured Elevation	
-25 48 36.139		+28 05 53.281		1438.200	
Delta Latitude	Delta Longitude	Delta Elevation	Mensuration Error		
0.205	-0.012	0.000	0.000		
Individual HE			Individual VE		
0.206			0.000		
ID	T&E Latitude	T&E Longitude	T&E Elevation	T&E CE90	T&E LE90
17	-25 48 43.856	+28 09 4.106	1444.000	0.000	0.000
					T&E Description CP #17
Measured Latitude		Measured Longitude		Measured Elevation	
-25 48 43.825		+28 09 4.121		1444.000	
Delta Latitude	Delta Longitude	Delta Elevation	Mensuration Error		
0.959	0.419	0.000	0.000		
Individual HE			Individual VE		
1.046			0.000		
ID	T&E Latitude	T&E Longitude	T&E Elevation	T&E CE90	T&E LE90
18	-25 48 37.225	+28 11 54.324	1454.620	0.000	0.000
					T&E Description CP #18
Measured Latitude		Measured Longitude		Measured Elevation	
-25 48 37.238		+28 11 54.361		1454.620	
Delta Latitude	Delta Longitude	Delta Elevation	Mensuration Error		
-0.400	1.044	0.000	0.000		
Individual HE			Individual VE		
1.118			0.000		
ID	T&E Latitude	T&E Longitude	T&E Elevation	T&E CE90	T&E LE90
19	-25 48 43.528	+28 15 0.374	1559.960	0.000	0.000
					T&E Description CP #19
Measured Latitude		Measured Longitude		Measured Elevation	
-25 48 43.533		+28 15 0.382		1559.960	
Delta Latitude	Delta Longitude	Delta Elevation	Mensuration Error		
-0.137	0.210	0.000	0.000		
Individual HE			Individual VE		
0.251			0.000		



ID	T&E Latitude	T&E Longitude	T&E Elevation	T&E CE90	T&E LE90
20	-25 48 42.925	+28 17 44.555	1446.500	0.000	0.000
					T&E Description
					CP #20
Measured Latitude		Measured Longitude		Measured Elevation	
-25 48 42.932		+28 17 44.568		1446.500	
Delta Latitude	Delta Longitude	Delta Elevation	Mensuration Error		
-0.208	0.385	0.000	0.000		
Individual HE			Individual VE		
0.437			0.000		
ID	T&E Latitude	T&E Longitude	T&E Elevation	T&E CE90	T&E LE90
21	-25 51 12.497	+28 05 50.230	1428.110	0.000	0.000
					T&E Description
					CP #21
Measured Latitude		Measured Longitude		Measured Elevation	
-25 51 12.489		+28 05 50.211		1428.110	
Delta Latitude	Delta Longitude	Delta Elevation	Mensuration Error		
0.249	-0.535	0.000	0.000		
Individual HE			Individual VE		
0.590			0.000		
ID	T&E Latitude	T&E Longitude	T&E Elevation	T&E CE90	T&E LE90
22	-25 51 11.691	+28 09 1.772	1476.530	0.000	0.000
					T&E Description
					CP #22
Measured Latitude		Measured Longitude		Measured Elevation	
-25 51 11.665		+28 09 1.788		1476.530	
Delta Latitude	Delta Longitude	Delta Elevation	Mensuration Error		
0.788	0.448	0.000	0.000		
Individual HE			Individual VE		
0.907			0.000		
ID	T&E Latitude	T&E Longitude	T&E Elevation	T&E CE90	T&E LE90
23	-25 51 14.426	+28 11 49.629	1440.470	0.000	0.000
					T&E Description
					CP #23
Measured Latitude		Measured Longitude		Measured Elevation	
-25 51 14.393		+28 11 49.610		1440.470	
Delta Latitude	Delta Longitude	Delta Elevation	Mensuration Error		
1.021	-0.514	0.000	0.000		
Individual HE			Individual VE		
1.143			0.000		



ID	T&E Latitude	T&E Longitude	T&E Elevation	T&E CE90	T&E LE90
24	-25 51 10.328	+28 15 5.543	1514.100	0.000	0.000
					T&E Description
					CP #24
Measured Latitude		Measured Longitude		Measured Elevation	
-25 51 10.328		+28 15 5.527		1514.100	
Delta Latitude	Delta Longitude	Delta Elevation	Mensuration Error		
0.023	-0.461	0.000	0.000		
Individual HE				Individual VE	
0.461				0.000	
ID	T&E Latitude	T&E Longitude	T&E Elevation	T&E CE90	T&E LE90
25	-25 51 11.253	+28 17 35.862	1507.580	0.000	0.000
					T&E Description
					CP #25
Measured Latitude		Measured Longitude		Measured Elevation	
-25 51 11.288		+28 17 35.856		1507.580	
Delta Latitude	Delta Longitude	Delta Elevation	Mensuration Error		
-1.072	-0.175	0.000	0.000		
Individual HE				Individual VE	
1.086				0.000	



APPENDIX N: MAA REPORT FOR STAGE 1 – EXPERIMENT 3(b) (ORTHO-IMAGE USING 25 GCPS AND THE 12 M DTM)

MAA Report for exp02b_25gcps_12mdtm_ortho						
Distance values are in meters						
Mean latitude error: -0.089833						
Mean longitude error: 0.031818						
Mean horizontal error (average HE): 0.450608						
Standard deviation latitude error: 0.345872						
Standard deviation longitude error: 0.416749						
Standard deviation horizontal error: 0.315185						
90% Circular Error (against T&E): 0.854518						
90% Circular Error (T&E and mensuration error included): 0.854518						
ID	T&E Latitude	T&E Longitude	T&E Elevation	T&E CE90	T&E LE90	
1	-25 40 48.898	+28 05 58.648	1378.640	0.000	0.000	
						T&E Description
Measured Latitude	Measured Longitude	Measured Elevation				
-25 40 48.900	+28 05 58.648	1378.640				
Delta Latitude	Delta Longitude	Delta Elevation	Mensuration Error			
-0.066	0.003	0.000	0.000			
Individual HE			Individual VE			
0.066			0.000			
ID	T&E Latitude	T&E Longitude	T&E Elevation	T&E CE90	T&E LE90	
2	-25 40 53.691	+28 08 43.169	1302.820	0.000	0.000	
						T&E Description
Measured Latitude	Measured Longitude	Measured Elevation				
-25 40 53.711	+28 08 43.185	1302.820				
Delta Latitude	Delta Longitude	Delta Elevation	Mensuration Error			
-0.612	0.450	0.000	0.000			
Individual HE			Individual VE			
0.760			0.000			
ID	T&E Latitude	T&E Longitude	T&E Elevation	T&E CE90	T&E LE90	
3	-25 40 51.185	+28 11 51.353	1251.130	0.000	0.000	
						T&E Description
Measured Latitude	Measured Longitude	Measured Elevation				
-25 40 51.197	+28 11 51.359	1251.130				
Delta Latitude	Delta Longitude	Delta Elevation	Mensuration Error			
-0.390	0.175	0.000	0.000			
Individual HE			Individual VE			
0.427			0.000			



ID	T&E Latitude	T&E Longitude	T&E Elevation	T&E CE90	T&E LE90
4	-25 40 48.373	+28 14 43.374	1283.270	0.000	0.000
T&E Description					
Measured Latitude		Measured Longitude	Measured Elevation		
-25 40 48.383		+28 14 43.379	1283.270		
Delta Latitude	Delta Longitude	Delta Elevation	Mensuration Error		
-0.309	0.157	0.000	0.000		
Individual HE			Individual VE		
0.346			0.000		
ID	T&E Latitude	T&E Longitude	T&E Elevation	T&E CE90	T&E LE90
5	-25 40 58.441	+28 17 44.854	1268.350	0.000	0.000
T&E Description					
Measured Latitude		Measured Longitude	Measured Elevation		
-25 40 58.437		+28 17 44.857	1268.350		
Delta Latitude	Delta Longitude	Delta Elevation	Mensuration Error		
0.129	0.070	0.000	0.000		
Individual HE			Individual VE		
0.147			0.000		
ID	T&E Latitude	T&E Longitude	T&E Elevation	T&E CE90	T&E LE90
6	-25 43 20.146	+28 06 12.816	1319.670	0.000	0.000
T&E Description					
Measured Latitude		Measured Longitude	Measured Elevation		
-25 43 20.154		+28 06 12.814	1319.670		
Delta Latitude	Delta Longitude	Delta Elevation	Mensuration Error		
-0.244	-0.036	0.000	0.000		
Individual HE			Individual VE		
0.247			0.000		
ID	T&E Latitude	T&E Longitude	T&E Elevation	T&E CE90	T&E LE90
7	-25 43 28.495	+28 08 51.254	1315.200	0.000	0.000
T&E Description					
Measured Latitude		Measured Longitude	Measured Elevation		
-25 43 28.489		+28 08 51.257	1315.200		
Delta Latitude	Delta Longitude	Delta Elevation	Mensuration Error		
0.176	0.106	0.000	0.000		
Individual HE			Individual VE		
0.205			0.000		

ID	T&E Latitude	T&E Longitude	T&E Elevation	T&E CE90	T&E LE90
8	-25 43 30.456	+28 11 45.362	1303.450	0.000	0.000
T&E Description					
Measured Latitude		Measured Longitude		Measured Elevation	
-25 43 30.445		+28 11 45.321		1303.450	
Delta Latitude	Delta Longitude	Delta Elevation	Mensuration Error		
0.361	-1.150	0.000	0.000		
Individual HE				Individual VE	
1.205				0.000	
ID	T&E Latitude	T&E Longitude	T&E Elevation	T&E CE90	T&E LE90
9	-25 43 30.035	+28 14 52.315	1380.200	0.000	0.000
T&E Description					
Measured Latitude		Measured Longitude		Measured Elevation	
-25 43 30.035		+28 14 52.318		1380.200	
Delta Latitude	Delta Longitude	Delta Elevation	Mensuration Error		
-0.017	0.102	0.000	0.000		
Individual HE				Individual VE	
0.104				0.000	
ID	T&E Latitude	T&E Longitude	T&E Elevation	T&E CE90	T&E LE90
10	-25 43 18.712	+28 17 37.661	1326.500	0.000	0.000
T&E Description					
Measured Latitude		Measured Longitude		Measured Elevation	
-25 43 18.712		+28 17 37.669		1326.500	
Delta Latitude	Delta Longitude	Delta Elevation	Mensuration Error		
0.014	0.225	0.000	0.000		
Individual HE				Individual VE	
0.226				0.000	
ID	T&E Latitude	T&E Longitude	T&E Elevation	T&E CE90	T&E LE90
11	-25 46 25.942	+28 06 4.674	1417.430	0.000	0.000
T&E Description					
Measured Latitude		Measured Longitude		Measured Elevation	
-25 46 25.968		+28 06 4.633		1417.430	
Delta Latitude	Delta Longitude	Delta Elevation	Mensuration Error		
-0.813	-1.140	0.000	0.000		
Individual HE				Individual VE	
1.400				0.000	

ID	T&E Latitude	T&E Longitude	T&E Elevation	T&E CE90	T&E LE90
12	-25 46 16.305	+28 08 48.334	1402.000	0.000	0.000
T&E Description					
Measured Latitude		Measured Longitude		Measured Elevation	
-25 46 16.327		+28 08 48.340		1402.000	
Delta Latitude	Delta Longitude	Delta Elevation	Mensuration Error		
-0.697	0.167	0.000	0.000		
Individual HE			Individual VE		
0.716			0.000		
ID	T&E Latitude	T&E Longitude	T&E Elevation	T&E CE90	T&E LE90
13	-25 46 18.155	+28 12 7.352	1355.070	0.000	0.000
T&E Description					
Measured Latitude		Measured Longitude		Measured Elevation	
-25 46 18.148		+28 12 7.357		1355.070	
Delta Latitude	Delta Longitude	Delta Elevation	Mensuration Error		
0.201	0.161	0.000	0.000		
Individual HE			Individual VE		
0.258			0.000		
ID	T&E Latitude	T&E Longitude	T&E Elevation	T&E CE90	T&E LE90
14	-25 46 6.549	+28 14 54.009	1400.290	0.000	0.000
T&E Description					
Measured Latitude		Measured Longitude		Measured Elevation	
-25 46 6.553		+28 14 53.999		1400.290	
Delta Latitude	Delta Longitude	Delta Elevation	Mensuration Error		
-0.132	-0.261	0.000	0.000		
Individual HE			Individual VE		
0.293			0.000		
ID	T&E Latitude	T&E Longitude	T&E Elevation	T&E CE90	T&E LE90
15	-25 46 5.504	+28 17 41.246	1398.000	0.000	0.000
T&E Description					
Measured Latitude		Measured Longitude		Measured Elevation	
-25 46 5.507		+28 17 41.254		1398.000	
Delta Latitude	Delta Longitude	Delta Elevation	Mensuration Error		
-0.094	0.207	0.000	0.000		
Individual HE			Individual VE		
0.227			0.000		

ID	T&E Latitude	T&E Longitude	T&E Elevation	T&E CE90	T&E LE90
16	-25 48 36.146	+28 05 53.281	1438.200	0.000	0.000
T&E Description					
Measured Latitude		Measured Longitude		Measured Elevation	
-25 48 36.144		+28 05 53.297		1438.200	
Delta Latitude	Delta Longitude	Delta Elevation	Mensuration Error		
0.063	0.434	0.000	0.000		
Individual HE			Individual VE		
0.438			0.000		
ID	T&E Latitude	T&E Longitude	T&E Elevation	T&E CE90	T&E LE90
17	-25 48 43.856	+28 09 4.106	1444.000	0.000	0.000
T&E Description					
Measured Latitude		Measured Longitude		Measured Elevation	
-25 48 43.845		+28 09 4.119		1444.000	
Delta Latitude	Delta Longitude	Delta Elevation	Mensuration Error		
0.324	0.361	0.000	0.000		
Individual HE			Individual VE		
0.485			0.000		
ID	T&E Latitude	T&E Longitude	T&E Elevation	T&E CE90	T&E LE90
18	-25 48 37.225	+28 11 54.324	1454.620	0.000	0.000
T&E Description					
Measured Latitude		Measured Longitude		Measured Elevation	
-25 48 37.216		+28 11 54.342		1454.620	
Delta Latitude	Delta Longitude	Delta Elevation	Mensuration Error		
0.259	0.516	0.000	0.000		
Individual HE			Individual VE		
0.578			0.000		
ID	T&E Latitude	T&E Longitude	T&E Elevation	T&E CE90	T&E LE90
19	-25 48 43.528	+28 15 0.374	1559.960	0.000	0.000
T&E Description					
Measured Latitude		Measured Longitude		Measured Elevation	
-25 48 43.518		+28 15 0.379		1559.960	
Delta Latitude	Delta Longitude	Delta Elevation	Mensuration Error		
0.329	0.139	0.000	0.000		
Individual HE			Individual VE		
0.358			0.000		



ID	T&E Latitude	T&E Longitude	T&E Elevation	T&E CE90	T&E LE90
20	-25 48 42.925	+28 17 44.555	1446.500	0.000	0.000
T&E Description					
Measured Latitude		Measured Longitude		Measured Elevation	
-25 48 42.936		+28 17 44.564		1446.500	
Delta Latitude	Delta Longitude	Delta Elevation	Mensuration Error		
-0.329	0.262	0.000	0.000		
Individual HE			Individual VE		
0.420			0.000		
ID	T&E Latitude	T&E Longitude	T&E Elevation	T&E CE90	T&E LE90
21	-25 51 12.497	+28 05 50.230	1428.110	0.000	0.000
T&E Description					
Measured Latitude		Measured Longitude		Measured Elevation	
-25 51 12.509		+28 05 50.209		1428.110	
Delta Latitude	Delta Longitude	Delta Elevation	Mensuration Error		
-0.362	-0.592	0.000	0.000		
Individual HE			Individual VE		
0.694			0.000		
ID	T&E Latitude	T&E Longitude	T&E Elevation	T&E CE90	T&E LE90
22	-25 51 11.691	+28 09 1.772	1476.530	0.000	0.000
T&E Description					
Measured Latitude		Measured Longitude		Measured Elevation	
-25 51 11.686		+28 09 1.770		1476.530	
Delta Latitude	Delta Longitude	Delta Elevation	Mensuration Error		
0.140	-0.046	0.000	0.000		
Individual HE			Individual VE		
0.147			0.000		
ID	T&E Latitude	T&E Longitude	T&E Elevation	T&E CE90	T&E LE90
23	-25 51 14.426	+28 11 49.629	1440.470	0.000	0.000
T&E Description					
Measured Latitude		Measured Longitude		Measured Elevation	
-25 51 14.412		+28 11 49.625		1440.470	
Delta Latitude	Delta Longitude	Delta Elevation	Mensuration Error		
0.450	-0.105	0.000	0.000		
Individual HE			Individual VE		
0.462			0.000		

ID	T&E Latitude	T&E Longitude	T&E Elevation	T&E CE90	T&E LE90
24	-25 51 10.328	+28 15 5.543	1514.100	0.000	0.000
T&E Description					
Measured Latitude		Measured Longitude		Measured Elevation	
-25 51 10.329		+28 15 5.558		1514.100	
Delta Latitude	Delta Longitude	Delta Elevation	Mensuration Error		
-0.021	0.427	0.000	0.000		
Individual HE			Individual VE		
0.427			0.000		
ID	T&E Latitude	T&E Longitude	T&E Elevation	T&E CE90	T&E LE90
25	-25 51 11.253	+28 17 35.862	1507.580	0.000	0.000
T&E Description					
Measured Latitude		Measured Longitude		Measured Elevation	
-25 51 11.273		+28 17 35.868		1507.580	
Delta Latitude	Delta Longitude	Delta Elevation	Mensuration Error		
-0.608	0.164	0.000	0.000		
Individual HE			Individual VE		
0.630			0.000		



APPENDIX O: MAA REPORT FOR STAGE 1 – EXPERIMENT 3(c) (ORTHO-IMAGE USING 25 GCPS AND THE 2 M DTM)

MAA Report for 25gcps_2mdtm_ortho

Distance values are in meters

Mean latitude error: -0.039672
 Mean longitude error: 0.020637
 Mean horizontal error (average HE): 0.387128
 Standard deviation latitude error: 0.357158
 Standard deviation longitude error: 0.295056
 Standard deviation horizontal error: 0.258363
 90% Circular Error (against T&E): 0.718221
 90% Circular Error (T&E and mensuration error included): 0.718221

ID	T&E Latitude	T&E Longitude	T&E Elevation	T&E CE90	T&E LE90
1	-25 40 48.898	+28 05 58.648	1378.640	0.000	0.000
T&E Description CP #1					
Measured Latitude		Measured Longitude		Measured Elevation	
-25 40 48.899		+28 05 58.648		1378.640	
Delta Latitude	Delta Longitude	Delta Elevation	Mensuration Error		
-0.039	0.004	0.000	0.000		
Individual HE			Individual VE		
0.039			0.000		
ID	T&E Latitude	T&E Longitude	T&E Elevation	T&E CE90	T&E LE90
2	-25 40 53.691	+28 08 43.169	1302.820	0.000	0.000
T&E Description CP #2					
Measured Latitude		Measured Longitude		Measured Elevation	
-25 40 53.710		+28 08 43.169		1302.820	
Delta Latitude	Delta Longitude	Delta Elevation	Mensuration Error		
-0.582	-0.012	0.000	0.000		
Individual HE			Individual VE		
0.582			0.000		
ID	T&E Latitude	T&E Longitude	T&E Elevation	T&E CE90	T&E LE90
3	-25 40 51.185	+28 11 51.353	1251.130	0.000	0.000
T&E Description CP #3					
Measured Latitude		Measured Longitude		Measured Elevation	
-25 40 51.198		+28 11 51.358		1251.130	
Delta Latitude	Delta Longitude	Delta Elevation	Mensuration Error		
-0.400	0.140	0.000	0.000		
Individual HE			Individual VE		
0.424			0.000		



ID	T&E Latitude	T&E Longitude	T&E Elevation	T&E CE90	T&E LE90
4	-25 40 48.373	+28 14 43.374	1283.270	0.000	0.000
					T&E Description
					CP #4
Measured Latitude		Measured Longitude		Measured Elevation	
-25 40 48.384		+28 14 43.382		1283.270	
Delta Latitude	Delta Longitude	Delta Elevation	Mensuration Error		
-0.341	0.232	0.000	0.000		
Individual HE				Individual VE	
0.413				0.000	
ID	T&E Latitude	T&E Longitude	T&E Elevation	T&E CE90	T&E LE90
5	-25 40 58.441	+28 17 44.854	1268.350	0.000	0.000
					T&E Description
					CP #5
Measured Latitude		Measured Longitude		Measured Elevation	
-25 40 58.435		+28 17 44.856		1268.350	
Delta Latitude	Delta Longitude	Delta Elevation	Mensuration Error		
0.173	0.055	0.000	0.000		
Individual HE				Individual VE	
0.181				0.000	
ID	T&E Latitude	T&E Longitude	T&E Elevation	T&E CE90	T&E LE90
6	-25 43 20.146	+28 06 12.816	1319.670	0.000	0.000
					T&E Description
					CP #6
Measured Latitude		Measured Longitude		Measured Elevation	
-25 43 20.154		+28 06 12.815		1319.670	
Delta Latitude	Delta Longitude	Delta Elevation	Mensuration Error		
-0.228	-0.021	0.000	0.000		
Individual HE				Individual VE	
0.229				0.000	
ID	T&E Latitude	T&E Longitude	T&E Elevation	T&E CE90	T&E LE90
7	-25 43 28.495	+28 08 51.254	1315.200	0.000	0.000
					T&E Description
					CP #7
Measured Latitude		Measured Longitude		Measured Elevation	
-25 43 28.489		+28 08 51.256		1315.200	
Delta Latitude	Delta Longitude	Delta Elevation	Mensuration Error		
0.168	0.067	0.000	0.000		
Individual HE				Individual VE	
0.181				0.000	

ID	T&E Latitude	T&E Longitude	T&E Elevation	T&E CE90	T&E LE90
8	-25 43 30.456	+28 11 45.362	1303.450	0.000	0.000
					T&E Description
					CP #8
Measured Latitude		Measured Longitude		Measured Elevation	
-25 43 30.444		+28 11 45.338		1303.450	
Delta Latitude	Delta Longitude	Delta Elevation	Mensuration Error		
0.367	-0.672	0.000	0.000		
Individual HE				Individual VE	
0.766				0.000	
ID	T&E Latitude	T&E Longitude	T&E Elevation	T&E CE90	T&E LE90
9	-25 43 30.035	+28 14 52.315	1380.200	0.000	0.000
					T&E Description
					CP #9
Measured Latitude		Measured Longitude		Measured Elevation	
-25 43 30.033		+28 14 52.318		1380.200	
Delta Latitude	Delta Longitude	Delta Elevation	Mensuration Error		
0.060	0.095	0.000	0.000		
Individual HE				Individual VE	
0.112				0.000	
ID	T&E Latitude	T&E Longitude	T&E Elevation	T&E CE90	T&E LE90
10	-25 43 18.712	+28 17 37.661	1326.500	0.000	0.000
					T&E Description
					CP #10
Measured Latitude		Measured Longitude		Measured Elevation	
-25 43 18.684		+28 17 37.654		1326.500	
Delta Latitude	Delta Longitude	Delta Elevation	Mensuration Error		
0.864	-0.203	0.000	0.000		
Individual HE				Individual VE	
0.888				0.000	
ID	T&E Latitude	T&E Longitude	T&E Elevation	T&E CE90	T&E LE90
11	-25 46 25.942	+28 06 4.674	1417.430	0.000	0.000
					T&E Description
					CP #11
Measured Latitude		Measured Longitude		Measured Elevation	
-25 46 25.967		+28 06 4.685		1417.430	
Delta Latitude	Delta Longitude	Delta Elevation	Mensuration Error		
-0.797	0.327	0.000	0.000		
Individual HE				Individual VE	
0.861				0.000	

ID	T&E Latitude	T&E Longitude	T&E Elevation	T&E CE90	T&E LE90
12	-25 46 16.305	+28 08 48.334	1402.000	0.000	0.000
					T&E Description
					CP #12
Measured Latitude		Measured Longitude		Measured Elevation	
-25 46 16.311		+28 08 48.322		1402.000	
Delta Latitude	Delta Longitude	Delta Elevation	Mensuration Error		
-0.201	-0.332	0.000	0.000		
Individual HE			Individual VE		
0.388			0.000		
ID	T&E Latitude	T&E Longitude	T&E Elevation	T&E CE90	T&E LE90
13	-25 46 18.155	+28 12 7.352	1355.070	0.000	0.000
					T&E Description
					CP #13
Measured Latitude		Measured Longitude		Measured Elevation	
-25 46 18.154		+28 12 7.351		1355.070	
Delta Latitude	Delta Longitude	Delta Elevation	Mensuration Error		
0.008	-0.012	0.000	0.000		
Individual HE			Individual VE		
0.014			0.000		
ID	T&E Latitude	T&E Longitude	T&E Elevation	T&E CE90	T&E LE90
14	-25 46 6.549	+28 14 54.009	1400.290	0.000	0.000
					T&E Description
					CP #14
Measured Latitude		Measured Longitude		Measured Elevation	
-25 46 6.552		+28 14 53.998		1400.290	
Delta Latitude	Delta Longitude	Delta Elevation	Mensuration Error		
-0.100	-0.287	0.000	0.000		
Individual HE			Individual VE		
0.304			0.000		
ID	T&E Latitude	T&E Longitude	T&E Elevation	T&E CE90	T&E LE90
15	-25 46 5.504	+28 17 41.246	1398.000	0.000	0.000
					T&E Description
					CP #15
Measured Latitude		Measured Longitude		Measured Elevation	
-25 46 5.506		+28 17 41.255		1398.000	
Delta Latitude	Delta Longitude	Delta Elevation	Mensuration Error		
-0.061	0.226	0.000	0.000		
Individual HE			Individual VE		
0.234			0.000		

ID	T&E Latitude	T&E Longitude	T&E Elevation	T&E CE90	T&E LE90
16	-25 48 36.146	+28 05 53.281	1438.200	0.000	0.000
					T&E Description
					CP #16
Measured Latitude		Measured Longitude		Measured Elevation	
-25 48 36.143		+28 05 53.297		1438.200	
Delta Latitude	Delta Longitude	Delta Elevation	Mensuration Error		
0.094	0.434	0.000	0.000		
Individual HE			Individual VE		
0.444			0.000		
ID	T&E Latitude	T&E Longitude	T&E Elevation	T&E CE90	T&E LE90
17	-25 48 43.856	+28 09 4.106	1444.000	0.000	0.000
					T&E Description
					CP #17
Measured Latitude		Measured Longitude		Measured Elevation	
-25 48 43.843		+28 09 4.102		1444.000	
Delta Latitude	Delta Longitude	Delta Elevation	Mensuration Error		
0.375	-0.122	0.000	0.000		
Individual HE			Individual VE		
0.395			0.000		
ID	T&E Latitude	T&E Longitude	T&E Elevation	T&E CE90	T&E LE90
18	-25 48 37.225	+28 11 54.324	1454.620	0.000	0.000
					T&E Description
					CP #18
Measured Latitude		Measured Longitude		Measured Elevation	
-25 48 37.241		+28 11 54.351		1454.620	
Delta Latitude	Delta Longitude	Delta Elevation	Mensuration Error		
-0.498	0.776	0.000	0.000		
Individual HE			Individual VE		
0.922			0.000		
ID	T&E Latitude	T&E Longitude	T&E Elevation	T&E CE90	T&E LE90
19	-25 48 43.528	+28 15 0.374	1559.960	0.000	0.000
					T&E Description
					CP #19
Measured Latitude		Measured Longitude		Measured Elevation	
-25 48 43.518		+28 15 0.378		1559.960	
Delta Latitude	Delta Longitude	Delta Elevation	Mensuration Error		
0.301	0.107	0.000	0.000		
Individual HE			Individual VE		
0.320			0.000		

ID	T&E Latitude	T&E Longitude	T&E Elevation	T&E CE90	T&E LE90
20	-25 48 42.925	+28 17 44.555	1446.500	0.000	0.000
					T&E Description
					CP #20
Measured Latitude		Measured Longitude		Measured Elevation	
-25 48 42.935		+28 17 44.564		1446.500	
Delta Latitude	Delta Longitude	Delta Elevation	Mensuration Error		
-0.295	0.275	0.000	0.000		
Individual HE			Individual VE		
0.404			0.000		
ID	T&E Latitude	T&E Longitude	T&E Elevation	T&E CE90	T&E LE90
21	-25 51 12.497	+28 05 50.230	1428.110	0.000	0.000
					T&E Description
					CP #21
Measured Latitude		Measured Longitude		Measured Elevation	
-25 51 12.508		+28 05 50.210		1428.110	
Delta Latitude	Delta Longitude	Delta Elevation	Mensuration Error		
-0.330	-0.554	0.000	0.000		
Individual HE			Individual VE		
0.645			0.000		
ID	T&E Latitude	T&E Longitude	T&E Elevation	T&E CE90	T&E LE90
22	-25 51 11.691	+28 09 1.772	1476.530	0.000	0.000
					T&E Description
					CP #22
Measured Latitude		Measured Longitude		Measured Elevation	
-25 51 11.685		+28 09 1.769		1476.530	
Delta Latitude	Delta Longitude	Delta Elevation	Mensuration Error		
0.174	-0.070	0.000	0.000		
Individual HE			Individual VE		
0.187			0.000		
ID	T&E Latitude	T&E Longitude	T&E Elevation	T&E CE90	T&E LE90
23	-25 51 14.426	+28 11 49.629	1440.470	0.000	0.000
					T&E Description
					CP #23
Measured Latitude		Measured Longitude		Measured Elevation	
-25 51 14.412		+28 11 49.626		1440.470	
Delta Latitude	Delta Longitude	Delta Elevation	Mensuration Error		
0.446	-0.086	0.000	0.000		
Individual HE			Individual VE		
0.455			0.000		

ID	T&E Latitude	T&E Longitude	T&E Elevation	T&E CE90	T&E LE90
24	-25 51 10.328	+28 15 5.543	1514.100	0.000	0.000
					T&E Description
					CP #24
Measured Latitude		Measured Longitude		Measured Elevation	
-25 51 10.330		+28 15 5.541		1514.100	
Delta Latitude	Delta Longitude	Delta Elevation	Mensuration Error		
-0.053	-0.046	0.000	0.000		
Individual HE			Individual VE		
0.070			0.000		
ID	T&E Latitude	T&E Longitude	T&E Elevation	T&E CE90	T&E LE90
25	-25 51 11.253	+28 17 35.862	1507.580	0.000	0.000
					T&E Description
					CP #25
Measured Latitude		Measured Longitude		Measured Elevation	
-25 51 11.257		+28 17 35.869		1507.580	
Delta Latitude	Delta Longitude	Delta Elevation	Mensuration Error		
-0.097	0.197	0.000	0.000		
Individual HE			Individual VE		
0.219			0.000		



APPENDIX P: MAA REPORT FOR STAGE 2 – EXPERIMENT 01 (ORTHO-IMAGE USING 10 TERRASAR-X ACQUIRED GCPS AND THE 2 M DTM)

MAA Report for terrasar-x_gcps_2mdtm_ortho_geographic

Distance values are in meters

Mean latitude error: -0.143141
 Mean longitude error: 0.213521
 Mean horizontal error (average HE): 1.061211
 Standard deviation latitude error: 0.645782
 Standard deviation longitude error: 0.997244
 Standard deviation horizontal error: 0.592826
 90% Circular Error (against T&E): 1.820917
 90% Circular Error (T&E and mensuration error included): 1.820917

ID	T&E Latitude	T&E Longitude	T&E Elevation	T&E CE90	T&E LE90
1	-25 40 49.311	+28 05 58.511	1374.660	0.000	0.000
T&E Description CP #1					
Measured Latitude		Measured Longitude		Measured Elevation	
-25 40 49.330		+28 05 58.497		1374.660	
Delta Latitude	Delta Longitude	Delta Elevation	Mensuration Error		
-0.585	-0.407	0.000	0.000		
Individual HE			Individual VE		
0.713			0.000		

ID	T&E Latitude	T&E Longitude	T&E Elevation	T&E CE90	T&E LE90
2	-25 40 51.884	+28 11 51.392	1246.370	0.000	0.000
T&E Description CP #2					
Measured Latitude		Measured Longitude		Measured Elevation	
-25 40 51.921		+28 11 51.385		1246.370	
Delta Latitude	Delta Longitude	Delta Elevation	Mensuration Error		
-1.148	-0.203	0.000	0.000		
Individual HE			Individual VE		
1.166			0.000		

ID	T&E Latitude	T&E Longitude	T&E Elevation	T&E CE90	T&E LE90
3	-25 40 59.687	+28 17 47.377	1265.130	0.000	0.000
T&E Description CP #3					
Measured Latitude		Measured Longitude		Measured Elevation	
-25 40 59.725		+28 17 47.447		1265.130	
Delta Latitude	Delta Longitude	Delta Elevation	Mensuration Error		
-1.148	1.958	0.000	0.000		
Individual HE			Individual VE		
2.270			0.000		



ID	T&E Latitude	T&E Longitude	T&E Elevation	T&E CE90	T&E LE90
4	-25 43 29.604	+28 08 51.890	1304.180	0.000	0.000
T&E Description CP #4					
Measured Latitude		Measured Longitude		Measured Elevation	
-25 43 29.617		+28 08 51.871		1304.180	
Delta Latitude	Delta Longitude	Delta Elevation	Mensuration Error		
-0.412	-0.549	0.000	0.000		
Individual HE			Individual VE		
0.686			0.000		
ID	T&E Latitude	T&E Longitude	T&E Elevation	T&E CE90	T&E LE90
5	-25 43 29.999	+28 14 50.877	1303.910	0.000	0.000
T&E Description CP #5					
Measured Latitude		Measured Longitude		Measured Elevation	
-25 43 30.029		+28 14 50.900		1303.910	
Delta Latitude	Delta Longitude	Delta Elevation	Mensuration Error		
-0.944	0.634	0.000	0.000		
Individual HE			Individual VE		
1.137			0.000		
ID	T&E Latitude	T&E Longitude	T&E Elevation	T&E CE90	T&E LE90
6	-25 46 26.499	+28 06 4.257	1400.260	0.000	0.000
T&E Description CP #6					
Measured Latitude		Measured Longitude		Measured Elevation	
-25 46 26.490		+28 06 4.243		1400.260	
Delta Latitude	Delta Longitude	Delta Elevation	Mensuration Error		
0.270	-0.397	0.000	0.000		
Individual HE			Individual VE		
0.480			0.000		
ID	T&E Latitude	T&E Longitude	T&E Elevation	T&E CE90	T&E LE90
7	-25 46 18.421	+28 12 9.383	1374.750	0.000	0.000
T&E Description CP #7					
Measured Latitude		Measured Longitude		Measured Elevation	
-25 46 18.429		+28 12 9.378		1374.750	
Delta Latitude	Delta Longitude	Delta Elevation	Mensuration Error		
-0.235	-0.156	0.000	0.000		
Individual HE			Individual VE		
0.282			0.000		



ID	T&E Latitude	T&E Longitude	T&E Elevation	T&E CE90	T&E LE90
8	-25 46 5.592	+28 17 41.083	1385.540	0.000	0.000
					T&E Description
					CP #8
Measured Latitude		Measured Longitude		Measured Elevation	
-25 46 5.599		+28 17 41.151		1385.540	
Delta Latitude	Delta Longitude	Delta Elevation	Mensuration Error		
-0.208	1.902	0.000	0.000		
Individual HE				Individual VE	
1.913				0.000	
ID	T&E Latitude	T&E Longitude	T&E Elevation	T&E CE90	T&E LE90
9	-25 48 49.178	+28 09 2.215	1423.740	0.000	0.000
					T&E Description
					CP #9
Measured Latitude		Measured Longitude		Measured Elevation	
-25 48 49.162		+28 09 2.180		1423.740	
Delta Latitude	Delta Longitude	Delta Elevation	Mensuration Error		
0.488	-0.991	0.000	0.000		
Individual HE				Individual VE	
1.105				0.000	
ID	T&E Latitude	T&E Longitude	T&E Elevation	T&E CE90	T&E LE90
10	-25 48 43.930	+28 15 1.545	1552.310	0.000	0.000
					T&E Description
					CP #10
Measured Latitude		Measured Longitude		Measured Elevation	
-25 48 43.914		+28 15 1.534		1552.310	
Delta Latitude	Delta Longitude	Delta Elevation	Mensuration Error		
0.494	-0.307	0.000	0.000		
Individual HE				Individual VE	
0.581				0.000	
ID	T&E Latitude	T&E Longitude	T&E Elevation	T&E CE90	T&E LE90
11	-25 51 15.544	+28 05 47.757	1422.540	0.000	0.000
					T&E Description
					CP #11
Measured Latitude		Measured Longitude		Measured Elevation	
-25 51 15.522		+28 05 47.742		1422.540	
Delta Latitude	Delta Longitude	Delta Elevation	Mensuration Error		
0.694	-0.427	0.000	0.000		
Individual HE				Individual VE	
0.815				0.000	



ID	T&E Latitude	T&E Longitude	T&E Elevation	T&E CE90	T&E LE90
12	-25 51 15.939	+28 11 51.975	1434.480	0.000	0.000
					T&E Description
					CP #12
Measured Latitude		Measured Longitude		Measured Elevation	
-25 51 15.916		+28 11 51.968		1434.480	
Delta Latitude	Delta Longitude	Delta Elevation	Mensuration Error		
0.693	-0.198	0.000	0.000		
Individual HE				Individual VE	
0.720				0.000	
ID	T&E Latitude	T&E Longitude	T&E Elevation	T&E CE90	T&E LE90
13	-25 51 14.189	+28 17 35.166	1505.010	0.000	0.000
					T&E Description
					CP #13
Measured Latitude		Measured Longitude		Measured Elevation	
-25 51 14.183		+28 17 35.235		1505.010	
Delta Latitude	Delta Longitude	Delta Elevation	Mensuration Error		
0.182	1.918	0.000	0.000		
Individual HE				Individual VE	
1.927				0.000	





APPENDIX Q: MAA REPORT FOR STAGE 2 – EXPERIMENT 02 (ORTHO-IMAGE USING ONLY SENSOR MODEL AND THE 2 M DTM)

MAA Report for sensor_model_no_gcps_2mdtm_ortho						
Distance values are in meters						
Mean latitude error: -5.805287						
Mean longitude error: 1.711381						
Mean horizontal error (average HE): 6.084747						
Standard deviation latitude error: 0.494120						
Standard deviation longitude error: 0.526876						
Standard deviation horizontal error: 0.357470						
90% Circular Error (against T&E): 6.542845						
90% Circular Error (T&E and mensuration error included): 6.542845						
ID	T&E Latitude	T&E Longitude	T&E Elevation	T&E CE90	T&E LE90	
1	-25 40 49.311	+28 05 58.511	1374.660	0.000	0.000	
						T&E Description
						CP #1
Measured Latitude		Measured Longitude		Measured Elevation		
-25 40 49.520		+28 05 58.545		1374.660		
Delta Latitude	Delta Longitude	Delta Elevation	Mensuration Error			
-6.439	0.944	0.000	0.000			
Individual HE			Individual VE			
6.508			0.000			
ID	T&E Latitude	T&E Longitude	T&E Elevation	T&E CE90	T&E LE90	
2	-25 40 51.884	+28 11 51.392	1246.370	0.000	0.000	
						T&E Description
						CP #2
Measured Latitude		Measured Longitude		Measured Elevation		
-25 40 52.074		+28 11 51.454		1246.370		
Delta Latitude	Delta Longitude	Delta Elevation	Mensuration Error			
-5.888	1.705	0.000	0.000			
Individual HE			Individual VE			
6.130			0.000			
ID	T&E Latitude	T&E Longitude	T&E Elevation	T&E CE90	T&E LE90	
3	-25 40 59.687	+28 17 47.377	1265.130	0.000	0.000	
						T&E Description
						CP #3
Measured Latitude		Measured Longitude		Measured Elevation		
-25 40 59.844		+28 17 47.449		1265.130		
Delta Latitude	Delta Longitude	Delta Elevation	Mensuration Error			
-4.842	1.998	0.000	0.000			
Individual HE			Individual VE			
5.238			0.000			



ID	T&E Latitude	T&E Longitude	T&E Elevation	T&E CE90	T&E LE90
4	-25 43 29.604	+28 08 51.890	1304.180	0.000	0.000
					T&E Description
					CP #4
Measured Latitude		Measured Longitude		Measured Elevation	
-25 43 29.799		+28 08 51.947		1304.180	
Delta Latitude	Delta Longitude	Delta Elevation	Mensuration Error		
-6.030	1.567	0.000	0.000		
Individual HE				Individual VE	
6.230				0.000	
ID	T&E Latitude	T&E Longitude	T&E Elevation	T&E CE90	T&E LE90
5	-25 43 29.999	+28 14 50.877	1303.910	0.000	0.000
					T&E Description
					CP #5
Measured Latitude		Measured Longitude		Measured Elevation	
-25 43 30.159		+28 14 50.978		1303.910	
Delta Latitude	Delta Longitude	Delta Elevation	Mensuration Error		
-4.958	2.812	0.000	0.000		
Individual HE				Individual VE	
5.700				0.000	
ID	T&E Latitude	T&E Longitude	T&E Elevation	T&E CE90	T&E LE90
6	-25 46 26.499	+28 06 4.257	1400.260	0.000	0.000
					T&E Description
					CP #6
Measured Latitude		Measured Longitude		Measured Elevation	
-25 46 26.699		+28 06 4.291		1400.260	
Delta Latitude	Delta Longitude	Delta Elevation	Mensuration Error		
-6.193	0.958	0.000	0.000		
Individual HE				Individual VE	
6.267				0.000	
ID	T&E Latitude	T&E Longitude	T&E Elevation	T&E CE90	T&E LE90
7	-25 46 18.421	+28 12 9.383	1374.750	0.000	0.000
					T&E Description
					CP #7
Measured Latitude		Measured Longitude		Measured Elevation	
-25 46 18.604		+28 12 9.446		1374.750	
Delta Latitude	Delta Longitude	Delta Elevation	Mensuration Error		
-5.647	1.731	0.000	0.000		
Individual HE				Individual VE	
5.906				0.000	

ID	T&E Latitude	T&E Longitude	T&E Elevation	T&E CE90	T&E LE90
8	-25 46 5.592	+28 17 41.083	1385.540	0.000	0.000
T&E Description CP #8					
Measured Latitude		Measured Longitude		Measured Elevation	
-25 46 5.774		+28 17 41.154		1385.540	
Delta Latitude	Delta Longitude	Delta Elevation	Mensuration Error		
-5.634	1.982	0.000	0.000		
Individual HE			Individual VE		
5.972			0.000		
ID	T&E Latitude	T&E Longitude	T&E Elevation	T&E CE90	T&E LE90
9	-25 48 49.178	+28 09 2.215	1423.740	0.000	0.000
T&E Description CP #9					
Measured Latitude		Measured Longitude		Measured Elevation	
-25 48 49.382		+28 09 2.272		1423.740	
Delta Latitude	Delta Longitude	Delta Elevation	Mensuration Error		
-6.313	1.575	0.000	0.000		
Individual HE			Individual VE		
6.506			0.000		
ID	T&E Latitude	T&E Longitude	T&E Elevation	T&E CE90	T&E LE90
10	-25 48 43.930	+28 15 1.545	1552.310	0.000	0.000
T&E Description CP #10					
Measured Latitude		Measured Longitude		Measured Elevation	
-25 48 44.117		+28 15 1.629		1552.310	
Delta Latitude	Delta Longitude	Delta Elevation	Mensuration Error		
-5.780	2.335	0.000	0.000		
Individual HE			Individual VE		
6.234			0.000		
ID	T&E Latitude	T&E Longitude	T&E Elevation	T&E CE90	T&E LE90
11	-25 51 15.544	+28 05 47.757	1422.540	0.000	0.000
T&E Description CP #11					
Measured Latitude		Measured Longitude		Measured Elevation	
-25 51 15.753		+28 05 47.791		1422.540	
Delta Latitude	Delta Longitude	Delta Elevation	Mensuration Error		
-6.451	0.945	0.000	0.000		
Individual HE			Individual VE		
6.520			0.000		

ID	T&E Latitude	T&E Longitude	T&E Elevation	T&E CE90	T&E LE90
12	-25 51 15.939	+28 11 51.975	1434.480	0.000	0.000
					T&E Description
					CP #12
Measured Latitude		Measured Longitude		Measured Elevation	
-25 51 16.130		+28 11 52.037		1434.480	
Delta Latitude	Delta Longitude	Delta Elevation	Mensuration Error		
-5.912	1.714	0.000	0.000		
Individual HE			Individual VE		
6.155			0.000		
ID	T&E Latitude	T&E Longitude	T&E Elevation	T&E CE90	T&E LE90
13	-25 51 14.189	+28 17 35.166	1505.010	0.000	0.000
					T&E Description
					CP #13
Measured Latitude		Measured Longitude		Measured Elevation	
-25 51 14.363		+28 17 35.237		1505.010	
Delta Latitude	Delta Longitude	Delta Elevation	Mensuration Error		
-5.382	1.980	0.000	0.000		
Individual HE			Individual VE		
5.734			0.000		

APPENDIX R: MAA REPORT FOR STAGE 3 – EXPERIMENT 01 (CLUSTER OF GCPS ON THE WEST SIDE OF THE IMAGE)

MAA Report for left_independant_2mdtm_ortho						
Distance values are in meters						
Mean latitude error: -3.503629						
Mean longitude error: 5.955728						
Mean horizontal error (average HE): 8.396816						
Standard deviation latitude error: 2.816383						
Standard deviation longitude error: 5.394742						
Standard deviation horizontal error: 3.778206						
90% Circular Error (against T&E): 13.238588						
90% Circular Error (T&E and mensuration error included): 13.238588						
ID	T&E Latitude	T&E Longitude	T&E Elevation	T&E CE90	T&E LE90	
1	-25 40 49.311	+28 05 58.511	1374.660	0.000	0.000	
						T&E Description
						CP #1
Measured Latitude		Measured Longitude		Measured Elevation		
-25 40 49.477		+28 05 58.442		1374.660		
Delta Latitude	Delta Longitude	Delta Elevation	Mensuration Error			
-5.123	-1.927	0.000	0.000			
Individual HE				Individual VE		
5.473				0.000		
ID	T&E Latitude	T&E Longitude	T&E Elevation	T&E CE90	T&E LE90	
2	-25 40 51.884	+28 11 51.392	1246.370	0.000	0.000	
						T&E Description
						CP #2
Measured Latitude		Measured Longitude		Measured Elevation		
-25 40 51.863		+28 11 51.619		1246.370		
Delta Latitude	Delta Longitude	Delta Elevation	Mensuration Error			
0.651	6.301	0.000	0.000			
Individual HE				Individual VE		
6.335				0.000		
ID	T&E Latitude	T&E Longitude	T&E Elevation	T&E CE90	T&E LE90	
3	-25 40 59.687	+28 17 47.377	1265.130	0.000	0.000	
						T&E Description
						CP #3
Measured Latitude		Measured Longitude		Measured Elevation		
-25 40 59.653		+28 17 47.781		1265.130		
Delta Latitude	Delta Longitude	Delta Elevation	Mensuration Error			
1.074	11.237	0.000	0.000			
Individual HE				Individual VE		
11.288				0.000		

ID	T&E Latitude	T&E Longitude	T&E Elevation	T&E CE90	T&E LE90
4	-25 43 29.604	+28 08 51.890	1304.180	0.000	0.000
					T&E Description
					CP #4
Measured Latitude		Measured Longitude		Measured Elevation	
-25 43 29.644		+28 08 51.959		1304.180	
Delta Latitude	Delta Longitude	Delta Elevation	Mensuration Error		
-1.241	1.901	0.000	0.000		
Individual HE			Individual VE		
2.270			0.000		
ID	T&E Latitude	T&E Longitude	T&E Elevation	T&E CE90	T&E LE90
5	-25 43 29.999	+28 14 50.877	1303.910	0.000	0.000
					T&E Description
					CP #5
Measured Latitude		Measured Longitude		Measured Elevation	
-25 43 30.021		+28 14 51.227		1303.910	
Delta Latitude	Delta Longitude	Delta Elevation	Mensuration Error		
-0.676	9.745	0.000	0.000		
Individual HE			Individual VE		
9.768			0.000		
ID	T&E Latitude	T&E Longitude	T&E Elevation	T&E CE90	T&E LE90
6	-25 46 26.499	+28 06 4.257	1400.260	0.000	0.000
					T&E Description
					CP #6
Measured Latitude		Measured Longitude		Measured Elevation	
-25 46 26.644		+28 06 4.191		1400.260	
Delta Latitude	Delta Longitude	Delta Elevation	Mensuration Error		
-4.481	-1.821	0.000	0.000		
Individual HE			Individual VE		
4.837			0.000		
ID	T&E Latitude	T&E Longitude	T&E Elevation	T&E CE90	T&E LE90
7	-25 46 18.421	+28 12 9.383	1374.750	0.000	0.000
					T&E Description
					CP #7
Measured Latitude		Measured Longitude		Measured Elevation	
-25 46 18.529		+28 12 9.653		1374.750	
Delta Latitude	Delta Longitude	Delta Elevation	Mensuration Error		
-3.325	7.496	0.000	0.000		
Individual HE			Individual VE		
8.200			0.000		

ID	T&E Latitude	T&E Longitude	T&E Elevation	T&E CE90	T&E LE90
8	-25 46 5.592	+28 17 41.083	1385.540	0.000	0.000
T&E Description CP #8					
Measured Latitude		Measured Longitude		Measured Elevation	
-25 46 5.676		+28 17 41.501		1385.540	
Delta Latitude	Delta Longitude	Delta Elevation	Mensuration Error		
-2.594	11.613	0.000	0.000		
Individual HE			Individual VE		
11.899			0.000		
ID	T&E Latitude	T&E Longitude	T&E Elevation	T&E CE90	T&E LE90
9	-25 48 49.178	+28 09 2.215	1423.740	0.000	0.000
T&E Description CP #9					
Measured Latitude		Measured Longitude		Measured Elevation	
-25 48 49.343		+28 09 2.339		1423.740	
Delta Latitude	Delta Longitude	Delta Elevation	Mensuration Error		
-5.090	3.438	0.000	0.000		
Individual HE			Individual VE		
6.142			0.000		
ID	T&E Latitude	T&E Longitude	T&E Elevation	T&E CE90	T&E LE90
10	-25 48 43.930	+28 15 1.545	1552.310	0.000	0.000
T&E Description CP #10					
Measured Latitude		Measured Longitude		Measured Elevation	
-25 48 44.227		+28 15 2.003		1552.310	
Delta Latitude	Delta Longitude	Delta Elevation	Mensuration Error		
-9.203	12.726	0.000	0.000		
Individual HE			Individual VE		
15.705			0.000		
ID	T&E Latitude	T&E Longitude	T&E Elevation	T&E CE90	T&E LE90
11	-25 51 15.544	+28 05 47.757	1422.540	0.000	0.000
T&E Description CP #11					
Measured Latitude		Measured Longitude		Measured Elevation	
-25 51 15.677		+28 05 47.666		1422.540	
Delta Latitude	Delta Longitude	Delta Elevation	Mensuration Error		
-4.120	-2.543	0.000	0.000		
Individual HE			Individual VE		
4.842			0.000		

ID	T&E Latitude	T&E Longitude	T&E Elevation	T&E CE90	T&E LE90
12	-25 51 15.939	+28 11 51.975	1434.480	0.000	0.000
					T&E Description
					CP #12
Measured Latitude		Measured Longitude		Measured Elevation	
-25 51 16.089		+28 11 52.237		1434.480	
Delta Latitude	Delta Longitude	Delta Elevation	Mensuration Error		
-4.655	7.270	0.000	0.000		
Individual HE			Individual VE		
8.633			0.000		
ID	T&E Latitude	T&E Longitude	T&E Elevation	T&E CE90	T&E LE90
13	-25 51 14.189	+28 17 35.166	1505.010	0.000	0.000
					T&E Description
					CP #13
Measured Latitude		Measured Longitude		Measured Elevation	
-25 51 14.408		+28 17 35.597		1505.010	
Delta Latitude	Delta Longitude	Delta Elevation	Mensuration Error		
-6.764	11.989	0.000	0.000		
Individual HE			Individual VE		
13.766			0.000		

APPENDIX S: MAA REPORT FOR STAGE 3 – EXPERIMENT 02 (CLUSTER OF GCPS ON THE EAST SIDE OF THE IMAGE)

MAA Report for gcps_right_2dtm_ortho						
Distance values are in meters						
Mean latitude error: 5.204709						
Mean longitude error: 4.781283						
Mean horizontal error (average HE): 7.925042						
Standard deviation latitude error: 3.951290						
Standard deviation longitude error: 4.423644						
Standard deviation horizontal error: 4.724900						
90% Circular Error (against T&E): 13.980002						
90% Circular Error (T&E and mensuration error included): 13.980002						
ID	T&E Latitude	T&E Longitude	T&E Elevation	T&E CE90	T&E LE90	
1	-25 40 49.311	+28 05 58.511	1374.660	0.000	0.000	
						T&E Description
						CP #1
Measured Latitude		Measured Longitude		Measured Elevation		
-25 40 48.993		+28 05 58.861		1374.660		
Delta Latitude	Delta Longitude	Delta Elevation	Mensuration Error			
9.833	9.735	0.000	0.000			
Individual HE			Individual VE			
13.837			0.000			
ID	T&E Latitude	T&E Longitude	T&E Elevation	T&E CE90	T&E LE90	
2	-25 40 51.884	+28 11 51.392	1246.370	0.000	0.000	
						T&E Description
						CP #2
Measured Latitude		Measured Longitude		Measured Elevation		
-25 40 51.647		+28 11 51.635		1246.370		
Delta Latitude	Delta Longitude	Delta Elevation	Mensuration Error			
7.322	6.758	0.000	0.000			
Individual HE			Individual VE			
9.964			0.000			
ID	T&E Latitude	T&E Longitude	T&E Elevation	T&E CE90	T&E LE90	
3	-25 40 59.687	+28 17 47.377	1265.130	0.000	0.000	
						T&E Description
						CP #3
Measured Latitude		Measured Longitude		Measured Elevation		
-25 40 59.691		+28 17 47.380		1265.130		
Delta Latitude	Delta Longitude	Delta Elevation	Mensuration Error			
-0.128	0.095	0.000	0.000			
Individual HE			Individual VE			
0.160			0.000			

ID	T&E Latitude	T&E Longitude	T&E Elevation	T&E CE90	T&E LE90
4	-25 43 29.604	+28 08 51.890	1304.180	0.000	0.000
					T&E Description
					CP #4
Measured Latitude		Measured Longitude		Measured Elevation	
-25 43 29.336		+28 08 52.244		1304.180	
Delta Latitude	Delta Longitude	Delta Elevation	Mensuration Error		
8.281	9.838	0.000	0.000		
Individual HE				Individual VE	
12.859				0.000	
ID	T&E Latitude	T&E Longitude	T&E Elevation	T&E CE90	T&E LE90
5	-25 43 29.999	+28 14 50.877	1303.910	0.000	0.000
					T&E Description
					CP #5
Measured Latitude		Measured Longitude		Measured Elevation	
-25 43 29.848		+28 14 51.038		1303.910	
Delta Latitude	Delta Longitude	Delta Elevation	Mensuration Error		
4.668	4.494	0.000	0.000		
Individual HE				Individual VE	
6.480				0.000	
ID	T&E Latitude	T&E Longitude	T&E Elevation	T&E CE90	T&E LE90
6	-25 46 26.499	+28 06 4.257	1400.260	0.000	0.000
					T&E Description
					CP #6
Measured Latitude		Measured Longitude		Measured Elevation	
-25 46 26.167		+28 06 4.637		1400.260	
Delta Latitude	Delta Longitude	Delta Elevation	Mensuration Error		
10.242	10.583	0.000	0.000		
Individual HE				Individual VE	
14.728				0.000	
ID	T&E Latitude	T&E Longitude	T&E Elevation	T&E CE90	T&E LE90
7	-25 46 18.421	+28 12 9.383	1374.750	0.000	0.000
					T&E Description
					CP #7
Measured Latitude		Measured Longitude		Measured Elevation	
-25 46 18.284		+28 12 9.524		1374.750	
Delta Latitude	Delta Longitude	Delta Elevation	Mensuration Error		
4.242	3.906	0.000	0.000		
Individual HE				Individual VE	
5.766				0.000	

ID	T&E Latitude	T&E Longitude	T&E Elevation	T&E CE90	T&E LE90
8	-25 46 5.592	+28 17 41.083	1385.540	0.000	0.000
					T&E Description
					CP #8
Measured Latitude		Measured Longitude		Measured Elevation	
-25 46 5.602		+28 17 41.021		1385.540	
Delta Latitude	Delta Longitude	Delta Elevation	Mensuration Error		
-0.322	-1.723	0.000	0.000		
Individual HE				Individual VE	
1.753				0.000	
ID	T&E Latitude	T&E Longitude	T&E Elevation	T&E CE90	T&E LE90
9	-25 48 49.178	+28 09 2.215	1423.740	0.000	0.000
					T&E Description
					CP #9
Measured Latitude		Measured Longitude		Measured Elevation	
-25 48 48.991		+28 09 2.459		1423.740	
Delta Latitude	Delta Longitude	Delta Elevation	Mensuration Error		
5.763	6.766	0.000	0.000		
Individual HE				Individual VE	
8.888				0.000	
ID	T&E Latitude	T&E Longitude	T&E Elevation	T&E CE90	T&E LE90
10	-25 48 43.930	+28 15 1.545	1552.310	0.000	0.000
					T&E Description
					CP #10
Measured Latitude		Measured Longitude		Measured Elevation	
-25 48 43.842		+28 15 1.602		1552.310	
Delta Latitude	Delta Longitude	Delta Elevation	Mensuration Error		
2.709	1.578	0.000	0.000		
Individual HE				Individual VE	
3.135				0.000	
ID	T&E Latitude	T&E Longitude	T&E Elevation	T&E CE90	T&E LE90
11	-25 51 15.544	+28 05 47.757	1422.540	0.000	0.000
					T&E Description
					CP #11
Measured Latitude		Measured Longitude		Measured Elevation	
-25 51 15.214		+28 05 48.092		1422.540	
Delta Latitude	Delta Longitude	Delta Elevation	Mensuration Error		
10.204	9.298	0.000	0.000		
Individual HE				Individual VE	
13.805				0.000	

ID	T&E Latitude	T&E Longitude	T&E Elevation	T&E CE90	T&E LE90
12	-25 51 15.939	+28 11 51.975	1434.480	0.000	0.000
					T&E Description
					CP #12
Measured Latitude		Measured Longitude		Measured Elevation	
-25 51 15.725		+28 11 52.127		1434.480	
Delta Latitude	Delta Longitude	Delta Elevation	Mensuration Error		
6.609	4.212	0.000	0.000		
Individual HE			Individual VE		
7.837			0.000		
ID	T&E Latitude	T&E Longitude	T&E Elevation	T&E CE90	T&E LE90
13	-25 51 14.189	+28 17 35.166	1505.010	0.000	0.000
					T&E Description
					CP #13
Measured Latitude		Measured Longitude		Measured Elevation	
-25 51 14.246		+28 17 35.044		1505.010	
Delta Latitude	Delta Longitude	Delta Elevation	Mensuration Error		
-1.761	-3.384	0.000	0.000		
Individual HE			Individual VE		
3.815			0.000		

APPENDIX T: MAA REPORT FOR STAGE 3 – EXPERIMENT 03 (CLUSTER OF GCPS ON THE NORTH SIDE OF THE IMAGE)

MAA Report for gcps_top_2dtm_ortho						
Distance values are in meters						
Mean latitude error: -3.676196						
Mean longitude error: -2.615097						
Mean horizontal error (average HE): 5.302920						
Standard deviation latitude error: 3.781919						
Standard deviation longitude error: 1.893448						
Standard deviation horizontal error: 3.181233						
90% Circular Error (against T&E): 9.379670						
90% Circular Error (T&E and mensuration error included): 9.379670						

ID	T&E Latitude	T&E Longitude	T&E Elevation	T&E CE90	T&E LE90	
1	-25 40 49.311	+28 05 58.511	1374.660	0.000	0.000	
						T&E Description
						CP #1

Measured Latitude		Measured Longitude		Measured Elevation		
-25 40 49.440		+28 05 58.490		1374.660		

Delta Latitude	Delta Longitude	Delta Elevation	Mensuration Error			
-3.982	-0.605	0.000	0.000			

Individual HE			Individual VE			
4.027			0.000			

ID	T&E Latitude	T&E Longitude	T&E Elevation	T&E CE90	T&E LE90	
2	-25 40 51.884	+28 11 51.392	1246.370	0.000	0.000	
						T&E Description
						CP #2

Measured Latitude		Measured Longitude		Measured Elevation		
-25 40 51.824		+28 11 51.397		1246.370		

Delta Latitude	Delta Longitude	Delta Elevation	Mensuration Error			
1.857	0.131	0.000	0.000			

Individual HE			Individual VE			
1.861			0.000			

ID	T&E Latitude	T&E Longitude	T&E Elevation	T&E CE90	T&E LE90	
3	-25 40 59.687	+28 17 47.377	1265.130	0.000	0.000	
						T&E Description
						CP #3

Measured Latitude		Measured Longitude		Measured Elevation		
-25 40 59.635		+28 17 47.292		1265.130		

Delta Latitude	Delta Longitude	Delta Elevation	Mensuration Error			
1.622	-2.379	0.000	0.000			

Individual HE			Individual VE			
2.879			0.000			

ID	T&E Latitude	T&E Longitude	T&E Elevation	T&E CE90	T&E LE90
4	-25 43 29.604	+28 08 51.890	1304.180	0.000	0.000
					T&E Description
					CP #4
Measured Latitude		Measured Longitude		Measured Elevation	
-25 43 29.621		+28 08 51.841		1304.180	
Delta Latitude	Delta Longitude	Delta Elevation	Mensuration Error		
-0.542	-1.377	0.000	0.000		
Individual HE			Individual VE		
1.480			0.000		
ID	T&E Latitude	T&E Longitude	T&E Elevation	T&E CE90	T&E LE90
5	-25 43 29.999	+28 14 50.877	1303.910	0.000	0.000
					T&E Description
					CP #5
Measured Latitude		Measured Longitude		Measured Elevation	
-25 43 29.999		+28 14 50.818		1303.910	
Delta Latitude	Delta Longitude	Delta Elevation	Mensuration Error		
-0.010	-1.651	0.000	0.000		
Individual HE			Individual VE		
1.651			0.000		
ID	T&E Latitude	T&E Longitude	T&E Elevation	T&E CE90	T&E LE90
6	-25 46 26.499	+28 06 4.257	1400.260	0.000	0.000
					T&E Description
					CP #6
Measured Latitude		Measured Longitude		Measured Elevation	
-25 46 26.637		+28 06 4.150		1400.260	
Delta Latitude	Delta Longitude	Delta Elevation	Mensuration Error		
-4.273	-2.968	0.000	0.000		
Individual HE			Individual VE		
5.202			0.000		
ID	T&E Latitude	T&E Longitude	T&E Elevation	T&E CE90	T&E LE90
7	-25 46 18.421	+28 12 9.383	1374.750	0.000	0.000
					T&E Description
					CP #7
Measured Latitude		Measured Longitude		Measured Elevation	
-25 46 18.526		+28 12 9.322		1374.750	
Delta Latitude	Delta Longitude	Delta Elevation	Mensuration Error		
-3.251	-1.699	0.000	0.000		
Individual HE			Individual VE		
3.669			0.000		

ID	T&E Latitude	T&E Longitude	T&E Elevation	T&E CE90	T&E LE90
8	-25 46 5.592	+28 17 41.083	1385.540	0.000	0.000
					T&E Description
					CP #8
Measured Latitude		Measured Longitude		Measured Elevation	
-25 46 5.711		+28 17 40.925		1385.540	
Delta Latitude	Delta Longitude	Delta Elevation	Mensuration Error		
-3.662	-4.392	0.000	0.000		
Individual HE			Individual VE		
5.718			0.000		
ID	T&E Latitude	T&E Longitude	T&E Elevation	T&E CE90	T&E LE90
9	-25 48 49.178	+28 09 2.215	1423.740	0.000	0.000
					T&E Description
					CP #9
Measured Latitude		Measured Longitude		Measured Elevation	
-25 48 49.354		+28 09 2.114		1423.740	
Delta Latitude	Delta Longitude	Delta Elevation	Mensuration Error		
-5.452	-2.813	0.000	0.000		
Individual HE			Individual VE		
6.135			0.000		
ID	T&E Latitude	T&E Longitude	T&E Elevation	T&E CE90	T&E LE90
10	-25 48 43.930	+28 15 1.545	1552.310	0.000	0.000
					T&E Description
					CP #10
Measured Latitude		Measured Longitude		Measured Elevation	
-25 48 44.326		+28 15 1.523		1552.310	
Delta Latitude	Delta Longitude	Delta Elevation	Mensuration Error		
-12.242	-0.603	0.000	0.000		
Individual HE			Individual VE		
12.257			0.000		
ID	T&E Latitude	T&E Longitude	T&E Elevation	T&E CE90	T&E LE90
11	-25 51 15.544	+28 05 47.757	1422.540	0.000	0.000
					T&E Description
					CP #11
Measured Latitude		Measured Longitude		Measured Elevation	
-25 51 15.672		+28 05 47.549		1422.540	
Delta Latitude	Delta Longitude	Delta Elevation	Mensuration Error		
-3.943	-5.807	0.000	0.000		
Individual HE			Individual VE		
7.019			0.000		

ID	T&E Latitude	T&E Longitude	T&E Elevation	T&E CE90	T&E LE90
11	-25 51 15.544	+28 05 47.757	1422.540	0.000	0.000
					T&E Description
					CP #11
Measured Latitude		Measured Longitude		Measured Elevation	
-25 51 15.672		+28 05 47.549		1422.540	
Delta Latitude	Delta Longitude	Delta Elevation	Mensuration Error		
-3.943	-5.807	0.000	0.000		
Individual HE			Individual VE		
7.019			0.000		
ID	T&E Latitude	T&E Longitude	T&E Elevation	T&E CE90	T&E LE90
12	-25 51 15.939	+28 11 51.975	1434.480	0.000	0.000
					T&E Description
					CP #12
Measured Latitude		Measured Longitude		Measured Elevation	
-25 51 16.111		+28 11 51.846		1434.480	
Delta Latitude	Delta Longitude	Delta Elevation	Mensuration Error		
-5.337	-3.593	0.000	0.000		
Individual HE			Individual VE		
6.433			0.000		
ID	T&E Latitude	T&E Longitude	T&E Elevation	T&E CE90	T&E LE90
13	-25 51 14.189	+28 17 35.166	1505.010	0.000	0.000
					T&E Description
					CP #13
Measured Latitude		Measured Longitude		Measured Elevation	
-25 51 14.467		+28 17 34.941		1505.010	
Delta Latitude	Delta Longitude	Delta Elevation	Mensuration Error		
-8.577	-6.242	0.000	0.000		
Individual HE			Individual VE		
10.608			0.000		



APPENDIX U: MAA REPORT FOR STAGE 3 – EXPERIMENT 04 (CLUSTER OF GCPS ON THE SOUTH SIDE OF THE IMAGE)

MAA Report for gcps_bottom_2dtm_ortho						
Distance values are in meters						
Mean latitude error: 1.348255						
Mean longitude error: -2.887899						
Mean horizontal error (average HE): 3.364686						
Standard deviation latitude error: 0.985375						
Standard deviation longitude error: 1.384710						
Standard deviation horizontal error: 1.313400						
90% Circular Error (against T&E): 5.047808						
90% Circular Error (T&E and mensuration error included): 5.047808						
ID	T&E Latitude	T&E Longitude	T&E Elevation	T&E CE90	T&E LE90	
1	-25 40 49.311	+28 05 58.511	1374.660	0.000	0.000	
						T&E Description
						CP #1
Measured Latitude		Measured Longitude		Measured Elevation		
-25 40 49.204		+28 05 58.387		1374.660		
Delta Latitude	Delta Longitude	Delta Elevation	Mensuration Error			
3.316	-3.469	0.000	0.000			
Individual HE			Individual VE			
4.799			0.000			
ID	T&E Latitude	T&E Longitude	T&E Elevation	T&E CE90	T&E LE90	
2	-25 40 51.884	+28 11 51.392	1246.370	0.000	0.000	
						T&E Description
						CP #2
Measured Latitude		Measured Longitude		Measured Elevation		
-25 40 51.881		+28 11 51.261		1246.370		
Delta Latitude	Delta Longitude	Delta Elevation	Mensuration Error			
0.086	-3.662	0.000	0.000			
Individual HE			Individual VE			
3.663			0.000			
ID	T&E Latitude	T&E Longitude	T&E Elevation	T&E CE90	T&E LE90	
3	-25 40 59.687	+28 17 47.377	1265.130	0.000	0.000	
						T&E Description
						CP #3
Measured Latitude		Measured Longitude		Measured Elevation		
-25 40 59.650		+28 17 47.185		1265.130		
Delta Latitude	Delta Longitude	Delta Elevation	Mensuration Error			
1.155	-5.339	0.000	0.000			
Individual HE			Individual VE			
5.462			0.000			

ID	T&E Latitude	T&E Longitude	T&E Elevation	T&E CE90	T&E LE90
4	-25 43 29.604	+28 08 51.890	1304.180	0.000	0.000
					T&E Description
					CP #4
Measured Latitude		Measured Longitude		Measured Elevation	
-25 43 29.549		+28 08 51.790		1304.180	
Delta Latitude	Delta Longitude	Delta Elevation	Mensuration Error		
1.702	-2.787	0.000	0.000		
Individual HE				Individual VE	
3.266				0.000	
ID	T&E Latitude	T&E Longitude	T&E Elevation	T&E CE90	T&E LE90
5	-25 43 29.999	+28 14 50.877	1303.910	0.000	0.000
					T&E Description
					CP #5
Measured Latitude		Measured Longitude		Measured Elevation	
-25 43 29.943		+28 14 50.733		1303.910	
Delta Latitude	Delta Longitude	Delta Elevation	Mensuration Error		
1.742	-4.010	0.000	0.000		
Individual HE				Individual VE	
4.372				0.000	
ID	T&E Latitude	T&E Longitude	T&E Elevation	T&E CE90	T&E LE90
6	-25 46 26.499	+28 06 4.257	1400.260	0.000	0.000
					T&E Description
					CP #6
Measured Latitude		Measured Longitude		Measured Elevation	
-25 46 26.406		+28 06 4.121		1400.260	
Delta Latitude	Delta Longitude	Delta Elevation	Mensuration Error		
2.868	-3.770	0.000	0.000		
Individual HE				Individual VE	
4.737				0.000	
ID	T&E Latitude	T&E Longitude	T&E Elevation	T&E CE90	T&E LE90
7	-25 46 18.421	+28 12 9.383	1374.750	0.000	0.000
					T&E Description
					CP #7
Measured Latitude		Measured Longitude		Measured Elevation	
-25 46 18.379		+28 12 9.258		1374.750	
Delta Latitude	Delta Longitude	Delta Elevation	Mensuration Error		
1.317	-3.492	0.000	0.000		
Individual HE				Individual VE	
3.732				0.000	

ID	T&E Latitude	T&E Longitude	T&E Elevation	T&E CE90	T&E LE90
8	-25 46 5.592	+28 17 41.083	1385.540	0.000	0.000
					T&E Description
					CP #8
Measured Latitude		Measured Longitude		Measured Elevation	
-25 46 5.569		+28 17 40.941		1385.540	
Delta Latitude	Delta Longitude	Delta Elevation	Mensuration Error		
0.716	-3.951	0.000	0.000		
Individual HE			Individual VE		
4.015			0.000		
ID	T&E Latitude	T&E Longitude	T&E Elevation	T&E CE90	T&E LE90
9	-25 48 49.178	+28 09 2.215	1423.740	0.000	0.000
					T&E Description
					CP #9
Measured Latitude		Measured Longitude		Measured Elevation	
-25 48 49.137		+28 09 2.184		1423.740	
Delta Latitude	Delta Longitude	Delta Elevation	Mensuration Error		
1.246	-0.880	0.000	0.000		
Individual HE			Individual VE		
1.526			0.000		
ID	T&E Latitude	T&E Longitude	T&E Elevation	T&E CE90	T&E LE90
10	-25 48 43.930	+28 15 1.545	1552.310	0.000	0.000
					T&E Description
					CP #10
Measured Latitude		Measured Longitude		Measured Elevation	
-25 48 43.854		+28 15 1.525		1552.310	
Delta Latitude	Delta Longitude	Delta Elevation	Mensuration Error		
2.328	-0.564	0.000	0.000		
Individual HE			Individual VE		
2.396			0.000		
ID	T&E Latitude	T&E Longitude	T&E Elevation	T&E CE90	T&E LE90
11	-25 51 15.544	+28 05 47.757	1422.540	0.000	0.000
					T&E Description
					CP #11
Measured Latitude		Measured Longitude		Measured Elevation	
-25 51 15.522		+28 05 47.696		1422.540	
Delta Latitude	Delta Longitude	Delta Elevation	Mensuration Error		
0.685	-1.699	0.000	0.000		
Individual HE			Individual VE		
1.832			0.000		

ID	T&E Latitude	T&E Longitude	T&E Elevation	T&E CE90	T&E LE90
11	-25 51 15.544	+28 05 47.757	1422.540	0.000	0.000
					T&E Description
					CP #11
Measured Latitude		Measured Longitude		Measured Elevation	
-25 51 15.522		+28 05 47.696		1422.540	
Delta Latitude	Delta Longitude	Delta Elevation	Mensuration Error		
0.685	-1.699	0.000	0.000		
Individual HE			Individual VE		
1.832			0.000		
ID	T&E Latitude	T&E Longitude	T&E Elevation	T&E CE90	T&E LE90
12	-25 51 15.939	+28 11 51.975	1434.480	0.000	0.000
					T&E Description
					CP #12
Measured Latitude		Measured Longitude		Measured Elevation	
-25 51 15.933		+28 11 51.940		1434.480	
Delta Latitude	Delta Longitude	Delta Elevation	Mensuration Error		
0.171	-0.993	0.000	0.000		
Individual HE			Individual VE		
1.008			0.000		
ID	T&E Latitude	T&E Longitude	T&E Elevation	T&E CE90	T&E LE90
13	-25 51 14.189	+28 17 35.166	1505.010	0.000	0.000
					T&E Description
					CP #13
Measured Latitude		Measured Longitude		Measured Elevation	
-25 51 14.183		+28 17 35.061		1505.010	
Delta Latitude	Delta Longitude	Delta Elevation	Mensuration Error		
0.193	-2.926	0.000	0.000		
Individual HE			Individual VE		
2.933			0.000		





**APPENDIX V: MAA REPORT FOR STAGE 3 – EXPERIMENT 05 (GCPS
DISTRIBUTED RANDOMLY ACROSS THE ENTIRE IMAGE)**

MAA Report for gcps_random_2dtm_ortho						
Distance values are in meters						
Mean latitude error: 0.516462						
Mean longitude error: 0.187905						
Mean horizontal error (average HE): 0.845465						
Standard deviation latitude error: 0.703862						
Standard deviation longitude error: 0.438169						
Standard deviation horizontal error: 0.524066						
90% Circular Error (against T&E): 1.517055						
90% Circular Error (T&E and mensuration error included): 1.517055						
ID	T&E Latitude	T&E Longitude	T&E Elevation	T&E CE90	T&E LE90	
1	-25 40 49.311	+28 05 58.511	1374.660	0.000	0.000	
						T&E Description
						CP #1
Measured Latitude		Measured Longitude		Measured Elevation		
-25 40 49.302		+28 05 58.512		1374.660		
Delta Latitude	Delta Longitude	Delta Elevation	Mensuration Error			
0.294	0.028	0.000	0.000			
Individual HE			Individual VE			
0.295			0.000			
ID	T&E Latitude	T&E Longitude	T&E Elevation	T&E CE90	T&E LE90	
2	-25 40 51.884	+28 11 51.392	1246.370	0.000	0.000	
						T&E Description
						CP #2
Measured Latitude		Measured Longitude		Measured Elevation		
-25 40 51.892		+28 11 51.391		1246.370		
Delta Latitude	Delta Longitude	Delta Elevation	Mensuration Error			
-0.249	-0.038	0.000	0.000			
Individual HE			Individual VE			
0.252			0.000			
ID	T&E Latitude	T&E Longitude	T&E Elevation	T&E CE90	T&E LE90	
3	-25 40 59.687	+28 17 47.377	1265.130	0.000	0.000	
						T&E Description
						CP #3
Measured Latitude		Measured Longitude		Measured Elevation		
-25 40 59.661		+28 17 47.356		1265.130		
Delta Latitude	Delta Longitude	Delta Elevation	Mensuration Error			
0.805	-0.575	0.000	0.000			
Individual HE			Individual VE			
0.989			0.000			

ID	T&E Latitude	T&E Longitude	T&E Elevation	T&E CE90	T&E LE90
4	-25 43 29.604	+28 08 51.890	1304.180	0.000	0.000
					T&E Description
					CP #4
Measured Latitude		Measured Longitude		Measured Elevation	
-25 43 29.604		+28 08 51.899		1304.180	
Delta Latitude	Delta Longitude	Delta Elevation	Mensuration Error		
0.001	0.238	0.000	0.000		
Individual HE			Individual VE		
0.238			0.000		
ID	T&E Latitude	T&E Longitude	T&E Elevation	T&E CE90	T&E LE90
5	-25 43 29.999	+28 14 50.877	1303.910	0.000	0.000
					T&E Description
					CP #5
Measured Latitude		Measured Longitude		Measured Elevation	
-25 43 29.982		+28 14 50.883		1303.910	
Delta Latitude	Delta Longitude	Delta Elevation	Mensuration Error		
0.536	0.166	0.000	0.000		
Individual HE			Individual VE		
0.561			0.000		
ID	T&E Latitude	T&E Longitude	T&E Elevation	T&E CE90	T&E LE90
6	-25 46 26.499	+28 06 4.257	1400.260	0.000	0.000
					T&E Description
					CP #6
Measured Latitude		Measured Longitude		Measured Elevation	
-25 46 26.505		+28 06 4.275		1400.260	
Delta Latitude	Delta Longitude	Delta Elevation	Mensuration Error		
-0.186	0.504	0.000	0.000		
Individual HE			Individual VE		
0.537			0.000		
ID	T&E Latitude	T&E Longitude	T&E Elevation	T&E CE90	T&E LE90
7	-25 46 18.421	+28 12 9.383	1374.750	0.000	0.000
					T&E Description
					CP #7
Measured Latitude		Measured Longitude		Measured Elevation	
-25 46 18.395		+28 12 9.398		1374.750	
Delta Latitude	Delta Longitude	Delta Elevation	Mensuration Error		
0.805	0.400	0.000	0.000		
Individual HE			Individual VE		
0.899			0.000		

ID	T&E Latitude	T&E Longitude	T&E Elevation	T&E CE90	T&E LE90
8	-25 46 5.592	+28 17 41.083	1385.540	0.000	0.000
					T&E Description
					CP #8
Measured Latitude		Measured Longitude		Measured Elevation	
-25 46 5.549		+28 17 41.063		1385.540	
Delta Latitude	Delta Longitude	Delta Elevation	Mensuration Error		
1.342	-0.561	0.000	0.000		
Individual HE			Individual VE		
1.454			0.000		
ID	T&E Latitude	T&E Longitude	T&E Elevation	T&E CE90	T&E LE90
9	-25 48 49.178	+28 09 2.215	1423.740	0.000	0.000
					T&E Description
					CP #9
Measured Latitude		Measured Longitude		Measured Elevation	
-25 48 49.178		+28 09 2.241		1423.740	
Delta Latitude	Delta Longitude	Delta Elevation	Mensuration Error		
-0.007	0.719	0.000	0.000		
Individual HE			Individual VE		
0.719			0.000		
ID	T&E Latitude	T&E Longitude	T&E Elevation	T&E CE90	T&E LE90
10	-25 48 43.930	+28 15 1.545	1552.310	0.000	0.000
					T&E Description
					CP #10
Measured Latitude		Measured Longitude		Measured Elevation	
-25 48 43.861		+28 15 1.550		1552.310	
Delta Latitude	Delta Longitude	Delta Elevation	Mensuration Error		
2.105	0.150	0.000	0.000		
Individual HE			Individual VE		
2.111			0.000		
ID	T&E Latitude	T&E Longitude	T&E Elevation	T&E CE90	T&E LE90
11	-25 51 15.544	+28 05 47.757	1422.540	0.000	0.000
					T&E Description
					CP #11
Measured Latitude		Measured Longitude		Measured Elevation	
-25 51 15.555		+28 05 47.794		1422.540	
Delta Latitude	Delta Longitude	Delta Elevation	Mensuration Error		
-0.323	1.018	0.000	0.000		
Individual HE			Individual VE		
1.068			0.000		

ID	T&E Latitude	T&E Longitude	T&E Elevation	T&E CE90	T&E LE90
12	-25 51 15.939	+28 11 51.975	1434.480	0.000	0.000
T&E Description					
CP #12					
Measured Latitude		Measured Longitude		Measured Elevation	
-25 51 15.930		+28 11 51.993		1434.480	
Delta Latitude	Delta Longitude	Delta Elevation	Mensuration Error		
0.275	0.477	0.000	0.000		
Individual HE			Individual VE		
0.551			0.000		
ID	T&E Latitude	T&E Longitude	T&E Elevation	T&E CE90	T&E LE90
13	-25 51 14.189	+28 17 35.166	1505.010	0.000	0.000
T&E Description					
CP #13					
Measured Latitude		Measured Longitude		Measured Elevation	
-25 51 14.147		+28 17 35.163		1505.010	
Delta Latitude	Delta Longitude	Delta Elevation	Mensuration Error		
1.314	-0.083	0.000	0.000		
Individual HE			Individual VE		
1.317			0.000		

APPENDIX W: A-GCP-ES DEVELOPMENT REQUEST LETTER

LETTER OF REQUEST

03 March 2016

To: Mr Chris Böhme
Pinkmatter Solutions, South Africa

From: Ivan Henrico (ivan.henrico@sita.co.za)
PhD Registered Student: University of Pretoria

ASSISTANCE WITH THE DEVELOPMENT OF A PYTHON SCRIPT TO EXTRACT GROUND CONTROL POINTS (GCPS)

1. I am currently registered at the University of Pretoria for my PhD in Geoinformatica, student number = 15025901. As part of my studies, I need to develop an automatic GCP extraction script that can be integrated with remote sensing image processing software (the use of PCI Pluggable Functions are proposed).

2. Due to my lack of experience in GIS software architecture and engineering, assistance is sought from Pinkmatter Solutions to develop this required script. Please take note of the fact that no financial costs can be made towards the development and assistance of this script. This script will only be used for my studies and will not be distributed for use to any other person, department or party. Where applicable, the necessary references towards the development and support of Pinkmatter Solutions will be made. Any usage and testing of the script will have to be requested from the University of Pretoria, the thesis author (myself) and my supervisor (Prof Ludwig Combrinck).

3. If assistance and support for this request is approved, then it is proposed to schedule a meeting between Pinkmatter Solutions and myself on 16 March 2016 to discuss the details pertaining to the development of this script.

Your kind consideration and approval will be highly appreciated.

Regards


Ivan Henrico

APPROVED / NOT APPROVED



**(MR CHRIS BÖHME)
PINKMATTER SOLUTIONS**



APPENDIX X: AUTOMATIC GCP EXTRACTION SCRIPT (A-GCP-ES)

```
import getopt
import os
from pci.asl import *
from pci.autochip2 import *
from pci.fimport import *
from pci.gcpipro import *
from pci.gcpwrit import *
import re
import sys

class CGcpData:
    def __init__(self, sample, line, lat, lon, height):
        self.sample = sample
        self.line = line
        self.lat = lat
        self.lon = lon
        self.height = height
    def get_lat(self):
        return self.lat
    def get_lon(self):
        return self.lon
    def get_height(self):
        return self.height
    def get_sample(self):
        return self.sample
    def get_line(self):
        return self.line

class CAIData:
    def __init__(self, inputFile, outputDirectory, chipDb, corrScore):
        self.inputFile = inputFile
        self.outputDirectory = outputDirectory
```



```
self.chipDb = chipDb
self.corrScore = corrScore
self.outputGcpLayer = -1
self.tempPixImage = os.path.join(self.outputDirectory, "TempImage.pix")
self.reportFilePath = os.path.join(self.outputDirectory, "Report.txt")
self.outputGcpFilePath = os.path.join(self.outputDirectory, "Gcps.txt")
def get_chip_db(self):
    return self.chipDb
def get_input_file(self):
    return self.inputFile
def get_output_directory(self):
    return self.outputDirectory
def get_corr_score(self):
    return self.corrScore
def get_output_gcp_layer(self):
    return self.outputGcpLayer
def get_temp_pix_image_path(self):
    return self.tempPixImage
def get_report_file_path(self):
    return self.reportFilePath;
def get_gcps(self):
    return self.gcps
def get_output_gcp_file(self):
    return self.outputGcpFilePath
def set_output_gcp_layer(self, gcpLayer):
    self.outputGcpLayer = gcpLayer
def set_gcps(self, gcps):
    self.gcps = gcps

def get_options(argv):
    counter = 0
    msg = 'main.py -i <path and name of image file> -o <path to output folder> -c <path
and name of chip database file> -r [min correlation strength, default set at (0.75)]'
    try:
```

```
    opts, args = getopt.getopt(argv, "hi:o:c:r:", [])
except getopt.GetoptError:
    print msg
    sys.exit(2)
corrScore = 0.75
for opt, arg in opts:
    if opt == '-h':
        print msg
        sys.exit()
    elif opt in ("-i"):
        inputFolder = arg
        counter = counter + 1
    elif opt in ("-o"):
        outputFolder = arg
        counter = counter + 1
    elif opt in ("-c"):
        chipDbFile = arg
        counter = counter + 1
    elif opt in ("-r"):
        corrScore = float (arg)
if counter != 3:
    print msg
    sys.exit(2)

return CAIData(inputFolder, outputFolder, chipDbFile, corrScore)

def remove_if_exists(filePath):
    if os.path.isfile(filePath):
        print "Removing file " + filePath
        os.remove(filePath)

def correlate_data(data):
    inPath = data.get_input_file()
    tempOutFile = data.get_temp_pix_image_path()
```



```
remove_if_exists(tempOutFile)
fimport(inPath, tempOutFile, [], u"AVERAGE", u"BAND")

chipfile = data.get_chip_db()
minScore = data.get_corr_score()
numgcps = []
# correlate the chip DB to the image
autochip2(tempOutFile, [], [], [], chipfile, "", "", [], u"FFTP", [], u"PIXEL", [minScore], "",
numgcps)
print "/-----\\"
print "|                               |"
print " " + str(numgcps[0]) + " GCPs correlated with success"
print "|                               |"
print "\\-----/"
# gets the GCP segment in the pix file
gcpSegments = asl(tempOutFile, u"brief", [215], u"")
gcpSegment = -1
for it in gcpSegments:
    if(it > gcpSegment):
        gcpSegment = it
data.set_output_gcp_layer(gcpSegment)
layer = []
# project the GCPs to Lat/Lon
gcppro(tempOutFile, [gcpSegment], "", [], u"LON", u"", u"", layer)
data.set_output_gcp_layer(layer[0])

def get_gcps(data):
    inFile = data.get_temp_pix_image_path()
    outFile = data.get_report_file_path()
    gcpLayer = data.get_output_gcp_layer()
    type = ["2D", "3D", "2DERR", "3DERR"]
    # write GCP to disk
    gcpwrit(inFile, [gcpLayer], outFile, type[1])
    gcps = []
```

```
prog = re.compile("^[\\d.]+\\s+[\\d.]+\\s+[\\d.]+\\s+([-\\d.]+)\\s+([-\\d.]+)\\s+([-\\d.]+)\\s+(\\w+)\\s+$")
with open(outFile, "r") as ins:
    for line in ins:
        m = prog.match(line)
        if(m):
            id = m.group(1)
            p = m.group(2)
            l = m.group(3)
            long = m.group(4)
            lat = m.group(5)
            height = m.group(6)
            gcpType = m.group(7)
            if(gcpType == "G"):
                gcps.append(CGcpData(float(p), float(l), float(lat), float(long), float(height)))
data.set_gcps(gcps)

#####
# final GCP text file generation
#####
def report_gcps(data):
    gcps = data.get_gcps()
    with open(data.get_output_gcp_file(), "w") as trg:
        # The header of the output
        # trg.write("#          LAT (Y)          LONG (X)  ELEVATION (Z)
            #          PIXEL X (COLUMN)          PIXEL Y (ROW)          GCP#\n")
        trg.write("#          LAT (Y)          LONG (X)  ELEV (Z)  PIXEL (X)
            #          PIXEL (Y)")
        trg.write("\n")
    for num, gcp in enumerate (gcps):
        line = str(num + 1) + "\t"
        # Lat Lon in degrees
        line += str(gcp.get_lat()) + "\t"
```



```
line += str(gcp.get_lon()) + "\t"
# height sample and line values
line += str(gcp.get_height()) + "\t"
line += str(gcp.get_sample()) + "\t"
line += str(gcp.get_line()) + "\t"
trg.write(line + "\n")

def clean_up(data):
    remove_if_exists(data.get_temp_pix_image_path())
    remove_if_exists(data.get_report_file_path())

def main(argv):
    # create chip DB using 'PNT2CHIP'
    data = get_options(argv)
    correlate_data(data)
    get_gcps(data)
    report_gcps(data)
    clean_up(data)
if __name__ == "__main__":
    main(sys.argv[1:])
```

APPENDIX Y: OPERATOR MAA REPORTS FOR INPUT GCPS ACCURACY COMPARISON

1. Operator #1

MAA Report for dim_phr1b_p_201306220821476_sen_643051101-001						
Distance values are in meters						
Mean latitude error: -0.002410						
Mean longitude error: -0.001481						
Mean horizontal error (average HE): 0.014083						
Standard deviation latitude error: 0.008202						
Standard deviation longitude error: 0.012514						
Standard deviation horizontal error: 0.005792						
90% Circular Error (against T&E): 0.021505						
90% Circular Error (T&E and mensuration error included): 0.021505						

ID	T&E Latitude	T&E Longitude	T&E Elevation	T&E CE90	T&E LE90	
1	-25 40 48.739	+28 05 58.453	1373.250	0.000	0.000	
						T&E Description
						CP #1

Measured Latitude		Measured Longitude		Measured Elevation		
-25 40 48.739		+28 05 58.453		1373.250		

Delta Latitude	Delta Longitude	Delta Elevation	Mensuration Error			
-0.014	0.018	0.000	0.000			

Individual HE				Individual VE		
0.023				0.000		

ID	T&E Latitude	T&E Longitude	T&E Elevation	T&E CE90	T&E LE90	
2	-25 40 58.711	+28 17 45.045	1263.080	0.000	0.000	
						T&E Description
						CP #2

Measured Latitude		Measured Longitude		Measured Elevation		
-25 40 58.711		+28 17 45.045		1263.080		

Delta Latitude	Delta Longitude	Delta Elevation	Mensuration Error			
-0.007	-0.003	0.000	0.000			

Individual HE				Individual VE		
0.008				0.000		

ID	T&E Latitude	T&E Longitude	T&E Elevation	T&E CE90	T&E LE90	
3	-25 46 18.213	+28 12 7.614	1370.510	0.000	0.000	
						T&E Description
						CP #3

Measured Latitude		Measured Longitude		Measured Elevation		
-25 46 18.213		+28 12 7.614		1370.510		

Delta Latitude	Delta Longitude	Delta Elevation	Mensuration Error			
0.006	0.006	0.000	0.000			

Individual HE				Individual VE		
0.009				0.000		



ID	T&E Latitude	T&E Longitude	T&E Elevation	T&E CE90	T&E LE90
4	-25 51 12.797	+28 05 50.429	1421.280	0.000	0.000
					T&E Description
					CP #4
Measured Latitude		Measured Longitude		Measured Elevation	
-25 51 12.797		+28 05 50.429		1421.280	
Delta Latitude	Delta Longitude	Delta Elevation	Mensuration Error		
-0.004	-0.013	0.000	0.000		
Individual HE			Individual VE		
0.013			0.000		
ID	T&E Latitude	T&E Longitude	T&E Elevation	T&E CE90	T&E LE90
5	-25 51 11.111	+28 17 35.640	1508.490	0.000	0.000
					T&E Description
					CP #5
Measured Latitude		Measured Longitude		Measured Elevation	
-25 51 11.111		+28 17 35.640		1508.490	
Delta Latitude	Delta Longitude	Delta Elevation	Mensuration Error		
0.007	-0.016	0.000	0.000		
Individual HE			Individual VE		
0.017			0.000		



2. Operator #2

MAA Report for dim_phr1b_p_201306220821476_sen_643051101-001

Distance values are in meters

Mean latitude error: 0.006164
 Mean longitude error: -0.104132
 Mean horizontal error (average HE): 0.110777
 Standard deviation latitude error: 0.011974
 Standard deviation longitude error: 0.204270
 Standard deviation horizontal error: 0.201195
 90% Circular Error (against T&E): 0.377536
 90% Circular Error (T&E and mensuration error included): 0.377536

ID	T&E Latitude	T&E Longitude	T&E Elevation	T&E CE90	T&E LE90
1	-25 40 48.739	+28 05 58.453	1373.250	0.000	0.000
T&E Description CP #1					
Measured Latitude		Measured Longitude		Measured Elevation	
-25 40 48.739		+28 05 58.453		1373.250	
Delta Latitude	Delta Longitude	Delta Elevation	Mensuration Error		
-0.009	0.008	0.000	0.000		
Individual HE			Individual VE		
0.012			0.000		

ID	T&E Latitude	T&E Longitude	T&E Elevation	T&E CE90	T&E LE90
2	-25 40 58.711	+28 17 45.045	1263.080	0.000	0.000
T&E Description CP #2					
Measured Latitude		Measured Longitude		Measured Elevation	
-25 40 58.711		+28 17 45.045		1263.080	
Delta Latitude	Delta Longitude	Delta Elevation	Mensuration Error		
-0.000	0.000	0.000	0.000		
Individual HE			Individual VE		
0.001			0.000		

ID	T&E Latitude	T&E Longitude	T&E Elevation	T&E CE90	T&E LE90
3	-25 46 18.213	+28 12 7.614	1370.510	0.000	0.000
T&E Description CP #3					
Measured Latitude		Measured Longitude		Measured Elevation	
-25 46 18.213		+28 12 7.614		1370.510	
Delta Latitude	Delta Longitude	Delta Elevation	Mensuration Error		
0.000	-0.001	0.000	0.000		
Individual HE			Individual VE		
0.001			0.000		



ID	T&E Latitude	T&E Longitude	T&E Elevation	T&E CE90	T&E LE90
4	-25 51 12.797	+28 05 50.429	1421.280	0.000	0.000
					T&E Description
					CP #4
Measured Latitude		Measured Longitude		Measured Elevation	
-25 51 12.796		+28 05 50.411		1421.280	
Delta Latitude	Delta Longitude	Delta Elevation	Mensuration Error		
0.018	-0.512	0.000	0.000		
Individual HE			Individual VE		
0.513			0.000		
ID	T&E Latitude	T&E Longitude	T&E Elevation	T&E CE90	T&E LE90
5	-25 51 11.111	+28 17 35.640	1508.490	0.000	0.000
					T&E Description
					CP #5
Measured Latitude		Measured Longitude		Measured Elevation	
-25 51 11.110		+28 17 35.640		1508.490	
Delta Latitude	Delta Longitude	Delta Elevation	Mensuration Error		
0.023	-0.016	0.000	0.000		
Individual HE			Individual VE		
0.028			0.000		

3. Operator #3

MAA Report for dim_phrlb_p_201306220821476_sen_643051101-001

Distance values are in meters

Mean latitude error: -0.000005
 Mean longitude error: 0.000052
 Mean horizontal error (average HE): 0.005209
 Standard deviation latitude error: 0.005556
 Standard deviation longitude error: 0.005113
 Standard deviation horizontal error: 0.005466
 90% Circular Error (against T&E): 0.012232
 90% Circular Error (T&E and mensuration error included): 0.012232

ID	T&E Latitude	T&E Longitude	T&E Elevation	T&E CE90	T&E LE90
1	-25 40 48.739	+28 05 58.453	1373.250	0.000	0.000
T&E Description CP #1					
Measured Latitude		Measured Longitude		Measured Elevation	
-25 40 48.739		+28 05 58.453		1373.250	
Delta Latitude	Delta Longitude	Delta Elevation	Mensuration Error		
-0.009	0.008	0.000	0.000		
Individual HE			Individual VE		
0.012			0.000		

ID	T&E Latitude	T&E Longitude	T&E Elevation	T&E CE90	T&E LE90
2	-25 40 58.711	+28 17 45.045	1263.080	0.000	0.000
T&E Description CP #2					
Measured Latitude		Measured Longitude		Measured Elevation	
-25 40 58.711		+28 17 45.045		1263.080	
Delta Latitude	Delta Longitude	Delta Elevation	Mensuration Error		
-0.001	0.001	0.000	0.000		
Individual HE			Individual VE		
0.001			0.000		

ID	T&E Latitude	T&E Longitude	T&E Elevation	T&E CE90	T&E LE90
3	-25 46 18.213	+28 12 7.614	1370.510	0.000	0.000
T&E Description CP #3					
Measured Latitude		Measured Longitude		Measured Elevation	
-25 46 18.213		+28 12 7.614		1370.510	
Delta Latitude	Delta Longitude	Delta Elevation	Mensuration Error		
0.000	-0.000	0.000	0.000		
Individual HE			Individual VE		
0.000			0.000		



ID	T&E Latitude	T&E Longitude	T&E Elevation	T&E CE90	T&E LE90
4	-25 51 12.797	+28 05 50.429	1421.280	0.000	0.000
					T&E Description
					CP #4
Measured Latitude		Measured Longitude		Measured Elevation	
-25 51 12.797		+28 05 50.429		1421.280	
Delta Latitude	Delta Longitude	Delta Elevation	Mensuration Error		
0.001	-0.001	0.000	0.000		
Individual HE			Individual VE		
0.001			0.000		
ID	T&E Latitude	T&E Longitude	T&E Elevation	T&E CE90	T&E LE90
5	-25 51 11.111	+28 17 35.640	1508.490	0.000	0.000
					T&E Description
					CP #5
Measured Latitude		Measured Longitude		Measured Elevation	
-25 51 11.111		+28 17 35.640		1508.490	
Delta Latitude	Delta Longitude	Delta Elevation	Mensuration Error		
0.009	-0.008	0.000	0.000		
Individual HE			Individual VE		
0.012			0.000		



4. Operator #4

MAA Report for dim_phrlb_p_201306220821476_sen_643051101-001

Distance values are in meters

Mean latitude error: 0.070814
 Mean longitude error: -0.014276
 Mean horizontal error (average HE): 0.111439
 Standard deviation latitude error: 0.058795
 Standard deviation longitude error: 0.070789
 Standard deviation horizontal error: 0.035605
 90% Circular Error (against T&E): 0.157066
 90% Circular Error (T&E and mensuration error included): 0.157066

ID	T&E Latitude	T&E Longitude	T&E Elevation	T&E CE90	T&E LE90
1	-25 40 48.739	+28 05 58.453	1373.250	0.000	0.000

T&E Description
CP #1

Measured Latitude	Measured Longitude	Measured Elevation
-25 40 48.736	+28 05 58.451	1373.250

Delta Latitude	Delta Longitude	Delta Elevation	Mensuration Error
0.086	-0.047	0.000	0.000

Individual HE	Individual VE
0.098	0.000

ID	T&E Latitude	T&E Longitude	T&E Elevation	T&E CE90	T&E LE90
2	-25 40 58.711	+28 17 45.045	1263.080	0.000	0.000

T&E Description
CP #2

Measured Latitude	Measured Longitude	Measured Elevation
-25 40 58.708	+28 17 45.042	1263.080

Delta Latitude	Delta Longitude	Delta Elevation	Mensuration Error
0.090	-0.101	0.000	0.000

Individual HE	Individual VE
0.135	0.000

ID	T&E Latitude	T&E Longitude	T&E Elevation	T&E CE90	T&E LE90
3	-25 46 18.213	+28 12 7.614	1370.510	0.000	0.000

T&E Description
CP #3

Measured Latitude	Measured Longitude	Measured Elevation
-25 46 18.212	+28 12 7.617	1370.510

Delta Latitude	Delta Longitude	Delta Elevation	Mensuration Error
0.036	0.097	0.000	0.000

Individual HE	Individual VE
0.103	0.000



ID	T&E Latitude	T&E Longitude	T&E Elevation	T&E CE90	T&E LE90
4	-25 51 12.797	+28 05 50.429	1421.280	0.000	0.000
					T&E Description
					CP #4
Measured Latitude		Measured Longitude		Measured Elevation	
-25 51 12.797		+28 05 50.427		1421.280	
Delta Latitude	Delta Longitude	Delta Elevation	Mensuration Error		
-0.016	-0.056	0.000	0.000		
Individual HE			Individual VE		
0.058			0.000		
ID	T&E Latitude	T&E Longitude	T&E Elevation	T&E CE90	T&E LE90
5	-25 51 11.111	+28 17 35.640	1508.490	0.000	0.000
					T&E Description
					CP #5
Measured Latitude		Measured Longitude		Measured Elevation	
-25 51 11.106		+28 17 35.641		1508.490	
Delta Latitude	Delta Longitude	Delta Elevation	Mensuration Error		
0.159	0.035	0.000	0.000		
Individual HE			Individual VE		
0.163			0.000		



5. Operator #5

MAA Report for dim_phrlb_p_201306220821476_sen_643051101-001

Distance values are in meters

Mean latitude error: -0.004822

Mean longitude error: 0.011877

Mean horizontal error (average HE): 0.042903

Standard deviation latitude error: 0.032399

Standard deviation longitude error: 0.028665

Standard deviation horizontal error: 0.013965

90% Circular Error (against T&E): 0.060799

90% Circular Error (T&E and mensuration error included): 0.060799

ID	T&E Latitude	T&E Longitude	T&E Elevation	T&E CE90	T&E LE90
1	-25 40 48.739	+28 05 58.453	1373.250	0.000	0.000

T&E Description
CP #1

Measured Latitude	Measured Longitude	Measured Elevation
-25 40 48.740	+28 05 58.454	1373.250

Delta Latitude	Delta Longitude	Delta Elevation	Mensuration Error
-0.055	0.042	0.000	0.000

Individual HE	Individual VE
0.070	0.000

ID	T&E Latitude	T&E Longitude	T&E Elevation	T&E CE90	T&E LE90
2	-25 40 58.711	+28 17 45.045	1263.080	0.000	0.000

T&E Description
CP #2

Measured Latitude	Measured Longitude	Measured Elevation
-25 40 58.711	+28 17 45.044	1263.080

Delta Latitude	Delta Longitude	Delta Elevation	Mensuration Error
0.010	-0.040	0.000	0.000

Individual HE	Individual VE
0.041	0.000

ID	T&E Latitude	T&E Longitude	T&E Elevation	T&E CE90	T&E LE90
3	-25 46 18.213	+28 12 7.614	1370.510	0.000	0.000

T&E Description
CP #3

Measured Latitude	Measured Longitude	Measured Elevation
-25 46 18.213	+28 12 7.615	1370.510

Delta Latitude	Delta Longitude	Delta Elevation	Mensuration Error
0.006	0.032	0.000	0.000

Individual HE	Individual VE
0.032	0.000





ID	T&E Latitude	T&E Longitude	T&E Elevation	T&E CE90	T&E LE90
4	-25 51 12.797	+28 05 50.429	1421.280	0.000	0.000
					T&E Description
					CP #4
Measured Latitude		Measured Longitude		Measured Elevation	
-25 51 12.798		+28 05 50.430		1421.280	
Delta Latitude	Delta Longitude	Delta Elevation	Mensuration Error		
-0.024	0.020	0.000	0.000		
Individual HE			Individual VE		
0.031			0.000		
ID	T&E Latitude	T&E Longitude	T&E Elevation	T&E CE90	T&E LE90
5	-25 51 11.111	+28 17 35.640	1508.490	0.000	0.000
					T&E Description
					CP #5
Measured Latitude		Measured Longitude		Measured Elevation	
-25 51 11.110		+28 17 35.640		1508.490	
Delta Latitude	Delta Longitude	Delta Elevation	Mensuration Error		
0.040	0.005	0.000	0.000		
Individual HE			Individual VE		
0.040			0.000		



6. Operator #6

MAA Report for dim_phrlb_p_201306220821476_sen_643051101-001

Distance values are in meters

Mean latitude error: -0.001293

Mean longitude error: -0.002790

Mean horizontal error (average HE): 0.018313

Standard deviation latitude error: 0.013679

Standard deviation longitude error: 0.013301

Standard deviation horizontal error: 0.006175

90% Circular Error (against T&E): 0.026226

90% Circular Error (T&E and mensuration error included): 0.026226

ID	T&E Latitude	T&E Longitude	T&E Elevation	T&E CE90	T&E LE90
1	-25 40 48.739	+28 05 58.453	1373.250	0.000	0.000

T&E Description
CP #1

Measured Latitude	Measured Longitude	Measured Elevation
-25 40 48.739	+28 05 58.453	1373.250

Delta Latitude	Delta Longitude	Delta Elevation	Mensuration Error
-0.013	0.019	0.000	0.000

Individual HE	Individual VE
0.023	0.000

ID	T&E Latitude	T&E Longitude	T&E Elevation	T&E CE90	T&E LE90
2	-25 40 58.711	+28 17 45.045	1263.080	0.000	0.000

T&E Description
CP #2

Measured Latitude	Measured Longitude	Measured Elevation
-25 40 58.711	+28 17 45.045	1263.080

Delta Latitude	Delta Longitude	Delta Elevation	Mensuration Error
-0.014	-0.004	0.000	0.000

Individual HE	Individual VE
0.014	0.000

ID	T&E Latitude	T&E Longitude	T&E Elevation	T&E CE90	T&E LE90
3	-25 46 18.213	+28 12 7.614	1370.510	0.000	0.000

T&E Description
CP #3

Measured Latitude	Measured Longitude	Measured Elevation
-25 46 18.213	+28 12 7.613	1370.510

Delta Latitude	Delta Longitude	Delta Elevation	Mensuration Error
-0.004	-0.021	0.000	0.000

Individual HE	Individual VE
0.022	0.000



ID	T&E Latitude	T&E Longitude	T&E Elevation	T&E CE90	T&E LE90
4	-25 51 12.797	+28 05 50.429	1421.280	0.000	0.000
					T&E Description
					CP #4
Measured Latitude		Measured Longitude		Measured Elevation	
-25 51 12.797		+28 05 50.429		1421.280	
Delta Latitude	Delta Longitude	Delta Elevation	Mensuration Error		
-0.000	-0.008	0.000	0.000		
Individual HE			Individual VE		
0.008			0.000		
ID	T&E Latitude	T&E Longitude	T&E Elevation	T&E CE90	T&E LE90
5	-25 51 11.111	+28 17 35.640	1508.490	0.000	0.000
					T&E Description
					CP #5
Measured Latitude		Measured Longitude		Measured Elevation	
-25 51 11.110		+28 17 35.640		1508.490	
Delta Latitude	Delta Longitude	Delta Elevation	Mensuration Error		
0.024	0.000	0.000	0.000		
Individual HE			Individual VE		
0.024			0.000		

